The Analyst

An international analytical science journal

Information for Authors

Full details of how to submit material for publication in The Analyst are given in the Instructions to Authors in the January issue. Separate copies are available on request.

The Analyst publishes original research papers, critical reviews, tutorial reviews, perspectives, news articles, book reviews and a conference diary.

Original research papers. The Analyst publishes full papers on all aspects of the theory and practice of analytical chemistry, fundamental and applied, inorganic and organic, including chemical, physical, biochemical, clinical, pharmaceutical, biological, environmental, automatic and computer-based methods. Papers on new approaches to existing methods, new techniques and instrumentation, detectors and sensors, and new areas of application with due attention to overcoming limitations and to underlying principles are all equally welcome.

Full critical reviews. These must be a critical evaluation of the existing state of knowledge on a particular facet of analytical chemistry.

Tutorial reviews. These should be informally written although they should still be a critical evaluation of a specific topic area. Some history and possible future developments should be given. Potential authors should contact the Editor before writing reviews.

Perspectives. These articles should provide either a personal view or a philosophical look at a topic relevant to analytical science. Alternatively, they may be relevant historical articles. Perspectives are included at the discretion of the Editor.

Particular attention should be paid to the use of standard methods of literature citation, including the journal abbreviations defined in Chemical Abstracts Service Source Index. Wherever possible, the nomenclature employed should follow IUPAC recommendations, and units and symbols should be those associated with SI.

Every paper will be submitted to at least two referees, by whose advice the Editorial Board of The Analyst will be guided as to its acceptance or rejection. Papers that are accepted must not be published elsewhere except by permission. Submission of a manuscript will be regarded as an undertaking that the same material is not being considered for publication by another journal.

Associate Scientific Editors. For the benefit of all potential contributors wishing to discuss the scientific content of their paper(s) a Group of Associate Scientific Editors exists. Requests for help or advice on scientific matters can be directed to the appropriate member of the Group (according to discipline). Currently serving Associate Scientific Editors are listed in each issue of The Analyst (and Analytical Communications).

Manuscripts (four copies typed in double spacing) should be addressed to:

H. S. Minhas, Managing Editor, or
J. F. Tyson, US Associate Editor

All queries relating to the presentation and submission of papers, should be addressed to the Publishing Division and any correspondence regarding accepted papers and proofs, should be directed to the Production Division for The Analyst. Members of the Analytical Editorial Board (who may be contacted directly or via the Editorial Office) would also welcome comments, suggestions and advice on general policy matters concerning The Analyst.

There is no page charge.

Fifty reprints are supplied free of charge.

Critical Review

Analytical Extraction of Additives From Polymers

Harold J. Vandenburg[a], Anthony A. Clifford*[a], Keith D. Bartle[a], John Carroll[b], Ian Newton[b], Louise M. Garden[b], John R. Dean[c] and Claire T. Costley[c]

[a] *School of Chemistry, University of Leeds, Leeds, UK LS2 9JT*
[b] *ICI Technology, Research and Technology Centre, P.O. Box 90, Wilton, Middlesbrough, Cleveland, UK TS90 8JE*
[c] *Department of Chemical and Life Sciences, University of Northumbria at Newcastle, Ellison Building, Newcastle-upon-Tyne, Tyne and Wear, UK NE1 8ST*

Summary of Contents

Introduction
Conventional Extraction Techniques
    Dissolution of the Polymer
    Liquid–Solid Extractions
New Developments in Extraction From Polymers
    SFE
    MAE
    ASE
Supercritical Fluid Extraction
    Extraction Process
Factors Affecting SFE From Polymers
    Effect of Supercritical CO_2 on Polymers
    Effect of Temperature and Pressure
    Effect of Flow Rate
    Effect of Modifiers
    Nature of the Extractant
    Effect of Particle Size
    Summary of SFE
Microwave Heating
Ultrasonic Extraction
ASE
Other Extraction Methods
Conclusions
References

Keywords: Review; polymer; supercritical fluid extraction; microwave-assisted extraction; liquid extraction

Harold Vandenburg graduated from Manchester Polytechnic where he studied Applied Chemistry part-time whilst working in quality control in the pharmaceutical/personal care sector. After working for a year in Australia and USA, he started six years of research on migration from polymers into foods at high temperatures at the Procter Department of Food Science at the University of Leeds. He obtained his PhD during this time. Still at the University of Leeds, but now at the School of Chemistry, he is undertaking research comparing the effectiveness of sample preparation methods for polymers and environmental samples.
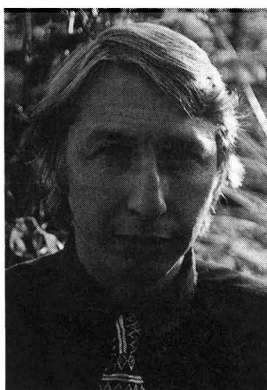
Introduction

Plastics contain many small molecules as well as the polymer itself. These include additives to alter the polymer properties or prolong the life of the polymer, such as plasticisers, antioxidants and ultraviolet (UV) light absorbers. There may also be processing aids, residual monomers, low molecular weight oligomers and inadvertent contaminants present. It is important for the manufacturer and regulators to know the level of these materials in the polymer to ensure the product is fit for its intended purpose. Food contact plastics are regulated by maximum concentrations allowable in the plastic, which applies to residual monomers and processing aids as well as additives.[1–3] There are some methods for determining concentrations of additives without extraction from the polymer, such as nuclear magnetic resonance spectrometry,[4] UV spectrometry,[5] and UV desorption–mass spectrometry.[6] However, in order to determine the levels in the polymer it is usually necessary to extract the compounds from the plastic quantitatively before analysis. The trade names and chemical names of many commonly used additives are given in Table 1.

Conventional Extraction Techniques

These can be divided into two categories: dissolution of the polymer and liquid–solid extraction methods. Many examples can be found in texts such as Crompton,[7] Haslam *et al.*[8] and Wheeler.[9] A review of extraction methods to 1992 is included in Cotton.[10]

Dissolution of the Polymer

A British Standard method[11] describes the dissolution of polymers in refluxing toluene, with re-precipitation of the polymer by addition of ethanol. Decalin heated to 110 °C has been used as a solvent for poly(ethylene) (PE)[12] and at 150 °C for poly(propylene) (PP).[13] The high molecular weight polymer precipitates out as the solution is cooled and the supernatant solution is filtered and analysed. Formic acid is used to dissolve poly(amides) before further fractionation, for example by liquid–liquid extraction with toluene for 18 h to remove lubricants.[14]

Poly(ethylene terephthalate) (PET) has been dissolved in hexafluoropropan-2-ol–dichloromethane mixtures and the polymer precipitated by addition of acetone or methanol.[15,16] Analysis of poly(vinyl chloride) (PVC) has traditionally been by sequential diethyl ether and methanol extractions to remove selected components, then dissolution of the polymer in tetrahydrofuran (THF). Centrifugation at two speeds would then produce two further fractions. Methanol would then be added to precipitate the polymer, and the methanol–THF would be evaporated and examined for non-extracted material.[7] This

process can be simplified by dissolving the polymer in THF, followed by centrifugation at 20 000 rev min^{-1} to remove mostly inorganic fillers. Addition of ethanol precipitates the polymer and polymeric additives. Polymeric plasticiser can be re-extracted from the precipitated polymer.[14]

Dissolution and re-precipitation therefore provides an effective method of extraction. The advantage is that there is no possibility of some analyte remaining bound in the polymer network, although inclusion of the analyte in the re-precipitated polymer can occur. There is often a considerable amount of 'waxes' in solution, which may need to be removed before further analysis. Some workers have considered this too time consuming[17] and prefer liquid–solid extractions.

Liquid–Solid Extractions

Here the analyte is extracted from the solid medium by a liquid, which is separated by physical means, such as filtration. There are many methods for carrying out these extractions including Soxhlet, sonication and shake-flask extractions. Spell and Eddy[17] studied the extraction of additives from PP at room temperature and found that required extraction time varied linearly with polymer density and decreased with increasing particle size. They also found a large variation in extraction time for different solvents and additives. By powdering the polymer to 50 mesh size, 98% extraction of 2,6-di-*tert*-butyl-4-methylphenol (BHT) was achieved by shaking at room temperature for 30 min with carbon disulfide. To achieve the same recovery with isooctane required 125 min, and 2000 min were required to recover Santonox with isooctane. The importance of small particles is further demonstrated by Newton.[14] Refluxing ground PP with chloroform for 1 h gives complete extraction. For films, 3 h are required and for unground granules 3 h are sufficient to provide an extract for identification purposes only. Ethoxylated tertiary amines can be extracted from PP by refluxing the ground material with 1,2-dichloroethane for 1 h. Refluxing the granules for 3 h gives only 85% extraction.

Soxhlet extraction has often been used, with a variety of solvents. Whilst this method eventually gives good extraction efficiencies, the extraction rate is slow. Times for extraction typically vary from 6 h[18] to 48 h.[19,20] Even with long extraction times recovery is not always good. Perlstein[21] obtained recoveries of only 59% for extraction of Tinuvin 320 from unground PVC after 16 h Soxhlet extraction with diethyl ether. However, recoveries rose to 97% from ground polymer. The choice of solvent is significant for the duration of the extraction. Wims and Swarin[22] found that talc filled PP needed 72 h extraction with chloroform, but only 24 h with THF. Thus, small particles are often essential to complete the extraction in reasonable times, and the solvents must be carefully selected to swell the polymer.

Solid–liquid extraction has been shown to be effective, but often very slow and requires large amounts of solvents. This results in dilute solutions requiring further concentration before analysis, which is time consuming and may result in the loss of volatile compounds. The use of large volumes of often toxic solvents is environmentally unsound, as well as expensive in purchase and disposal costs. Some effort needs to be made to select the most appropriate solvent for the extraction. Therefore, there are great savings to be made if the extraction time and the solvent usage can be reduced.

New Developments in Extraction From Polymers

The principal objectives of any technique to replace 'traditional' extraction methods is to complete the extraction in less time, using less solvent and also have the possibility of automating the process. Recent articles[23,24] describe some new techniques, such as supercritical fluid extraction (SFE), microwave-assisted extraction (MAE) and accelerated solvent extraction (ASE), and some applications are summarized. Although the purpose of this review is not to describe the techniques in detail, a brief description is given.

SFE

SFE uses fluids above their critical temperature and pressure. These supercritical fluids have densities and diffusivities between those of liquids and gasses. The solvating power is

Table 1 Commonly used additives in polymers

Trade name	Chemical name
BHT	2,6-Di-*tert*-butyl-4-methylphenol
Chimassorb 81	2-Hydroxy-4-*n*-octoxybenzophenone
Chimassorb 944	Poly(*N*-1,1,3,3-tetramethylbutyl-*N'*,*N'''*-di(2,2,6,6-tetramethylpiperidinyl)-*N'*,*N'''*-melaminoditrimethylene
Cyasorb UV 531	2-Hydroxy-4-*n*-octoxybenzophenone
DSTDP	Distearyl 3,3'-thiodipropionate
Erucamide	13-*cis*-Docosenamide
Ionox 330	1,3,5-Trimethyl-2,4,6-tris(3,5-di-*tert*-butyl-4-hydroxybenzyl)benzene
Irgafos 168	Tris(2,4-di-*tert*-butylphenyl) phosphite
Irganox 1010	Pentaerythrityl-tetrakis(3,5-di-*tert*-butyl-4-hydroxyphenyl) propionate
Irganox 1076	Octadecyl-3,5-di-*tert*-butyl-*R*-hydroxyhydrocinnamate
Irganox 1098	*N*,*N'*-Bis{[3-(3',5'-di-*tert*-butyl-4'-hydroxyphenyl)-(propionyl)]}-hexamethylenediamine
Irganox 3114	1,3,5-Tris(3,5-di-*tert*-butyl-4-hydroxybenzyl)*s*-triazine 2,4,6-(1*H*, 3*H*,5*H*)trione
Isonox 129	2,2'-Ethylidenebis(4,6-di-*tert*-butylphenol)
Nauguard 524	Tris(2,4-di-*tert*-butylphenyl) phosphite
Santonox	4,4-Thiobis(6-*tert*-butyl-*m*-cresol)
Tinuvin 328	2-(2'-Hydroxy-3,3,5-di-*tert*-amylphenyl)benzotriazole
Tinuvin 770	Bis(2,2,6,6-tetramethylpiperidin-4-yl) sebacate
Tinuvin P	2-(2-Hydroxy-5-methylphenyl)-2*H*-benzotriazole
Topanol CA	1,1,3-Tris(2-methyl-4-hydroxy-5-*tert*-butylphenyl)butane
Ultranox 626	Bis(2,4-di-*tert*-butylphenyl)pentaerythritol diphosphite
Weston 618	Distearylpentaerythritol diphosphite

related to the density, which in turn depends on pressure and temperature. Increasing pressure at constant temperature increases density and solvating power. However, increasing temperature at constant pressure decreases density and hence solvating power. CO_2 is most widely used as solvent because of its convenient critical temperature (31.3 °C) and pressure (7.4 MPa), low cost, low toxicity and non-explosive character. Liquid solvents called modifiers are sometimes added to the CO_2 in order to increase solubility or displace analytes from a matrix.

MAE

Sample and solvent are placed in a container and heated using microwave energy. The technique has evolved from closed-vessel microwave acid digestions. The apparatus typically consists of closed vessels with temperature and pressure control, allowing the solvent to be heated under pressure above its normal boiling-point and remain liquid. The solvent must contain a component with a high relative permittivity to be heated by microwaves. Carousels of extraction vessels may be used, allowing for simultaneous extraction of up to 12 samples.

ASE

The sample is loaded into an extraction cell and solvent is pumped into the cell, which is heated in an oven. The temperature and pressure are programmed by the user. Pressure is applied to keep the solvent liquid above its normal boiling-point. After the pre-set extraction time, more solvent is pumped through the cell into the collecting vessel and the remaining solvent is purged into the collecting vessel with nitrogen. The equipment is automated, allowing up to 24 sequential extractions to be programmed.

In this paper, published accounts of laboratory methods for the extraction from polymers are reviewed. The new methods are here compared with each other and with traditional methods. Although there is a considerable literature on SFE, there are few reports on the other novel techniques.

Supercritical Fluid Extraction

SFE has been used for a great many matrices, including the extraction of environmental contaminants, natural products and food processing as well as polymers, which are discussed in several reviews.[25–29] Extraction from polymers is one of the more recent uses of SFE. Early experiments established that SFE of polymers was a viable extraction method and could be much faster than traditional methods. Anton *et al.*[30] extracted oligomers and an unidentified additive from an ethylene–propylene O-ring using CO_2 at 25 °C and 6.6 MPa for 1 h. A second extraction produced more analyte, indicating that the extraction was not complete after the first hour. Hirata and Okamoto[31] found that additives could be extracted at 90% recoveries from PE and PP films using CO_2 at 25.4 MPa and 35 °C within 2 h, compared with 24 h for Soxhlet extraction. Cotton *et al.*[32] showed that SFE of additives and oligomers from PP, nylon, PET and poly(ether-ether ketone) (PEEK) were possible. Irganox 1010, Irgafos 168 and erucamide were extracted from ground PE and Tinuvin 770 from PP at 92–95% recoveries in 15 min at 42.9 MPa and 60 °C. At 14.3 MPa the same recovery was achieved in 30 min.[33] Following these successful extractions the optimum extraction conditions have been investigated.

Extraction Process

The two main factors in SFE are solubility of extractant in the fluid and rate of mass transfer out of the matrix. The mass transfer from the polymer is by diffusion from the bulk polymer to the surface, where dissolution in the supercritical fluid (SF) can occur. Bartle *et al.*[34] described a simple model for extraction from spherical particles called the 'hot ball' model. This assumed that the concentration of extractant in the SF was effectively zero, and the only limiting step was transfer out of the matrix by a process which could be modelled as diffusion. This successfully predicted the characteristics of the extraction curve of $\ln(m/m_0)$ *versus* time for extraction of BHT from PP (where m_0 is the initial concentration in the plastic and m is the amount remaining in the plastic). These are that the curve falls steeply initially, as the extractant is extracted from the surface, and then becomes linear (Fig. 1). There were deviations from the predicted onset of the linear portion and of the extrapolated intercept of the linear portion with the m/m_0 axis. These were explained in terms of non-spherical particles, solubility limitations and non-uniform distribution of the extractant in the polymer. The success of the model indicates that the basic processes can be modelled as diffusion. However, the deviations indicate that solubility and other factors are also significant.

The linear part of the logarithmic plot can be extrapolated to determine the concentration of an extractant without complete extraction by using three extraction periods of equal duration. The amount m_0 can be found using the equation $m_0 = m_1 + [(m_2)^2/(m_2 - m_3)]$. The first extraction must be long enough such that the second and third extractions are on the linear portion of the curve. The extrapolation method successfully gave the extractable amount of BHT from PP. The model was extended to cover polymer films and non-uniform distribution of the extractant in PET as an example.[35] The temperature chosen (70 °C) was just above the glass transition temperature (T_g) (69 °C), but the amount extracted was considerably less than that extracted by Soxhlet extraction. Thus, much of the trimer is unavailable to SFE at this temperature. This is consistent with the findings of Ashby,[36] who found that the overall migration from PET into olive oil was negligible until a temperature of 130 °C was reached. The effect of solubility on extraction was incorporated into the model by Bartle *et al.*[37] using extraction of Irgafos 168 from PP to test the model. At 70 °C, the effect of increased pressure (solubility) on the extraction curve was to increase the slope of the initial steep $\ln(m/m_0)$ curve and increase the slope of the linear portion of the graph, *i.e.*, increased extraction rate. The
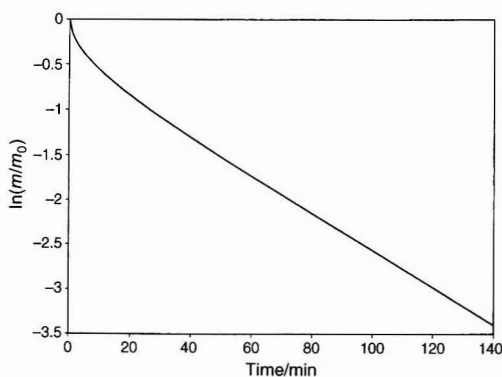

Fig. 1 Example of $\ln(m/m_0)$ plot for SFE from polymers using the 'hot ball' model.

effects of pressure and flow rate on extraction are explained theoretically by Clifford *et al.*[38]

A method for direct observation of the extraction process in real-time is described by Howdle *et al.*[39] using an organometallic complex. The IR absorption bands are sensitive to the environment, and therefore a shift in the spectrum occurs when the complex is extracted from the polymer. This allows monitoring of the extraction process *in situ*.

SFE is therefore an effective method of extraction from polymers. There are several factors that can affect the success of SFE: temperature, pressure, time, addition of modifier, the matrix and the compound extracted. The interaction of these variables is particularly complex for extraction from polymers, partly because the solvent can interact with the polymer.

Factors Affecting SFE From Polymers

Effect of Supercritical CO_2 on Polymers

CO_2 can be dissolved in polymers and effectively plasticise and swell them. A high pressure view cell with a sapphire window has been used to measure the swelling of soils and plant materials during treatment with supercritical CO_2.[40] A direct relationship was observed between the degree of swelling and the efficiency of extraction. Similar effects would be expected from polymers, with the size of the effect depending on the amount of CO_2 absorbed. The amount of CO_2 absorbed will depend on temperature, pressure and the polymer concerned. Shieh *et al.*[41,42] studied the effects of supercritical CO_2 on nine crystalline and 11 amorphous polymers. The appearance, mass changes, physical properties and solubility of CO_2 were examined after removal from the fluid. The amorphous polymers were most affected, many exhibiting significant swelling, particularly poly(methyl methacrylate) (PMMA). T_g was measured for PMMA and glycol-modified poly(ethylene terephthalate) (PETG) and was found to be depressed after exposure to CO_2. Crystalline polymers were plasticised less than the amorphous polymers. The T_g of PET was found to be depressed by 52 °C when CO_2 was sorbed at 2 MPa.[43] The greater effect on amorphous polymers is expected as it has been reported that CO_2 is not soluble in the crystalline regions of polymers.[44] The strength of the effect on PMMA was possibly explained by investigations using Fourier transform infrared spectrometry (FTIR), which determined that there were specific Lewis acid–base type interactions between the carbonyl group in PMMA and CO_2.[45] No such interaction was found in PE, and a weak interaction was found between CO_2 and the π system of poly(styrene) (PS). Therefore, we can expect the greatest swelling and plasticisation in amorphous polymers with electron donating groups. Extraction at temperatures above T_g will generally be much faster than below T_g. Kalospiros and Paulaitis[46] have developed a molecular thermodynamic model for predicting solvent-induced glass transitions as a function of sorbed gas in the polymer. However, CO_2 can also induce crystallisation in polymers at lower temperatures,[47] which would be expected to reduce the rate of diffusion. Condo and co-workers[48,49] measured the depression of the T_g of PMMA, poly(ethyl methacrylate) (PEMA) and poly(methyl methacrylate-*co*-styrene) (SMMA60) by CO_2 *in situ*, using creep compliance in a high pressure cell. The relationship with pressure and temperature was not simple, and four types of behaviour were predicted and found. The phenomenon of reverse vitrification was identified, where the polymer undergoes a glass to liquid transition by decreasing the temperature. This means that some polymers may be plasticised under much milder conditions of temperature and pressure than was previously believed.

The interaction of CO_2 with polymers can rapidly swell and plasticise the polymer, resulting in much faster diffusion and hence extraction. The plasticisation alters the T_g and softening

points, and therefore the temperature and pressure selected for the extraction can be lower than would be expected from physical data available on the polymer.

Effect of Temperature and Pressure

Diffusion in polymers is a slow process with diffusion coefficients of the order of 10^{-10} cm^2 s^{-1} at 40 °C. The rate of diffusion follows an exponential Arrhenius form with temperature, rate $\propto A \exp(-E/RT)$, where E is the activation energy, R is the gas constant and T the absolute temperature. This would indicate that increasing the temperature would exponentially increase the diffusion rate. If the solubility in the SF is not limiting, then higher temperature would lead to higher extraction rate. However, increase in temperature decreases the density of a SF at constant pressure, which reduces the solubility of the extractant in the SF. Therefore, it might be expected that a rise in temperature would lead to a rise in extraction rate, up to a point where solubility in the SF became a limiting factor. Increasing the temperature can also cause the polymer to undergo a transition from a glassy to a rubbery form at the glass transition temperature. The diffusion in the rubbery form is much faster than the crystalline glassy form. Therefore, a sharp rise in extraction rate would be expected at the T_g.

Increasing the pressure increases the density of the SF and therefore the solubility of the extractant. At low temperatures, when the extraction is almost completely diffusion-limited, this should have little effect. The situation is further complicated because supercritical CO_2 can plasticise a polymer and lower the T_g. The amount of lowering increases with amount of fluid in the polymer, which depends on the pressure and temperature. Supercritical CO_2 has a much greater effect on amorphous polymers than on crystalline polymers. Therefore, the effect of pressure and temperature would be expected to be more pronounced in amorphous polymers. Increasing the pressure may increase the extraction rate in amorphous polymers, even when solubility does not limit the extraction as the plasticisation of the polymer increases with absorbed CO_2.

The effect of temperature on extraction of oligomers from PET was studied by Kuppers.[50] Extraction at a constant CO_2 density of 0.5 g cm^{-3} (hence changing pressure) showed an increase in the rate of extraction of trimer from PET from 40 to 160 °C, but there was no jump at the T_g. Increasing the density at the same temperature gave even higher extraction rates, indicating that solubility is also limiting the extraction. However, it is possible that increased plasticisation of the polymer at higher pressures was responsible for the increase rather than the increased solubility. Plotting extraction at constant pressure (changing density) against T showed a sharp increase at T_g, then a flattening of the curve at high temperatures, presumably as solubility again became limiting. The lack of a jump in the constant density curve may indicate a change in the T_g at higher pressures of CO_2.

Cotton *et al.*[51] extended the work on PET film to higher temperatures. They found an increase in extraction with temperature at constant pressure (40.6 MPa), but no discontinuity at T_g. Above 215 °C some melting took place, causing agglomeration which slowed extraction and blocked the restrictor, so 215 °C was the highest temperature used for extractions. The extrapolation method at this temperature gives quantitative recoveries using 3 × 30 min extractions, and 95% recoveries using 3 × 15 min extractions. The intercept of the extrapolated linear portion of the graph is lower than at 70 °C, indicating that solubility, as well as diffusion from the polymer, affects the extraction at the higher temperature. Schmidt *et al.*[52] analysed carbonic acid diphenyl ester from poly(butylene terephthalate) (PBT) by SFE. At room-temperature, six times less was extracted than at 55 °C. Hunt and Dowle[53] found that extraction of diisooctyl phthalate (DIOP) and Topanol CA from

ground PVC increased with temperature up to 90 °C at 45 MPa, then levelled off, presumably as solubility became the limiting factor. The extraction rate increased on increasing the pressure from 35 to 40 MPa at 45 °C; increasing the pressure further to 45 MPa had no further effect.

The extraction of dioctylphthalate (DOP) and dibutylphthalate (DBP) plasticisers from PVC was also measured for 25 min extractions by Marin *et al.*[54] At a pressure of 52 MPa, the amount extracted by CO_2 increased from 50 to 80 °C, at which temperature extraction was almost complete within the 25 min. At a constant temperature of 70 °C, increasing the pressure from 22 to 60 MPa increased the amount extracted from approximately 79 to 95%. At 100 °C, the same pressure increase led to a marginal increase in extraction from 95 to 98%. As the extraction is close to completion at the higher temperatures, it is not possible to see the full effect of the pressure increase. However, from solubility considerations, the effects should be greater at higher temperatures because the extraction then becomes solubility-limited.

Extraction of tris(nonylphenyl) phosphite, Irganox 1076 and Weston 618 from low-density PE (LDPE) film was measured at 45.6 MPa at different temperatures.[55] At 60 °C, only 40–60% was extractable. However, by heating to 150 °C, which is 10 °C above the melting-point, >95% was recovered. This is against the general finding that heating above the melting-point reduces extraction rate as melting reduces the surface area of ground samples. Extraction of *N,N*-ethylenebisstearamide from PS increased from 77 to 94% by increasing the temperature from 60 to 150 °C. Extraction efficiency of BHT and Irganox 1010 from freeze-ground PP increased from 30 to 90 °C at a pressure of 30.4 MPa.[56] At 90 °C, 60 min were sufficient for complete extraction of all additives except for Irganox 1010. During the extraction of flame retardants from poly(urethane) (PU), Mackay and Smith[57] found that extraction at 30.4 MPa was rapid and quantitative within 10 min at 60 °C, whereas at 20.3 MPa recoveries were lower, and at 10.1 MPa some flame retardants were hardly extracted at all.

The effect of pressure in selective extractions was pointed out by Engelhardt *et al.*[58] At 15.2 MPa and 45 °C, erucamide was extracted from PE. By increasing the pressure to 20.3 MPa, an Irganox-type antioxidant was also extracted. They linked the SFE conditions needed to extract materials with their retention using reversed-phase (RP) HPLC. If 90% organic modifier is needed to elute a compound from an RP HPLC column, then an extraction pressure of 15.2–20.3 MPa is sufficient. If a compound elutes with 50–60% organic modifier by HPLC, then the pressure for SFE using CO_2 needs to be 35.5 MPa.

Cotton *et al.*[59] measured the extraction of Irgafos 168, Irganox 1010 and Tinuvin 770 from PP pellets and ground PP. Increasing pressure gave increased extraction rates at 50 °C up to a limit of 30.4 MPa, after which solubility no longer limited the extraction. The rate increased sharply with increasing temperature, up to the melting-point of the polymer. Once melting occurs the particles coalesce and the surface area decreases. The diffusion coefficient was found to be two orders of magnitude higher than from previously published data. This was explained by the plasticisation and swelling of the polymer by sorbed CO_2. The value of the extrapolation procedure was demonstrated by successfully determining the total concentrations of Irganox 1010 and Irgafos 168 in less time than was required to complete the extraction from ground PP. For the larger pellets, low results were obtained from the extrapolation because the $\ln(m/m_0)$ *versus* time plot had not reached the linear portion after the first extraction period.

Recovery of dialkyl organotin stabilisers from freeze-ground, unplasticised PVC at 17.7 MPa was found to increase with temperature up to 90 °C, then levelled off with further temperature increases, presumably as solubility became limiting.[60] Similarly, the recovery at 90 °C increased with increasing

pressure up to 15.2 MPa and then levelled off as diffusion became limiting. The extraction was complete within 60 min at 90 °C and 17.7 MPa. No data are given for recoveries above 90 °C at pressures above 17.7 MPa, but unless melting had commenced at this temperature the extraction rate should be enhanced as solubility-limiting behaviour would be reached at a higher temperature.

Extraction of ethylbenzene from PS was neither completely diffusion nor solubility limited, leading to unusual T and P relationships.[61] The polymer was significantly swelled by the CO_2, leading to a 10^6-fold increase in diffusivity of ethylbenzene in the polymer. T_g was lowered from 100 to 50 °C by only 6 MPa of CO_2.

Roston *et al.*[62] used SFE to extract a sustained release drug covalently bonded to poly(butadiene). Optimum pressure for the extraction was 33.5 MPa. Increasing the pressure above this reduced the amount extracted. These workers suggest that this decrease at higher pressures was due to recovery increasing with linear velocity of extracting media through the cell up to a certain velocity, then decreasing. Decreased trapping efficiency at faster flow rates is also a possibility. The temperature could not be raised above 75 °C because the drug is not thermally stable. Significant swelling of the polymer was noted; 85% of the drug was recovered in 45 min with a further 5% recovered in the subsequent 30 min.

Extraction of Irgafos 168, Irganox 1076 and Irganox 1010 from PE powder increased with increasing temperature at 30.4 MPa.[63] However, at 15.2 MPa the amount extracted during the first 30 min initially increased with temperature as diffusion was faster, but then fell as solubility-limiting behaviour took over. The amount extracted at longer times was always higher at higher temperatures, as the concentration in the extracting fluid fell and diffusion control was re-established. At 50 °C, increasing pressure had little effect as the extraction was almost completely diffusion-controlled. At 80 °C, the extraction rate increased from 20.3 to 30.4 MPa. The recovery at 25.4 MPa and 80 °C was higher than by 36 h Soxhlet extraction with hexane. Lou *et al.*[64] examined the extraction of caprolactam from nylon 6, and dimer and trimer from PBT. Extraction of caprolactam during the first 30 and 120 min increased with increasing temperature from 50 to 170 °C. No jump at the T_g was apparent, implying that the CO_2 had suppressed the T_g. However, during extraction from PBT, the amount of the dimer extracted after 120 min was highest at 150 °C and for the trimer at 110 °C. This indicates that the larger trimer is less soluble than the dimer, and extraction becomes solubility-limited at a lower temperature.

The effect of temperature on the extraction of styrene dimers and trimers from PS was demonstrated by Jordan *et al.*[65] A very low density of CO_2 was used (0.184 g cm^{-3}), and kept constant at different temperatures. Extraction at 120 °C (10.8 MPa) produced eight times more dimers and trimers than extraction at 80 °C (8.8 MPa). The effect of the density of CO_2 was examined by extracting at 120 °C at 20.3 MPa. The extraction time was reduced so that the same total amount of CO_2 was used as in the lower pressure experiment. Exact comparisons of peak areas were not possible because the chromatographic system was overloaded, but at the higher pressures a sample size about 25% of that used at the lower pressure caused saturation. Therefore, the higher pressure extraction resulted in significantly greater extraction.

The effects of pressure are more pronounced for extraction from an amorphous rubber. Burgess and Jackson[66] found that extraction of carbon tetrachloride from chlorinated poly-(isoprene) could be completed within 40 min at 60 °C and 21 MPa, and not at higher temperatures or pressures. The normal T_g is 120 °C, but the softening point is lowered by the CO_2 at high pressures. Therefore, increasing the pressure at high temperatures lowered the softening point and the polymer particles coalesced, reducing the surface area. Extractions on

crystalline polymers at low temperatures usually show little improvement with increasing pressure. However, in this case at 40 °C the extraction improves with increasing pressure. At this low temperature the extraction is unlikely to be solubility-limited, and therefore the greater extraction is probably due to increased swelling of the polymer at higher pressures.

The polymer matrix affects the extraction efficiency, as demonstrated by Juo et al.,[67] who extracted Chimassorb 944, distearyl 3,3'-thiodipropionate (DSTDP), Irganox 1010, Irganox 1076, Tinuvin 144, Irganox 1098, Ionox 330 and oxidised Nauguard 524 from LDPE and high-density PE (HDPE). Both polymers were extracted at 60.8 MPa and 40 °C, for 30 min for LDPE and 5 h for HDPE. All additives were extracted from the LDPE, whereas some additives would not extract from HDPE even with 3% methanol modifier.

Generally, diffusion from the polymer is the rate-limiting process, particularly during the later stages. Therefore, for optimum extraction, a high temperature should be used to maximise diffusion. High pressure should also be used for rapid extractions, both to increase solubility of the analyte and to plasticise the polymer. However, high pressures may lower the softening point of the polymer, and therefore the optimum conditions need to be experimentally determined.

Effect of Flow Rate

The flow rate will affect the extraction only if the extraction is solubility-limited. In this way changes to flow rate are similar to changes in pressure. The effects of pressure and flow rate on SFE from polymers have been modelled.[38] For a solubility-limited extraction, increasing the pressure will increase the rate of extraction up to the point at which diffusion becomes rate-limiting. At faster flow rates, the pressure limit will occur at lower pressure. Therefore, increasing the flow rate has a similar effect to increasing the pressure. This does not take into account the increased plasticisation of the polymer at higher pressures of CO_2. Hawthorne et al.[68] found that the flow rate had little effect on extraction of alkylbenzenes from PS beads except at a very low flow rate of 0.25 ml min^{-1}. For extraction of antioxidant from PE powder, there was little effect of flow rate at 50 °C, but some effect was noted at 80 °C as the faster diffusion at the higher temperature raised the concentration in the fluid.[63] In contrast, Baner et al.[69] found a marked reduction in the time to determine total extractables from Biopol (a biodegradable polymer) with increased flow rate. At a flow rate of 1.5 ml min^{-1}, the extraction took 40–50 min, reducing to about 15 min with a flow rate of 4.5 ml min^{-1} and 8 min for 8.5 ml min^{-1}. As the total volume of CO_2 is similar in each case, it seems that this extraction is almost completely solubility-limited.

Effect of Modifiers

CO_2 is characterised as a non-polar solvent with a solubility parameter similar to hexane. It does, however, have some affinity with slightly polar molecules because of its molecular quadrupole. For more polar molecules the addition of polar modifiers is used to increase the polarity of the supercritical phase and the solubility of polar compounds. In extraction from environmental matrices, binding of the extractant to active sites is very important, and the modifier can displace the extractant from the matrix, increasing extractability. This is less likely to be a factor in extraction of polymers. However, if they are similar in molecular character, modifiers can act by swelling the polymer, increasing diffusion and extraction rates. Modifiers used for this purpose may be non-polar or aromatic as well as polar. Therefore, modifiers may enhance extraction even when solubility is not a limiting factor.

Hunt and Dowie[53] found that only 50% of Topanol CA would extract from PVC at 45 MPa and 90 °C within 30 min. The

addition of methanol modifier enhanced the extraction. The recoveries increased with increasing methanol concentration in the SF from 2 to 15%. The total present in the polymer was not accurately known; therefore, it was not known whether the recovery was quantitative. Mixed messages on modifiers come from the work of Kuppers.[50] Dichloromethane (DCM) enhanced extraction of oligomers from PET, the higher oligomers being most affected. Using methanol or propan-2-ol completely prevented extraction. The reason for the latter finding is not explained.

Recovery of oligomers and caprolactam from ground nylon 6 was poor using CO_2 at 60 °C.[70] Addition of methanol to the extraction vessel during a 5 min static extraction period enhanced extraction, which was almost complete for caprolactam in 15 min. For oligomers the recovery was lower, but was further improved by using 7.5% methanol during the dynamic extraction stage. Methanol enhanced the extraction of caprolactam from nylon for Jordan et al.[65] Spiking the extraction cell with methanol before extraction with CO_2 at 75 °C and 25.3 MPa extracted approximately three times as much caprolactam as the same extraction conditions without methanol. The same amount of caprolactam spiked onto Celite was completely recovered using CO_2 only, indicating that solubility limitations were not the reason for the low recovery from the polymer. These workers suggest that the methanol was swelling the polymer and therefore enhancing the extraction rate. Lou et al.[64] examined the effect of modifiers on extraction of caprolactam from nylon 6, and dimer and trimer from PBT. The modifiers (hexane, chloroform, methanol and benzene) were spiked into the extraction cell for an initial static extraction period. Methanol was the most effective modifier for nylon and chloroform for extraction from PBT. When compared with extraction using unmodified CO_2, the modifiers had the most effect at lower temperatures. In fact, at higher temperature the amount extracted at longer times was lower than when using CO_2 alone. This was thought to be due to a shrinking of the polymer after the modifier had been extracted from the cell. Improvements in extraction efficiencies could be achieved at both diffusion and solubility limiting conditions, indicating that the modifiers worked both by swelling the polymer and increasing solubility.

Addition of benzene during a static extraction with CO_2 for 30 min improved recoveries of antioxidant from PE powder.[63] Benzene was selected as it is known to swell PE, and this was thought to be the main reason for the greater recoveries. However, for Irganox 1010 the greater solubility was also thought to be significant. Garde et al.[71] optimised the extraction of antioxidants from PP. They found that the best methods used two static extractions of 30 min, one with hexane and one with methanol. Use of methanol as modifier in a 60 min dynamic extraction only slightly enhanced the recoveries, indicating that swelling of the polymer is the most important factor.

Propane added to CO_2 had little effect on the extraction of chlorofluorocarbons (CFCs) from PU foams.[72] Using unground foam, the time required for 99% extraction was 1.5 h, whereas with addition of propane (6% m/m) 2 h were needed. However, using material ground to 0.2 cm particle size, 1 h was needed with CO_2 alone and only 0.6 h with addition of propane.

Compounds may be added to the supercritical phase as a reactant rather than as a simple modifier. Roston et al.[62] used formic acid to hydrolyse the bond between the polymer and a drug. Using methanol as a modifier there was almost no extraction. Cedergren et al.[73] extracted nicotine from PE patches using modified CO_2. They found that 1 M triethylamine in methanol was the best modifier. The tertiary amine was added to prevent reaction with the CO_2, which could lead to insoluble carbamates. Pre-treatment of the PE with concentrated triethylamine together with a static extraction stage gave the best recoveries.

Modifiers generally accelerate extraction when the modifier interacts with the polymer more than CO_2. The modifier can then cause greater swelling than with CO_2 alone. Therefore, methanol is useful when extracting from polar nylons, and aromatic modifiers from non-polar poly(olefins). The greater solubility in modified CO_2 is most effective when extracting large or polar molecules.

Nature of the Extractant

The nature of the extractant affects extraction in both solubility and diffusion limiting cases. The larger the molecule the slower the diffusion in the polymer, and hence the slower the extraction. High molecular weight compounds tend to be less soluble in supercritical CO_2 and hence solubility will also limit the extraction more for larger molecules. The extraction of DIOP from PVC at 45 MPa and 90 °C was almost complete after 20 min, whereas the polar Topanol CA was only 50% extracted.[53] Irganox 1010 has proved difficult to extract in a number of cases when smaller compounds were extracted.[56,63] Higher nylon oligomers also proved difficult to extract.[70] Extraction of flame retardants at 30.4 MPa for 10 min at 60 °C was complete for molecules of molecular weights 286, 388 and 472 Da, but the largest molecule with a molecular weight of 571 Da was only 77% extracted.[57]

There are some reports of smaller molecules extracting slower than larger molecules. The plasticiser DOP extracted faster from a 100 + 50 PVC–plasticiser blend than the smaller DBP.[54] This was attributed to DBP being more strongly bonded to matrix sorption sites than DOP. However, it should be noted that DOP may be a more effective plasticiser than DBP, hence leading to faster extraction rates.

Effect of Particle Size

As one of the limiting steps in extraction is diffusion to the surface of the polymer, the particle size or film thickness is extremely important.[52,53,59,60,70,74] The diffusion coefficient of additives in polymers at 40 °C is typically about 10^{-10} cm^2 s^{-1}. The rate of diffusion (s^{-1}) is proportional to D/L^2, where L is the length of the shortest dimension. As a first approximation, therefore, for an extraction time of 1000 s (17 min) a particle diameter of 0.3 mm is required. Therefore, grinding of the polymer is often an essential step in the analysis. An exception to this is the extraction of thin films and foams, for which the shortest dimension is small. Garde et al.[71] could extract no more than 50% of antioxidants from PP pellets, but could achieve 90% recoveries from the same polymer extruded into film. Loss of volatile additives is possible owing to the heat generated by grinding polymers. Therefore, the polymer must be frozen, usually with liquid nitrogen, before grinding.

Hexabromocyclododecane was extracted from PS styrofoam and Irganox 1010 from PE ethafoam within 30 min at 150 °C at 45.6 MPa.[55] Flame retardants were extracted from PU foam within 5 min at 30.4 MPa, 60 °C.[57] A different approach to avoiding the need to grind the sample was taken by Mackay and Smith.[75] Examination of polymer samples (unplasticised PVC) after SFE revealed that the CO_2 had not penetrated into the core of the sample, and recoveries were low. The polymer was dissolved in THF and an internal standard added. The solvent was evaporated and the resulting polymer samples were extracted with CO_2 at 50 °C, 35.5 MPa for 10 min. Extraction was far from complete, but the internal standard extracted to the same extent as the analyte and the correct analysis result was obtained.

Extraction of additives from liquid polymers has been achieved by bonding them onto silica.[76] Additives from poly(alkylene glycol) and sorbitan ester were extracted by SFE with CO_2 at 45 °C. Oligomers were co-extracted, but most of these could be removed by a silica guard column.

Non-quantitative extraction of additives from a range of polymers was demonstrated by Braybrook and Mackay[77] for biocompatability testing. Solvent extraction is problematical for this purpose because solvent residues interfere with the biocompatability test. Mackay and Smith[78] showed the value of on-line SFE–SFC–MS by identifying a range of additives from PU. Some of these additives could not be analysed by GC–MS.

Summary of SFE

SFE can provide a method for extracting additives from polymers. It is much faster than Soxhlet extraction. Grinding of the sample is usually necessary except for thin films and foams. Extractions are likely to be fastest from amorphous polymers, but the temperature must be carefully chosen to be lower than the softening point under experimental conditions. This softening point is likely to be lower than that of the polymer at atmospheric pressure, and the conditions of temperature and pressure must be carefully selected. For crystalline polymers, the temperature should be as high as possible without onset of melting, and the pressure also should be as high as possible to ensure no solubility limitations and maximum plasticisation of the polymer. Most difficulty is likely to be experienced with extraction of high molecular weight and/or polar compounds. The use of a modifier is likely to enhance the extraction in these cases. The modifier should be one that is known to swell the polymer. For extractions that still take a long time, an extrapolation procedure can be used to determine concentration in the plastic without complete extraction.

Microwave Heating

Microwave-assisted sample preparation techniques are widely used in analytical laboratories, largely in the field of digestion of samples. Zlotorzynski[79] reviewed the use of microwave radiation in analysis and suggested that microwave extraction is in its infancy. Reviews on the applications of microwave-assisted sample preparation have recently been published.[80,81] There are several publications on MAE in environmental analysis, but few on extraction from polymers. The advantages of MAE are that samples can be rapidly heated and several samples can be extracted simultaneously. The sample can be contained in a pressure-resistant vessel with safety valves. The solvent can therefore be heated above its normal boiling-point. At 1.2 MPa, the temperature reached in a pressure vessel with acetone is 164 °C, with dichloromethane 140 °C, and with acetonitrile 194 °C.[81] The high temperatures will accelerate diffusion through the polymer and hence improve extraction rates. The high temperature may increase the swelling of the polymer owing to greater solvent–polymer interaction at higher temperatures. Another advantage compared with Soxhlet extraction is that any composition of solvent mixtures can be used. During Soxhlet extraction the solvent is the vapour condensate, which will only have the same composition as a mixture of solvents if an azeotropic mixture is used.

The solvent selected must have a high relative permittivity to be heated by microwaves; therefore, pure hydrocarbons cannot be used. Freitag and John[82] used acetone–heptane (1 + 1) to extract additives from LDPE, HDPE and PP. After grinding to 20 mesh, 91–97% of Irgafos 168, Chimassorb 81 and Irganox 1010 were extracted within 6 min from HDPE and within 3 min from PP and LDPE. Molecular weight had a significant effect, with Irganox 1010 being the slowest to extract. 1,1,1-Trichloroethane gave slightly faster extractions, but is environmentally less desirable. The order of extraction of Irganox 1010 from the polymers was PP > LDPE > HDPE, although the scatter of the LDPE results was fairly high. Dissolution of larger particles in toluene–1,2-dichlorobenzene was effected in 5 min. However,

the dissolution method gave only 85% recovery of the additives from the PE samples, although 95% recovery was achieved from the PP. Extractions from larger pellets were less efficient. The vessels were pressurised, but the temperatures and pressures reached were not reported.

Nielson[83] compared microwave extraction with sonication for HDPE, PP and LDPE. BHT, Irganox 1010 and Irganox 1076 could be extracted at >90% recoveries from ground HDPE in 20 min at 50% power. Two solvent systems were used: propan-2-ol–cyclohexane (1 + 1) and DCM–propan-2-ol (98 + 2). In each case the propan-2-ol was present to absorb the microwave energy and the other solvent to swell the polymer. The sample was stirred at 5 min intervals. The polymer was ground to 20 mesh, and 5 g of plastic were used to 50 ml of solvent. This is a much larger sample than the 50–100 mg typically used in SFE. Butylated hydroxy ethylbenzene (BHEB), Isonox 129 and erucamide slip agent were extracted from LDPE using the same conditions. From PP, Irganox 3114, Irganox 1010, Irganox 1076, Irgafos 168, Tinuvin 328, Ultranox 626, Cyasorb UV 531, BHT and AM 340 could be extracted from the ground polymer (20 mesh) [5 g of plastic to 50 ml of solvent, DCM–propan-2-ol (98 + 2)] in 20 min at 20% power, with stirring required every 5 min. Only the Irganox 3114 had a low recovery of 79%.

When larger pellets were used the recoveries were also high, except for Irganox 1010, for which only 50% recovery was possible without grinding. The vessels were not pressurised and the temperature using the DCM–propan-2-ol mixture did not exceed 50 °C.

Costley *et al.*[84] report on extraction of cyclic trimer from PET using a variety of solvents heated to 120 °C in pressure vessels. The polymer fused at temperatures above 120 °C with DCM; therefore, higher temperatures were not investigated. Extraction for 2 h with DCM at 120 °C gave the same extraction as 24 h Soxhlet extraction with xylene as solvent. MAE using hexane–acetone (1 + 1), water, acetone and acetone–DCM (1 + 1) all gave much lower recoveries than DCM at 120 °C.

From these examples, MAE appears to be a rapid and effective technique for polymer extractions. The solvent can be selected to swell the polymer, provided that some microwave absorbing solvent is also present. The polymer needs to be ground for efficient extraction. However, there are too few reports for firm conclusions to be drawn.

Ultrasonic Extraction

Ultrasonic extraction works principally by agitating the solution and producing cavitation in the liquid. This would be expected to enhance the rate of transfer across the polymer/liquid boundary layer, but not to increase the diffusion of compounds within the polymer. There are several reports of ultrasonic extraction from polymers. Brandt[85] extracted tri(nonylphenyl) phosphite (TNPP) from a styrene–butadiene polymer using 2 × 20 min extractions with isooctane as solvent. This compares with 2 × 1 h extractions for boiling under reflux. Nielson[83] compared ultrasonic extraction with MAE for extraction of a variety of analytes from PP, LDPE and HDPE (see under Microwave Heating). For all samples, the ultrasonic extraction could be achieved within 1 h, provided that the samples were stirred every 10 min. For LDPE and PP most compounds were extracted within 10 min. The exception was Irganox 1010, which required 1 h for >90% extraction. Further experiments by Nielson[86] on extraction from HDPE using the same regime confirmed these results. However, where phosphite antioxidants are present the use of DCM–cyclohexane was preferred as it prevented hydrolysis of the phosphite by the alcohol.

Caceres *et al.*[87] used the same solvent mixtures as Nielson[83] to extract Tinuvin 770 and Chimassorb 944 from HDPE. The additives could only be extracted at less than 20% recoveries from pellets using ultrasonic extractions of up to 5 h. The size

of the pellets is not given, but the fact that the sample was not ground may be the reason for the difference in results. Extraction of Chimassorb 81 from LDPE and ethylene-vinyl acetate polymer (EVA) was achieved with 6 h standing of the sample under DCM (maceration) followed by 3 × 20 min sonication.[88] The initial maceration time allowed swelling of the polymer. The extraction time using maceration alone was 48 h. In this case it was important to avoid high temperatures as these could degrade the analyte.

Ultrasonic extraction from polymers has given some reasonably fast extractions, but the advantages over shaking the sample have not been widely demonstrated.

ASE

Lou *et al.*[89] extracted monomers and oligomers from nylon and PBT using hexane as extraction solvent in a home-made ASE. They investigated the effect of temperature, pressure and flow rate with 20 min static followed by 30 min dynamic extractions. Pressure was found to have no effect other than to keep the solvents liquid at high temperature and flow rate had little effect between 0.4 and 2 ml min^{-1}. Extraction efficiencies increased in all cases as the temperature was raised from 50 to 170 °C, which was attributed to faster diffusion rates. These workers observed that solvents which are good swelling agents, and hence give fastest extractions during Soxhlet extraction, tend to dissolve the polymer at the high temperatures used during ASE. Dissolved polymer re-precipitates on cooling and can block transfer lines in the instrument. Solvents therefore cannot be selected on the basis of those used for atmospheric pressure extractions. Hexane was used in the extractions even though it gives poor recoveries during Soxhlet extraction. Lou *et al.* point out that selection of a suitable extraction solvent is probably the most difficult step in optimising ASE, as there are few data on the solubility of polymers in solvents at high temperatures. These workers had previously analysed the same polymers using SFE with pure and modified CO_2[64] and compared the result with that obtained using pure CO_2 at 170 °C and 30.7 MPa. The recoveries for ASE for caprolactam from nylon and the dimer and trimer from PBT are 1.1, 6.5 and 37.6 times higher, respectively, than those obtained with SFE. However, at these conditions the SFE was not optimum, particularly for the dimer and trimer, where the peak extraction after 30 min occurred at 110 and 90 °C, respectively. This extraction peak at low temperatures clearly indicates solubility-limited extractions. Addition of modifier (methanol for nylon and chloroform for PBT) during the static extraction stage further increased recoveries from SFE, particularly for the dimer and trimer, but recoveries were still higher with ASE by approximately 1.5 times for the dimer and trimer. No experiments were performed with modified CO_2 during the dynamic extraction. From these results, it appears that ASE offers significant advantages over SFE with CO_2 alone for extraction of compounds with a low solubility in CO_2.

Other Extraction Methods

Some new variations on the dissolution theme have recently been published. Staal *et al.*[90] dissolved polycarbonate and polysulfone in THF and precipitated them onto a C_{18} guard column. A gradient elution from 50 + 50 water–THF as non-solvent to 100% THF successively eluted the additives, then the oligomers and finally the polymer itself. No quantitative work was reported The method could be adapted by altering the solvent programme to separate the compounds of interest.

Another way to separate the additives from the polymer after dissolution was explored by Nerin *et al.*[91] They linked a high-performance size-exclusion chromatography (SEC) column with a normal-phase HPLC column, *via* a three-way switching

valve. The polymer elutes from the SEC column first and is drained through the valve. The valve is then switched to allow the additives onto the analytical HPLC column.

One problem with the dissolution method is that high boiling solvents are usually required to dissolve the polymer. The solvent is therefore difficult to remove after precipitation of the polymer. This was addressed by Macko and co-workers[92,93] who used an autoclave to dissolve HDPE in heptane at 160–170 °C, well above the normal boiling-point. The polymer was precipitated by cooling, and after filtration the additives could be determined by direct analysis of the resulting solution by normal-phase HPLC. Alternatively, the solvents were relatively easy to remove by evaporation. The dissolution took 1 h, and the complete analysis time was 3 h.

Caceres *et al.*[87] compared several methods for extraction of Tinuvin 770 and Chimassorb 944 from HDPE pellets. Room temperature diffusion into chloroform and ultrasonication gave less than 20% extraction. Soxtec extraction with DCM for 4 h resulted in only 50% extraction. Dissolution of the polymer in

dichlorobenzene at 160 °C for 1 h followed by re-precipitation of the polymer with propan-2-ol gave 65–70% recovery. The most successful method was boiling under reflux with toluene at 160 °C for 2–4 h, which extracted 95% of both additives. The relatively poor performance of the Soxtec extraction compared with the reflux extraction is probably due to the large difference in temperature between the boiling solvents. The pellets were not ground and the size was not specified.

Conclusions

There are several methods that can be used for the extraction of low molecular weight material from polymers. The principal points of each are given in Table 2. Table 3 shows a summary of the extraction papers discussed here.

There is a choice to be made between inexpensive, simple equipment giving long extraction times and more expensive but rapid techniques. Soxhlet extraction will generally extract all additives, but extraction times can be as long as 48 h. During

Table 2 Summary of extraction techniques

	Soxhlet	SFE	Microwave	Sonication	ASE
Solvent	Any	CO_2 (possibly modified)	Must contain a microwave absorbing component	Any	Any
Typical sample size	1–5 g	10–100 mg	1–5 g	1–5 g	1–10 g
Analysis time	6–24 h	20 min–2 h	30–60 min	40–60 min	15 min
Solvent usage	50–100 ml	10 ml	30 ml	30–50 ml	30–50 ml
Advantages	Inexpensive, widely accepted	Low solvent use, fast, can be automated	Fast, low solvent use, can extract multiple solvents simultaneously	Economical	Low solvent use automated, any solvent possible
Disadvantages	Slow, large solvent use	Expense, may take time to optimise method	Expense, not sufficient body of evidence for extraction from plastics	Not always effective	Expense, not sufficient body of evidence for extraction from plastics

Table 3 Polymer extraction summary

Polymer	Additive	Extraction technique	Comments	Ref.
Solid–liquid extraction—				
Poly (ethylene terephthalate)	Cyclic trimer and other oligomers up to the heptamer	Dissolution followed by precipitation	0.1 g of polymer was dissolved in dichloromethane and hexafluoropropan-2-ol (7 + 3 v/v 10 ml) and then acetone was added to precipitate the high molecular mass polymer. The sample was filtered, concentrated to dryness and the residue dissolved in dimethylacetamide. Positive ion atmospheric-pressure chemical ionisation (APCI) was used to analyse the extracts	15
Poly (ethylene terephthalate)	Butyric acid (1), Malathion (2), Diazinon (3). All are recycling by-products	Dissolution/ precipitation	(1) PET was dissolved in a large volume of hexafluoropropanol and dichloromethane. Large oligomers were then removed from the solution by polymer precipitation using acetone. Additives (2) and (3) as before but precipitated using methanol. Average recoveries from spiked samples were 80–98%	16
Poly (vinyl chloride)	Dioctyl phthalate	Dissolution/ precipitation	Sample dissolved in THF and centrifuged at 20 000 rev min^{-1}. Polymer is then precipitated using ethanol and isolated by filtration. The filtrate is evaporated to dryness and analysed	94
Poly(vinyl chloride) and poly(vinyl chloride)–vinyl acetate copolymer	Tinuvin 320; Cyasorb UV 9; Uvinul N-539	Soxhlet extraction	PVC film or finely ground PVC particles (1 g). Soxhlet extraction with diethyl ether for 16 h; evaporation to dryness; precipitate dissolved in THF (10 ml); filtration through Millipore Teflon filter of 0.5 µm pore size. Recoveries ranged from 65% (unground PVC, diameter 2–10 mm) to 94% (ground, *i.e.*, <0.5 mm) for Tinuvin 320; 59% (unground PVC, diameter 2–10 mm) to 97% (ground, *i.e.*, <0.5 mm) for Cyasorb UV-9; and 89% (film, thickness 150 µm) to 95% (ground, *i.e.*, <0.5 mm) for Uvinul N-539	95

Table 3 *continued*

Polymer	Additive	Extraction technique	Comments	Ref.
Poly(propylene)	Chimassorb 944	Dissolution/precipitation	Polymer was dissolved in decalin at 150 °C and re-precipitated by cooling	13
Polyamides	Lubricants, *e.g.*, stearic acid and ethylene bis-stearamide	Dissolution followed by liquid–liquid extraction	Dissolve 5 g of polymer in 30 ml of formic acid and extract with 150 ml of toluene for 18 h	14
Polycarbonate, polysulfone	Additives, monomers and oligomers	Dissolution	THF dissolution of polymer samples. Preliminary note on the on-line extraction of polymers by multiple solvents on packed HPLC columns.	90
Poly(ethylene)	Cyasorb 531	Soxhlet extraction	Powdered sample (100 g) Soxhlet-extracted with 500 ml hexane or chloroform for 12 h. This was repeated three times. Then the extract was filtered and filtrate evaporated to dryness. Soluble fractions of low molecular weight polymers were removed from the individual extracts using methanol followed by evaporation to dryness and dissolution in chloroform. Chromatographic identification only	96
Poly(ethylene)	Irganox 1010, Irgafos 168, α-tocopherol	Disolution with hot heptane under pressure	Polymer (1 g, cut into slices) was dissolved in heptane at 160–170 °C under elevated pressure in an autoclave. Polymer precipitated by cooling and supernatant analysed by HPLC. 2 h per sample needed for complete analysis.	92, 93
Poly(ethylene) (high-density)	BHT, Irganox anti-oxidants, Isonox, Cyasorb, Am 340, MD 1024, Irgafos 168	Ultrasonic extraction	Use of cyclohexane–dichloromethane as extraction solvent reduces risk of hydrolysis of Irgafos 168. 30–40 min of ultrasonic extraction needed for complete extraction.	86
Poly(ethylene) (high-density)	Tinuvin 770, Chimassorb 944	Soxtec, ultrasonic extraction, room temperature diffusion, dissolution, reflux	Boiling HDPE pellets under reflux with toluene was the most successful method	87
Poly(ethylene) (low-density)	Ionol, Santanox, oleamide	Flask-shaker	Pelletised (7-mesh) LDPE (5 g) was shaken with solvents (10 ml). Carbon disulfide extracted Ionol and Santanox in about 2 h, much faster than isooctane. Extraction with powdered (50-mesh) LDPE was much faster	17
Poly(ethylene) (low-density)	Chimassorb 81	Ultrasonic extraction and maceration	Ground polymer (0.25 g) was placed in dichloromethane (3 ml), shaken and kept in the dark for 6 h, followed by 3 × 15 min ultrasonic extractions. This gave same extraction as 48 h of standing in the dark	88
Poly(ethylene) (low-density)	DSTDP; Irganox 1035; Santonox R; peroxide initiator Vulcup	Soxhlet extraction	Poly(ethylene) film (5 g) Soxhlet-extracted with 100 ml THF, extract concentration to 5 ml. Chromatographic identification only	97
Polymer	DLTDP; DSTDP; TNPP; Goodrite 3114; Weston 618; Topanol CA, Irganox 1076; Cyasorb UV 531	Solid–liquid extraction from polymers by soaking in boiling solvents	Reflux pressed foil samples with boiling CH_2Cl_2 for 2 h; evaporate to dryness; solution in 5 ml THF; filtration through 0.5 µm Millipore Teflon filter	20
Poly(propylene)	Irganox 1010, Irganox 1330, Irgafos 168, Irganox 3114, Atmer 163 and Tinuvin 326	Soxhlet extraction	Soxhlet extraction using chloroform (50 ml). Optimum extraction obtained in 1 h using sieved (< 1.18 mm) freeze-ground samples (3 g). For film and granular samples, 3 h extraction necessary	14
Poly(propylene)	Tinuvin 770; Hostavin TMN 20; Tinuvin 144	Soxhlet extraction	Sample (10 g) in powder or pellet form was extracted. Kumagawa extraction with $CHCl_3$ for 16 h, extract concentration to 20 ml under a flow of nitrogen; then 80 ml of acetone added to precipitate oligomers. Sample filtered and washed with hot acetone; filtrate concentrated under a flow of nitrogen and finally made up to volume (10 ml) with $CHCl_3$. Results for poly(propylene) pellets were 96.2% for Tinuvin 770 and 95.6% for Hostavin TMN 20	95
Poly(propylene)	DLTDP; DSTDP; TNPP; BHT; Goodrite 3114; Weston 618; Topanol CA; Irganox 1076; Cyasorb UV 531; oleamide; erucamide; Ethyl 330; stearamide; Irganox 1010	Soxhlet extraction	Sample (50 g) in pellet form. Soxhlet extraction with 250 ml CH_2Cl_2 for 48 h; evaporate to dryness; re-dissolving in 5 ml THF; filtration through Millipore Teflon filter of 0.5 µm pore size. Good results (88–120% recovery) reported for two out of three samples	20
Poly(propylene)	Irganox 1010; Irgafos 168; Tinuvin 770; erucamide; Irganox 3114; Tinuvin 440; Tinuvin P	Soxhlet extraction	Sample (10 g) in pellet form. Soxhlet extraction with diethyl ether for 15 h; evaporation to dryness; wax precipitation by refluxing with 5 ml ethanol; cooling; filtration. Qualitative data only	98

Table 3 *continued*

Polymer	Additive	Extraction technique	Comments	Ref.
Poly(propylene)	BHT, Topanol CA, Irganox 1076	Cold liquid solvent extraction	Sample of beads or shavings (1 g). Overnight extraction with 5 ml of acetonitrile at ambient temperature in a sealed amber-coloured vial with constant stirring. Qualitative only	99
Poly(propylene)	DSTDP, BHT, Topanol CA, Santowhite powder	Cold liquid solvent extraction	Sample (4 g of 8-mesh pellets) shaken in a 50 ml screw-capped, darkened glass vial with (a) 20 ml THF or (b) CH_2Cl_2 for 24 h at room temperature	22
Poly(propylene) co-polymer	Irganox 1330	Solid–liquid extraction from polymers by soaking in boiling solvents	Sample frozen and pulverised (0.5–5.0 g). Refluxing for 40 min under nitrogen purging using 25–100 ml of decalin, hexane, $CHCl_3$ and THF. After cooling, samples filtered through Whatman GF/A microfibre filter. For quantitative work a 100-fold molar excess of BHT (0.5–1.5 mg l^{-1}) was added to the extraction solvent to protect Irganox 1330 from oxidation during extraction. Results indicate that all solvents gave good recoveries provided that the sample was milled to a particle size of < 1.0 mm	100
Poly(styrene) (styrenic polymer)	External lubricants	Dissolution followed by evaporation	Wash 20 g of poly(styrene) resin with ethanol. Collect washings and evaporate to dryness with nitrogen. Dissolve residue in chloroform. Analyse using FTIR	101
Poly(styrene) (styrenic polymer)	Internal lubricants	Dissolution followed by evaporation	Dissolve 20 g of resin in 150 ml of dichloromethane. Add 100 ml of ethanol dropwise to precipitate polymer. Analyse using FTIR	101
PVC, PE	BHT, tinuvin 326, Tinuvin 327, Irganox 1076, Cyasorb UV 9, Cyasorb UV 1084	Dissolution, separation of polymer by size-exclusion chromatography	Polymer dissolved and separated by SEC. Polymeric fraction diverted to waste and fraction containing analytes directed to silica HPLC column. Qualitative data only	88
Styrene–butadiene rubber	Tris(nonylated phenyl) phosphite	Ultrasonic extraction	Ultrasonic extraction with isooctane for 2 × 20 min gave same extraction as 2 × 1 h for boiling under reflux	85

Supercritical fluid extraction—

Polymer	Additive	Extraction technique	Comments	Ref.
Biodegradable lactide-*co*-glycoside	Oligomers, stearic acid, anthraquinone-based dye	SFE	Screening method for *in vitro* cytotoxicity testing. SFE extracts not contaminated with solvent residues	77
Biopol	Triacetin, total extractables	SFE	40 °C, 35 MPa, 10 min; CO_2 only. Pieces were cut from a bottle. Faster flow rates gave faster extraction with almost complete recovery after 8 min at a flow rate of 8.5 ml min^{-1}	69
Nylon	Caprolactam	SFE	SFE–SFC with CO_2 only on milled polymer at 35 MPa and 75 °C showed extractable caprolactam. Addition of methanol modifier to the extraction cell significantly increased the amount of extracted caprolactam. The methanol was thought to act by swelling the polymer rather than through enhanced solubility.	65
Nylon 6	Caprolactam and oligomers	SFE	SFE conditions: temperature, 60–80 °C; CO_2 density, 0.85 g ml^{-1}. Extraction effeciencies higher than methanol Soxhlet extractions. Use of 7.5% methanol modifier and additional modifier in extraction cell necessary for high extraction efficiencies	70
Nylon 6	Caprolactam	SFE and Soxhlet extraction	Study of modifier addition and temperature variation. Conditions for SFE: modified supercritical CO_2; temperature, 50–170 °C; pressure, 30 MPa; extraction time, 20 min static and 30 min dynamic. Comparable results obtained by both techniques. Chloroform, benzene and methanol as modifiers had a large effect at low temperatures, the effect decreased at higher temperatures	64
Nylon pellets	Cyclic trimer and ethyl bis-stearamide	SFE	On-line SFE–SFC. Conditions for SFE: CO_2 only; temperature, 70 °C; pressure, 5–40 MPa sample size: 5–10 mg. Qualitative only	32
Poly(butylene terephthalate)	Dimer/trimer	SFE and Soxhlet extraction	Study of modifier addition and temperature variation. Conditions for SFE: chloroform-modified supercritical CO_2; temperature, 50 °C; pressure, 30 MPa; extraction time, 20 min static and 30 min dynamic. Comparable results obtained for the dimer extraction; lower recovery by SFE for the trimer (73%). Chloroform was the most effective modifier, followed by benzene and methanol	64
Poly(butylene terephthalate) polymers	Volatiles	SFE	On-line–GC. Conditions for SFE: CO_2 only; temperature, 55 °C; pressure, 20 MPa; extraction time, 10 min. Average recovery from a 25 µm sample thickness is 98%	52
Poly(ethylene terephthalate)	Cyclic trimer	SFE and Soxhlet extraction	On- and off-line SFE–SFC. SFE conditions: CO_2 only; temperature, 70 °C; pressure, 40 MPa; extraction time, 13 consecutive 30 min extractions, *i.e.*, over a period of 6.5 h. Poor recovery obtained, as compared with Soxhlet, by SFE	35
Poly(ethylene terephthalate)	Cyclic trimer	SFE and liquid solvent extraction	CO_2 only; temperature, 90–215 °C; pressure, 40 MPa; extraction time, 30 min. Sample size: 0.02–3 g of film. Soxhlet conditions: Sample size, 12–13 g of film; solvent, xylene; extraction time, 24 h. Good results obtained by SFE at elevated temperature	51
Poly(ethylene terephthalate)	Cyclic trimer	SFE	On-line SFE–SFC: conditions for SFE: CO_2 only; temperature, 70 °C; pressure, 5–40 MPa. Sample size: 5–10 mg. Qualitative only	

Table 3 *continued*

Polymer	Additive	Extraction technique	Comments	Ref.
Poly(ethylene terephthalate)	Cyclic trimer and other oligomers	SFE	Conditions: supercritical CO_2 with and without modifiers used (methanol, isopropyl alcohol, dichloromethane and acetone); temperature, 40–150 °C; density, 0.5–0.9 g ml^{-1}. Sample size: 0.75 g of ground PET chips or 1 g of PET fibres. The use of isopropyl alcohol and methanol as modifiers prevented extraction; a 7% dichloromethane modified supercritical CO_2 was beneficial. A three-stage SFE procedure was recommended using supercritical CO_2 only	50
Poly(vinyl chloride)	Diisooctyl phthalate (DIOP) as plasticizer, chlorinated polyethylene wax, Topanol	SFE and liquid solvent extraction	Conditions for SFE: CO_2 only; temperature, 45–115 °C; pressure, 7–45 MPa; extraction time, 0.5–435 min. Sample size: 0.2–0.4 g. Analysis using off-line packed SFC. Results for SFE compare favourably with those obtained using liquid extraction and the actual formulation value	53
Poly(vinyl chloride)	Stabilizers	SFE and dissolution/precipitation	Screening method for food contact plastics, non-quantitative. SFE extracted same stabilizers as precipitation method	5
Poly(vinyl chloride)	Tinuvin P	SFE	Polymer was dissolved in THF and internal standard added. The polymer was re-cast and extracted with CO_2 at 50 °C and a pressure of 30 MPa for 10 min. Extraction was far from complete, but the internal standard compensated and good analyses were obtained	75
Poly(vinyl chloride)	Dibutyl phthalate, dioctyl phthalate	SFE and Soxhlet extraction	Best SFE conditions: temperature,95 °C; pressure, 48 MPa; extraction time, 25 min; unmodified CO_2. Extraction efficiency was 98% compared with 5 h Soxhlet extraction with cyclohexane	54
Poly(vinyl chloride)	Organotin stabiliser	SFE	SFE conditions: pressure, 18 MPa; formic acid modifier; temperature optimum at 90 °C. Extraction complete within 60 min	60
Poly(vinyl chloride)	Diisooctyl phthalate, diethylhexyl phthalate,BHT, Tinuvin P, tributyltin chloride, vinyl chloride monomer	SFE	Screening method for *in vitro* cytotoxicity testing; therefore, not quantitative. SFE conditions: pressure, 42 MPa; temperature, 50–150 °C. Main advantage over solvent extraction is that the extracts are not contaminated with toxic solvent residues	77
Poly(alkylene glycol (PAG)	Additives	SFE	SFE conditions: temperature, 45 °C; pressure, 30 MPa; CO_2 only. PAG was adsorbed into silica and extracted with CO_2. An in-line silica column was used to remove co-extracted oligomers	76
Poly(isoprene)	Carbon tetrachloride	SFE	Optimum extraction conditions 60 °C at 21 MPa, CO_2 only. Increasing the temperature caused softening and agglomeration of rubber particles. Increasing the pressure lowered the softening temperature of the rubber and therefore also caused the particles to agglomerate	66
Poly(styrene)	Ethylbenzene	SFE	CO_2 only, temperature from 50 to 100 °C, pressure: 7–12 MPa. Supercritical CO_2 swelled the polymer, lowered T_g and resulted in a 10^6-fold increase in diffusivity of ethylbenzene in PS. A model used to estimate diffusivity in the swelled polymer is presented	61
Poly(styrene)	Alkylbenzenes	SFE	CO_2 only. SFE was limited by diffusion within the polymer rather than solubility in the CO_2. Fastest extractions therefore employ small particle size and either static or dynamic extraction	68
Poly(styrene)	Styrene dimers and trimers	SFE	CO_2 only. 9–11 MPa, 80–120 °C. On-line SFE–SFC was effective at identifying additives and oligomers. The rate of extraction increased with temperature	65
Poly(urethane) foams	CFCs	SFE	SFE conditions: 50 °C at 11 MPa. Supercritical CO_2 extracted much more than liquid CO_2 and nitrogen. Addition of propane modifier seems to increase extraction rate slightly. Ground foam extracted much faster than un-ground foam	72
Poly(ethylene)	Erucamide acid amide	SFE	On-line SFE-capillary SFC. CO_2 only; temperature, 45 °C; pressure, 15 MPa; extraction time, 15 min. Sample size: 2.7 mg. Example chromatogram presented	58
Poly(ethylene)	Irganox	SFE	On-line SFE–capillary SFC. CO_2 only; temperature, 45 °C; pressure, 20 MPa; extraction time, 30 min. Sample size: 9 mg. Example chromatogram presented	58
Poly(ethylene)	Chimassorb, Tinuvin 144, Irganox 1098, oxidised Nauguard 524, Irganox 1010, DSTDP, Irganox 1076 and Ionox 330	SFE and Soxhlet extraction	SFE conditions: CO_2 only; temperature, 40 °C; pressure, 60 MPa; extraction time, 30 min and 5 h for low- and high-density poly-(ethylene) samples, respectively. Sample size: 0.2 g. Soxhlet: 1 g sample extracted with 100 ml of toluene for 3 h. After cooling, 20 ml of ethanol added to precipitate low molecular weight polymer. Extract solutions filtered, dried and reconstituted in CH_2Cl_2 prior to analysis. Similar mass spectra obtained by both extraction techniques	67
Poly(ethylene)	Additives	SFE	Conditions for SFE: CO_2 only; temperature, 65 °C; pressure, 15 MPa; extraction time, 10 min. Sample size: 3 mg of film	102
Poly(ethylene)	Irganox 1010, Irganox 1076, Irgafos 168	SFE and Soxhlet extraction	Conditions for SFE: temperature, 50–80 °C; pressure, 15–30 MPa, CO_2 and benzene-modified CO_2. Results at 80 °C and 30 MPa generally fastest, with amount extracted sometimes exceeding that from Soxhlet extraction. Benzene modifier increased extraction rates, particularly at lower temperatures	63
Poly(ethylene)	Nicotine	SFE	SFE conditions: pressure, 21 MPa; temperature, 60 °C; CO_2 modified with triethylamine; extraction time, 20 min	73

Table continued on next page

Table 3 *continued*

Polymer	Additive	Extraction technique	Comments	Ref.
Poly(ethylene) (low-density)		SFE	On-line SFE–SFC analysis. SFE conditions: temperature, 100 °C; pressure, 45 MPa. Typical extraction time 20 min for ground polymer samples (30–50 mesh)	74
Poly(ethylene) (low-density)	Paraffins and olefins	SFE	Screening method for *in vitro* cytotoxicity testing	77
Poly(ethylene) and poly(propylene)	Irganox 1010, BHT, erucamide, Tinuvin 770, Irgafos 168, Isonox 129 and DLTDP	SFE	On-line SFE–SFC. SFE conditions: CO_2 only; temperature, 50 °C; pressure, 14 and 43 MPa; extraction time, 15 and 30 min. Accurate quantification and high extraction efficiency reported.	33
Poly(ethylene), poly(styrene)	BHT, BHEB, Isonox 129, Irganox 1076, Irganox 1010, Irgafos 168, Cyasorb 3346, Cyanox 1790, stearyl stearamide, HBCD and erucamide	SFE	On-line SFE–SFE. CO_2 only; temperature, 150 °C; pressure, 46 MPa; extraction time, 30 min. Typical recoveries ranged from 86 to 108%	55
Polymer	Misoprostol	SFE	Formic acid modified CO_2 used to extract misoprostol steroid drug from polymer to which it is covalently bonded. Formic acid hydrolyses covalent bond	62
Poly(propylene)	BHT, Tinuvin 326, Seenox DM and Irganox 1010	SFE and liquid solvent extraction	On-line SFE–capillary SFC. CO_2 only; temperature, 30–90 °C; pressure, 30 MPa; extraction time, 30 min. Qualitative results only. Selectivity of extraction investigated	56
Poly(propylene)	Apple aroma compounds	SFE and liquid solvent extraction	Conditions for SFE: CO_2 only; temperature, 10–70 °C; pressure, 6–12 MPa; extraction time, 5–20 min. Sample size: 10 mg of film. Analysis using on-line GC. Results for SFE compare favourably (96–105% recovery) with those obtained using liquid solvent (dichloromethane) extraction	94
Poly(propylene)	Irganox 1010, Irganox 1076, total extractables	SFE	40 °C, 35 MPa, 10 min, CO_2 only, 30 μm film. SFE extracted more material than 4 h Soxhlet extraction with dichloromethane	69
Poly(propylene)	Irganox 1076, Irgafos 168, Hostanox SE-02	SFE	SFE conditions: temperature, 60 °C; CO_2 density, 0.85 g ml^{-1}. Optimum extraction used two static extractions with hexane and methanol modifiers	71
Poly(propylene), poly(ethylene)	Cyasorb UV 531, Topanol OC, Irganox 1330, Irganox 1010, Irganox 1076	SFE	SFE conditions: 25.6 MPa, 35 °C, CO_2 only. 2 h extraction was required for complete extraction	31
Poly(urethane) foams	Amgard TCEP, Amgard TMCP, Amgard V6 and Thermolin 101	SFE	On-line SFE–SFC. SFE conditions: CO_2 only; temperature, 60 °C; pressure, 30 MPa; extraction time, 5 min. Good recoveries obtained compared with solvent extraction	75
Poly(urethane)	Oligomers, TPP, BHT, Irganox 1010, Irganox 1076	SFE	Screening method for *in vitro* cytotoxicity testing	77
Poly(urethanes) [Pellethane, estane, and 90-N poly(urethane) Ellastolan]	BHT, residual ethers, plasticisers (either an adipate acid or a phthalate ester)	SFE	On-line SFE–SFC–MS. Conditions for SFE: CO_2 only; temperature, 60 °C; pressure, 30 MPa; extraction time, 10 min. Feasibility study	78

Microwave-assisted extraction (MAE) and ASE—

Polymer	Additive	Extraction technique	Comments	Ref.
Poly(propylene) and poly(ethylene) (powdered)	Irganox 1010, Irgafos 168, Chimassorb 81	MAE	Hexane–acetone (1 + 1)—max. 6 min. 1,1,1-Trichloroethane—max. 3 min. Microwave power, 70%; solvent volume, 30 ml for both	82
HDPE, LDPE, PP	Irganox 1010, Irgafox 168, Cyasorb UV 531, BHT	Microwave heating, atmospheric pressure	Cyclohexane–propan-2-ol (1 + 1) found to be the best solvent for extraction from poly(olefins). 20 min extraction time typical	83
Poly(ethylene terephthalate)	Cyclic trimer	MAE and Soxhlet extraction	MAE conditions: sample size, 8 g of film; solvent, xylene + water or dichloromethane (40 ml); extraction time, 30–120 min; temperature, 70–120 °C. Soxhlet conditions: sample size, 15–20 g of film; solvent, xylene (190 ml); extraction time, 24 h. Good agreement between both extraction methods	84
PBT	Dimers and trimers	ASE	Freeze-ground samples extracted with hexane at temperature from 50 to 70 °C. Extraction rate increased with temperature. Pressure had no effect other than to keep solvent liquid. Extraction faster than SFE with CO_2 alone	89
Nylon-6	Caprolactam	ASE	Freeze-ground samples extracted with hexane at temperatures from 50 to 170 °C. Extraction rate increased with temperature. Pressure had no effect other than to keep solvent liquid. Extraction faster than with SFE with CO_2 alone, but very similar to CO_2 with methanol modifier	89

such long extractions and subsequent concentration steps there is a possibility of losses of volatile or thermally labile components. The selection of extraction solvent can make a large difference to the extraction time. However, the equipment is inexpensive, and once set up requires little 'hands-on' attention. SFE has been shown to provide a much faster extraction method than Soxhlet extraction. In most cases rapid and quantitative extraction has been achieved using ground samples or thin films. The method needs to be optimised for pressure, temperature and modifier. Equipment exists which can extract several samples simultaneously and which can be programmed to extract up to 28 samples consecutively. Microwave-assisted extraction offers a rapid method for the extraction of up to 12 samples simultaneously. The equipment is also much more expensive than that for Soxhlet extraction, and there are relatively few publications concerning this method. ASE has been found to be effective in extraction from environmental samples and has great potential for extraction from polymers. The main problem is likely to be selection of extraction solvent which does not dissolve the polymer at high temperature. Although ASE uses liquid solvents, the total solvent usage may not be higher than through the use of modifiers with SFE.

In conclusion, Soxhlet extraction is inexpensive and well established, but time consuming. Of the newer methods, only SFE has been available long enough for large amounts of published evidence to become available. Amongst the applications of analytical SFE, extractions of polymers have been the most successful, although a few cases are problematical. Other newer methods show promise, but cannot yet be assessed from a wide range of published data.

References

1   EEC 89/109, *Off. J. Eur. Comm.*, 1989, **L40**, 38.
2   EEC 90/128, *Off. J. Eur. Comm.*, 1990, **L349**, 26.
3   EEC 92/39, *Off. J. Eur. Comm.*, 1992 , **L168**, 21.
4   Schilling, F. C., and Kuck, V. J., *Polym. Degradation Stab.*, 1991, **31**, 141.
5   Brauer, B., Funke, T., and Schulenbergschell, H., *Dtsch. Lebensm. Rundsch.*, 1995, **91**, 381.
6   Wright, S. J., Dale, M. J., Langridge-Smith, P. R. R., Zhan, Q., and Zenobi, R., *Anal. Chem.*, 1966, **68**, 3585.
7   Crompton, T. R., *The Analysis of Plastics*, Pergamon Press, Oxford, 1984.
8   Haslam, J., Willis, H. A., and Squirrel, D. C. M., *Identification and Analysis of Plastics*, Iliffe Books, London, 2nd edn., 1977.
9   Wheeler, D. A., *Talanta*, 1968, **15**, 1315.
10 Cotton, N. J., PhD Thesis, University of Leeds, 1992
11 British Standard 2782, Part 4, Method 405D, 1965.
12 Schabron, J. F., and Fenska, L. E., *Anal. Chem.*, 1980, **52**, 1411.
13 Freitag, W., *Fresenius' Z. Anal. Chem.*, 1983, **316**, 495.
14 Newton, I. D., in *Polymer Characterisation*, ed. Hunt, B. J., and James, M. I., Blackie, Glasgow, 1993, pp. 8–36.
15 Barns, K. A., Damant, A. P., Startin, J. R., and Castle, L., *J. Chromatogr. A*, 1995, **712**, 191.
16 Komolprasert, V., Lawson, A. R., and Hargraves, W. A., *J. Agric. Food Chem.*, 1995, **43**, 1963.
17 Spell, H. L., and Eddy, R. D., *Anal. Chem.*, 1960, **32**, 1811.
18 Crompton, T. R., *Eur. Polym. J.*, 1968, **4**, 473.
19 Majors, R. E., *J. Chromatog. Sci.*, 1970, **8**, 339.
20 Haney, M. A., and Dark, W. A., *J. Chromatogr. Sci.*, 1980, **18**, 655.
21 Perlstein, P., *Anal. Chim. Acta*, 1983, **149**, 21
22 Wims, A. M., and Swarin, S. J., *J. Appl. Polym. Sci.*, 1975, **19**, 1243.
23 Majors, R. E., *LC–GC*, 1995, **13**, 82.
24 Majors, R. E., *LC–GC*, 1996, **14**, 88.
25 Chester, T. L., Pinkston, J. D., and Raynie, D. E., *Anal. Chem.*, 1992, **64**, 153R.
26 Chester, T. L., Pinkston, J. D., and Raynie, D. E., *Anal. Chem.*, 1994, **66**, 106R.
27 Levy, J. M., *HRC–J. High Resolut. Chromatogr.*, 1994, **17**, 212.

28 Camel, V., Tambute, A., and Caude, M., *Analusis*, 1992, **20**, 503.
29 Smith, C. G., Smith, P. B., Pasztor, A. J., Mckelvy, M. L., Meunier, D. M., Froelicher, S. W., and Ellaboudy, A. S., *Anal. Chem.*, 1993, **65**, R 217.
30 Anton, K., Menes, R., and Widmer, H. M., *Chromatographia*, 1988, **26**, 221.
31 Hirata, Y., and Okamoto, Y., *J. Microcol. Sep.*, 1989, **1**, 46.
32 Cotton, N. J., Bartle, K. D., Clifford, A. A., Ashraf, S., Moulder, R., and Dowle, C. J., *HRC–J. High Resolut. Chromatogr.*, 1991, **14**, 165.
33 Ryan, T. W., Yocklovich, S. G., Watkins, J. C., and Levy, E. J., *J. Chromatogr.*, 1990, **505**, 273.
34 Bartle, K. D., Clifford, A. A., Hawthorne, S. B., Lagenfield, J. J., Miller, D. J., and Robinson, R., *J. Supercrit. Fluids*, 1990, **3**, 143.
35 Bartle, K. D., Boddington, T., Clifford, A. A., Cotton, N. J., and Dowle, C. J., *Anal. Chem.*, 1991, **63**, 2371.
36 Ashby, R., *Food Addit. Contam.*, 1988, **5**, 485.
37 Bartle, K. D., Boddington, T., Clifford, A. A., and Hawthorne, S. B., *J. Supercrit. Fluids*, 1992, **5**, 207.
38 Clifford, A. A., Bartle, K. D., and Zhu, S. A., *Anal. Proc.*, 1995, **32**, 227.
39 Howdle, S. M., Ramsay, J. M., and Cooper, A. I., *J. Polym. Sci. B: Polym. Phys.*, 1994, **32**, 541.
40 Fahmy, T. M., Paulitis, M. E., Johnson, D. M., and McNally, M. E. P., *Anal. Chem.*, 1993, **65**, 1462.
41 Shieh, Y. T., Su, J. H., Manivannan, G., Lee, P. H. C., Sawan, S. P., and Spall, W. D., *J. Appl. Polym. Sci.*, 1996, **59**, 695.
42 Shieh, Y. T., Su, J. H., Manivannan, G., Lee, P. H. C., Sawan, S. P., and Spall, W. D., *J. Appl. Polym. Sci.*, 1996, **59**, 707.
43 Chiou, J. S., Barlow, J. W., and Paul, D. R., *J. Appl. Polym. Sci.*, 1985, **30**, 3911.
44 Michaels, A. S., and Bixler, H. J., *J. Polym. Sci.*, 1961, **L**, 393.
45 Kazarian, S. G., Vincent, M. F., Bright, F. V., Liotta, C. L., and Eckert, C. A., *J. Am. Chem. Soc.*, 1996, **118**, 1729.
46 Kalospiros, N. S., and Paulaitis, M. E., *Chem. Eng. Sci.*, 1994, **49**, 659.
47 Handa, Y. P., Roovers, J., and Wang, F., *Macromolecules*, 1994, **27**, 5511.
48 Condo, P. D., and Johnston, K. P., *J. Polym. Sci. B: Polym. Phys.*, 1994, **32**, 523.
49 Condo, P. D., Paul, D. R., and Johnston, K. P., *Macromolecules*, 1994, **27**, 365.
50 Kuppers, S., *Chromatographia*, 1992, **33**, 434.
51 Cotton, N. J., Bartle, K. D., Clifford, A. A., and Dowle, C. J., *J. Chromatogr. Sci.*, 1993, **31**, 157.
52 Schmidt, S., Blomberg, L., and Wannnman, T., *Chromatographia*, 1989, **28**, 400.
53 Hunt, T. P., and Dowle, C. J., *Analyst*, 1991, **116**, 1299.
54 Marin, M. L., Jiminez, A., Lopez, J., and Vilaplana, J., *J. Chromatogr. A*, 1996, **750**, 183.
55 Ashraf-Khorassani, M., Boyer, D. S., and Levy, J. M., *J. Chromatogr. Sci.*, 1991, **29**, 517.
56 Daimon, H., and Hirata, Y., *Chromatographia*, 1991, **32**, 549.
57 Mackay, G. A., and Smith, R. M., *Analyst*, 1993, **118**, 741.
58 Engelhardt, H., Zapp, J., and Kolla, P., *Chromatographia*, 1991, **32**, 527.
59 Cotton, N. J., Bartle, K. D., Clifford, A. A., and Dowle, C. J., *J. Appl. Polym. Sci.*, 1993, **48**, 1607.
60 Oudsema, J. W., and Poole, C. F., *HRC–J. High Resolut. Chromatogr.*, 1993, **16**, 198.
61 Dooley, K. M., Launey, D., Becnel, J. M., and Caines, T., *ACS Symp. Ser.*, 1995, **608**, 269.
62 Roston, D. A., Sun, J. J., Collins, P. W., Perkins, W. E., and Tremont, S. J., *J. Pharm. Biomed. Anal.*, 1995, **13**, 1513.
63 Lou, X. W., Janssen, H. G., and Cramers, C. A., *J. Microcol. Sep.*, 1995, **7**, 303.
64 Lou, X. W., Janssen, H. G., and Cramers, C. A., *J. Chromatogr. Sci.*, 1996, **34**, 282.
65 Jordan, S. L., Taylor, L. T., Seemuth, P. D., and Miller, R. J., *Text. Chem. Color.*, 1997, **29**, 25.
66 Burgess, A. N., and Jackson, K., *J. Appl. Polym. Sci.*, 1992, **46**, 1395.
67 Juo, C. G., Chen, S. W., and Her, G. R., *Anal. Chim. Acta*, 1995, **311**, 153.
68 Hawthorne, S. B., Galy, A. B., Schmitt, V. O., and Miller, D. J., *Anal. Chem.*, 1995, **67**, 2723.

69 Baner, L., Bucherl, T., Ewender, J., and Franz, R., *J. Supercrit. Fluids*, 1992, **5**, 213.

70 Venema, A., Vandeven, H. J. F. M., David, F., and Sandra, P., *HRC–J. High Resolut. Chromatogr.*, 1993, **16**, 522.

71 Garde, J. A., Galotto, J., Catala, R., and Gavara, R., presented at the ILSI Symposium on Food Packaging: Ensuring the Quality and Safety of Foods, September 11–13, 1996, Budapest, Hungary.

72 Filardo, G., Galia, A., Gambino, S., Silvestri, G., and Poidomani, M., *J. Supercrit. Fluids*, 1996, **9**, 234.

73 Cedergren, L., Fors, S., and Jonn, S., presented at the 3rd European Symposium on Analytical SFC and SFE organized in conjunction with the 6th International Symposium on SFC and SFE, September 6–8, 1995, Uppsala, Sweden.

74 Ashraf-Khorassani, M., and Levy, J. M., *HRC–J. High Resolut. Chromatogr.*, 1990, **13**, 742.

75 Mackay, G. A., and Smith, R. M., *HRC–J. High Resolut. Chromatogr.*, 1995, **18**, 607.

76 Hunt, T. P., Dowle, C. J., and Greenway, G., *Analyst*, 1993, **118**, 17.

77 Braybrook, J. H., and Mackay, G. A., *Polym. Int.*, 1992, **27**, 157.

78 Mackay, G. A., and Smith, R. M., *J. Chromatogr. Sci.*, 1994, **32**, 455.

79 Zlotorzynski, A., *Crit. Rev. Anal. Chem.*, 1995, **25**, 43.

80 Smith, F. E., and Arsenault, E. A., *Talanta*, 1996, **43**, 1207.

81 Renoe, B. W., *Am. Lab.*, 1994, August, 34.

82 Freitag, W., and John, O., *Angew. Makromol. Chem.*, 1990, **175**, 181.

83 Nielson, R. C., *J. Liq. Chromatogr.*, 1991, **14**, 503.

84 Costley, C. T., Dean, J. R., Newton, I., and Carroll, J., *Anal. Commun.*, 1997, **34**, 89.

85 Brandt, H. J., *Anal. Chem.*, 1961, **33**, 1390.

86 Nielson, R. C., *J. Liq. Chromatogr.*, 1993, **16**, 1625.

87 Caceres, A., Ysambert, F., Lopez, J., and Marquez, N., *Sep. Sci. Technol.*, 1996, **31**, 2287.

88 Nerin, C., Salafranca, J., and Cacho, J., *Food Addit. Contam.*, 1996, **13**, 243.

89 Lou, X., Janssen, H., and Cramers, C. A., *Anal. Chem.*, 1997, **69**, 1598.

90 Staal, W. J., Cools, P., Vanherk, A. M., and German, A. L., *Chromatographia*, 1993, **37**, 218.

91 Nerin, C., Salafranca, J., Cacho, J., and Rubio, C., *J. Chromatogr. A*, 1995, **690**, 230.

92 Macko, T., Siegl, R., and Lederer, K., *Angew. Makromol. Chem.*, 1995, **227**, 179.

93 Macko, T., Furtner, B., and Lederer, K., *J. Appl. Polym. Sci.*, 1996, **62**, 2201.

94 Nielson, T. J., Jagerstad, I. M., Oste, R. E., and Sivik, B. T. G., *J. Agric. Food Chem.*, 1991, **39**, 1234.

95 Sevini, F., and Marcato, B., *J. Chromatogr. A*, 1983, **260**, 507.

96 Lehotay, J., Danecek, J., Liska, O., Lesko, O. J., and Brandsteterova, E., *J. Appl. Polym. Sci.*, 1980, **25**, 1943.

97 Majors, R. E., and Johnson, E. L., *J. Chromatogr. Sci.*, 1978, **167**, 17.

98 Raynor, M. W., Bartle, K. D., Davies, I. L., Williams, A., Clifford, A. A., Chalmers, J. M., and Cook, B. W., *Anal. Chem.*, 1988, **60**, 427.

99 Vargo, J. D., and Olson, K. L., *Anal. Chem.*, 1985, **57**, 672.

100 Gasslander, U., and Jaegfeldt, H., *Anal. Chim. Acta*, 1984, **166**, 243.

101 Kumur, T., *Analyst*, 1990, **115**, 1319.

102 Hirata, Y., Nakata, F., and Horihata, M., *J. High Resolut. Chromatogr.*, 1988, **11**, 81.

Evaluation of Parallel Factor Analysis for the Resolution of Kinetic Data by Diode-array High-performance Liquid Chromatography

Peter Hindmarch, Keyhandokht Kavianpour and Richard G. Brereton*

School of Chemistry, University of Bristol, Cantock's Close, Bristol, BS8 1TS, UK

The PARAFAC algorithm for factor analysis of three or higher way datasets is summarised. A series of simulations of kinetic profiles of two-way diode-array HPLC data is described. A three-phase reaction system of reactant, intermediate and product is used to illustrate the method, each closely eluting and with similar spectra based on experimental HPLC with diode-array detection of chlorophyll degradation products. A kinetic parameter is varied to change the relative concentration of the intermediate in each series of simulations. Several indices of quality of reconstruction are introduced. It is concluded that the number of factors used to model the data is crucial to the quality of reconstruction. A good approach is first to use fewer factors than are expected, then increasing the number until each elution profile shows a single maximum.

Keywords: Deconvolution; PARAFAC; high-performance liquid chromatography; kinetics; chlorophyll

Three-way data are common in analytical chemistry.[1,2] An example is a series of chromatograms recorded in time. If these chromatograms consist, in turn, of two-way data such as in HPLC with diode-array detection (DAD) or GC–MS, the full series of chromatograms may be regarded as a three-way dataset. One mode is time or sample number, whereas the other modes are elution time and a spectroscopic parameter, such as wavelength or mass number. Conventionally, each chromatogram is analysed independently by factor analysis or multivariate calibration, but this ignores the fact that there are components common to the entire series of chromatograms with similar spectra and elution profiles. Treating the entire dataset as one three-dimensional block provides more information than treating each chromatogram separately.

There are several methods for three-dimensional factor analysis,[3–7] and it is the purpose of this paper to evaluate one of the most common, called PARAFAC. In this approach, the three-dimensional data are decomposed into a series of factors, each relating to one of the three physical variables.

Theory

PARAFAC (parallel factor analysis) is a method of decomposing a three-way data array, or tensor, into a series of two-way arrays. The original algorithms were developed by psychometricians for the decomposition of multiblock data.[8–11] Mathematically, PARAFAC can be seen as a simplification of the Tucker3 Model proposed by Tucker,[12] in which a three-way $I \times J \times K$ array is decomposed into three loadings matrices $A(I \times L)$, $B(J \times M)$ and $C(K \times N)$, where L, M and N are the number of factors in the first, second and third modes, respectively. I, J, and K may be regarded as the number of samples, elution times and wavelengths, respectively. In most areas of chemistry, L, M and N will be equal and are the number of detectable components in a mixture, making the chemometric problem simpler than the psychometric problem.

In this case, a three-way array (or tensor) X, whose dimensions are sample number, elution time and spectral wavelength in the case of HPLC–DAD, is decomposed into three matrices A, B and C such that,

$$x_{i,j,k} = \sum_{1}^{F} a_{i,f} b_{j,f} c_{k,f} + e_{i,j,k} \tag{1}$$

where F is the number of factors used in the model and e is the error term. A is a matrix of I rows consisting of sample numbers and L columns consisting of the number of detectable components in the mixture; B and C correspond to the elution profiles and spectra of these L components. This model can also be written as

$$\underline{X} = \sum_{1}^{F} a_f \otimes b_f \otimes c_f + \underline{E} \tag{2}$$

where $\otimes$ represents the ternary tensor product of the three vectors. The field of tensor algebra as applied to chemical data is discussed extensively elsewhere.[13] The definition and representation of tensor products varies depending on the context, but it is sufficient here to state that the tensor product of vectors $_{I,1}a$, $_{J,1}b$ and $_{K,1}c$ is a vector with co-ordinates $x_i y_j z_k$. Combining all of these vectors over all factors gives the three-way data matrix. Graphically, the PARAFAC model for a three-way, two-component system is shown in Fig. 1.

The simplest way of implementing a PARAFAC model is by alternating least squares. Starting with a known three-way matrix, $\underline{X}$, and two randomly initiated loadings matrices, A and B, the third loadings matrix, C, can be estimated. Then, from this new estimate of C, A and B then C can be successively estimated and so on until there is convergence in the model.

The advantage of this approach is that, apart from the number of factors, F, no prior knowledge of the system is required. Furthermore, apart from scaling considerations, PARAFAC produces a unique solution. However, as it is a numeric rather than an analytical method, care must be taken to ensure that the algorithm converges properly and operates at an acceptable speed. The theory of the PARAFAC algorithm is discussed further elsewhere,[14–16] as also are further applications to calibration.[17–20] Practical applications, however, have been limited.[21–23]

Method

Experimental

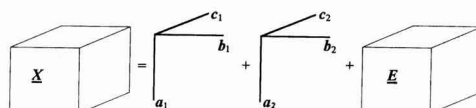Spectra of three chlorophyll degradation products were obtained experimentally from a Waters (Milford, MA, USA)

Fig. 1 Graphical representation of the PARAFAC method.

Model 990 HPLC–DAD system. For chlorophyll degradation mixtures, closely eluting compounds often possess very similar spectral characteristics, posing real problems in resolution by chemometric means. Spectra were recorded between 350 and 800 nm at 2 nm intervals.

A common problem involves detecting crucial intermediates that are present in low concentrations, *e.g.*, in the reaction A → B → C, where the first reaction is slow and the second is fast. A full kinetic model for the pathway requires the detection of B, which may be present in small amounts, dependent on the relative rates of the two reactions. If HPLC is employed to study such reactions, the intermediate, which may be a stereoisomer of the parent compound, could have very similar elution profiles and spectra to one of the other components. This situation is well established in the study of the degradation of chlorophyll by HPLC .

Simulation Design

The data were designed to simulate the degradation of chlorophyll-*a* products investigated elsewhere.[24] Each three-way dataset is constructed from modes representing elution profiles, spectra and degradation profiles of each component.

Three spectra obtained experimentally were used to represent three compounds with very similar spectral characteristics. The elution profiles were simulated and the degradation profiles represent a series of HPLC–DAD traces used to monitor a three-reactant system.

The three species formed are assumed to form part of a reaction series, where the reactant (R) is converted into an intermediate (I), which is then converted into a product (P).

Elution Profiles

The elution data matrix is represented by $_{20,3}A$, representing 20 chromatographic points in time. The chromatographic profile of compound l (where $l = 1, 2$ and 3 for the reactant, intermediate and product, respectively) at time I is given by $a_{l,i}$. Each column of A is an individual elution profile represented in this simulation by Gaussians centred at points 10, 14 and 6 in time and given by

$$a_{i,1} = e^{-\frac{(i-10)^2}{6}} \tag{5}$$

$$a_{i,2} = e^{-\frac{(i-14)^2}{6}} \tag{6}$$

$$a_{i,3} = e^{-\frac{(i-6)^2}{6}} \tag{7}$$

The data are designed so that the product elutes first, followed by the reactant and then the intermediate. The elution profiles are shown graphically in Fig. 2.
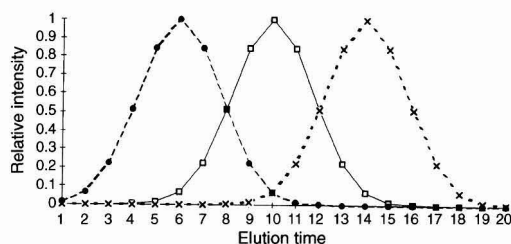

Fig. 2 Simulated elution profiles. □, Reactant; ×, intermediate; and ●, product.

Spectra

Spectra were chosen from previous work to represent each component. Brereton and co-workers[24,25] have shown that in chlorophyll degradation studies the ratio of absorbances between the two absorbance maxima, at approximately 430 and 665 nm, respectively, is very diagnostic. These spectra were chosen so that the reactant and the intermediate had spectra with similar features. Table 1 gives the spectral characteristics of each component. The spectra, shown in Fig. 3, were scaled to constant maximum absorbance and stored as $_{226,3}B$, where each column represents a spectrum taken between 350 and 800 nm, digitised at a resolution of 2 nm, *i.e.*, 226 readings per spectrum.

Degradation profiles

The degradation profiles were designed to represent a reactant decreasing in concentration as the experiment proceeds, a minor intermediate increasing to a maximum, then decreasing and a product increasing in concentration. Concentrations are such that at any time the total concentration of all species is constant. The degradation data matrix $_{20,3}C$ represents the concentration of the three components at 20 sampling points throughout the experiment where the three columns represent the reactant, intermediate and product respectively. The profiles for each component are given by

$$c_{k,1} = 5e^{-k/8} \tag{8}$$

$$c_{k,2} = (5 - 5e^{-k/8})e^{-k/d} \tag{9}$$

$$c_{k,3} = 5 - 5e^{-k/8} + e^{-k/d} - 5e^{-(k/8 + k/d)} \tag{10}$$

where k is the sample number arranged sequentially in time and d is a parameter varying according to the relative significance and kinetic stability of the intermediate. The greater the value of d the slower is the decomposition of the intermediate, and so the easier it is to detect. Different simulations were performed at different values of d and simulated degradation profiles are shown in Fig. 4.

Table 1 Position of maxima of designed and predicted elution profiles.

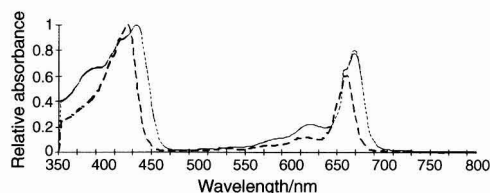|	Elution maximum		
	Reactant	Intermediate	Product
	10	14	6
Rate parameter, d	Factor 1	Factor 2	Factor 3
1	10	10	6
3	10	10	6
5	10	6	14
10	6	10	14
20	14	6	10

Fig. 3 Experimentally obtained spectra used in the simulations. Solid line, reactant; dotted line, intermediate; and dashed line, product.

Formation of three-way data set

The three-way, three-component model $_{20,226,20}$ X is formed by

$$x_{i,j,k} = \sum_{f=1}^{F} a_{i,f} b_{j,f} c_{k,f} \qquad (11)$$

where f is the component number and F is the number of components, which in this study is three. Five datasets were created in which the rate constant, d, was 1, 3, 5, 10 and 20.

Application of PARAFAC Algorithm

No pre-processing is performed on the data in this paper. The issue of pre-processing of three-way arrays is more complex than for the two-way case. Centring can be performed across either one, two or three of the modes and can distort the trilinear model. The order of any pre-processing is also critical. These issues have been discussed elsewhere.[9,15,26,27]

The datasets were decomposed by the PARAFAC written in Matlab 4.2 (Mathworks, Natick, MA, USA).

The algorithm was used to extract three factor matrices from each simulated dataset initialised using random vectors and a convergence limit of 1×10^{-6} between successive estimates of the sum of squares of the misfit.

Indicators of Quality of Reconstruction

Various functions can be used to compare the results from the simulations with the design data.

Component sum of squares

This gives a measure of the size of each component and factor, which aids in the identification of factors and gives an indication of their purity. The size of each predicted component, $\hat{S}_f$, is given by

$$\hat{S}_f = \sum_{i=1}^{I} \sum_{j=1}^{J} \sum_{k=1}^{K} (\hat{a}_{i,f} \hat{b}_{j,f} \hat{c}_{k,f})^2 \qquad (12)$$

The values obtained for the predicted model using eqn. (12) can be compared to the size of the true components, S_f, calculated in the same manner as above, but with the estimated vectors replaced by their true equivalents.

The square root of the ratio of the estimated to the true sum of squares, Q_f, is given by

$$Q_f = \sqrt{\hat{S}_f / S_f} \qquad (13)$$

The closer this value is to unity, the better is the modelling of the factor f. The concentration of the reactant will decrease
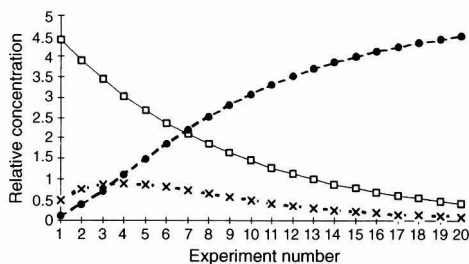

Fig. 4 Simulated degradation profiles. $\square$, Reactant; $\times$, intermediate; and $\bullet$, product.

identically from sample to sample in each simulation. The relative concentration of the intermediate will increase with increasing d and the product will decrease. The total concentration of the reactant, intermediate and product at any one point will always be constant, but the sum of squares will not.

Regression

For each of the elution, spectral and degradation modes, the predicted data are regressed on to the real data. In each case a matrix R can be obtained, often called a rotation or transformation matrix. For example, for the elution data, if A is the true elution datum, $\hat{A}$ is the predicted data and R_A is the rotation matrix, then

$$\hat{A} = AR_A \qquad (14)$$

R_A is found by the pseudo-inverse:

$$R_A = (A'A)^{-1} A'\hat{A} \qquad (15)$$

For a good model, each column and row of the rotation matrix contains only one value significantly greater than zero.

Using the rotation matrices obtained above and the rotation matrix, a 'predicted true' dataset can be obtained, denoted by a circle overscript, *e.g.* for the elution data

$$\mathring{A} = \hat{A}R_A^{-1} \qquad (16)$$

Calculating a residual root mean sum of squares $RMSEP(A)$ between the actual true and predicted true data, across each matrix, gives a further indication of the quality of regression:

$$RMSEP(A) = \sqrt{\frac{\sum_{i=1}^{I} \sum_{f=1}^{F} (\mathring{a}_{i,f} - \hat{a}_{i,f})^2}{I \times F}} \qquad (17)$$

Spectral characteristics and elution maxima

A simple measure of the success of the decomposition can obtained by comparing the predicted design parameters with those listed in Table 1. From the predicted elution data the position of the maximum of each component can be obtained as the maximum of each column of $\hat{A}$. Similarly, the positions of the two absorbance maxima and their ratio can be computed from the estimated spectral data.

Results

Most methods for factor analysis depend first on determining the number of significant factors. This is particularly true when the aim is to model the entire dataset. The importance of detecting and modelling all significant components in two-way factor analysis has been discussed in the context of mid-infrared (MIR) spectrometry.[28,29] If a third significant factor is ignored, then the information from this compound is mixed with the other two compounds. In contrast, if a third factor is small it may become confused with the other two factors if a three-factor model is employed. PARAFAC depends crucially on a prior estimate of the number of significant factors as shown below. The following section reports the results assuming a three component mixture and the subsequent section a two component mixture.

Another important aspect is that the order in which the factors are extracted may differ according to how the algorithm is implemented, *e.g.*, the starting point of the iterations. This

means that, over a series of datasets, the first factor may correspond to physically different compounds in each run, so it is first necessary to reorder the factors according to presumed physical significance. In some cases, where the interpretation of each factor is in doubt, this can be difficult. In the tables, the factors are ordered according to the order in which they were extracted.

Three-factor Systems

The predicted maxima positions of the elution profiles, in terms of elution index for the three component, three-factor system, are given in Table 2. At the levels where d, the kinetic rate parameter, is low, *i.e.*, 1 and 3, the PARAFAC algorithm fails to position the three components correctly, whereas at higher levels of d all three components are correctly determined.

Table 2 lists the spectral parameters determined from the predicted data. In all cases the product (factor 3 at $d = 1$ and 3, factor 2 at $d = 5$ and 20 and factor 1 at $d = 10$) is predicted well, with a peak ratio of 1.65, and a low-wavelength absorbance maximum at 424 or 426 nm. There is a slight problem with predicting the high-wavelength absorbance maximum at higher values of d, presumably because the prediction ability decreases

as the amount of intermediate increases. However, the high-wavelength absorption maximum is always $\leqslant 660$ nm. A 4 nm shift in position represents only two sampling points in the wavelength direction.

In this study, the data were designed with very similar spectral parameters and the PARAFAC algorithm has successively determined these, so it is trivial to establish the correspondence between components and factors. However, this will not always be true and in cases where there are several very similar components, a confident identification of the factors based on spectral parameters may not be possible.

The component sum of squares for the true and predicted data are given in Table 3. At all levels the size of the product is predicted remarkably well. The reactant and intermediate, however, are only closely estimated at the two higher levels of d. This can be understood by considering that the reactant and product had similar spectral characteristics. At the lower levels of d, the intermediate is relatively minor compared with the reactant, but as the intermediate increases in significance at higher levels of d, it is easier for the algorithm to distinguish between them.

The elution profiles for $d = 1$ and 20 are presented graphically in Fig. 5. It is obvious that the product and intermediate are not distinguished when d is low; these two

Table 2 Design and predicted spectral parameters for the three factor model.

Design	Reactant	Intermediate	Product
Spectral ratio	1.28	1.24	1.65
Absorbance max. 1/nm	434	434	424
Absorbance max. 2/nm	670	670	660
$d = 1$—	Factor 1	Factor 2	Factor 3
Spectrum ratio	1.29	1.28	1.65
Absorbance max. 1/nm	436	436	426
Absorbance max. 2/nm	670	670	660
$d = 3$—			
Spectrum ratio	1.30	1.27	1.65
Absorbance max. 1/nm	434	434	424
Absorbance max. 2/nm	670	670	660
$d = 5$—			
Spectrum ratio	1.28	1.65	1.24
Absorbance max. 1/nm	434	426	436
Absorbance max. 2/nm	670	660	670
$d = 10$—			
Spectrum ratio	1.65	1.28	1.24
Absorbance max. 1/nm	424	424	434
Absorbance max. 2/nm	658	668	668
$d = 20$—			
Spectrum ratio	1.24	1.65	1.28
Absorbance max. 1/nm	434	424	434
Absorbance max. 2/nm	668	656	668

Table 4 Prediction ratios, Q_f, for the two- and three-component models

		Ratio Q_f			
	Three-component model			Two-component model	
d	Reactant	Intermediate	Product	Reactant	Product
1	0.9999	10.2884	0.7218	1.0060	1.0009
3	0.9999	3.3054	0.6465	1.0416	1.0021
5	1.0000	0.9836	0.9493	0.9972	1.0892
10	1.0002	0.9829	0.9646	1.2003	0.9942
20	1.0197	0.9402	1.0001	n/a	n/a

Table 5 Root mean square error of prediction (RMSEP) for the three-factor models

	Data mode		
d	A	B	C
1	1.1×10^{-7}	4.19×10^{-7}	3.5×10^{-8}
3	4.2×10^{-8}	2.89×10^{-8}	2.3×10^{-8}
5	1.4×10^{-8}	2.89×10^{-8}	3.5×10^{-8}
10	3.7×10^{-8}	2.3×10^{-8}	3.6×10^{-8}
20	3.37×10^{-8}	3.55×10^{-7}	2.63×10^{-8}

Table 3 Size of each design component and factors for the two- and three-component systems

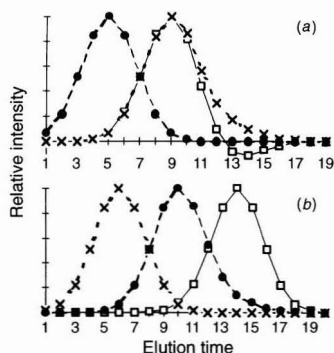|	Rate parameter, d				
	1	3	5	10	20
Reactant	9100	9100	9100	9100	9100
Intermediate	8	167	591	2570	7165
Product	14827	13416	11750	7637	3547
Three-component system—					
Factor 1	842	1825	8201	7640	6334
Factor 2	4741	3803	11751	8463	3547
Factor 3	14285	13412	572	2483	9461
Two-component system—					
Factor 1	9209	9872	11684	13111	5317
Factor 2	14312	13473	10795	7549	15294

Fig. 5 Elution profiles obtained for the three factor models at (*a*) $d = 1$ and (*b*) $d = 20$.

species have similar spectral characteristics. Figs. 6(a) and (b) are representations of the corresponding spectra and it can be seen that they are recovered well.

It can be concluded that when the number of components is correctly known, the PARAFAC algorithm produces excellent decomposition results. These results are the best when all of the components are relatively significant, as shown by the square root of the ratios of predicted to true sum of squares, Q_f, given in Table 4, and the $RMSEP$ in Table 5. For the elution data, A,

Table 6 Position of maxima of predicted elution profiles for the two factor model

	Elution maximum	
d	Factor 1	Factor 2
1	10	6
3	10	6
5	6	10
10	10	6
20	6	10

improves considerably from the $d = 1$ to the $d = 20$ level. There is also an improvement, but to a lesser extent, for the spectral data. The error in the kinetic profiles is reasonably constant at each level.

Two factor Systems

The PARAFAC algorithm was repeated on the datasets but with two rather than three factors used to model the data. The elution and spectral parameters found are given in Tables 6 and 7, respectively. As can be seen from Table 6, at each level of d the algorithm appears to detect successfully the reactant and product without any interference from the intermediate. Note that the product should elute at datapoint 6 and the reactant at datapoint 10.

Again, in Table 7, it appears that the two-component model produces good predictions of the spectrum ratios and absorbance maxima at each level of d, although the peak ratio for the product (1.56) is lower at $d = 20$.

However, when the sum of squares of the factors and components are computed (Table 3), the situation is not so straightforward. At the lower two levels of the intermediate the
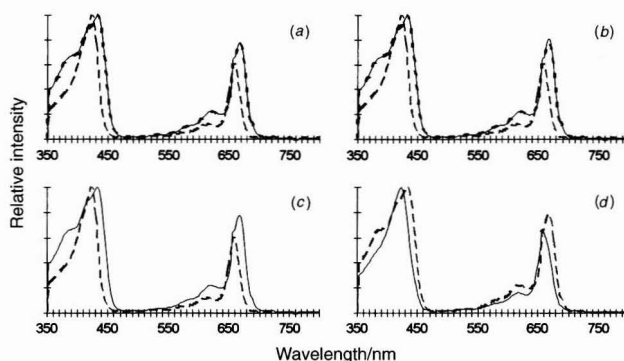
Fig. 6 Predicted spectra for (a) three factors at $d = 1$, (b) three factors at $d = 2$, (c) two factors at $d = 1$ and (d) two factors at $d = 20$.
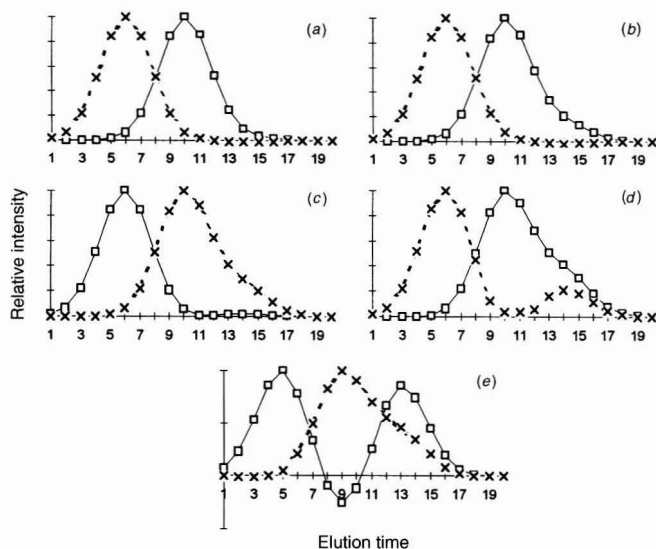
Fig. 7 Elution profiles obtained for the two factor models at (a) $d = 1$, (b) $d = 3$, (c) $d = 5$, (d) $d = 10$ and (e) $d = 20$.

factors predict the size of the component reasonably well, but at the higher levels it becomes more difficult to distinguish the factors. This result reinforces the observation from above that a univariate measure such as elution maximum is not a sophisticated measure of data quality and a multivariate method, utilising the data from all available modes, should always be used in preference. This is important as the PARAFAC algorithm distributes all of the observed systematic variance between the factors in the model, so that these are not necessarily pure factors.

Unlike the three-factor model above, predictions for the two factor model are better when the unmodelled component is relatively insignificant. As can be seen in Table 4, as the level of the intermediate increases the quality of reconstruction of the spectrally similar reactant decreases, but this is only observed when a multivariate measure such as the sum of squares or the rotation matrices is used. The quality of the product also falls but less significantly. Because at the $d = 20$ level a confident determination of the identification of the reactant and product cannot be made, the prediction ratio therefore cannot be calculated.

The five recovered elution profiles are shown in Fig. 7. These supplement the data in Table 6; it is obvious that for $d = 20$ the first factor has, in fact, two clear maxima. Interestingly, the intermediate is confused with the product and predicted as one factor, despite the difference in both spectral characteristics and elution profiles. This unexpected result can be explained in terms of kinetic profiles; the level of intermediate builds up rapidly and then decreases with time, and so the kinetics of the two compounds are fairly similar. Two components with identical kinetics but different spectra and elution profiles could be modelled as a single factor. Visual inspection of the predicted chromatograms in Fig. 7(*c*)–(*e*) should provide clues that the number of predicted components is too few, and so lead to rerunning the model including further components. The spectra, Fig. 6(*c*) and (*d*), are recovered well again.

Conclusions

PARAFAC is a powerful approach for resolving out series for two-way chromatograms recorded over a number of samples. The methods can be extended to three-way or higher data, *e.g.*, chromatograms could be recorded at different pH values and times; the change in chromatography with pH complements the change in intensity with time.

Table 7 Predicted spectral parameters for the two factor model. The design parameters are given in Table 1

	Factor 1	Factor2
$d = 1$—		
Spectrum ratio	1.28	1.65
Absorbance max. 1/nm	436	426
Absorbance max. 2/nm	670	660
$d = 3$—		
Spectrum ratio	1.28	1.65
Absorbance max. 1/nm	436	426
Absorbance max. 2/nm	670	660
$d = 5$—		
Spectrum ratio	1.65	1.28
Absorbance max. 1/nm	426	436
Absorbance max. 2/nm	660	670
$d = 10$—		
Spectrum ratio	1.27	1.65
Absorbance max. 1/nm	436	426
Absorbance max. 2/nm	670	660
$d = 20$—		
Spectrum ratio	1.56	1.27
Absorbance max. 1/nm	426	436
Absorbance max. 2/nm	660	670

The dataset in this paper is demanding, with the following properties. The middle chromatographic peak has no composition 1 or selective region, and most factor analysis methods find it difficult to resolve out unselective peaks. The spectra of the reactant and intermediate are almost identical, with similar spectra ratios and absorbance maxima, and also partially co-elute. Approaches such as windows factor analysis and evolutionary factor analysis will not resolve out neighbouring peaks with very similar spectra; these will simply be modelled by one principal component. Even two-dimensional peak purity methods such as derivatives depend on change in spectral composition over elution time and simply would not detect a difference between the reactant and intermediate. By using PARAFAC on a series of chromatograms, these peaks can be distinguished provided that the concentration of the intermediate is not too low. Hence PARAFAC has potential as a major technique for the resolution and quantification of a series of two-way of chromatograms, often in cases where normal factor analysis methods will fail.

The major drawback is that a good estimate of the number of components is required in advance for sensible models. If this is unknown, it is better to perform the models with fewer components first to see whether there are any elution profiles with more than one maximum. If so, the algorithm can be repeated, increasing the number of components until unimodal elution profiles are achieved.

Appendix

List of Notation Used

i	Elution time index
I	Total number of elution points (20)
j	Spectral wavelength index
J	Number of points in each spectrum (226)
k	Sample number
K	Number of reaction times (20)
A	Elution data matrix, with individual point $a_{l,i}$
B	Spectra data matrix, with individual point $b_{l,j}$
C	Concentration data matrix, with individual point $c_{l,k}$
l	Component number
L	Number of components
d	Kinetic rate parameter
$\underline{X}$	Three-way data, with individual point $x_{i,j,k}$
f	Factor number
F	Total number of factors

Three-way matrices are represented by underlined uppercase bold italic characters, *e.g.*, $\underline{X}$, two-way matrices by uppercase bold italic characters, *e.g.*, A, vectors by lower case bold italic characters, *e.g.*, a_f, and scalars by non-bold characters. Estimated variables are denoted by a 'hat,' *e.g.*, $\hat{A}$, except in eqns. (16) and (17), where the 'estimated true' data are represented by a circle overscript. Dimensions of matrices are given as left-hand side subscripts, *e.g.*, $_{20,10}A$ is a matrix of 20 rows by 10 columns.

References

1 Geladi, P., *Chemom. Intell. Lab. Syst.*, 1989, **7**, 11.
2 Ståhle, L., *Chemom. Intell. Lab. Syst.*, 1989, **7**, 95.
3 Mitchell, B. C., and Burdick, D. S., *Chemom. Intell. Lab. Syst.*, 1993, **20**, 149.

4 Wold, S., Geladi, P., Esbensen, K., and Öhman, J., *J. Chemom.*, 1987, **1**, 41.
5 Kvalheim, O. M., and Grung, B., *Chemom. Intell. Lab. Syst.*, 1995, **29**, 213.
6 Smilde, A. K., and Doornbos, D. A., *J. Chemom.*, 1991, **5**, 345.
7 Tauler, R., Smilde, A. K., Kowalski, B., *J. Chemom.*, 1995, **9**, 31.
8 Cattell, R., *Psychol. Bull.*, 1952, **49**, 499.
9 Kruskal, J. B., *Psychometrika*, 1976, **41**, 281.
10 Sands, R., and Young, F., *Psychometrika*, 1980, **45**, 39.
11 Kroonberg, P. M., and de Leeuw, J., *Psychometrika*, 1980, **45**, 69.
12 Tucker, L., in *Problems of Measuring Change*, ed. Harris, C., University of Wisconsin Press, Madison, WI, 1963, p. 122.
13 Burdick, D. S., *Chemom. Intell. Lab. Syst.*, 1995, **28**, 229.
14 Harshman, R. A., and Lundy, M. E., *Comput. Stat. Data Anal.*, 1994, **18**, 39.
15 Smilde, A. G., *Chemom. Intell. Lab. Syst.*, 1992, **15**, 143.
16 Henrion, R., *Chemom. Intell. Lab. Syst.*, 1994, **25**, 1.
17 Bro, R., and Heimdal, H., *Chemom. Intell. Lab. Syst.*, 1996, **34**, 85.
18 Smilde, A. K., *J. Chemom.*, 1992, **6**, 11.
19 Smilde, A. K., Van der Graaf, P. H., Doornbos, D. A., Steerneman, T., and Sleurink, A., *Anal. Chim. Acta*, 1990, **235**, 41.
20 Bro, R., *J. Chemom.*, 1996, **10**, 47.
21 Booksh, K. S., Muroski, A. R., and Myrick, M. L., *Anal. Chem.*, 1996, **68**, 3539.
22 Bro, R., *Chemom. Intell. Lab. Syst.*, 1996, **34**, 85.
23 Smilde, A. K., Tauler, R., Henshaw, J. M., Burgess, L. W., and Kowalski, B. R., *Anal. Chem.*, 1994, **66**, 3345.
24 Brereton, R. G., Rahmani, A., Liang, Y., Z., and Kvalheim, O. M., *Photochem. Photobiol.*, 1993, **57**, 1048.
25 Elbergali, A. K., Brereton, R. G., and Rahmani A., *Analyst*, 1995, **120**, 2207.
26 Harshman, R. A., and Lundy, M. E., in *Research Methods for Multimode Data Analysis*, ed. Law, H. G., Snyder, C. W., Hattie, J. A., and McDonald, R. P., Praeger, New York, 1984, p. 216.
27 Ten Berge, J. M. F., in *Multiway Data Analyses*, ed. Coppi, R., and Bolasco, S., Elsevier, Amsterdam, 1989, p. 53.
28 Gurden, S. P., Brereton. R. G., and Groves, J. A., *Analyst*, 1996, **121**, 441.
29 Gurden, S. P., Brereton, R. G., and Groves, J. A., *Chemom. Intell. Lab. Syst.*, 1994, **23**, 123.

Raman Spectral Estimation *via* Fast Orthogonal Search

Michael J. Korenberg[*a], **Colin J. H. Brenan**[b] **and Ian W. Hunter**[b]

[a] *Department of Electrical and Computer Engineering, Queen's University, Kingston, Ontario, Canada K7L 3N6*
[b] *Department of Mechanical Engineering, Room 3-147, Massachusetts Institute of Technology, Cambridge, MA 02139, USA*

A Fourier transform (FT) spectrometer measures the autocorrelation (interferogram) of radiation emitted from a source and estimates the optical power spectral density through application of the discrete Fourier transform (DFT) to the recorded interferogram. Although a widely used method, FT spectrometry suffers because its frequency resolution is limited to the sampling rate divided by the number of time-series data points. A large number of points are therefore required to resolve an optical spectrum properly. In this paper, it is shown that a noise-resistant technique known as fast orthogonal search (FOS) can be used to achieve accurate optical spectrum estimation. Further, it is shown that frequency accuracy comparable to the DFT applied to the full interferogram can be obtained with FOS even if the original interferogram is contaminated with noise and then reduced by a factor of up to 10 by irregularly spaced sampling. The FOS application presented here is for the estimation of Raman spectra from interferograms acquired with an FT Raman spectrometer.

Keywords: Spectrum estimation; Raman spectroscopy; irregular sampling; discrete Fourier transform

Beginning with the early work of Michelson,[1] the Fourier transform (FT) spectrometer has become an increasingly important tool for optical spectral measurement. The FT spectrometer in its most general form is constructed from a two-beam, wavefront- or amplitude-division interferometer. After division of an incident optical field of wavenumber σ_0 ($= 1/\lambda_0$) into two equi-amplitude beams, an optical path length difference, Δs, is imposed on the field of each beam on propagation through the interferometer. Interference of the two fields at the interferometer output generates an irradiance, J, that varies as a function of Δs:

$$J(\Delta s) = B(\sigma_0)\cos(2\pi\sigma_0\,\Delta s) \tag{1}$$

where B is the optical power at σ_0 and

$$\Delta s = 2(n_1 x_1 - n_2 x_2) \tag{2}$$

where, for $i = 1$ or 2, n_i and x_i are the refractive index and length of the *i*th interferometer arm, respectively. For a polychromatic field illuminating the interferometer, the interferogram, $J(\Delta s)$, and optical spectrum are a cosine Fourier transform pair:[2,3]

$$J(\Delta s) = \int_{-\infty}^{+\infty} B(\sigma)\cos(2\pi\sigma\Delta s)\mathrm{d}\sigma \tag{3}$$

and the interferogram is formally equivalent to the autocorrelation of the input optical field through the Wiener–Khitnitche theorem.[4] Hence the essence of FT spectrometry is to measure the optical field autocorrelation with the interferometer and recover the optical power spectrum by application of the discrete Fourier transform (DFT).

DFT-based spectral estimation requires the interferogram to be sampled at equi-spaced intervals and at a rate at least twice the maximum wavenumber, σ_{max}, of the optical signal (Nyquist sampling criterion). For an *N*-point data record sampled at frequency $\sigma_s = 2\sigma_{max}$, the DFT estimate will have a spectral resolution

$$\Delta\sigma = \frac{2\sigma_{max}}{N} \tag{4}$$

and a spectral range, $\delta\sigma$, equal to σ_{max}. The FT spectrometer resolving power R ($= \delta\sigma/\Delta\sigma$) equals $N/2$ or

$$R = \frac{\Delta s_{max}}{\bar{\lambda}} \tag{5}$$

for a maximum optical path length difference, Δs_{max}, and light of mean wavelength $\bar{\lambda}$.

The time required to record an *N*-point interferogram, T, depends on the means by which Δs is systematically varied. Most commonly, one interferometer mirror is moved relative to the other and measurement of J at specified optical path differences yields the interferogram as a time-series signal.[5–7] If the measurement time per interferogram point equals δt, the total time to measure the interferogram is simply $T = N\delta t$. Assuming that optical shot noise dominates, the FT spectral signal-to-noise ratio (S/N) has been shown to scale as $1/\sqrt{N}$.[8] Clearly, for an FT spectrometer based on a scanning mirror configuration, operation of the spectrometer at a high resolving power greatly increases the time to acquire an interferogram that yields an acceptable spectral S/N.

Attempts to minimize T can adversely impact on the spectral resolution, spectral range and S/N. These restrictions are alleviated with an FT spectrometer fabricated from a static two-beam interferometer and an array photosensor with N equi-spaced photosensitive elements for recording the interferogram distributed across the detector array.[9–12] For the same S/N, the acquisition time is decreased by N (known as the multi-channel advantage[9]) compared with a scanning mirror-type FT spectrometer but with a restricted spectral resolution since the number of array photoelements is usually a small fixed number.

Given the above considerations, it would be particularly advantageous in many spectroscopic applications (*e.g.*, imaging or time-resolved measurement) to estimate spectra from a smaller number of sample points, N, in order to minimize total measurement time, T, whilst simultaneously retaining a high spectral S/N and resolving power, R. Alternatively, for the static, two-beam interferometer, minimizing N will result in a smaller instrument or, equivalently, achieve higher resolution of the optical spectrum for a given size of instrument. A number of parametric methods have been proposed, such as the Prony and Pisarenko methods, the maximum entropy method, and various autoregressive moving average-based estimators,[13] to obtain frequency resolutions comparable to the DFT but with a reduced number of sample points (*i.e.*, smaller N) or, conversely, to obtain finer frequency resolution than is afforded by the DFT for the same N. However, in all of these methods the model order must be selected, and the first two additionally
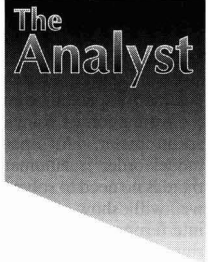
require solution of a polynomial equation, which may be of high degree.

Accordingly, we demonstrate the application of a recent parametric spectral estimator, fast orthogonal search (FOS),[14] to the estimation of Raman spectra acquired with an FT-Raman spectrometer.[7] As opposed to the techniques listed above, model order is automatically determined in FOS; moreover, there is no need to solve a polynomial equation. Most important, we will show that reduction in the number of Raman interferogram points by a factor of 10 through irregular sampling and application of FOS to the reduced data set generates a spectral estimate comparable in frequency resolution to a DFT applied to the full interferogram. We also demonstrate that the FOS spectral estimator is relatively insensitive (compared with the DFT estimator) to additive noise over a large range of interferogram S/N. Optical spectrometers utilizing the FOS algorithm and irregularly spaced sampling may have important applications in process control or monitoring.

Method

There is a special benefit provided by FOS which is not readily available with the other spectral methods discussed above, namely the ability to handle conveniently time series which are unequally spaced or missing some data.[14] This capability stems from the implicit orthogonalization procedure that FOS employs, and does not involve interpolation to 'fill in' missing data values, which would introduce error.

The ability of FOS to cope with unequally spaced data permits irregular sampling of the interferogram and, further, the irregular sampling permits accurate resolution of high frequencies in the optical spectrum using fewer interferogram points than required by the DFT and other parametric spectral estimators. This can be understood through consideration of a time series obtained by sampling at the Nyquist frequency. Suppose next that a large number of data points are randomly deleted. Since some points would still remain closely proximate, high-frequency information would not be lost, yet far fewer points would be required for processing the time series to extract its spectral content. As noted, this exploits the capability of FOS to accept unequally spaced data without introducing error, unlike the other above-mentioned spectral methods. Why FOS has this ability is explained next.

Denote the irregularly-spaced data points by $y(n)$, sampled at times $t = t(n)$, $n = 0, ..., N - 1$. Then FOS enables one to build up a concise sinusoidal series model:

$$y(n) = \sum_{m=0}^{M} a_m p_m(n) + e(n) \qquad (6)$$

where $p_0(n) = 1$, and for $i = 1, 2, ...,$

$$p_{2i-1}(n) = \cos \omega_i t(n) \qquad (7)$$

$$p_{2i}(n) = \sin \omega_i t(n) \qquad (8)$$

and $e(n)$ is the equation error.

The frequencies ω_i in eqns. (7) and (8) are found by systematically searching through a candidate set of frequencies $\omega_A, \omega_B, ...$ These candidate frequencies are not required to be commensurate with, or integral multiples of, the fundamental frequency corresponding to the record length. The candidate frequencies can be selected with *a priori* knowledge of the specific frequencies sought or they could simply be frequencies distributed in frequency bands of interest.

In particular, for $i = 1, 2, ...,$ and $M = 2i$ we set ω_i equal to that candidate frequency resulting in the greatest reduction in mean-square error (MSE) when the term pair

$$T_i(n) = a_{2i-1}p_{2i-1}(n) + a_{2i}p_{2i}(n) \qquad (9)$$

is added to the model of eqn. (6). An implicit orthogonalization of the term pairs, achieved *via* a slightly modified Cholesky decomposition, is used to obtain a computationally efficient procedure[14] for building up the sinusoidal series model. Because the $t(n)$ in eqns. (7) and (8) are the actual instants when the samples $y(n)$ were taken, and these instants are used in defining the $T_i(n)$ (which are implicitly orthogonalized), the unequal spacing of the data contributes no error.

Results

A comparative analysis of DFT and FOS spectral estimates is based on a double-sided Raman interferogram for neat methanol measured at equi-spaced scan mirror positions with an FT Raman spectrometer to yield an interferogram containing 6294 data points. The interferogram was zero-padded to 8192 points in order to treat the data set as a time series obtained with a sampling rate of 8192 Hz. After application of the Hamming window, the DFT was applied to obtain the Raman spectrum shown in Fig. 1(*a*), having a spectral resolution of 26 cm⁻¹ (2.6 Hz). As expected, the spectrum derived here compares with the previously published Raman spectrum of methanol.[15] Application of FOS to the original 6294 point interferogram generates a Raman spectrum similar to that obtained with the 8192 point DFT but with a slightly higher spectral resolution of 20 cm⁻¹ (2 Hz) [Fig. 1(*b*)]. To obtain this Raman spectral estimate, FOS searched through 200 candidate frequencies equi-spaced between 1700 and 2098 Hz (−3480 to 500 cm⁻¹) inclusive and selected the 40 most significant frequencies. The amplitudes of those frequencies are plotted in Fig. 1(*b*) and the amplitudes of unselected frequencies were set to zero. The small difference in spectral peak positions between the FOS and DFT spectra is attributed to their slightly different spectral resolutions.

We now proceed to demonstrate a major difference between the DFT and FOS spectral estimators by recovering *via* FOS the methanol Raman spectrum with only 10% of the original interferogram data. At the same time, we will illustrate the pronounced capability of FOS to cope with noise contamination
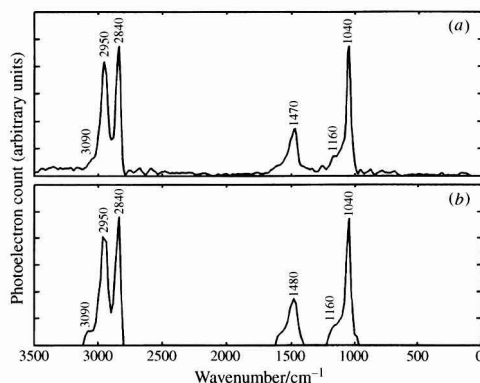

Fig. 1 Comparison of the Raman spectrum of methanol estimated from a 6294 point interferogram with two different algorithms. (*a*) Raman spectrum resulting from application of the DFT to the 6294 point interferogram, Hamming windowed and zero padded to 8192 points. (*b*) Raman spectral estimate that results from the direct application of FOS to the 6294 point raw interferogram. Divisions on the vertical axes are proportional to the photoelectron count and the horizontal axes indicate spectral position in wavenumbers.

of the interferogram. We began by adding to the full interferogram zero-mean white Gaussian noise whose variance was 10% of that of the interferogram. Then, 621 of the 6294 points in the noisy interferogram were randomly selected and FOS was directly applied without any additional processing to this reduced data set. Again, FOS searched through 200 candidate frequencies equi-spaced between 1700 and 2098 Hz, and the amplitudes of selected frequencies are shown in Fig. 2(*a*). The following stopping criterion was used.[16] FOS required, in order to continue, that the greatest reduction achievable by adding a further frequency, divided by the mean square of the current residue, exceed a threshold divided by the number of data points. This criterion (which follows immediately from using a standard correlation test) helps to avoid choosing frequencies which are merely fitting noise. A threshold of 10.9 was used here, roughly corresponding to 99.9% confidence limits. Comparison of Fig. 2(*a*) with 1(*a*) shows that the Raman spectrum estimated from 10% of the noisy data using FOS is remarkably similar to the DFT result obtained from the full 6294 point interferogram with no added noise. Fig. 2(*b*) and (*c*) show, for 50% and 100% noise contamination, respectively, the FOS estimated Raman spectra using the same 621 point irregular sampling sequence. It is impressive that with only 10% of the original interferogram points and interferogram S/Ns as low as 1 (100% additive noise) that the FOS algorithm recovers the major spectral components of the Raman spectrum.

Note that the irregular spacing of the 621 point reduced data set was crucial to successful recovery of the spectrum. Had, instead, every tenth point been selected from the original data, the sampling rate would have been only about 820 Hz, suitable for recovering frequencies up to about 410 Hz but certainly not those at higher frequencies where most, if not all, of the spectral information in the interferogram is situated. Fig. 3(*a*) shows the unproductive result of applying the DFT in this situation, where no noise was added to the reduced data set. On the other hand, if the original sampling frequency of 8192 Hz is maintained but

621 data points were selected equally spaced to either side of the zero lag position (310 data points to either side) then the resulting DFT spectral estimate will have a resolution limit of 260 cm^{-1} (26 Hz) [Fig. 3(*b*)], over ten times larger than the resolution observed with FOS applied to a data set with the same number of points. Again, no noise was added to the reduced data set used to obtain the DFT spectral estimate. Thus a FOS spectral analysis of a randomly reduced noisy data set results in substantially higher spectral resolution than is possible with a DFT spectral estimator applied to a clean interferogram with the same number of points. Comparison of Fig. 3(*a*) and (*b*) with Fig. 2(*a*) is particularly relevant in those situations where the number of sampled interferogram points must be minimized. Similarly accurate FOS Raman spectral estimates from reduced interferograms have also been observed for other condensed phase organic and inorganic samples. Moreover, it has been shown that the recovery of the major spectral components in a Raman spectrum from a randomly reduced interferogram *via* FOS is not critically dependent on the particular random sampling sequence employed.

Conclusions

We have introduced for optical spectrum estimation the use of a recent spectral estimator called fast orthogonal search[14,16] and compared its performance with the discrete Fourier transform on an interferogram recorded with an FT spectrometer. The specific example given here is the estimation of the Raman spectrum of methanol from its interferogram measured with an FT Raman spectrometer. The FOS algorithm does not impose the same restriction on sampling of the interferogram as the DFT; therefore, FOS requires far fewer interferogram data points than the DFT to obtain a spectral estimate of comparable resolution to a DFT estimate that utilizes the entire interferogram data record. Consequently, the reduced number of interferogram points needed to obtain a given spectral resolu-
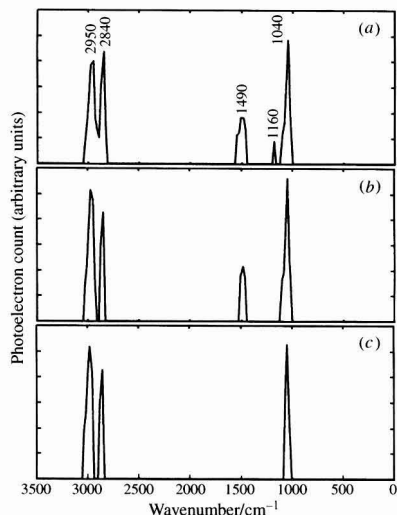

Fig. 2 Raman spectral estimate of methanol by FOS applied to a 621 point reduced interferogram generated by resampling a noisy 6294 point interferogram with a random sampling sequence. In (*a*), the noise added to the original interferogram had a variance equal to 10% of the variance of the original interferogram. In (*b*) and (*c*), the noise variance was 50% and 100%, respectively, and the peaks occurred at the same positions as marked in (*a*).
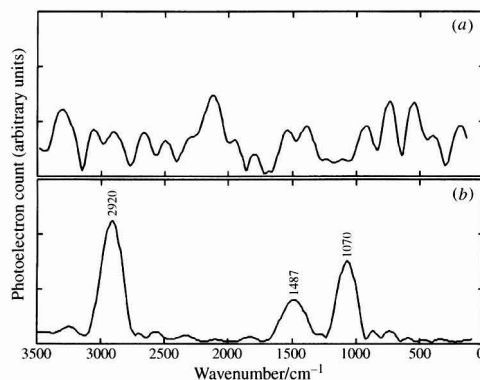

Fig. 3 Comparison of the Raman spectrum of methanol estimated from the DFT applied to (*a*) a reduced 621 point interferogram produced by resampling the original interferogram at a new sampling rate that is one tenth the original sampling frequency and (*b*) a reduced 621 point interferogram composed of 310 points equally distributed to either side of the original interferogram zero lag position. The sampling rate of this reduced interferogram is identical with that of the original interferogram. Note that no noise was added to the original interferogram before the reduced interferograms were obtained. In (*a*) and (*b*), the reduced interferograms were Hamming windowed and zero padded to 8192 points. These spectra should be compared with that in Fig. 2(*a*), estimated by FOS from an equal number of interferogram points (which had additionally been corrupted with noise).

tion *via* FOS implies substantial performance improvements for existing FT spectrometers when measurement time must be minimized and suggests new interferometric spectrometer designs based on the irregular sampling strategy allowed by FOS. This is especially pertinent for a spectrometer having an array photosensor where the number of array photoelements is typically small.

To illustrate the differences between the DFT and FOS spectral estimators, a 6294 point Raman interferogram of neat methanol acquired with an FT Raman spectrometer was analyzed with each algorithm. First, the FOS and DFT Raman spectra computed from the full Raman interferogram were shown to be similar. Next, the interferogram was contaminated with additive Gaussian white noise and then resampled with an irregular (random) sampling sequence to generate a new interferogram having one tenth the points (621 points) of the original data set. Application of FOS to the reduced noisy interferogram generated a Raman spectrum remarkably similar to the DFT spectral estimate using the full clean interferogram data record (6294 points). As expected, application of the DFT to reduced data sets of 621 points failed to generate estimates comparable to the Raman spectrum obtained from the original interferogram even though the reduced sets did not have added noise, unlike those analyzed by FOS.

The FOS method is general and robust and could be an alternative to the DFT in other FT-based spectrochemical analytical techniques. This would include atomic emission, visible or infrared absorption, nuclear magnetic resonance, electron paramagnetic resonance and ion cyclotron spectrometry.

References

1   Michelson, A. A., *Philos. Mag.*, 1891, **5**, 338.
2   *Fourier Transform Infrared Spectroscopy: Applications to Chemical Systems*, ed. Ferraro, J. R., and Basile, L. J., Academic Press, New York, 1978.
3   Nordstrom, R. J., in *Fourier, Hadamard and Hilbert Transforms in Chemistry*, ed. Marshall, A. G., Plenum Press, New York, 1982, p. 21.
4   Saleh, B. E. A., and Teich, M. C., *Fundamental of Photonics.*, Wiley, New York, 1991.
5   Hirschfeld, T., and Chase, D. B., *Appl. Spectrosc.*, 1986, **40**, 133.
6   Bell, R. J., *Introductory Fourier Transform Spectroscopy*, Academic Press, New York, 1972.
7   Brenan, C. J. H., and Hunter, I. W., *Appl. Spectrosc.*, 1995, **49**, 1086.
8   Kahn, F. D., *Astrophys. J.*, 1959, **129**, 518.
9   Zhao, J., and McCreery, R. L., *Appl. Spectrosc.*, 1996, **50**, 1209.
10 Moller, K. D., *Appl. Opt.*, 1995, **34**, 1493.
11 Junttila, M.-L., *Appl. Opt.*, 1992, **31**, 4106.
12 Okamoto, T., Kawata, S., and Minami, S., *Appl. Opt.*, 1984, **23**, 269.
13 Kay, S. M., *Modern Spectral Estimation: Theory and Application*, Prentice-Hall, Englewood Cliffs, NJ, 1988.
14 Korenberg, M. J., *Biol. Cybern.*, 1989, **60**, 267.
15 *Raman/IR Atlas of Organic Compounds*, ed. Schrader, B., and Meier, W., Verlag Chemie, Weinheim, 1977, p. A3-04.
16 Korenberg, M., in *Non-linear Vision: Determination of Neural Receptive Fields, Function, and Networks*, ed. Pinter, R. B., and Nabet, B., CRC Press, Boca Raton, FL, 1992, ch.7.

Microfabricated Flow Chamber for Fluorescence-based Chemistries and Stopped-flow Injection Cytometry

Peter S. Hodder[*a], **Gert Blankenstein**[b] and **Jaromir Ruzicka**[a]

[a] *Department of Chemistry, University of Washington, P.O. Box 351700, Seattle, WA 98195, USA*
[b] *Mikroelektronik Centret (MIC), Technical University of Denmark, Building 345E, DK-2800 Lyngby, Denmark*

A microfabricated flow chamber (MFC) suitable for performing liquid-based fluorimetric assays is introduced. Precision delivery of microliter volumes of sample and reagent to the MFC is accomplished by a double-syringe-pump flow injection analysis (FIA) apparatus. The FIA–MFC system also combines the 'sheath flow' technique (traditionally used in flow cytometry) and stopped-flow FIA as a way to allow sample and reagent streams to be mixed reproducibly. The applicability of this FIA–MFC system to bioanalytical assays is demonstrated by performing an enzymatic assay with an artificial fluorigenic substrate to determine the activity of Savinase, a proteolytic enzyme. When coupled to a fluorescence microscope platform, quantitative analysis of the reaction product is possible. Experiments showed that the FIA–MFC system was capable of performing the assay with good reproducibility of injection (1.5%), and linearity of response (r^2 = 0.9997) in activity ranges of analytical interest. Owing to the incorporation of flow cytometry sheath flow principles into an FIA format, the FIA–MFC system is a suitable tool for cytometric studies.

Keywords: *Flow injection; microfabrication; enzyme; fluorescence; microscopy; flow cytometry*

Recently, microfabricated devices have demonstrated promise as alternatives to conventional analytical instruments. The most obvious benefits of using such technology are the lower sample and reagent volumes necessary for analysis, with a concomitant decrease in the amount of waste generated. These benefits are of particular interest to the biotechnology community, where both small amounts of sample (DNA, cellular suspensions) and expensive reagents (enzymes, fluorescent probes, antibodies) are available for bioanalysis. In addition, since the dimensions of a typical microfabricated structure are by definition small, microscopic arrays consisting of hundreds to thousands of copies of a particular structure can be fabricated in order to perform repetitive chemistries in a highly parallel fashion.[1] Researchers have conceived the concept of placing many different microfabricated structures on a single chip where sampling, sample preparation, sample delivery, reaction with reagent and detection could be integrated. Termed micro-total analytical systems', or μ-TAS,[2] this concept has recently been an area of very active research. Currently most μ-TAS devices are 'hybrid' systems, where macroscale components (*e.g.*, lasers, photomultiplier tubes, pumps, power supplies, microscopes) are clustered around a microfabricated structure.

With a variety of detection methods having been successfully demonstrated in microfabricated structures,[3–5] it is now important to consider the development of suitable automation of sample and reagent handling. The method ultimately chosen should allow manipulation of a variety of fluids (aqueous or non-aqueous, filtered or containing suspended matter) in an automated and highly reproducible fashion. Flow injection

analysis (FIA) is an analytical technique that has demonstrated its utility in performing a variety of chemistries.[6] It has been adapted as a mode of operation for a number of μ-TAS systems, and a recent review has been published on microfabricated structures that employ FIA using *in situ* electroosmotic pumping schemes to manipulate small volumes of aqueous solutions.[7] It would be desirable with chemistries of biotechnological interest to pump organic solvents in microfabricated structures (*e.g.*, combinatorial synthesis chemistries for drug discovery), which ranges from difficult to impossible if one uses electroosmotic flow as a pumping scheme.[8] However, at present FIA-based hydrodynamic fluid manipulation in microfabricated structures is problematic, presumably because of the imprecision that results from using a traditional FIA peristaltic pump to manipulate microliter-scale volumes in microfabricated structures. In addition, advances in the design of intricate miniature hydrodynamic-based pumps that can be incorporated directly into microfabricated structures have fragility concerns associated with their deployment in a μ-TAS format.[9] With few exceptions, such devices are subject to fouling (through entrapment of particulate or air bubbles), back-pressure and pulsation effects.

Since the foremost research goal in our laboratory is to develop a robust yet microfabricated stopped-flow cytometer, where analysis of cell suspensions *via* FIA techniques is possible, we have chosen FIA-compatible, high-precision stepper-motor syringe pumps that represent a useful alternative for hydrodynamic manipulation of fluid in a microfabricated structure. Computer control of the pumps allows reproducible delivery of small volumes (nl–μl) at low flow rates (nl–μl min^{-1}) without sacrificing the application of FIA techniques based on reverse or stopped-flow modes. In addition, the incorporation of robust, commercially available syringe-pumps into a μ-TAS format is convenient since the pumps and valves are located remotely from the microfabricated structure, allowing easy loading and delivery of sample and reagent and fast optimization of flow parameters. The apparatus presented in this paper takes advantage of both traditional FIA methodology and microfabrication techniques to study and exploit mixing by (i) construction a microfabricated flow chamber (MFC) with a novel architecture that serves as a confluence point for three streams, (ii) design of a two-stream (sample and reagent) 'sheath flow' pumping scheme and (iii) employment of stopped-flow FIA methodology. The aim of this work was the construction of a hybrid μFIA system that offers the biotechnology researcher flexibility in experimental design, allowing both biochemical and cytochemical studies to be performed in a robust research apparatus that consumes microliter volumes of sample and reagent per assay.

Experimental

Reagents

The enzyme–substrate reaction used in the FIA–MFC system is similar to a method described in detail elsewhere.[10] Savinase

(Novo Nordisk Industries, Copenhagen, Denmark), is a subtilisin (EC 3.4.21.14) alkaline endoprotease of the serine type. Its proteolytic activity has a broad substrate specificity, and it is used as a laundry detergent additive for removing protein-based stains. A concentrated powder containing 1% pure enzyme was used for activity determination. The activity units of the powder were stated on the vial as 3.17 KNPU g^{-1}, where KNPU (Kilo Novo Protease Unit) is the Novo-Nordisk internal unit used for expression of protease activity.[11] From a stock standard solution of 0.010 KNPU ml^{-1} (i.e., 10 mKNPU ml^{-1}), nine working standard solutions of 0.078, 0.156, 0.313, 0.625, 1.25, 2.5, 5, 8 and 10 mKNPU ml^{-1} were prepared. TRIS-HCl Buffer (0.100 M, pH 8.3) containing 0.010 M CaCl$_2$ was used to dissolve the enzyme and substrate solutions. 7-[N-(α-Succinyl-L-alanyl-L-alanyl-L-(phenylalanyl)amino]-4-methylcoumarin is an artificial fluorigenic substrate that consists of an 7-amino-4-methylcoumarin fluorophore (AMC) covalently attached to a tripeptide substrate (AAF). The AAF–AMC substrate allows quantitative determination of fluorescence as the fluorophore is released from the tripeptide by proteolytic action.[12] A working solution of substrate (4 mM) was made by first dissolving the substrate in N,N-dimethylformamide and then buffer so that the final concentration of N,N-dimethylformamide was 10% v/v. For enzyme activity determination, 1 mM substrate solutions were made from this working solution as required. This concentration was chosen so that pseudo-zero-order reaction kinetics would be maintained during the course of the assay.[13] All solutions were stored refrigerated (4 °C) and the substrate stock solution was protected from light to prevent photochemical degradation. All enzymatic reactions were carried out at room temperature. For tracer studies, sodium fluorescein was dissolved in sodium borate buffer (pH 10) so that its final concentration was 5 mM. Except for the enzyme, all chemicals were acquired from Sigma (St. Louis, MO, USA).

Microfabricated Flow Chamber

MFC construction started with the microfabrication of the desired design in a silicon {100} chip, prepared by standard photolithography and wet-etch techniques.[14] The depth of all etched channels was 50 μm and widths of the channels varied from 150 to 580 μm. These dimensions were chosen to allow pumping of solutions containing dissolved particulate and gas with minimum clogging effects. After etching, the chip was electrostatically bonded (400 °C, 1000 V) on one side to a thin glass window (about 1 mm thick). On the other side of the chip, holes were made at the channel entrances and exits, and gold-plated tubes (spring contact sockets, id 0.86 mm, od 0.97 mm; Newark Electronics, Chicago, IL, USA) were epoxied into place. The spring contact sockets served as tubing connectors that allowed coupling to FIA tubing. When completed, the typical size of the entire structure (including the tubing connectors) was 13 × 8 × 15 mm (Fig. 1).

Flow Injection Analysis

FIA system with two Cavro XL3000 high-precision computer-controlled stepper-motor syringe pumps (Cavro Scientific Instruments, Sunnyvale, CA, USA) was used (Fig. 2). Each syringe (250 or 500 μl) was connected to a two-way Cavro XL Smart Valve. The valves switched positions between the syringes' respective buffer and reagent reservoirs (to load the syringes) and the MFC (to inject of their contents). The FIA system was controlled through the serial port of a Toshiba laptop computer running a QuickBasic 4.5 computer program (Microsoft, Seattle, WA, USA). The FIA system was connected to the MFC via a sample injector valve (Upchurch, Oak Harbor, WA, USA) with a 20 μl sample loop. The valve was placed physically close to the MFC to minimize dispersion of the

injected sample. An Upchurch tee valve was used to split the sheath stream so that it entered the two outer inlets of the MFC. Microline tubing (Cole Parmer, Chicago, IL, USA) of 0.51 mm id was used for all fluidic connections. Except for mating the tubing to MFC tubing connectors, Upchurch Teflon flangeless fittings with ferrules were used.

Fluorescence Detection

The MFC was mounted on the stage of a Axiovert 100 inverted epiluminescent microscope (Carl Zeiss, Oberkochen, Germany) with a fluorescence filter set to allow detection of the AMC fluorophore. The glass window bonded to the MFC permitted focusing of the etched channels by a Zeiss 10×, 0.50 NA Fluar objective. The objective was used to bring a small region of the center channel of the MFC into focus. This region was then framed in the photomultiplier tube viewfinder. This region had the dimensions of 1800 × 580 × 50 μm, which corresponds to an analytical volume of 52 nl. A fluorescence spectrometer with a 75 W xenon short-arc light source (Photon Technology International, South Brunswick, NJ, USA) was coupled to the microscope via a fiber optic cable. The monochromators of the spectrometer were set to an excitation wavelength of 370 nm
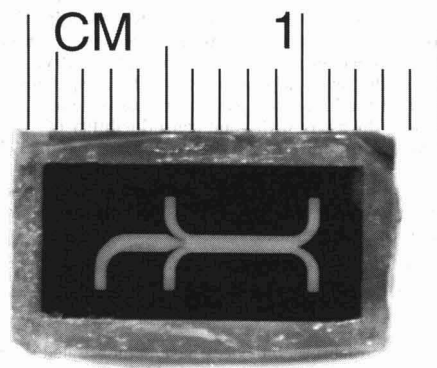

Fig. 1 Top view of a microfabricated flow chamber (MFC). The MFC has three fluid inlets that impinge upon a center channel, and has two outlets.
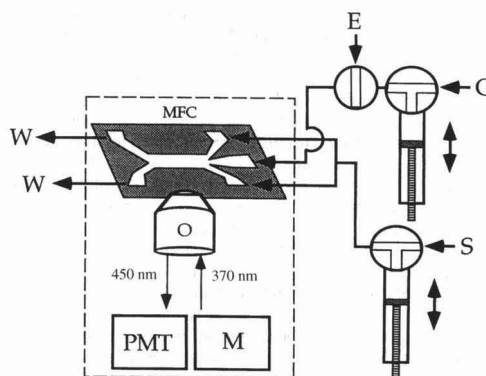

Fig. 2 Schematic diagram of FIA–MFC system. C = 'core' syringe (filled with carrier buffer); S = sheath syringe (filled with substrate); E = enzyme sample introduced into injector valve, W = waste vial. Box in broken lines contains MFC in the fluorescence microscope platform. M = monochromator; PMT = photomultiplier tube detector; O = microscope objective.

with a 20 nm bandpass to allow selective excitation of the free AMC fluorophore over excitation of the substrate–fluorophore complex. A 400 nm long pass dichroic (Chroma Technology, Brattleboro, VT, USA) and 450 nm emission filter with a 65 nm bandpass (Omega Optical, Brattleboro, VT, USA) were used to allow only the fluorescence of the free fluorophore to be detected by the photomultiplier tube.

Results and Discussion

Theoretical Considerations for Assay Design

The MFC was designed to act as a mixing tee integrated with a flow cell where sample and reagent streams merge in such a way that the sample stream is bounded on both sides by reagent streams [Fig. 3(a)]. This containment of a central stream by an outer stream is termed 'sheath flow', a hydrodynamic technique traditionally employed in flow cytometry.[15] Sheath flow typically consists of a faster flowing annular outer stream ('sheath') that surrounds a slower flowing cylindrical inner ('core') stream. In flow cytometry, sheath flow serves the purpose of collimating cellular suspensions so that each cell follows a narrow, well defined trajectory and thereby cell-by-cell analysis is possible. Other prototypes of the MFC design take advantage of the sheath flow principle for sorting of cellular suspensions.[16] In the FIA–MFC system, it is important to note that as long as the sheath and core streams flow, laminar flow prevails and only a negligible amount of diffusional mixing occurs at the periphery of the sheath and core stream interface (see equations below).

Mixing of sample and reagent in flow injection systems is facilitated by injecting a plug of sample into a flowing stream of reagent and allowing sufficient dispersion to occur before the sample–reagent mixture reaches the detector.[6] In stopped-flow FIA, mutually dispersed reagent and sample zones flow into a cell which is interfaced with a detector suitable for measurement of some species of the ensuing chemical reaction.[17] During the stopped-flow period, the species of interest (*e.g.*, a fluorescent product of the reaction) is formed and measured. The advantage of the stopped-flow method in biotechnological applications is that it allows continuous monitoring of a reaction rate, a parameter of great interest, without an excessive consumption of reagent (*cf.*, continuous flow methodologies).
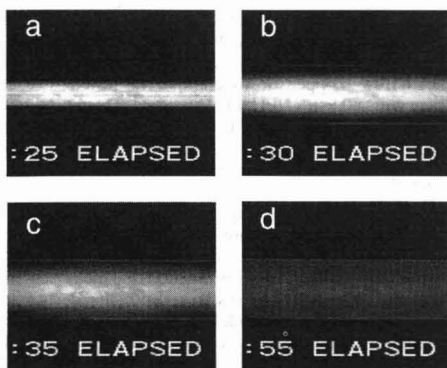
Fig. 3 Snapshots of the FIA–sheath flow principle. Images taken from center channel of MFC. Core syringe loaded with fluorescein tracer and sheath syringe loaded with buffer. The time elapsed (in seconds) from the start of the FIA assay is given at the bottom. As the sheath and core syringes flow, laminar flow is observed at $t = 25$ s (a), just before stopping the flow at $t = 26$ s. Upon stopping of syringes, mixing of the core stream into the sheath stream is recorded at successive time intervals from $t = 30$ s (b), 35 s (c) and 55 s (d) after the beginning of the assay.

When addressing mixing in microfabricated structures (and in many FIA systems), consideration must be given to the behavior of fluids at micrometer dimensions if one wishes to design a functional FIA-based assay. In this context, much emphasis has been placed on the Reynolds number (*Re*), which can be described as the ratio of inertial to viscous forces, and is useful for describing whether a flowing liquid is turbulent (*Re* > 2000) or laminar (*Re* ≪ 2000).[18] This can be readily seen by inspection of a hydraulic equation used to calculate *Re*:

$$Re = \frac{(D_{eq})v_{av}\rho}{\mu} \quad (1)$$

where D_{eq} is the effective diameter of the structure through which the liquid is flowed, v_{av} is the average linear velocity of the liquid, ρ its density and μ its viscosity. Assuming the liquid is Newtonian and incompressible and low volumetric flow rates are employed (< 1 ml min^{-1}), the D_{eq} term dominates at micrometer dimensions and low *Re*s result. Therefore, microfabricated structures are being designed to exploit diffusion-based mass transport since convective mixing is thought to be difficult to achieve. The Einstein–Smoluchowski equation is useful for estimating the time required for a species to diffuse a given distance:

$$t = \frac{\langle(\Delta x)^2\rangle}{2D} \quad (2)$$

where $\langle(\Delta x)^2\rangle$ is the average square of the displacement in the *x*-direction through which diffusion will occur and D is the diffusion coefficient of a molecule in a given phase (D is typically 10^{-5} cm^2 s^{-1} for molecules in liquids at STP). With this in mind, researchers have constructed elaborate devices for promoting diffusional mixing in liquids by creating conditions where $\langle(\Delta x)^2\rangle$ is minimized. For example, a microfabricated multi-stage, multi-layer lamination assembly was designed to optimize diffusional mixing of species by splitting and rejoining continuously flowing sample and reagent streams through a complex three-dimensional network.[19] However, owing to their small channel widths, such designs may have inherent drawbacks with handling biological samples where the presence of particulate is typical.

Therefore, this work exploited a different path, *viz.*, the use of stopped-flow FIA methodology in combination with a sheath flow technique to facilitate mixing in the MFC and allow the determination of a species of interest in a biochemical reaction. In terms of traditional wet chemistry, the laminar sheath flow in the MFC can be thought of as a means to confine sample and reagent in their separate beakers until the experimenter decides that the conditions are optimum to measure a chemical reaction. By simultaneously stopping the core and sheath flows, the sheath–core boundary collapses and mixing of the now stationary sample and reagent streams occurs [Fig. 3(b)–(d)]. It is important to note that the sheath flow serves as a type of multi-lamination technique, where the width of the streams (*i.e.*, 'channels' of sample and reagent) can be set by changing the ratio of sheath to core flow rates. This is advantageous for experiments where cell suspensions are used in order to avoid clogging effects while at the same time allowing mixing to occur on a convenient time scale when the sheath and core flows have stopped: the dimensions of the channel, subdivided by the three streams, promotes mixing of sample and reagent species, since they need only displace a short distance (about 200 μm) before penetrating each other. Substitution of typical experimental run parameters into eqn. (2) yields 20 s as the required time for a substrate molecule on the periphery of the core–sheath boundary to diffuse to the other side of the enzyme stream. Furthermore, experiments also showed that mixing after stopping had an additional component to mixing: the abrupt

stopping of flow caused an expansion of the core stream into the sheath stream. This phenomenon, which lasted of the order of < 1 s, promoted reproducible mixing of the sheath and core streams. This could result from artifactual processes, such as the syringes not stopping at precisely the same time once a command is given to stop. Also, it is not possible to describe this behavior in terms of *Re*. Once the flow is stopped, the Reynolds conditions do not apply. The utility of the stopped-flow approach for mixing slowly diffusing species (such as microbeads with cells) will be investigated further.

To run an enzymatic assay (Fig. 4), the core and sheath syringes were loaded with 33.5 µl of TRIS buffer and 67.0 µl of substrate solution, respectively. While the syringes were loading, the downstream injector valve was turned to the load position and 20 µl of enzyme standard solution were loaded into the sample loop. After the syringes had been loaded, the injector valve was turned to the inject position and the contents of the core and sheath syringes were dispensed to the MFC. To allow rapid delivery of sample and reagent to the MFC, the volumetric flow rates were chosen to be 250 µl min^{-1} for the sheath stream and 125 µl min^{-1} for the core stream. Note that this choice of flow rates resulted in laminar flow (*Re* = 2) of three equally sized streams (about 200 µm width) when viewed under the microscope. Once the syringes had finished delivering their loaded volumes, they stopped simultaneously for 50 s. This cessation was coordinated so that the FIA peak of the injected enzyme solution was trapped in the MFC. Upon stopping, the increase in fluorescence with time was measured, corresponding to the increase in concentration of released AMC fluorophore from the AAF–AMC complex. After the measuring time, the syringes were loaded again (sheath 250 µl, core 125 µl) to rinse the MFC. This was followed by an additional rinse step with 250 µl of buffer by the core syringe. The assay was then repeated for each standard.

The completeness of mixing was of some concern in preliminary experiments prior to discovering the effectiveness of the stopped-flow approach. Since preliminary experiments with tracer solutions suggested that agitation-based mixing schemes would be beneficial in decreasing the mixing time, this was investigated. However, experiments incorporating these mixing schemes with the enzyme–substrate system gave similar results to the stopped flow approach, and therefore the agitation-based mixing scheme was not explored further. To increase the sensitivity of the assay at low enzyme activity, it was found that increasing the measuring time was possible until enough fluorescent product was generated by enzymatic action to be

Fig. 4 Fluorescence spectra of 10 successive Savinase enzymatic assays in the MFC–FIA system, 0–10 mKNPU ml^{-1}. Each assay is started by injecting contents of core and sheath syringes into the MFC. Upon stopped flow, an increase in fluorescence corresponding to the generation of fluorescent product is observed. Enzyme is then rinsed out at the end of the assay.

detected. Therefore, a measuring time of 50 s was chosen as a convenient time scale in order to exploit the dynamic range of the system while at the same time quantify enzyme activities of analytical interest (0.1–0.5 mKNPU ml^{-1}).[20]

The total volumes of substrate and buffer solution volumes were, 317 and 408 µl per assay, respectively, exceeding many-fold the volume of the flow system. The majority of this volume comes from the washing steps of the FIA routine. This was found necessary to insure that the hydrophilic protease did not adhere to the walls of the flow chamber where it would give residual activity, resulting in a carryover which was especially conspicuous if higher activity samples were assayed in succession. Although other schemes were considered, such as acidic washes to deactivate residual enzyme activity or double injection of sample and reagent, they were not explored with the FIA–MFC system for reasons of fluidic simplicity. Otherwise, a further reduction in volumes would be facilitated by replacing the traditional FIA tubing used in this research with micrometer-diameter fused silica capillary tubing typically used in capillary electrophoresis. The recent introduction of commercially available connectors[21] suitable for mating fused silica tubing to injector valves, splitting tees, *etc.*, will facilitate the further minimization of sample and reagent volumes consumed per assay.

Data Analysis

Fluorescence spectra were collected and analyzed using the software utility that came with the spectrometer. The window of time (Δ*t*) used for calculation of the slope of each spectra was 50–90 s. This window was found sufficient to allow mixing to occur and enough product to be detected. Since the slope of the linear portion of each spectrum is directly proportional to the enzyme activity in pseudo-zero-order kinetics, a linear equation should result if the slope of the linear portion of each spectra is plotted *versus* the enzyme activity of each of the enzyme standards. As can be seen in the spectra, the 8 and 10 mKNPU ml^{-1} standards show non-linearity of the fluorescence signal (measured in cps, photon counts per second) over the selected time window, as the fluorescent signal measured at these activities, especially with the 10 mKNPU ml^{-1} standard, exceeds the linear range of the photomultiplier tube detector. However, a linear calibration curve ([Δcps Δ*t*$^{-1}$] = 2266 [mKNPU ml^{-1}] + 93.328, r^2 = 0.9997, *n* = 8) was calculated for the range of enzyme activities from 0.08 to 8 mKNPU ml^{-1}. With the points used, the FIA–MFC technique was linear over a two decade range. Reproducibility of injection and mixing of the sheath flow–stopped-flow technique was tested by repeating the assay with a 0.8 mKNPU ml^{-1} standard. The reproducibility was found to be 1.5% (*n* = 3).

Conclusion

Stopped flow of streams brought together in a microfabricated flow chamber that permits monitoring of reaction products in real time is a novel approach to mixing that combines aspects of flow cytometry and FIA to allow reaction rate measurements on biochemical and biological systems. Both the design of the MFC and the choice of the model enzyme chemistry were based on the employment of a fluorescence microscope platform as a detector. The use of the fluorescence microscope as a detector reflects its importance and utility in routine biological studies and its ability to image cellular processes. The hybrid µFIA system presented in this paper takes advantage of a high-precision syringe pump FIA apparatus, microfabrication technology and fluorescence microscopy to allow both mixing and subsequent chemical analysis of small volumes of fluid in an automated, highly reproducible fashion. The MFC itself can be thought of as both a nanoliter volume mixing chamber and
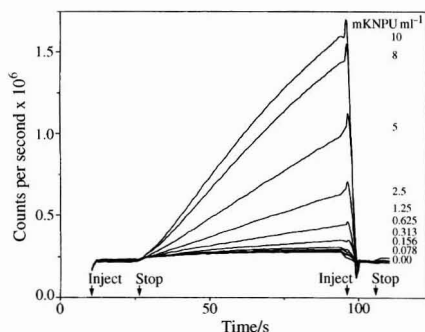
microscale flow cell suitable for performing a variety of fluorescence-based assays. Since hydrodynamically based pumping schemes are employed, the FIA–MFC system is insensitive to the use of different solvents, allowing greater flexibility in the choice of reagent chemistries (*cf.*, electro-osmotic-based pumping schemes). The microfabricated structure incorporates no moving parts and is therefore robust. However, in order to access even smaller volumes of sample and reagent per assay, further optimization of the system hardware is necessary.

The study of mixing and reaction kinetics carried out in this μFIA format is a stepping stone towards the development of a stopped-flow cytometer designed to study reaction kinetics in cellular suspensions. Future research will be directed towards minimizing volumes of sample and reagent used for analysis and also applying the FIA–MFC system to cell studies where the sheath flow will contain certain fluorescent probes, agonists or antagonists, while the core stream will contain cell suspensions of interest.

References

1 Borman, S., *Chem. Eng. News*, 1995, **73**, 37.
2 Manz, A., Graber, N., and Widmer, H. M., *Sens. Actuators B*, 1990, **1**, 244.
3 Liang, Z., Chiem, N., Ocvirk, G., Tang, T., Fluri, K., and Harrison, J. D., *Anal. Chem.*, 1996, **68**, 1040.
4 Effenhauser, C., Manz, A., Widmer, H. M., *Anal. Chem.*, 1995, **67**, 2284.
5 Reay, R. J., Flannery, A. F., Storment, C. W., Kounaves, S. P., and Kovacs, G. T. A., *Sens. Actuators B*, 1996, **34**, 450.
6 Ruzicka, J., and Hansen, E. H., *Flow Injection Analysis*, Wiley, New York, 2nd edn., 1988.
7 Haswell, S. J., *Analyst*, 1997, **122**, 1R.
8 Dasgupta, P. K., and Liu, S., *Anal. Chem.*, 1994, **66**, 1792.
9 Zengerle, R., Stehr, M., Freygang, M., Haffner, H., Messner, S., Rossberg, R., and Sandmaier, H., in *AMI Special Issue μTAS '96*, ed. Widmer, H. M., Verpoorte, E., and Barnard, S., AMI Basle, 1996, pp. 91–93.
10 Ruzicka, J., and Gübeli, T., *Anal. Chem.*, 1991, **63**, 1680.
11 *Savinase Product Sheet*, Novo Nordisk Industries, Copenhagen, Detergent Enzyme Division.
12 Kanaoka, Y., Takahashi, T., Nakayama, H., and Tanizawa, K., *Chem. Pharm. Bull.*, 1985, **33**, 1721.
13 Hansen, E. H., and Jensen, A., *Talanta*, 1993, **40**, 1891.
14 Kovacs, G. T. A., Petersen, K., and Albin, M., *Anal. Chem.*, 1996, **68**, 407A.
15 Kachel, V., Fellner-Feldegg, H., and Menke, E., in *Flow Cytometry and Sorting*, ed. Melamed, M. R., Lindmo, T., and Mendelsohn, M. L., Wiley-Liss, New York, 2nd edn., 1990, ch. 3.
16 Blankenstein, G., Scampavia, L., Branebjerg, J., Larsen, U. D., and Ruzicka, J., in *AMI Special Issue μTAS '96*, ed. Widmer, H. M., Verpoorte, E., and Barnard, S., AMI, Basle, 1996, pp. 82–84.
17 Christian, G. D., and Ruzicka, J., *Anal. Chim. Acta*, 1992, **261**, 11.
18 Bird, R. B., Stewart, W. E., and Lightfoot, E. N., *Transport Phenomena*, Wiley, New York, 1960, ch. 1–2.
19 Branebjerg, J., Gravesen, P., Krog, J. P., and Nielsen, C. R., in Proceedings of the 9th International Workshop on Micro Electro Mechanical Systems, San Diego, CA, 1996, pp. 441–446.
20 *Analytical Method AF 220/1-GB*, Novo Nordisk Industries, Copenhagen, Enzymes Division, 1986.
21 *Catalog of Chromatography and Fluid Transfer Fittings*, Upchurch Scientific, Oak Harbor, WA, 1997, pp. 25–26.

Determination of Phenoxy Acid Herbicides From Aqueous Samples by Improved Clean-up on Polymeric Pre-columns at High pH

René B. Geerdink*[a], Sylvia van Tol-Wildenburg[a], Wilfried M. A. Niessen[b] and Udo A. Th. Brinkman[b]

[a] RIZA, P.O. Box 17, 8200 AA Lelystad, The Netherlands
[b] Department of Analytical Chemistry, Free University, De Boelelaan 1083, 1081 HV Amsterdam, The Netherlands

An improved procedure for the determination of phenoxy acid herbicides in environmental water samples is reported. The procedure consists in solid-phase extraction (SPE) of 60 ml water samples on a polymeric pre-column at pH 2.8, a clean-up step at high pH and subsequent desorption and ion-pair LC separation at pH 8.8. The main improvements are in the basic clean-up step and in the LC eluent composition. The release of compounds which are electrostatically bound to the precolumn is favoured by a washing step with 0.1 mol l^{-1} sodium hydroxide solution. As regards LC, gradient elution is applied using solvents with low buffer and ion-pairing concentrations. The detection limits for the phenoxy acids (UV detection at 232 nm) are 5–20 ng l^{-1} for tap water samples. At the 0.1 µg l^{-1} spiking level, the RSD is 6% (n = 7) and the recoveries are better than 83% for all analytes. The long-term reproducibility typically has RSD values of 5% (n = 7). The method was successfully tested on water samples from various origins, and the results obtained with the present on-line SPE–LC–UV procedure were found to compare well with those obtained with procedures involving SPE combined off-line with GC–MS or flow injection MS–MS.

Keywords: Phenoxy acid herbicides; solid-phase extraction–liquid chromatography–UV detection; high-pH clean-up; aqueous samples

In our laboratory, the determination of phenoxy acid herbicides (for names and structures, see Table 1) in surface water is performed according to a previously described method.[1,2] The method essentially consists in on-line analyte enrichment from a small sample volume at pH 3, pre-column clean-up and an isocratic ion-pair LC separation on a polymeric column. However, over the years some of the initial conditions were changed because of maintenance problems. As an example, the high buffer salt concentration and the high pH of the washing solvent caused rapid deterioration of the LC pumps and valves, and were therefore modified. In addition, in order to simplify the procedure, heart-cutting of the pre-column desorption solvent[2] was omitted. All modifications were evaluated by testing spiked tap water samples and comparing the results obtained with the initial conditions. In general, the modified procedures could be used successfully for analyses of tap water and water from the main Dutch rivers, the Rhine and Meuse.
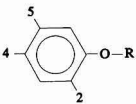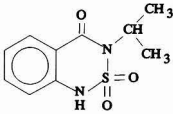
However, surprisingly, the analysis of spiked surface water samples showed large differences in analyte recoveries depending on the origin of the sample. Problems were experienced especially with samples from rural areas and were expected to be due to the presence of relatively large amounts of humic material. In order to improve the reliability of the procedure and to enhance the recovery of the analytes in, especially, the rural-area samples, the total analytical procedure has now been further modified and optimized. As a check, the results of the final solid-phase extraction (SPE)–LC–UV procedure were compared with those obtained by means of flow injection analysis (FIA)– MS–MS and GC–MS.

Experimental

Reagents

All chemicals and solvents were of analytical-reagent grade. HPLC-grade methanol, acetonitrile, sodium hydroxide, ammo-

Table 1 Structures of phenoxy acid herbicides and bentazone

Analyte			PHENOXY ACID Analyte structure				BENTAZONE	
Abbreviation	Peak No.	pK_a	2	4	5	R		CAS No.
MCPA	1	3.1	CH$_3$	Cl	H	CH$_2$COOH		94-74-6
MCPP	2	3.6	Cl	Cl	H	CH$_2$COOH		94-75-7
2,4-D	3	2.8	CH$_3$	Cl	H	CH(CH$_3$)COOH		7085-19-0
2,4-DP	4	2.7	Cl	Cl	H	CH(CH$_3$)COOH		120-36-5
Bentazone	5	3.2						25057-89-0
MCPB	6	4.6	Cl	Cl	Cl	CH$_2$COOH		93-76-5
2,4-DB	7	4.4	CH$_3$	Cl	H	(CH$_2$)$_3$COOH		94-81-5
2,4,5-T	8	2.8	Cl	Cl	H	(CH$_2$)$_3$COOH		94-82-6
2,4,5-TP	9	3.6	Cl	Cl	Cl	CH(CH$_3$)COOH		93-72-1

nium acetate, perchloric acid and water were obtained from J. T. Baker (Deventer, The Netherlands) and tetrabutylammonium hydrogensulfate from Fluka (Buchs, Switzerland). Chlorophenoxycarboxylic acids were obtained from Riedel-de Haën (Hannover, Germany) and Promochem (Wesel, Germany) and bentazone from Promochem.

Equipment

A Waters (Millipore, Bedford, MA, USA) Model 600E pump was used to deliver the eluent. A fully automated Prospekt (Spark, Emmen, The Netherlands) cartridge exchange system with two additional valves was used to control the flow scheme during analysis. The solvent delivery unit (SDU) of the Prospekt was provided with two additional six-port solvent selection valves for the wetting and conditioning of the pre-columns, the washing solvents and the aqueous samples. A Model 785A programmable absorbance detector (Applied Biosystems, H. I. Ambacht, The Netherlands) was operated at 232 nm. The column thermostat was a Mistral from Spark. Chromatograms were recorded and integrated by a Millipore data station using Baseline 810 or Millenium 2020 software.

For MS detection, a Finnigan TSQ-700 mass spectrometer (Finnigan MAT, San Jose, CA, USA) equipped with a Finnigan thermospray interface (TSP-2) was used; the experimental conditions were as in previous work.[3]

Procedures

Stock standard solutions of the chlorophenoxy acids and bentazone were prepared by weighing approximately 5 mg of each component and dissolution in 50 ml of methanol; they were stored at -20 °C. These solutions were diluted with ultrapure water and acidified to pH 2.8 with 0.1 mol l^{-1} HClO$_4$, to obtain individual and mixed working standard solutions which were stored at 4 °C. Spiked sample solutions were prepared by diluting the stock standard solutions with tap or surface water and acidifying them to pH 2.8 with 0.1 mol l^{-1} HClO$_4$.

Pre-columns (10 × 2 mm id), pre-packed with 15–25 µm PLRP-S styrene–divinylbenzene copolymer (Polymer Laboratories, Church Stretton, UK), were wetted with 2 ml of methanol (2 ml min^{-1}) and activated with 2 ml of 0.001 mol l^{-1} HClO$_4$ (1 ml min^{-1}) prior to use. Preconcentration of the samples (60 ml) was performed at 2 ml min^{-1}. Details of the clean-up procedure are described below.

LC separations were carried out at 50 °C on a 250 × 4.6 mm id column pre-packed with 5 µm, 100 Å PLRP-S using an acetonitrile–water gradient (for details, see Table 2 and later text).

Results and Discussion

The trace-level determination of phenoxy acids in surface water with an isocratic LC separation often creates problems because

Table 2 Gradient elution procedure D

Time/ min	Flow rate/ ml min^{-1}	A* (%)	B* (%)
0	1.0	70	30
5		70	30
25		30	70
26		70	30
30		70	30
60	0.05	70	30

* Solvent A: acetonitrile–water (20 + 80 v/v) with 0.0125 mol l^{-1} borate buffer in aqueous phase and 0.003 mol l^{-1} TBA. Solvent B: acetonitrile–water (40 + 60 v/v) with 0.0125 mol l^{-1} borate buffer in aqueous phase and 0.003 mol l^{-1} TBA.

most analyte peaks are eluted on a sharply decreasing baseline caused by a high humic acid hump in the early part of the chromatogram. This is demonstrated in Fig. 1, where the chromatogram of a standard solution is compared with that of a surface water sample. It will be obvious that the presence of the hump will cause difficulties during peak integration. Moreover, changing the sample volume applied to the pre-column causes a shift in the retention time of the MCPB and 2,4-DB (peaks 7 and 8), which are co-eluted in the system. This is demonstrated in Fig. 2, in which three tap water samples acidified to pH 3, of 30, 60 and 150 ml were applied to the pre-column and subsequently subjected to separation by LC. One should also note that, even with tap water samples, the baseline is not straight because of the presence of the dissolved organic carbon (DOC) which is not removed during tap water preparation from surface water. As is to be expected, the peak areas of all compounds of interest increased with increasing sample volume, *i.e.*, they were two- and five-fold higher for the 60 and 150 ml samples, respectively, compared with the 30 ml sample. However, with the 150 ml sample, the peaks of MCPB and 2,4-DB shifted to longer retention times and were now co-eluted with 2,4,5-TP (peak 9). One explanation of the shift is that it is due to the amount of acid applied to the pre-column. Obviously, a larger volume of high-pH solution will be necessary to ionize the compounds among which MCPB and 2,4-DB have the highest pK_a values. Desorption with the ion-pair-containing acetonitrile–water (30 + 70 v/v) eluent at pH 8.8 does not occur sufficiently rapidly for these two compounds, although the pH used ensures complete dissociation of all compounds with pK_a 2.7–4.6. This
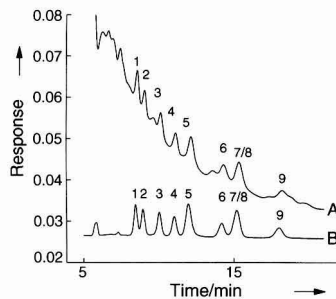

Fig. 1 SPE–LC–UV of acid herbicides after preconcentration of (A) surface water and (B) a standard solution. Conditions: 60 ml sample, spike 1.0 µg l^{-1}; washing solvent, acetonitrile–water (4 + 96 v/v), pH 3, 1 ml; system, 10 × 2 mm id pre-column packed with 20 µm PLRP-S, 250 × 4.6 mm id analytical column packed with 5 µm PLRP-S; eluent, acetonitrile–water (30 + 70 v/v), containing 0.0125 mol l^{-1} TB and 0.003 mol l^{-1} borate buffer, pH 8.8, flow-rate 1.0 ml min^{-1}; UV detection, 232 nm. Peaks: 1, MCPA; 2, 2,4-D; 3, MCPP; 4, 2,4-DP; 5, bentazone; 6, 2,4,5-T; 7/8, MCPB/ 2,4-DB; 9, 2,4,5-TP.
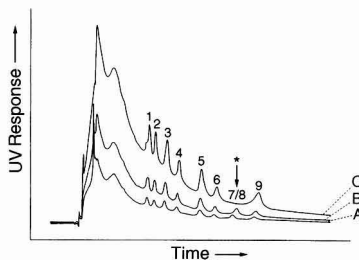

Fig. 2 SPE–LC–UV of acid herbicides after preconcentration of (A) 30, (B) 60 and (C) 150 ml of tap water spiked with 0.25 µg l^{-1} of each component. For conditions, see Fig. 1. At asterisk: MCPB/2,4-DB.

suggests that the buffer strength may be an important parameter.

In order to improve the LC separation, several conditions of the procedure were re-examined.

Analytical LC Separation

In Table 3 the conditions from refs. 1 and 2 (columns A and B, respectively) and the initial conditions used in this work (column C) are summarized. As discussed in the Introduction, the conditions of column C are the result of earlier improvements.

First, the influence of the pH used during sorption, *i.e.*, the pH of the sample, and the pH used during desorption, *i.e.*, the pH of the eluent, were studied in the ranges 2.0–3.5 and 7.5–9.5, respectively. The results showed that a low sample pH (2.0) gave less reproducible results than higher pHs: the RSD values of the retention times of the test analytes were about 5% and 0.1% at pH 2.0 and 2.8, respectively ($n = 7$). On the other hand, varying the eluent pH over the range indicated had no significant effect.

Next, gradient elution was introduced and the ion-pair reagent (TBA) and the borate buffer salt concentrations were optimized in order to obtain a low and non-fluctuating baseline during elution of the analytes of interest. The TBA concentration was studied in the range 0.001–0.006 mol l^{-1} and the borate concentration in the range 0.005–0.025 mol l^{-1}. The proper eluent composition for separation turned out to be a linear gradient for 20 min from 26 + 74 to 34 + 66 v/v acetonitrile–water with constant concentrations of 0.003 mol l^{-1} TBA and 0.0125 mol l^{-1} borate buffer of pH 8.8 (Table 3, column D). With these conditions, chromatograms of tap, surface and rural water samples all showed the desired baseline during analyte elution, even though there still was a baseline offset due to matrix constituents with surface and rural water.

Influence of Matrix Constituents

The trace-level determination of phenoxy acids generally requires extensive clean-up to remove humic constituents. These interfering compounds with their many acidic and phenolic substituents are difficult to separate from the similar phenoxy acids. In actual practice, pre-treatment techniques such as ultrafiltration,[2] on-line dialysis with (hollow-fibre) membranes[4] or a dual pre-column procedure (PLRP-S and anion exchanger)[5] are not sufficient for the analysis of surface water with concentrations down to 0.1 µg l^{-1}. With tap and groundwater, detection limits of ≤0.1 µg l^{-1} are more easily

achieved with off-line SPE on C_{18}-bonded silica at neutral pH using an ion-pairing mechanism.[6]

In another study on the preconcentration of a broad range of acidic, basic and neutral compounds from surface water adjusted to pH 13,[7] the selectivity did improve considerably, but only 2–5 ml samples could be handled without breakthrough. This resulted in poor detection limits of 0.5–1.3 µg l^{-1}. As an alternative, in a previous paper[2] pre-column clean-up with up to 7 ml of 0.1 mol l^{-1} aqueous sodium hydroxide was described. At that time, the LC eluent contained a commercial ion-pair reagent, low-UV PIC A (Waters), with a high buffer salt concentration that caused rapid deterioration of the pump heads. The target analytes were, admittedly, quantitatively recovered from the pre-column, probably owing to the additional 'mass effect' of the buffer salt; however, the humic acid hump in the chromatogram was still pronounced. In addition, owing to the high maintenance costs, the robustness of the procedure was not satisfactory.

As regards alternatives, the use of a clean-up procedure with a solution containing 1–5% of acetonitrile did not cause breakthrough of the analytes. However, the recoveries of the analytes (spiked at 0.25 and 1.0 µg l^{-1}) from rural samples were not constant and often much lower than those from tap water. Typical examples are presented in Table 4. In several instances, the analyte recoveries were below 60%; however, duplicate runs gave the same result, indicating that the nature of the sample and not the analytical procedure was the main cause of the problem.

Several of the above samples were also subjected to analysis by FIA–MS–MS, a rapid screening procedure which was described in detail in a previous paper.[3] To illustrate the problems then encountered, in one sample 3 µg l^{-1} of bentazone was found with FIA–MS–MS, whereas there was no peak at the retention time of bentazone in the LC–UV trace. This, and other, false-negative results indicate that the phenoxy acids are not, or incompletely, sorbed from these samples on the pre-column or, more likely, that they are sorbed on the pre-column but not desorbed by the LC eluent. With the latter explanation, the surface of the polymeric sorbent is considered to become coated by humic substances during the preconcentration process, which now acts as a (modified) stationary phase extracting the analytes of interest. Since bonding to this humic phase is stronger than bonding to the polymeric phase, analyte recoveries will be low(er). Moreover, in such a situation conventional clean-up procedures will not be successful because, with the release of the matrix constituents, the analytes will also be released and recoveries will be poor. Therefore, a washing step with water containing a few per cent of acetonitrile will only be efficient if relatively clean samples such as tap and ground

Table 3 Schematic representation of methods used to determine phenoxy acids and bentazone

		Procedure			
	Parameter	A	B	C	D
LC	Eluent	Acetonitrile–water (30 +70)	Acetonitrile–water (30 +70)	Acetonitrile–water (30 +70)	A: acetonitrile–water (20 + 80) B: acetonitrile–water (40 + 60)
	Elution	Isocratic	Isocratic	Isocratic	Gradient (see Table 2)
	Buffer	No	Low-UV PIC A reagent	0.0125 mol l^{-1} borate	0.0125 mol l^{-1} borate
	pH	11	8.3	8.8	8.8
	Ion pair	0.01 mol l^{-1} TBA	0.005 mol l^{-1} TBA	0.003 mol l^{-1} TBA	0.003 mol l^{-1} TBA
Sample	pH	3	3	2.8	2.8
	Heart-cut	No	Yes	No	No
	Clean-up	100 µl acetonitrile–water (30 + 70), pH 3	1 ml 0.1 mol l^{-1} sodium hydroxide solution, pH 12.5	1 ml acetonitrile–water (4 + 96), pH 3	1 ml sodium hydroxide solution, pH 11

water are analysed and matrix constituents are not dominant. Rural water samples, however, need more drastic clean-up procedures such as high-pH washing.

High-pH *Clean-up*

The pre-column washing with up to 7 ml of 0.1 mol l^{-1} sodium hydroxide solution referred to above was followed by heart-cutting of the pre-column eluent; this caused a considerable decrease in the matrix interferences. The explanation then provided was that the humic substances are highly polar molecules which were easily eluted from the pre-column without dragging along the analytes of interest. However, this explanation needs further extension. Application of a high-pH solvent to the pre-column will result in a charged humic phase. This phase can still interact with the, also charged, phenoxy acids and the polymeric sorbent, the interaction being due to charge-transfer complexation between the aromatic styrene–divinylbenzene copolymer with its π-electron pairs and the electrophilic humic and phenoxy acids.[8] The binding energies of these interactions on polymeric pre-columns are higher than hydrophobic interactions,[9] which are the main retention forces if C$_{18}$-bonded silica is applied for the analysis of water for these compounds. This may also explain why such large volumes of high-pH washing solvents (7–10 ml) can be used without analyte breakthrough. The explanation also supports the results of Aiken *et al.*,[10] who reported that the order of breakthrough of fulvic acids on polymeric resins at pH 13 is the same as that at pH 2 (note that C$_{18}$-type phases show a different retention mechanism with humic-bound compounds passing through and non-bound compounds being retained[11,12]).

Desorption of the, now very polar, pre-column with the aqueous pH 8.8 eluent resulted in the quantitative and instantaneous release of all phenoxy compounds and the remaining humic material.

In summary, application of 1 ml of sodium hydroxide solution (pH 11) for clean-up and the linear LC gradient of procedure D for separation gave excellent baselines and good recoveries for all types of water samples studied. Fig. 3 shows a typical example of a tap and a rural-area water sample. Table 5 shows that the recoveries from the rural samples determined with gradient elution (procedure D) are much higher than those with the isocratic procedure C. The recoveries are essentially quantitative (80–110%) for all but one analyte (bentazone, 70–80%). In other words, the desired rapid release of the analytes is indeed effected by the introduction of the high-pH washing step.

Analytical Data

The limits of detection, set at three times the standard deviation ($n = 7$), which were determined using tap water spiked at the

Table 4 Analyte recoveries (%) from rural-area samples spiked at the 0.25 and 1.0 μg l^{-1} levels and determined with procedure C. Values corrected for blank values

	Sample 1		Sample 2		Sample 3	
Analyte	+0.25	+1.0	+0.25	+1.0	+0.25	+1.0
MCPA	68	74	60	53	62	64
MCPP	52	73	56	64	57	76
2,4-D	60	67	46	62	53	62
2,4-DP	56	75	47	64	52	75
MCPB/2,4-DB	76	85	58	82	61	80
2,4,5-T	42	107	64	63	102	62
2,4,5-TP	32	65	40	77	48	66
Bentazone	76	87	60	86	60	82

0.01–0.02 μg l^{-1} level, were 5–20 ng l^{-1} for all nine analytes (60 ml samples). The repeatability and recovery of the procedure were determined with tap water spiked at the 0.1 μg l^{-1} level. The recoveries invariably were > 83% with RSD values of 3–7% ($n = 7$). The reproducibility of the procedure was tested by analysing one freshly prepared sample each week (spiking level 0.1 μg l^{-1}), for seven weeks; the RSD values were 2–10%.

The method was also tested by spiking several samples from a rural area at three levels, 0.25, 0.5 and 1.0 μg l^{-1}. The samples were analysed in our laboratory with the optimized SPE–LC–UV procedure D and with FIA–MS–MS. The sample set was also analysed by a contract agency which used a GC–MS procedure. Table 6 shows that the present procedure works well at all levels with mean recoveries > 80%. At the 0.25 μg l^{-1} level, the recovery for some of the compounds is lower; however, these recoveries are comparable with the results of the other procedures. The precision of the method (reference material from the contract laboratory at 0.2 μg l^{-1}) is excellent with recoveries of 97–109% and RSDs of 4–6% ($n = 5$). In general, the SPE–LC–UV results compare well with those from the FIA–MS–MS procedure (in which an internal standard is used) at all levels tested, whereas the GC–MS results were
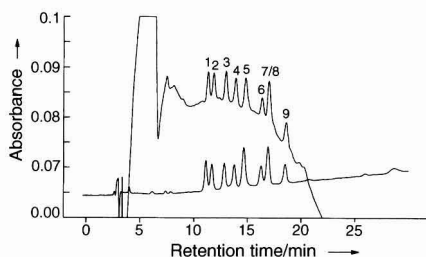
Fig. 3 SPE–LC–UV of acid herbicides after preconcentration of 60 ml of rural (top) and tap (bottom) water spiked with 0.25 μg l^{-1} of each component, using procedure D. System: 10 × 2 mm id pre-column packed with 20 μm PLRP-S, 250 × 4.6 mm id analytical column packed with 5 μm PLRP-S; UV detection, 232 nm. For gradient elution conditions, see Table 2. Peaks: 1, MCPA; 2, 2,4-D; 3, MCPP; 4, 2,4-DP; 5, bentazone; 6, 2,4,5-T; 7/8, MCPB/2,4-DB; 9, 2,4,5-TP.

Table 5 Analyte recoveries (%) from rural-area samples spiked at the 1.0 μg l^{-1} level and determined with procedures C and D. Values corrected for blank values

		Sample No.				
Analyte	Procedure	1	2	3	4	5
MCPA	C	50	66	72	64	76
	D	85	79	83	91	78
MCPP	C	85	91	84	88	73
	D	106	83	103	98	95
2,4-D	C	62	59	54	61	54
	D	91	78	86	95	83
2,4-DP	C	79	85	80	80	76
	D	105	80	112	101	101
MCPB/2,4-DB	C	89	87	64	87	86
	D	95	76	100	95	76
2,4,5-T	C	86	75	67	85	–*
	D	87	92	75	87	89
2,4,5-TP	C	88	90	–*	88	81
	D	110	81	–*	108	120
Bentazone	C	58	65	55	65	51
	D	70	84	77	71	77

* – Not determined.

Table 6 Recovery and precision, expressed as RSD, at 0.2 μg l⁻¹ and mean results (μg l⁻¹) for phenoxy acids and bentazone spiked at 0.25, 0.5 and 1.0 μg l⁻¹ in four rural-area samples and determined with FIA–MS–MS (A), SPE–LC–UV (B) and GC–MS (C). Values corrected for blank values

Analyte	Recovery (%)	RSD (%)	Spike 1.0 μg l⁻¹			Spike 0.5 μg l⁻¹			Spike 0.25 μg l⁻¹		
			A	B	C	A	B	C	A	B	C
MCPA	104	5.9	0.79	0.94	0.78	0.39	0.42	0.39	0.19	0.18	0.21
MCPP	101	3.3	0.79	0.73	0.82	0.43	0.42	0.45	0.21	0.20	0.22
2,4-D	102	6.2	0.98	0.90	0.58	0.50	0.49	0.36	0.23	0.20	0.18
MCPB	–*	–	0.63	–	0.42	0.34	–	0.24	0.17	–	0.14
2,4-DP	97	4.3	0.83	1.03	0.71	0.45	0.50	0.36	0.30	0.26	0.21
2,4-DB	109	4.9	0.78	0.94	0.32	0.46	0.49	0.18	0.14†	0.20	0.15‡
2,4,5-T	99	4.1	1.05	0.84	0.37	0.50	0.44	0.23	0.23	0.19	0.16
2,4,5-TP	104	5.8	0.79	0.87	0.52	0.42	0.50	0.31	0.32	0.28‡	0.19
Bentazone	109	4.0	0.72	0.66	0.24	0.41	0.43	0.14	0.20	0.17	0.13‡

* Not determined. † Not detected in two samples; average for two samples. ‡ Not detected in one sample; average for two samples.
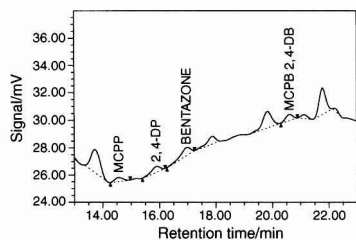
Fig. 4 SPE–LC–UV of 60 ml of rural water using procedure D. For conditions, see Fig. 3.

sometimes disappointing, probably owing to low conversion yields during derivatization.

Routine

Procedure D has been in use for about 2 years and is one of the ISO 9001/9002 methods in our laboratory. About 100 samples are analysed each year and the robustness of the procedure turned out to be excellent.

Fig. 4 shows an example of an SPE–LC–UV trace from a rural water sample. In this sample, four compounds are detected at concentrations of 0.05–0.1 μg l⁻¹. From Fig. 4, it is clear that at this level these compounds are readily detected, owing to the improved clean-up of the pre-column.

Conclusions

Two previously reported procedures for the trace-level determination of phenoxy acid herbicides and bentazone were evaluated and the conditions changed in order to improve the practicability for a variety of water samples. The introduction of an LC gradient instead of isocratic elution caused a less fluctuating baseline, which resulted in improved detection limits. Lowering the buffer salt and ion-pair concentrations helped to prolong the lifetime of the LC system.

Washing the pre-column with water containing 4% acetonitrile turned out to be effective and reliable only if relatively clean samples were analysed. Washing the pre-column with a high-pH solution, which induces the formation of charge-transfer complexes between the humic phase and the polymeric sorbent, turned out to be a much more powerful option. The compounds of interest and the remaining humic constituents are instantaneously released from this phase on introducing the LC eluent. The analyte recovery is now satisfactory (>70%) even for samples with a high humic content. The repeatability and reproducibility of the total analytical procedure are good and detection limits for 60 ml samples are as low as 5–20 ng l⁻¹. The results obtained for spiked rural-area samples with the present SPE–LC–UV procedure turned out to be essentially the same as those with a (much more expensive) FIA–MS–MS procedure and at least as good as those with a conventional GC–MS procedure, which has the disadvantage of requiring derivatization.

References

1 Geerdink, R. B., van Balkom, C. A. A., and Brouwer, H.-J., *J. Chromatogr.*, 1989, **481**, 275.
2 Geerdink, R. B., Graumans, A. M. B. C., and Viveen, J., *J. Chromatogr.*, 1991, **547**, 478.
3 Geerdink, R. B., Kienhuis, P. G. M., and Brinkman, U. A. Th., *Chromatographia*, 1994, **39**, 311.
4 van de Merbel, N. C. F., Lagerwerf, M., Lingeman, H., and Brinkman, U. A. Th., *Int. J. Environ. Anal. Chem.*, 1994, **54**, 105.
5 Vera-Avila, L. E., Padilla, P. C., Hernandez, M. G., and Meraz, J. L. L., *J. Chromatogr. A*, 1996, **731**, 115.
6 Ballinova, A., *J. Chromatogr. A*, 1996, **728**, 319.
7 Pijlman, L., *Technical Report*, RIZA, Lelystad, 1991.
8 LeCloire, P., Lelacheur, R. M., Johnson, J. D., and Christman, R. F., *Water Res.*, 1990, **24**, 1151.
9 McDowell, R. D., *LC–GC Int.*, 1994, **7**, 638.
10 Aiken, G. R., Thurman, E. M., Malcolm, R. L., and Walton, H. F., *Anal. Chem.*, 1979, **51**, 1799.
11 Gremm, T., Huber, S., and Frimmel, F. H., *Vom Wasser*, 1993, **80**, 109.
12 Landrum, P. F., Nihart, S. R., Eadle, B. J., and Gardner, W. S., *Environ. Sci. Technol.*, 1984, **18**, 187.

Extraction of Hexaconazole From Weathered Soils: a Comparison Between Soxhlet Extraction, Microwave-assisted Extraction, Supercritical Fluid Extraction and Accelerated Solvent Extraction

S. P. Frost[a], J. R. Dean[*a], K. P. Evans[b], K. Harradine[c], C. Cary[c] and M. H. I. Comber[d]

[a] *Department of Chemical and Life Sciences, University of Northumbria at Newcastle, Ellison Building, Newcastle upon Tyne, UK NE1 8ST*
[b] *Zeneca Specialties, P.O. Box 42, Hexagon House, Blackley, Manchester, UK M9 8ZS*
[c] *Zeneca Agrochemicals, Jealott's Hill Research Station, Bracknell, Berkshire, UK RG12 6EY*
[d] *Brixham Environmental Laboratory, Zeneca Ltd., Freshwater Quarry, Brixham, Devon, UK TQ5 8BA*

Extraction of hexaconazole residues which had been weathered over periods of time varying between 0 and 52 weeks was undertaken from two characterized soils. The various extraction techniques considered were Soxhlet extraction, microwave-assisted extraction, supercritical fluid extraction and accelerated solvent extraction. The results indicated that the physico-chemical properties of the soil are an important factor in the extraction of weathered residues of hexaconazole from soil. Overall the results obtained by accelerated solvent extraction were comparable to those obtained by Soxhlet extraction. Some matrix dependence of supercritical fluid extraction and microwave-assisted extraction was noted for the aged (52 week) sampled sandy loam soil. This effect was not evident for any of the extraction techniques using the sandy clay soil. The best precision was obtained for the automated accelerated solvent extraction system.

Keywords: Supercritical fluid extraction; microwave-assisted extraction; accelerated solvent extraction; hexaconazole; weathered soils

The need to change the nature of the solvent, the amount of solvent used and the time required to undertake an extraction from a matrix, whether it is soil, textiles or organic matter, has been the driving force behind the development of various techniques in recent years to challenge the long standing and proven method of Soxhlet extraction.[1–4] Substantial progress has been made towards developing improved techniques such as supercritical fluid extraction (SFE), microwave-assisted extraction (MAE) and accelerated solvent extraction (ASE). This paper reports the results found in a comparative study between these techniques for the extraction of the broad spectrum systemic triazole fungicide hexaconazole from weathered soil samples.

Supercritical fluid extraction has been the focus of much research for the preparation of samples from solid matrices. It is a popular method owing to the nature of the supercritical fluid CO_2, which is commonly used. Its critical parameters are low and it is inexpensive compared with HPLC-grade solvents, chemically inert and non-toxic. Many workers have used it for the extraction of non-polar and moderately polar environmental contaminants such as polycyclic aromatic hydrocarbons (PAHs),[5,6] although it has generally been found that the addition of a polar modifier, commonly methanol, is required for the extraction of more polar compounds and also to improve the recoveries of apolar compounds. This work has been extended to take into account the importance of increased temperature in

the extraction process. Yang *et al.*[7] found that increased temperatures, much higher than those normally encountered in SFE experiments, gave improved recoveries of PAHs from environmental samples.

The use of microwave energy to extract organic compounds from contaminated soil was first reported in 1986–87.[8,9] Microwave energy is non-ionizing radiation that causes molecular motion by migration of ions and rotation of dipoles, but does not induce changes in molecular structure. Rapid heating within an organic sample with a permanent dipole moment is brought about by alignment of the molecules, followed by their rapid return to disorder. Therefore, for the extraction process to be efficient, the sample obviously has to be contained in a solvent with a permanent dipole moment. In experiments carried out by several workers,[10–12] mainly on the extraction of PAHs, a solvent mixture of hexane–acetone (1 + 1) was used. Like SFE, MAE has created interest for the recovery of organic pollutants from environmental matrices because of the necessity to reduce organic solvent consumption and the speed of extraction. Typically, 30–40 ml of the organic solvent are used with extraction times of 5–20 min per sample. Since the analyte is typically contained within a closed vessel during extraction, the temperature of the solvent can be raised above its boiling point whilst under pressure. In addition, multiple sample extractions can be undertaken simultaneously under the same conditions.

More recently, ASE has emerged and is gaining in popularity.[13,14] This technique uses conventional liquid organic solvents at elevated temperatures (50–200 °C) and pressures [1500–2000 psi (1 psi = 6894.76 Pa)] to extract solid samples quickly and with smaller solvent volumes, typically 10–20 ml. The sample is enclosed in a high-pressure stainless-steel cell and, after an initial heating process, the sample is allowed to interact statically with the pressurized solvent for a predetermined time period, after which it is purged from the cell by compressed nitrogen into a collection vial. The whole process takes < 15 min per sample. As the system is fully automated, samples can be run sequentially.

Experimental

Weathered Canadian soil samples were supplied by Zeneca Agrochemicals (Bracknell, Berkshire, UK). These consisted of soil samples which had been collected at various times after hexaconazole application. Two soil types were evaluated. Each soil sample was air dried for 48 h and sieved through a 2–3.5 mm sieve prior to storage at −18 °C. Each soil was collected at various times after hexaconazole application and stored until

required. Soil A was collected over 0, 1 and 52 weeks, corresponding to soils A1, A2 and A3, respectively, and soil B was collected over 1 and 52 weeks, corresponding to soils B2 and B3, respectively.

Extraction Procedures

The levels of hexaconazole in each soil were quantified initially by Soxhlet extraction. Amounts of 40 g of soil were weighed into a 25×100 mm extraction thimble, 80 ml of acetonitrile–water $1 + 1$ were placed in a round-bottomed flask and the extraction was carried out for 6 h. Each extract was diluted with 2 ml of glass distilled water and partitioned into 5 ml of dichloromethane, reduced to dryness and re-diluted in 1 ml of dichloromethane. Samples were transfered on to dichloromethane (DCM) pre-wetted silica ISOLUTE columns (International Sorbent Technology, Hengoed, Mid-Glamorgan, UK), washed with DCM–MeOH $(95 + 5)$ (2 ml), and eluted with DCM–MeOH $(95 + 5)$ (2.5 ml). The eluate evaporated to dryness and re-diluted in acetone–hexane $(20 + 80)$ for subsequent analysis.

Supercritical fluid extraction was carried out on a Jasco (Tokyo, Japan) SFE instrument which possesses a second pump for modifier addition and a back-pressure regulator (BPR), which allows independent control of the extraction pressure. SFC-grade CO_2 purchased from Air Products (Sunderland, UK) was combined with HPLC-grade methanol (HiPerSolv, BDH Laboratory Supplies, Poole, Dorset, UK). The optimum conditions for extraction were as follows: pressure, 250 kg cm^{-2} (1 kg cm^{-2} = 98 066 Pa); temperature, 55 °C; proportion of methanol modifier, 20%; and extraction time, 20 min. These conditions were determined using laboratory slurry spiked soils.[15] However, as slurry spiked samples may not relate to weathered soil samples, the effects of extraction time were evaluated further. The flow rate was maintained at 2 ml min^{-1} and the pump head was cooled by means of a re-circulating coolant. A sample of approximately 4 g was accurately weighed into a stainless-steel extraction cell and placed inside the oven, where it was allowed to equilibrate to the set temperature for 5 min. Next the cell was filled with the supercritical CO_2 and methanol modifier *via* the pumps and allowed to interact statically with the analyte–matrix for a further 5 min with the

pumps switched off. After this, the pumps were restarted and the dynamic period was initiated for the determined period. The extract was collected by inserting the end of the BPR through a PTFE-lined septum into a collection vial containing a small volume of methanol (5 ml). Depressurized samples were vented through a cyano-bonded solid-phase extraction (SPE) cartridge (Varian, Walton-on-Thames, UK), pre-wetted with methanol. Upon completion of the extraction, the cartridge was back-flushed with 2×2 ml of methanol, then 1 ml of 1 ppm internal standard (UK-46,253, Pfizer Central Research, Kent, UK) was added to each extract. Soil samples (A1–A3) were subjected to a pre-chromatographic clean-up using C_{18} (Phase Separations, Queensferry, Clwyd, UK) SPE cartridges, pre-wetted with methanol, to remove largely non-polar contaminants. The cartridge was eluted with 5 ml of methanol and filtered through 0.2 µm Acrodiscs (Phase Separations). Samples B2 and B3 were filtered using 0.2 µm Acrodiscs only. Each sample was heated to 45 °C in a water-bath and reduced in volume to 1 ml under a stream of compressed air.

Microwave-assisted extraction was carried out using a Milestone 1200 Mega unit (Milestone, Rome, Italy). Soil samples (5 g) were accurately weighed into the Teflon liner of the extraction vessel and 30 ml of acetone (analytical-reagent grade, Rathburn, Walkerburn, UK) added. The vessels were sealed and extractions were carried out at 115 °C at 1000 W for 15 min. After extraction, the vessels were allowed to cool to 40 °C, typically taking 30 min, before opening. The contents were filtered through a size 4 sintered glass filter and 1 ml of internal standard (in acetone) was added. All soil samples were subjected to a pre-chromatographic clean-up using C_{18} (Phase Separations) cartridges, pre-wetted with methanol, to remove largely non-polar contaminants. The cartridge was eluted with 5 ml of methanol and then filtered through 0.2 µm Acrodiscs (Phase Separations). Finally, the filtered sample was reduced in volume to 1 ml.

Accelerated solvent extraction was carried out using an ASE 200 system (Dionex, Camberley, Sussex, UK). Acetone (AnalaR) was used as the solvent to implement the extractions. Samples of 5 g of the soils were weighed into the stainless-steel extraction cells (11 ml capacity) and the dead volume was filled with pre-cleaned sand (Dionex). After temperature equilibration (5 min), extraction was carried out at 2000 psi at 100 °C for 10 min then 1 ml of 5 ppm internal standard was added and the

Table 1 Extraction of hexaconazole from aged soil samples.* All values in mg kg^{-1}

Soil	No. of weeks after application of hexaconazole	Soxhlet extraction†	Supercritical fluid extraction	Microwave-assisted extraction	Accelerated solvent extraction
A1, sandy loam soil	0	0.14	Mean 0.074 RSD 7.4% $n = 5$	Mean 0.080 RSD 8.1% $n = 4$	Mean 0.124 RSD 3.8% $n = 5$
A2, sandy loam soil	1	0.12	Mean 0.087 RSD 5.4% $n = 4$	Mean 0.104 RSD 7.8% $n = 4$	Mean 0.127 RSD 4.4% $n = 6$
A3, sandy loam soil	52	0.07	Mean 0.034 RSD 7.2% $n = 4$	Mean 0.035 RSD 23.0% $n = 4$	Mean 0.093 RSD 1.8% $n = 6$
B2, sandy clay soil	1	0.14	Mean 0.119 RSD 10.1% $n = 4$	Mean 0.134 RSD 14.7% $n = 4$	Mean 0.136 RSD 1.9% $n = 6$
B3, sandy clay soil	52	0.08	Mean 0.072 RSD 8.4% $n = 4$	Mean 0.073 RSD 4.6% $n = 4$	Mean 0.070 RSD 3.4% $n = 6$

* All soils taken from a depth of 0–5 cm. Sandy loam soil: 5.7% organic matter; 81% sand; 8% silt; 11% clay and pH 7.4. Sandy clay soil: 1.5% organic matter; 53% sand; 25% silt; 22% clay and pH 8.3. † Typical RSD < 15%.

samples were reduced to 1 ml before being filtered through 0.2 μm Acrodiscs only.

Chromatographic Analysis

MAE and ASE samples were analysed using a Fisons (Crawley, Sussex, UK) Model 8000 gas chromatograph equipped with an electron capture detector. The following chromatographic conditions were found to be suitable for the analysis: a 1 μl sample was injected, on-column, on to a 60 m × 0.25 mm id DB1 column with a 0.25 μm film thickness. The oven temperature was ramped from 70 to 280 °C at 35 °C min^{-1} and held at 280 °C for 14 min, with a helium flow rate of 2.0 ml min^{-1}. Calibration curves were prepared with standards of 0.05, 0.1, 0.2, 0.5 and 1.0 ppm, giving correlation coefficients of 0.9966 (ASE) and 0.9985 (MAE).

SFE samples were analysed with a Varian Star 3400 gas chromatograph equipped with an electron capture detector. Volumes of 1 μl were injected *via* a split–splitless injector on to a 60 m × 0.25 mm id DB5 column with a 0.25 μm film thickness. The oven temperature was ramped from 80 to 270 °C at 40 °C min^{-1} and held at 270 °C for 14 min. A calibration

Fig. 1 Gas chromatogram of hexaconazole after microwave-assisted extraction: (*a*) prior to and (*b*) after C$_{18}$ SPE clean-up.

curve was prepared with standards as above, with a correlation coefficient of 0.9996.

Results and Discussion

Time studies were carried out for SFE extractions over 20, 40 and 60 min using soil A3. The mean recoveries ($n = 2$) were 0.045, 0.047 and 0.044 mg kg^{-1} for 20, 40 and 60 min extraction, respectively. As similar recoveries were achieved over all time periods, the extraction time was maintained at 20 min for speed of analysis. The results from multiple extractions from ASE, SFE and MAE were compared with those obtained using Soxhlet extraction (Table 1). For the sandy clay soil with an organic matter content of 1.5% (B2 and B3) good recoveries were achieved for all three methods compared with the recoveries obtained using Soxhlet extraction. However, consideration of the RSD values reveals that ASE generally produced far superior results on both the 1 and 52 week samples. This is probably due to the use of a fully automated system where sample handling is kept to a minimum.

However, the results obtained for the soil with a higher organic matter content (5.7%), the sandy loam soil (soil samples A1–A3), showed greater variation between recoveries. SFE gave recoveries approximately 50% of those achieved by Soxhlet extraction, although the RSD remained within acceptable levels (5 and 7%). Similar results were achieved with MAE, but the RSD for the 52 week sample was 23.0%, indicating the poor repeatability. ASE, however, gave recovery data in good agreement with the Soxhlet extraction data at all levels of weathering with RSD values ranging between 1 and 4%.

In terms of the actual extract produced from each technique, ASE produced the cleanest chromatographic sample, with no interfering or co-eluting peaks. In contrast, MAE samples produced a far 'dirtier' extract, which required pre-chromatographic clean-up. The interference was a single large tailing peak (retention time $t_R = 7.0$ min) which co-eluted close to the peak of interest (hexaconazole, $t_R = 8.5$ min) and produced rapid degeneration of the column efficiency (see, for example, Fig. 1). SFE extracted samples required the pre-chromatographic clean-up of the high organic content soils only, to allow the analyte signal to be resolved, as many peaks were eluted from these samples.

Conclusions

The nature of the analyte–matrix interaction is dependent on the composition of the soil, although its ability to be recovered is dependent upon the extraction conditions and the efficiency of the system. MAE can handle several samples simultaneously and is rapid, although long cool-down periods are required and poor recoveries were achieved for high organic content soils. SFE gave results similar to MAE without the need for several sample handling stages, although actual extraction periods were longer with this method. ASE gave good recoveries for all sample types used in this study, with rapid extraction times, and was the only technique to give results comparable to those obtained using the conventional Soxhlet extraction technique.

References

1   van der Velde, E. G., de Haan, W., and Liem, A. K. D., *J. Chromatogr.*, 1992, **626**, 135.
2   Lopez-Avila, V., Young, R., and Teplitsky, N., *J. AOAC Int.*, 1996, **79**, 142.
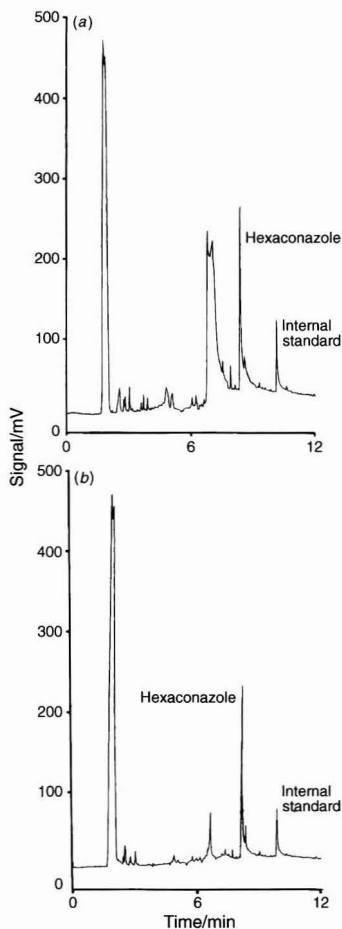
3   David, M. D., and Seiber, J. N., *Anal. Chem.*, 1996, **68**, 3038.
4   Bowadt, S., Johansson, B., Wunerli, S., Zennegg, M., de Alencastro, L. F., and Grandjean, D., *Anal. Chem.*, 1995, **67**, 2424.
5   Barnabas, I. J., Dean, J. R., Hitchin, S. M., and Owen, S. P., *Anal. Chim. Acta*, 1994, **291**, 261.
6   Barnabas, I. J., Dean, J. R., Hitchin, S. M., and Owen, S. P., *J. Chromatogr. Sci.*, 1994, **32**, 547.
7   Yang, Y., Gharaibeh, A., Hawthorne, S. B., and Miller, D. J., *Anal. Chem.*, 1995, **67**, 641.
8   Ganzler, K., Salgo, A., and Valko, K., *J. Chromatogr.*, 1986, **371**, 299.
9   Ganzler, K., and Salgo, A., *Z. Lebensm.-Unters. Forsch.*, 1987, **184**, 274.
10 Barnabas, I. J., Dean, J. R., Fowlis, I. A., and Owen, S. P., *Analyst*, 1995, **120**, 1897.

11 Lopez-Avila, V., Benedicto, J., Charan, C., and Young, R., *Environ. Sci. Technol.*, 1995, **29**, 2709.
12 Lopez-Avila, V., Young, R., Benedicto, J., Ho, P., and Kim, R., *Anal. Chem.*, 1995, **67**, 2096.
13 Dean, J. R., *Anal. Comm.*, 1996, **33**, 191.
14 Richter, B. E., Jones, B. A., Ezzel, J. L., and Porter, N. L., *Anal. Chem.*, 1996, **68**, 1033.
15 Frost, S. P., Dean, J. R., Evans, K. P., Harradine, K., Cary, C., and Comber, M. H. I., in preparation.

Speciation Analysis of Chromium Using Cryptand Ethers

Elena Andrés García* and Domingo Blanco Gomis

Departamento de Química Física y Analítica, Facultad de Química, Universidad de Oviedo, Oviedo, Spain

The speciation analysis of chromium was studied using sequential solvent extraction of Cr^{III} and Cr^{VI} (previously reduced to Cr^{III}) with cryptand 2.2.1 as the ligand and eosin as a counter ion, in combination with spectrofluorimetry. A linear working range from the detection limit (1 ng ml^{-1}) to 150 ng ml^{-1} of chromium was obtained. The proposed method was successfully applied to the determination of Cr^{III} and Cr^{VI} in sea-water and chromium in certified coal samples.

Keywords: Chromium; speciation; cryptand ether; ion-pair extraction; spectrofluorimetry

Chromium is one of the essential trace elements in the human body; it appears to play a role in the metabolism of glucose and certain lipids, mainly cholesterol.[1–3] However, nowadays the main reason for studying this element lies in its toxic nature. The biochemical toxicology of different compounds varies considerably with the chemical form and entrance route into the body. Thus, Cr^{VI} compounds are approximately 100 times more toxic than Cr^{III} salts, owing to their high oxidation potential and the ease with which they penetrate biological membranes. Consequently, it is of great importance in environmental studies and studies of food contamination to determine the level and oxidation state of chromium since excessive amounts of this element, particularly in the more toxic Cr^{VI} form, are detrimental to health as this element may be involved in the pathogenesis of certain diseases such as lung and gastrointestinal cancers. Speciation studies of chromium have been carried out in natural waters,[4] crayfish,[5] galvanic waste waters,[6] drilling fluid wastes,[7] activated sludge,[8] tannery effluent,[9] welding dust,[10] waste waters,[11] etc. In the environment, air chromium particulates play a role in the oxidation of sulfur dioxide and the formation of acidic aerosols involved in global acid rain.[12]

The most common techniques for the determination of chromium are AAS employing flame or electrothermal atomization and ICP-AES, and more recently ICP-MS, although by themselves they only yield information on total concentrations. This is the reason why speciation analysis of Cr has already been investigated by means of the application of different techniques, such as precipitation, adsorption, solvent extraction and chromatography.[6,13–15]

One approach to this problem is to use macrobicyclic compounds (cryptand ethers) with cavities of the right size to accommodate the chromium metal cation.[16] Cryptand ether 2.2.1 was used here. Although the product is not fluorescent, direct fluorimetric determination of the cation is possible by solvent extraction of the ion-pair formed by the cryptate complex and a highly fluorescent organic anion.

In this paper, we describe the sequential extraction and spectrofluorimetric determination of trace amounts of Cr^{III} and Cr^{VI} (previously reduced to Cr^{III} with ethanol) by using cryptand 2.2.1 and eosin as a counter ion. The proposed method was successfully applied to the speciation analysis of chromium in sea-water and for the determination of chromium in samples of coal certified by the Community Bureau of Reference.

Experimental

Reagents

All reagents were of analytical-reagent grade. Doubly distilled and de-mineralized water was used throughout.

Stock standard solutions of Cr^{III} and Cr^{VI} (1 g l^{-1}) were prepared by dissolving chromium sulfate and potassium dichromate in acidified water. All working standard solutions were freshly prepared by dilution of the appropriate stock standard solution with acidified water.

Solutions of cryptand 2.2.1 (10^{-4} M) were prepared by dissolving the commercial product (Kryptofix; Merck, Darmstadt, Germany) in water to which perchloric acid had been added and through which argon had been passed in order to remove carbon dioxide and to avoid carbonation of the cryptand. The solutions were stored in polyethylene flasks. Acidic eosin solutions (10^{-4} M) were prepared by, dissolving pure eosin (synthesized by reaction of Br^-–BrO_3^- with fluorescein in acidified aqueous acetone[17]) in alkaline water (pH 8–9). Buffer solutions were prepared with 0.5 or 0.1 M TRIS-HCl.

Apparatus

Fluorescence intensity measurements and spectra were obtained with a Perkin-Elmer (Norwalk, CT, USA) LS-5 spectro-fluorimeter equipped with a Model 3600 data station. The excitation and emission slit widths were both 2.5 nm and standard 1 cm silica cells were used. The temperature of the sample cell was kept constant within ±1 °C by using a Julabo Paratherm III thermostat system. A WTW-D812 Model 319, pH meter, calibrated against Radiometer (Copenhagen, Denmark) buffers, was used for pH measurements of the aqueous phase.

Procedure

Pipette standard Cr^{III} and Cr^{VI} solutions into a 10 ml centrifuge tube, add 0.3 ml of the cryptand 2.2.1 stock standard solution, 1 ml of buffer solution and 0.3 ml of eosin solution and dilute to 5 ml with water (final pH 9 ± 0.1). After mixing, add 5 ml of 1,2-dichloroethane and extract the Cr^{III} complex by shaking for 10 min. Allow the phases to separate and transfer 4 ml of the aqueous phase into a centrifuge tube, add 0.3 ml of ethanol to reduce Cr^{VI} to Cr^{III} and 0.3 ml of the cryptand 2.2.1 stock standard solution and dilute to 5 ml with water. After mixing, add 5 ml of 1,2-dichloroethane and extract the new Cr^{III} complex by shaking for 10 min. The organic phases were previously equilibrated with buffered aqueous phase. Measure the fluorescence intensity, I_f, of the 1,2-dichloroethane phases at 549 nm (excitation wavelength 534 nm).

Run a reagent blank in the same way and subtract its fluorescence from that of the sample.

For the analysis of coal, 2 g of the sample were first pre-treated by adding a small volume of NaOH. Combustion then

took place in an oxygen bomb, and finally the resulting sample was diluted to 50 ml with water.

Results and Discussion

Optimization of Extraction Conditions

Various acidic fluorescent dyes of the fluorescein group [fluorescein, dichlorofluorescein, tetrabromofluorescein (eosin), tetraiodofluorescein (erythrosin) and tetrachlorotetrabromofluorescein (Rose Bengal)] as counter ions in different extraction solvents (toluene, chlorobenzene, carbon tetrachloride, chloroform, 1,2-dichloroethane and dichloromethane) were tested. The results showed that the system eosin–1,2-dichloroethane gave the best fluorescence signal.

Fig. 1 shows the excitation and emission spectra of the blank and the complex extracted by following the general procedure. The excitation spectrum has a maximum at 534 nm and the emission maximum is at 549 nm. The spectra were not corrected for variations in the emission characteristics of the lamp or for the response characteristics of the photomultiplier. A spectral bandpass of 2.5 nm was used for both absorption and fluorescence.

The ion-pair extraction of chromium has a complicated dependence on pH, owing to the basic nature of the cryptand, the dissociation of eosin and hydrolysis of the cation. Taking into account the pK_a values of mono- and diprotonated cryptand 2.2.1,[18] the stability constant of the chromium hydroxide complex[19] and the pK_a values of eosin,[20] it can be inferred that the ion pair would be extractable from an alkaline medium.

Fig. 2 shows the effect of pH in the range 6–12 on the fluorescence intensity for 0.1 µg ml^{-1} of chromium. The

fluorescence is maximum with extraction at pH 8–10 and pH 9 (TRIS buffer) was selected for subsequent assays.

Reagent Concentrations

The effect of the variation of the cryptand 2.2.1 and eosin concentrations on the fluorescence signal of the extract was studied for a fixed amount (0.1 µg) of chromium and a single extraction step. Fig. 3 shows that the optimum concentrations are not less than 3.0×10^{-6} M cryptand 2.2.1 (for a fixed eosin concentration of 3.8×10^{-5} M) and 3.0×10^{-6} M eosin (with a fixed cryptand 2.2.1 concentration of 3.8×10^{-5} M). The molar ratio of cryptand 2.2.1 to chromium was 2 and that of eosin to chromium was 1.5. Therefore, a stoichiometry 2 : 4 : 3 (metal : ligand : counter ion) was established, where the metal cation was located between two macrobicyclic rings with a sandwich type structure. The eosin to chromium ratio must be 3 : 2 so as to neutralize the charge.

Rate of Extraction and Stability of the Extract

The first extraction of Cr^{III} is maximal after a 3 min shaking time. The fluorescence produced in the organic layer remains constant for at least 24 h under normal laboratory conditions.

The rate of the second extraction is slower owing to the reduction of Cr^{VI} to Cr^{III} by ethanol. In fact, the fluorescence signal reaches a maximum after a 10 min shaking time.

In the extraction procedure, it is important to add the cryptand 2.2.1 before pH adjustment. The recommended order is chromium, cryptand 2.2.1, eosin and TRIS buffer solution.

Effect of Ionic Strength

The influence of ionic strength, I (from 0.01 to 0.25 M, adjusted with TRIS), is shown in Fig. 4. The fluorescence intensity of the organic phase, and therefore the extraction of the chromium ion pair, decrease quickly at $I > 0.1$. Preliminary results showed that increasing the ionic strength promotes poorer association of the metal–cryptand complex with the eosinate anion and hence extraction.

Calibration Graph, Detection Limit and Precision

The calibration graph was linear from the detection limit up to 150 ng ml^{-1} of chromium. The detection limit (evaluated as the
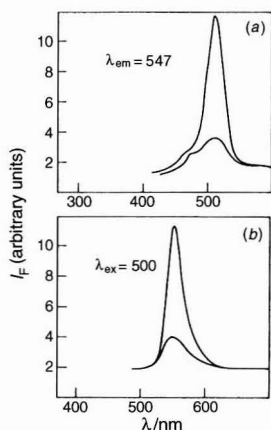
Fig. 1 (a) Excitation and (b) emission spectra of the chromium ion-association complex and blank.
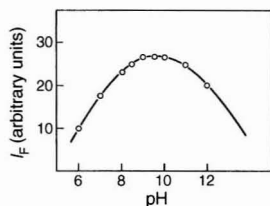
Fig. 2 Variation of the fluorescence intensity of the chromium ion-association complex with pH.
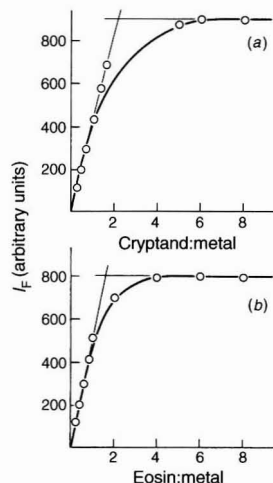
Fig. 3 Influence of the concentration of (a) cryptand 2.2.1 and (b) eosin on fluorescence intensity.

concentration corresponding to three times the standard deviation of the blank signal) was 1 ng ml⁻¹. The RSD, evaluated by repeated analysis of standards containing 100 ng ml⁻¹, was 1.6%.

Effect of Foreign Ions

To evaluate the selectivity attainable, chromium was extracted in the presence of a number of foreign ions capable of forming stable complexes with cryptand 2.2.1 and certain common anions. The tolerance limit was set as the concentration of foreign ions that produced a variation in the apparent recovery of 100 ng ml⁻¹ of chromium greater than three times the RSD (*i.e.*, variations > ±5%).

The results are summarized in Table 1. It can be seen that large amounts of alkali metal ions do not interfere. Among the rest of the cations tested, thallium can be tolerated up to a 10-fold molar excess, silver, zinc and lead up to five-fold, calcium and mercury up to two-fold and cadmium and strontium only up to one-fold.

The interference of cadmium and strontium cations could be reduced by increasing the ionic strength above 0.1 M since, in previous work,[21,22] we have observed a strong decrease in the extraction of strontium and cadmium with increase in the ionic strength of the aqueous phase.

The common anions chloride, sulfate, phosphate and nitrate had a negligible effect even for amounts above 10⁴ times that of chromium.

Determination of Chromium in Real Samples

The proposed method was tested by applying it to the determination of chromium in sea-water and coal (obtained from the combustion of pulverized coal). The coal samples had been certified by the Community Bureau of Reference (BCR).

The effect of sea-water matrices, collected at two points (near and far from a river mouth) on the beach at Gijón (northern

Spain), on the determination of low levels of chromium by the proposed method was investigated by recovery studies. Sea-water samples were spiked with 10, 20 and 40 μg l⁻¹ of Cr^{III} and Cr^{VI} and analysed using the proposed method. As can be seen in Table 2, neither of the samples is polluted with Cr^{VI}. However, both samples are polluted with Cr^{III}, and the sea-water sample collected near the river mouth has a greater amount (25 μg l⁻¹) of Cr^{III}. The recoveries ranged between 91.4 and 106.4%, showing acceptable precision.

For the analysis of coal, a portion of the coal sample solution (2.5 ml) was extracted according to the proposed procedure. The results, given in Table 3, are in good agreement with the certified value.

Conclusion

The sensitivity, selectivity and applicability that can be achieved by using cryptands in the speciation of chromium have been demonstrated. Sequential ion-pair extraction was applied to the separation of the species in real samples, so that the

Table 1 Effect of foreign ions (M) on the determination of 100 μg l⁻¹ of chromium

Cation or anion	M : Cr molar ratio	Apparent recovery (%)
Li⁺	1000	100.3
Na⁺	1000	98.2
K⁺	1000	102.1
Cs⁺	1000	99.6
NH₄⁺	500	105.6
Tl⁺	10	95.7
Ag⁺	5	98.2
Mg²⁺	1000	96.4
Ca²⁺	2	99.1
Sr²⁺	1	94.8
Ba²⁺	500	97.7
Cu²⁺	10	99.3
Pb²⁺	5	103.4
Cd²⁺	1	105.3
Hg²⁺	2	95.6
Ni²⁺	500	96.9
Zn²⁺	5	94.9
Co²⁺	1000	100.6
Fe³⁺	100	100.1
Al³⁺	1000	98.8
NO₃⁻	20000	101.7
Cl⁻	20000	100.6
PO₄³⁻	10000	98.6
SO₄²⁻	10000	95.7
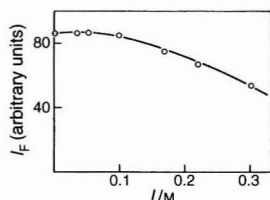
Fig. 4 Effect of ionic strength on fluorescence intensity.

Table 2 Recovery studies of Cr^{III} and Cr^{VI} added to two sea-water samples

Sea-water sample	Chromium species	Concentration in water/μg l⁻¹	Concentration added/μg l⁻¹	Found/μg l⁻¹	Recovery (%)
A	Cr^{III}	25.0	10	34.5	95.0
			20	46.3	106.4
			40	66.3	104.9
B		15.1	10	24.7	96.0
			20	35.7	103.2
			40	54.8	99.3
A	Cr^{VI}	Not detected	10	9.1	91.4
			20	20.1	100.5
			40	40.7	101.6
B		Not detected	10	9.8	98.0
			20	20.0	100.0
			40	40.4	101.0

Table 3 Determination of Cr^{III} in BCR coal certified reference material

Coal sample	Cr^{III} concentration/ $\mu g\ g^{-1}$	
	Certified value	Proposed method
1	31.3 ± 2.0	34.3 ± 1.8
2	32.7 ± 1.7	35.4 ± 1.5

procedure described here can be used for speciation analysis of other elements if the extraction system is chosen adequately, since selectivity depends on the stability constants of the cryptate complexes and the nature of the counter ion and the solvent used for extraction.

References

1   Anderson, R. A., *Clin. Physiol. Biochem.*, 1986, **4**, 31.
2   Merian, E., and Geldmacher, R., *Metalle in der Umwelt, Verteilung, Analytik und Biologische Relevanz*, VCH,Weinheim, 1984.
3   Versieck, J., and Cornelis, R., *Trace Elements in Human Plasma or Serum*, CRC Press, Boca Raton, FL, 1989.
4   Crespon Romero, R. M., Yebra Biurrun, M. C., and Bermejo Barrera, M. P., *Anal. Chim. Acta*, 1996, **327**, 37.
5   Bundy, K., Millet, L., Bollinger, J., and Anderson, M., *FASEB J.*, 1966, **10**, 1007.
6   Andrle, C. M., Jakubowski, N., and Broekaert, J. A. C., *Spectrochim. Acta, Part B*, 1997, **52**, 189.
7   Ghode, R., Muley, R., and Sarin, R., *Chem. Speciation Bioavailability*, 1995, **7**, 133.
8   Imai, A., and Gloyna, E. F., *Water Environ. Res.*, 1996, **68**, 301.
9   Walsh, A. R., and Ohalloran, J., *Water Res.*, 1996, **30**, 2393.
10   Girard, L., and Huber, J., *Talanta*, 1966, **43**, 1965.
11   Pantsarkallio, M., and Manninen, P. K. G., *J. Chromatogr.*, 1996, **750**, 89.
12   Fifield, F. W., and Haines, P. J., *Environmental Analytical Chemistry*, Blackie, Glasgow, 1995.
13   Lopez, A., Rotunno, T., Palmisano, F., Passino, R., Tiravanti, G., and Zambonin, G., *Environ. Sci. Technol.*, 1991, **25**, 1262.
14   Hill, S. J., Bloxham, M. J., and Worsfold, P. J., *J. Anal. At. Spectrom.*, 1993, **8**, 499.
15   Jakubowski, N., Jepkens, B., Stuewer, D., and Berndt, H., *J. Anal. At. Spectrom.*, 1994, **9**, 193.
16   Lehn, J. M., and Sauvage, J. P., *J. Am. Chem. Soc.*, 1975, **97**, 6700.
17   Fompeydie, D., Onur, F., and Levillain, *Bull. Soc. Chim. Fr.*, 1982, II-5.
18   Dietrich, B., Lehn, J. M., and Sauvage, J. P., *Tetrahedron Lett.*, 1969, 2885.
19   Ringbom, A., *Complexation in Analytical Chemistry*, Alhambra, Madrid, 1979, p. 347. (Spanish translation).
20   Levillain, P., and Fompeydie D., *Anal. Chem.*, 1985, **57**, 2561.
21   Gomis, D. B., Alonso, E. F., García, E. A., and Abrodo, P. A., *Talanta*, 1989, **36**, 1237.
22   Blanco, D., Fuente, E., and Arias, P., *Microchim. Acta*, 1989, **14**, 59.

Correlation Between Inclusion Formation Constant and Distribution Coefficient in a Liquid–Liquid Extraction System Consisting of Hydrocarbon Solvents and Aqueous Dimethyl Sulfoxide Solutions of β-Cyclodextrin

Masaki Tachibana* and Nobutoshi Kiba

Department of Applied Chemistry and Biotechnology, Faculty of Engineering, Yamanashi University, Kofu, Yamanashi 400, Japan

Carbazole was used as a fluorescence probe for the investigation of the correlation between the apparent formation constant (K_f) for an inclusion complex of β-cyclodextrin (CD) and the distribution coefficient (K_d) on liquid–liquid extraction. Single batch extractions of carbazole were performed at 25 ± 1 °C from three types of hydrocarbon solvents into an aqueous dimethyl sulfoxide (DMSO) phase containing CD or nothing. Both the K_f and K_d values for carbazole can be determined simultaneously under the same conditions on the basis of the extraction data. A plot of log K_f *versus* log K_d gives a straight line in both extraction systems of heptane and dodecane, with good correlations (0.9996 and 0.9992) and similar slopes (−0.675 and −0.672). The experimental results obtained from the cyclohexane–aqueous DMSO system suggest that the hydrocarbon used as the organic phase competes with carbazole for complexation with CD. The linear relationship is embodied in the form of an empirical equation, log K_{fOB} = −0.673 log K_d + log (K_{fCR}/K_{fHY}), where K_{fOB} is the observed K_f value for a 1 : 1 carbazole–CD complex in the aqueous DMSO medium and K_{fCR} and K_{fHY} are the absolute K_f values in water for the carbazole– and hydrocarbon–CD complexes, respectively.

Keywords: Correlation; inclusion formation constant; distribution coefficient; liquid–liquid extraction; carbazole–β-cyclodextrin complexation

Cyclodextrins (CDs) are cyclic oligosaccharides joined via α-1,4-linkages of glucopyranose units into a cone-shaped torus. The most commonly used CDs are those containing six, seven and eight glucopyranose units, and are referred to as α-, β- and γ-cyclodextrins, respectively. These compounds and the related derivatives are well known for their ability to form guest–host inclusion complexes with a variety of molecules on the basis of spatial fitting. Such a stereoselective interaction plays an important role in analytical chemistry. The knowledge of the formation constant (K_f) for a given complex is necessary to predict and understand better the interaction between cyclodextrin and the guest. Therefore, the K_f values for various cyclodextrin complexes have been evaluated by a wide variety of analytical techniques, including spectroscopy,[1,2] chromatography,[3,4] capillary electrophoresis,[5,6] pulse polarography[7] and other methods.[8–11]

Several applications of CDs in extraction processes have also been reported.[12–14] In such cases, CDs are normally added to the aqueous phase on liquid–liquid extraction in order to enhance partitioning of organic compounds from the organic phase. Size selectivity of CDs is often observed in complex samples, especially among polycyclic aromatic compounds (PACs).[12,15] However, the effect of the additions has been little discussed in connection with the K_f values, and further with basic parameters on solvent extraction, such as the distribution ratio (D) and the distribution coefficient (K_d). The reason is probably the difficulty in determining these parameter values at the same time. In most studies, the application of CDs to extraction processes resulted in undesirable precipitation from the aqueous phase.

A previous investigation in our laboratory showed that a few PACs could be selectively extracted from a hydrocarbon phase into a water–dimethyl sulfoxide (DMSO) solution of β-cyclodextrin (CD) without the precipitation process.[16] In addition, the extraction technique was applied to the determination of the apparent K_f value for a 1 : 1 carbazole–CD complex in the aqueous DMSO medium.[17] We noted that in this technique not only K_f but also K_d can be measured at the same time and under the same conditions. Both values of K_f and K_d will provide significant information regarding equilibrium of an analyte in a liquid–liquid extraction system containing CDs. There have been a few reports relating the K_f value to the K_d value in order to elucidate the binding forces contributing to the interaction of CDs with organic substances.[18,19] However, the correlation between these two values has remained obscure because the K_d values were independently derived from extraction data without the interaction.

In the present paper, a reliable correlation between K_f and K_d was studied in three types of extraction systems consisting of three different hydrocarbons and aqueous DMSO media, using carbazole as an appropriate probe. Although a good linear relationship between log K_f and log K_d for carbazole in a heptane–aqueous DMSO extraction system was observed previously,[17] it was not within the scope of the previous study to confirm the relationship. In this work, the linearity of the log K_f *versus* log K_d plot was clearly demonstrated on the basis of extraction data for carbazole from both dodecane and heptane. Furthermore, the results from the cyclohexane system suggested the competitive CD complexation of carbazole with the hydrocarbon solvent. A plausible relationship between K_f and K_d was consequently proposed in the form of an empirical equation, based on some assumptions associated with these experimental results. We expect to find such a correlation between K_f and K_d for other species and/or extraction systems, although the findings obtained in our work may be limited to carbazole in hydrocarbon–aqueous DMSO two-phase systems. It will be worthwhile for the selective separation of complicated PAC samples to correlate the two equilibrium constants relating to the CD interaction and liquid–liquid distribution.

Experimental

Apparatus

Synchronous spectrofluorimetric measurements were performed on a Hitachi (Tokyo, Japan) Model 650-40 spectrofluorimeter equipped with a Model 056 recorder. A 150 W xenon

arc lamp was used as the excitation source and a 1.00 cm pathlength quartz cell as the measurement vessel. Both excitation and emission bandwidths were always set at 2.5 nm. All batch extractions were carried out using a Irie (Tokyo, Japan) TS shaker in an air-conditioned room at 25 ± 1 °C. Either 50 cm³ separating funnels or 15×160 mm test-tubes with well fitting ground glass stoppers were used for the extractions.

Chemicals

Carbazole was purified by zone melting after the removal of anthracene present as a main impurity with pre-treatments based on the Diels–Alder reaction with maleic anhydride.[20] β-Cyclodextrin of guaranteed-reagent grade was purchased from Tokyo Kasei Kogyo (Tokyo, Japan) and used as received. Dimethyl sulfoxide was purified by repetition of the sequential operations of freezing partially, discarding the remaining liquid and re-melting the available solid.[21] Heptane and cyclohexane were of analytical-reagent grade for fluorimetry (Kanto Chemical, Tokyo, Japan). Commercially available dodecane of guaranteed-reagent grade was further shaken with a mixture of concentrated sulfuric and nitric acid, washed with water, dried over anhydrous calcium chloride and finally passed through an activated alumina open column. Distilled water and ethanol were of analytical-reagent grade for HPLC (Kanto Chemical) and used as received.

Extraction Procedure

Three different stock standard solutions of carbazole were first prepared at a concentration of 500 mmol m⁻³ in three hydrocarbon solvents, heptane, dodecane and cyclohexane. Working standard solutions were obtained by dilution of these stock standard solutions with the corresponding hydrocarbons at three different carbazole concentrations, 5.0, 10 and 25 mmol m⁻³. Water–DMSO solutions of CD were prepared at eight consecutive concentrations in the range 0–10 mol m⁻³. In these preparations, CD was initially dissolved in a suitable amount of DMSO and the DMSO solution was diluted with distilled water to give a 10 mol m⁻³ CD concentration. The other CD solutions were then produced by diluting the 10 mol m⁻³ solution with the corresponding water–DMSO medium. The DMSO concentrations in these media ranged from 10 to 60% v/v.

Single batch extraction of carbazole was performed by shaking an aliquot (2–10 cm³) of the working solution with a suitable portion (1–16 cm³) of the CD solution for 3 min mechanically, either in a separating funnel or a test-tube with a tightly fitting glass stopper. In this extraction system the concentrations of carbazole in the two phases were almost unchanged after shaking for more than 1.5 min. Therefore, a shaking time of 3 min was adopted for rapid batch extractions. The separating funnels were used when the sum of the solution volumes was more than 11 cm³, but for smaller volumes the test-tubes were convenient. In the latter case, only the upper hydrocarbon layer to be measured was pipetted off, without discarding the bottom aqueous layer after the separation of the two phases. All extraction procedures were carried out in an air-conditioned room at 25 ± 1 °C after solutions and glassware had been placed in it for at least 30 min to ensure temperature equilibrium.

Synchronous Spectrofluorimetric Measurements

The synchronous scanning technique was applied to the fluorimetric measurements of carbazole in hydrocarbon solvents before and after extractions. On extraction from 5.0 mmol m⁻³ working standard solutions into various water–DMSO solutions of CD, synchronous fluorescence spectra of

the separated hydrocarbon layers were measured directly with a wavelength interval ($\Delta\lambda$) of 7 nm. The peak intensities at 337 nm in the spectra were obtained by the baseline method and the relative values were calculated by use of the intensity of a carbazole standard solution. The relative intensities were regarded as the fluorescence of carbazole remaining in the hydrocarbon phase and employed for calculating the distribution ratio (D) or distribution coefficient (K_d) for carbazole in the two-phase system. In such cases, a 5.0 mmol m⁻³ hydrocarbon solution of carbazole saturated with the corresponding water–DMSO medium was used for the measurement of the initial intensity, instead of the original 5.0 mmol m⁻³ solution. This is because the synchronous fluorescence intensities of carbazole in pure hydrocarbons decrease to a discernible extent owing to saturation with a trace amount of the water–DMSO medium. The medium-saturated hydrocarbon solutions of carbazole were prepared by adding 0.5 cm³ of the aqueous medium to 100 cm³ of the original solution, stirring the immiscible mixture vigorously and allowing it to clear on standing. The prepared 5.0 mmol m⁻³ carbazole solution was also used as the above-mentioned standard for evaluation of the relative synchronous fluorescence intensities.

When extractions were performed at higher carbazole concentrations, the separated hydrocarbon phases were diluted with ethanol prior to the measurements in order to ensure a linear relationship. In these cases, an aliquot (3 cm³ at 10 mmol m⁻³ and 2 cm³ at 25 mmol m⁻³ carbazole concentrations) of the hydrocarbon layer was pipetted into a calibrated flask (5 and 10 cm³, respectively) and diluted to the mark with ethanol. Synchronous spectral intensities of the resulting hydrocarbon–ethanol mixtures were measured at a peak at 343 nm with $\Delta\lambda = 7$ nm. As the standards, 6.0 and 5.0 mmol m⁻³ carbazole solutions in 40 and 80% v/v ethanol mixtures, respectively, with the corresponding hydrocarbons were used. These solutions were readily prepared by diluting the carbazole working standard solutions with ethanol. The calibration graphs for carbazole were linear in the concentration ranges 0–5.0 and 0–6.0 mmol m⁻³ using the three types of hydrocarbons and various hydrocarbon–ethanol mixtures.

Determination of K_f and K_d Values

Application of solvent extraction to the determination of the apparent formation constant for a 1:1 complex of carbazole with CD was detailed in a previous paper.[17] On extraction of carbazole from a hydrocarbon solvent into an aqueous CD medium, according to the proposed theory, the following two equations are applicable at the same time:

$$K_f = \frac{[CR-CD]_a}{[CR]_a [CD]_a} \qquad (1)$$

$$D = \frac{[CR]_a + [CR-CD]_a}{[CR]_h} \qquad (2)$$

where K_f and D are the apparent formation constant for the 1:1 carbazole–CD complex formed in the aqueous phase and the distribution ratio for carbazole in the two-phase extraction system, respectively, [CR], [CD] and [CR–CD] are the equilibrium concentrations of the free carbazole, free CD and complex and the subscripts a and h denote the aqueous and hydrocarbon phases, respectively. In the absence of CD, on the other hand, the distribution coefficient (K_d) for carbazole between the two phases is simply defined according to the basic theory for solvent extraction by

$$K_d = [CR]_a/[CR]_h \qquad (3)$$

Combination of eqns. (1), (2) and (3) and rearrangment yield

$$D = K_d + K_d K_f [CD]_a \qquad (4)$$

When the initial concentration of CD in the water–DMSO medium ($[CD]_{a0}$) is in large excess compared with the concentration of the complex, the reasonable simplification $[CD]_a = [CD]_{a0}$ can be made. Eqn. (4) can be therefore expressed as

$$D = K_d + K_d K_f [CD]_{a0} \qquad (5)$$

In eqn. (5), the D and K_d values can be obtained experimentally by measuring the fluorescence intensities of carbazole present in the hydrocarbon phase before and after extraction. Also, a plot of D *versus* $[CD]_{a0}$ would be found to be linear if the assumption of $1:1$ stoichiometry is applicable to the inclusion complex. The value of K_f can consequently be determined from the slope and intercept of the linear plot according to eqn. (5).

In our work, D and K_d were originally determined by synchronous fluorimetric measurements of hydrocarbon phases after extraction with and without CDs, respectively. The apparent K_f value was subsequently calculated by dividing the slope of the D *versus* $[CD]_{a0}$ plot by the observed K_d value, not from the intercept of the plot. Since the D *versus* $[CD]_{a0}$ plots

tend to show upwards concave curvature at high CD concentrations, it seems reasonable to calculate in this way.

Results and Discussion

Heptane–Aqueous DMSO Extraction System

Single batch extraction of carbazole from heptane into various water–DMSO media were performed 384 times at 25 ± 1 °C under partly different conditions, that is, solution volumes of hydrocarbon 2–10 cm^3 and aqueous DMSO 1–16 cm^3 and concentrations of carbazole 5.0, 10 and 25 mmol m^{-3}, CD 0–10 mol m^{-3} and DMSO 10, 20, 30, 40, 50 and 60% v/v. The distribution ratio for carbazole determined from these extractions is plotted as a function of the initial concentration of CD (Fig. 1), together with the distribution coefficient, $K_d = D$ when $[CD]_{a0} = 0$. Also, a few values accessible for the correlation between K_f and K_d were calculated from the extraction data.

The parameter values given in Table 1 are grouped into six columns based on differences in the DMSO concentration. In each column, K_d was determined by averaging a series of values available from the eight different extractions with only the
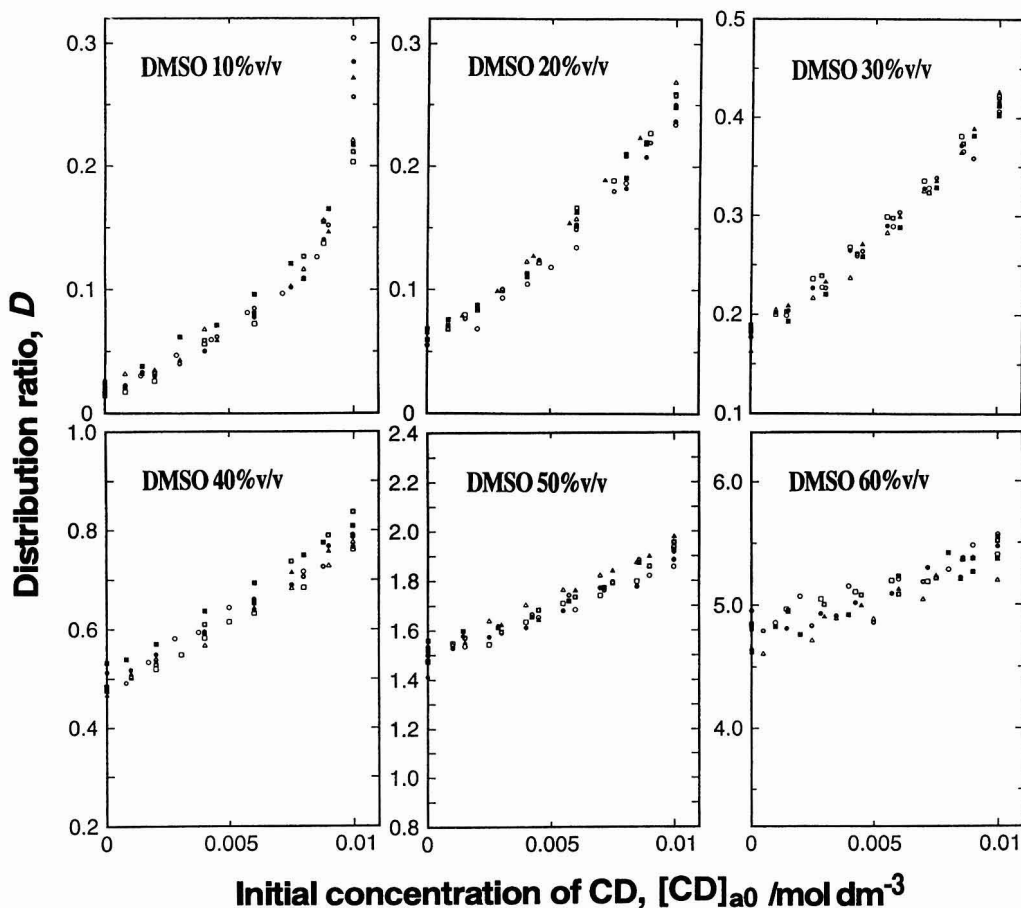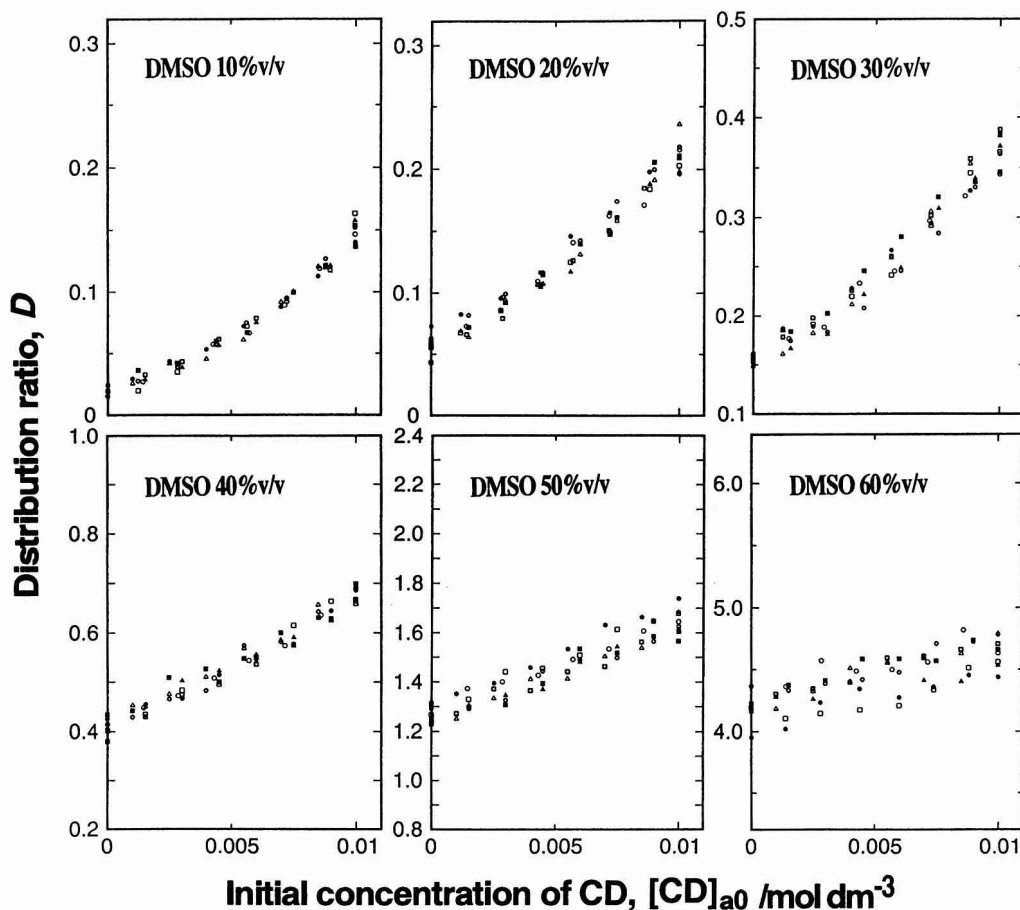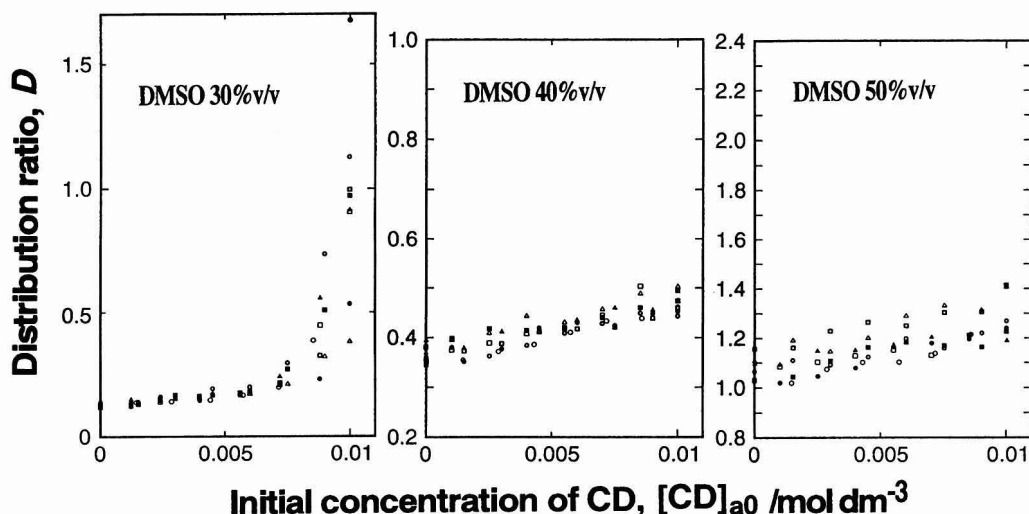

Fig. 1   Plot of the distribution ratio for carbazole *versus* the initial concentration of CD observed in a liquid–liquid extraction system consisting of heptane and aqueous DMSO (10–60% v/v).

water–DMSO medium. The RSD was then calculated for the K_d, in order to assess the precision. Each D *versus* $[CD]_{a0}$ plot is composed of the 64 data points measured at the same DMSO concentration.

As can be seen from Fig. 1, deviation from linearity of the plot is observed at higher $[CD]_{a0}$ and lower DMSO concentrations. In order to determine the K_f value according to eqn. (5), therefore, a linear regression analysis for the D *versus* $[CD]_{a0}$ plot was applied to only 40 data points in the lower $[CD]_{a0}$ range of 0–6 mol m^{-3}. The slope of the linear plot is given in Table 1, together with the correlation coefficient. Finally, the apparent K_f value for the carbazole–CD complex in the water–DMSO medium was calculated from dividing the slope by the observed K_d value as mentioned above.

Table 1 indicates that the increase in K_d becomes pronounced with increasing DMSO concentration, having good RSD values at the higher concentrations. This is to be expected owing to the high solvent power of DMSO for carbazole. This power will result in a large variation in concentration of carbazole in the heptane phase before and after extraction. On the other hand, the slope of the D *versus* $[CD]_{a0}$ plots does not increase as much as K_d, and the correlation coefficient goes through a maximum value at a DMSO concentration of 30% v/v. The smaller correlation at lower concentrations was attributable to the large deviation from the linear plots, and that at higher concentrations to the slight difference between the amounts of carbazole extracted with CD-free and -containing solutions. As can be seen from Table 1, the apparent K_f value given by the slope–K_d correlation decreases successively from 480 dm^3 mol^{-1} in 10% to 13.0 dm^3 mol^{-1} in 60% v/v DMSO medium. When the third component is dissolved in an aqueous CD medium as the organic modifier, other workers have suggested competitive complexation of the modifier compounds[22,23] or the presence of a ternary complex.[24,25] The decrease in K_f in this system may also be interpreted in terms of the assumption that the presence of DMSO in water breaks up the carbazole–CD complex competitively and assists carbazole in leaving the CD cavity.

Dodecane–Aqueous DMSO Extraction System

Carbazole in dodecane was extracted with water–DMSO media under the same conditions as described for the heptane–aqueous DMSO system, and the D *versus* $[CD]_{a0}$ plot was constructed in the same manner (Fig. 2). Table 2 gives the parameter values for carbazole in this extraction system. Comparison of Table 2 with Table 1 reveals that there is little difference in the parameter values for carbazole between dodecane and heptane. This similarity should be predictable to some extent from the similar structures of these two straight-chain hydrocarbons. On closer inspection, however, it is found that there are some differences on comparing the dodecane with the heptane solvent. The values of K_d and the slope in the dodecane system are slightly smaller than the corresponding values in the heptane system, except for the slope at a 50% v/v DMSO concentration. The

slight decrease in K_d can be ascribed to the difference in solubility of carbazole between the two hydrocarbons, but it is difficult to interpret the decrease in the slope of the D *versus* $[CD]_{a0}$ plot. Further, the correlation for the D *versus* $[CD]_{a0}$ plot in the dodecane system is poor compared with that in the heptane system, although it is better at a 10% v/v DMSO concentration. Probably this is due to the lower reproducibility of the synchronous spectrofluorimetric measurements of carbazole in dodecane.

Cyclohexane–Aqueous DMSO Extraction System

Extractions of carbazole from cyclohexane into CD solutions were tried under the same conditions as described in the above two systems. At DMSO concentrations < 30% v/v, however, it was impossible to estimate valid values of D and K_d for carbazole owing to precipitation from the aqueous DMSO solutions. Although the precipitation was observed even at 30% v/v DMSO at higher CD concentrations, the D values were measurable for $[CD]_{a0}$ lower than approximately 6 mol m^{-3}. A possible explanation for this phenomenon has already been offered by Sanemasa *et al.*,[26] who reported[26] that CD is easily precipitated from its aqueous solution upon introducing cyclohexane vapour into the solution, coprecipitating PACs at the same time. Therefore, such precipitation observed in the less concentrated DMSO media may be regarded as due to a complicated complex of CD with cyclohexane (and in part with carbazole).

Fig. 3 and Table 3 provide the D *versus* $[CD]_{a0}$ plot and the parameter values for carbazole, respectively, for DMSO concentrations ranging only from 30 to 50% v/v. The data at 60% v/v DMSO concentration were not evaluated because of the insensitivity to the extraction of carbazole. In this cyclohexane system, an appreciably poorer correlation for the linear plots of D *versus* $[CD]_{a0}$ is revealed by Fig. 3 and/or the correlation coefficients in Table 3. This poor correlation is due to the nature of the carbazole extraction, that is, a slight increase in the amount of carbazole with a large increase in the amount of CD. There may be some uncertainty in this system regarding the determination of the values of both the slope and the related K_f. However, the results for the cyclic hydrocarbon should be useful for comparison with those for the above straight-chain hydrocarbons. Table 3 indicates that the apparent K_f values at 30 and 40% v/v DMSO concentrations can be clearly distinguished from those in the heptane and dodecane systems, in spite of the similar decreases in K_d values. Anigbogu *et al.*[3] pointed out that differences in the experimental conditions and probing techniques could result in significant differences in K_f. In this extraction technique, however, large differences in K_f values were observed under the same conditions and using the same method, although there is a difference in type of hydrocarbon. This implies that the hydrocarbons used as the organic phase compete with carbazole for CD complexation. It may therefore be concluded that the estimated K_f for the carbazole–CD

Table 1 Parameter values obtained from data on solvent extraction of carbazole from heptane into various aqueous DMSO solutions of CD

Value	Concentration of DMSO (% v/v)					
	10	20	30	40	50	60
Mean K_d for 8 measurements	0.0216	0.0651	0.180	0.490	1.50	4.75
RSD of K_d measurements (%)	21.1	7.7	4.5	4.5	3.1	2.7
Slope of D *versus* $[CD]_{a0}$ plot*/dm^3 mol^{-1}	10.4	14.7	19.7	27.4	38.4	61.6
Correlation coefficient for the plot*	0.9600	0.9687	0.9808	0.9536	0.9311	0.7658
K_f (slope/K_d)/dm^3 mol^{-1}	480	226	109	55.9	25.6	13.0

* Linear regression analysis was applied to 40 data points in the $[CD]_{a0}$ range 0–6 mol m^{-3} in the plot.

complex must be considered as a relative value to that for the hydrocarbon–CD complex.

Linear Relationship Between log K_f and log K_d

The apparent formation constant is a measure of the complexation of carbazole with CD in a given water–DMSO medium. On the other hand, the distribution coefficient is a measure of the distribution of carbazole between a hydrocarbon solvent and the medium in the absence of CD. Therefore, these two

equilibrium constants, K_f and K_d, should be essentially independent of each other even if the hydrocarbon has a competitive effect on the carbazole–CD complexation.

Application of linear regression analysis to each of the six data from the heptane and dodecane extraction systems led to the equations log K_f = −0.675 log K_d + 1.547 (r = −0.9996) and log K_f = −0.672 log K_d + 1.511 (r = −0.9992), respectively. Because of the small number of data points (n = 3), regression analysis was not applied to the results from the cyclohexane system. As can be seen from the above equations,

Fig. 2 Plot of the distribution ratio for carbazole *versus* the initial concentration of CD observed in a liquid–liquid extraction system consisting of dodecane and aqueous DMSO (10–60% v/v).

Table 2 Parameter values obtained from data on solvent extraction of carbazole from dodecane into various aqueous DMSO solutions of CD

Value	Concentration of DMSO (% v/v)					
	10	20	30	40	50	60
Mean K_d for 8 measurements	0.0201	0.0593	0.157	0.412	1.27	4.19
RSD of K_d measurements (%)	16.4	13.6	2.9	4.4	2.6	2.7
Slope of D versus $[CD]_{a0}$ plot*/dm³ mol⁻¹	9.06	12.9	17.1	23.6	38.6	49.5
Correlation coefficient of the plot*	0.9744	0.9635	0.9581	0.9535	0.90006	0.6395
K_f (slope/K_d)/dm³ mol⁻¹	451	217	109	57.2	30.5	11.8

* Linear rergression analysis was applied to 40 data points in the $[CD]_{a0}$ range 0–6 mol m⁻³ in the plot.

the plot of log K_f versus log K_d gives straight lines with good correlations (0.9996 and 0.9992) and similar slopes (-0.675 and -0.672). These results suggest that the slope of the log K_f versus log K_d plot remains unaltered with changes to the extraction system. Fig. 4 illustrates log–log plots of the two equilibrium constants in all three hydrocarbon–aqueous DMSO extraction systems. The slopes of the three lines are identical, being the mean of the two values obtained from the heptane and dodecane systems. It is found that the above assumption is satisfactorily applicable to the case of the cyclohexane system. From these results, therefore, we conclude that there is a linear correlation between log K_f and log K_d for carbazole evaluated by the extraction method. In addition, the slope of the linear plot should be constant in different liquid–liquid extraction systems consisting of hydrocarbons and aqueous DMSO solutions. The reason for the unchanged slope is not clear, but it might arise from an unchanged fitting of the carbazole molecule into the CD cavity in different solvent environments.

Interpretation of Empirical Equation

On the above supposition, the correlation between K_f and K_d for carbazole in the hydrocarbon–aqueous DMSO systems can be expressed as

$$\log K_f = -0.673 \log K_d + A \qquad (6)$$

where A denotes the intercept of the linear plot and varies according to the hydrocarbon used as the organic phase in extraction. It is found from eqn. (6) that the value of K_f depends only on A when log $K_d = 0$ ($K_d = 1$). In addition, the apparent K_f value for carbazole can, in fact, be considered as a relative value resulting in competition with the hydrocarbon solvent. In order to generalize eqn. (6), we shall assume from the above viewpoint that K_f (observed) $= K_f$ (carbazole)/K_f (hydrocarbon). On the basis of this additional assumption, therefore, eqn. (6) can be replaced by

$$\log K_{fOB} = -0.673 \log K_d + \log (K_{fCR}/K_{fHY}) \qquad (7)$$

where K_{fOB} is the observed K_f value for a 1 : 1 carbazole–CD complex in a given water–DMSO medium and K_{fCR} and K_{fHY}

are the absolute K_f values in neat water for the carbazole– and hydrocarbon–CD complexes, respectively. Eqn. (7) is a plausible empirical equation, but it is difficult to verify the validity at present because of the lack of both K_{fCR} and K_{fHY} values measured at the same time.

Fortunately, however, some apparent K_{fHY} values for heptane and cyclohexane have been published and could serve for the inspection of eqn. (7). When eqn. (6) is applied to the two different hydrocarbon solvents, heptane and cyclohexane, the intercepts of the corresponding linear plots are expressed according to eqn. (7) as $A_{HP} = \log (K_{fCR}K_{fHP})$ and $A_{CY} = \log (K_{fCR}/K_{fCY})$, where the subscripts HP and CY represent heptane and cyclohexane, respectively. Consequently, the difference between A_{HP} and A_{CY} can be written as follows:

$$\begin{aligned} A_{HP} - A_{CY} &= \log (K_{fCR}/K_{fHP}) - \log (K_{fCR}/K_{fCY}) \\ &= \log (K_{fCR} K_{fCY}/K_{fHP} K_{fCR}) \\ &= \log (K_{fCY}/K_{fHP}) \end{aligned} \qquad (8)$$

In this work, the statistically established values of A for heptane, dodecane and cyclohexane were 1.548, 1.510 and 1.238, respectively. Substitution of the two values of interest into eqn. (8) resulted in log $(K_{fCY}/K_{fHP}) = 0.310$, that is, $K_{fCY}/K_{fHP} = 2.04$. Sanemasa and co-workers[27,28] studied the K_{fHY} values in an aqueous medium at 25 °C by making use of the volatilization rate of hydrocarbon molecules. The K_{fHP} and K_{fCY} values that they determined were 69 ± 4 and 156 ± 8 dm^3 mol^{-1}, respectively. Therefore, a simple calculation from their data gives a K_{fCY}/K_{fHP} ratio of 2.26 (with variations in the range 2.03–2.52). On the other hand, Wishnia and Lappi[29] presented the dissociation constant; which is the reciprocal of the formation constant ($1/K_f$) for heptane– and cyclohexane–CD 1 : 1 complexes in the range 0–50 °C. The values given in their table for the heptane and cyclohexane complexes were 0.37 and 0.182 mol m^{-3}, respectively, at 20 °C and 0.39 and 0.199 mol m^{-3}, respectively, at 30 °C. Further application of their results indicated that $K_{fCY}/K_{fHP} = 2.03$ at 20 °C and 1.96 at 30 °C. These values of the K_{fCY}/K_{fHP} ratio are in fair agreement with the value calculated in our work. Therefore, these results suggest that there is a reasonable correlation between K_{fOB} and K_d values for carbazole, and also that the correlation can be expressed in the form of the empirical eqn. (7).

Fig. 3 Plot of the distribution ratio for carbazole *versus* the initial concentration of CD observed in a liquid–liquid extraction system consisting of cyclohexane and aqueous DMSO (30–50% v/v).

Conclusion

Liquid–liquid extraction of carbazole was performed from three types of hydrocarbon solvents into water–DMSO solutions of CD in order to determine the values of the apparent formation constant and the distribution coefficient at the same time. A linear relationship between the $\log K_f$ and $\log K_d$ for carbazole was substantiated on the basis of the extraction data. Since the slope of the $\log K_f$ *versus* $\log K_d$ plot obtained with the dodecane system was similar to that with the heptane system, it was assumed that the slope does not vary with changes in hydrocarbon phase. The reason for the unchanged slope is not clear at the present stage of our limited study. Further and more extensive studies may be necessary in order to confirm the assumption. From the results with the cyclohexane system, on the other hand, it was concluded that the apparent K_f value observed for a 1 : 1 carbazole–CD complex is a relative value resulting in competition with the hydrocarbon solvent. An empirical equation was finally proposed as a reasonable correlation between the observed K_f and K_d values for carbazole in these hydrocarbon–aqueous DMSO extraction systems. Emphasis was placed on the interpretation of the intercept of the linear $\log K_f$ *versus* $\log K_d$ plot. Although it is unknown what the slope of the plot represents, the concept of the relative K_f value

as the intercept was pertinent to the empirical equation. Also, it is not clear whether such a correlation can be found or not for species other than carbazole. However, the good linearity of the $\log K_f$ *versus* $\log K_d$ plot may be attractive in further analytical investigations, such as for the prediction of selective separations from complicated mixtures and application of CD-containing solvent extraction to practical samples.

References

1   Muñoz de la Peña, A., Ndou, T., Zung, J. B., and Warner, I. M., *J. Phys. Chem.*, 1991, **95**, 3330.
2   Chokchainarong, S., Fennema, O. R., and Connors, K. A., *Carbohydr. Res.*, 1992, **232**, 161.
3   Anigbogu, V. C., Muñoz de la Peña, A., Ndou, T. T., and Warner, I. M., *Anal. Chem.*, 1992, **64**, 484.
4   Loukas, Y. L., Antoniadou-Vyza, E., Papadaki-Valiraki, A., and Machera, K. G., *J. Agric. Food Chem.*, 1994, **42**, 944.
5   Gareil, P., Pernin, D., Gramond, J.-P., and Guyon, F., *J. High Resolut. Chromatogr.*, 1993, **16**, 195.
6   Baumy, Ph., Morin, Ph., Dreux, M., Viaud, M. C., Boye, S., and Guillaumet, G., *J. Chromatogr. A*, 1995, **707**, 311.
7   Choi, H.-S., Chang, C.-J., and Knevel, A. M., *Pharm. Res.*, 1992, **9**, 582.
8   Georgiou, M. E., Georgiou, C. A., and Koupparis, M. A., *Anal. Chem.*, 1995, **67**, 114.
9   Li, S., and Purdy, W. C., *Anal. Chem.*, 1992, **64**, 1405.
10   Valsami, G. N., Koupparis, M. A., and Macheras, P. E., *Pharm. Res.*, 1992, **9**, 94.
11   McCormack, S., Russell, N. R., and Cassidy, J. F., *Electrochim. Acta*, 1992, **37**, 1939.
12   Blyshak, L. A., Rossi, T. M., Patonay, G., and Warner, I. M., *Anal. Chem.*, 1988, **60**, 2127.
13   Harangi, J., and Nánási, P., *Anal. Chim. Acta*, 1984, **156**, 103.
14   Matsunaga, K., Imanaka, M., Ishida, T., and Oda, T., *Anal. Chem.*, 1984, **56**, 1980.
15   Elliott, N. B., Prenni, A. J., Ndou, T. T., and Warner, I. M., *J. Colloid Interface Sci.*, 1993, **156**, 359.
16   Tachibana, M., and Furusawa, M., *Analyst*, 1995, **120**, 437.
17   Tachibana, M., Furusawa, M., and Kiba, N., *J. Inclusion Phenom. Mol. Recognit. Chem.*, 1995, **22**, 313.
18   Matsui, Y., and Mochida, K., *Bull. Chem. Soc. Jpn.*, 1979, **52**, 2808.
19   Uekama, K., Hirayama, F., Nasu, S., Matsuo, N., and Irie, T., *Chem. Pharm. Bull.*, 1978, **26**, 3477.
20   Furusawa, M., Takeuchi, T., Sekido, K., and Shimizu, H., *Kogyo Kagaku Zasshi*, 1963, **66**, 1811.
21   Tachibana, M., and Furusawa, M., *Bull. Chem. Soc. Jpn.*, 1988, **61**, 2353.
22   Mohseni, R. M., and Hurtubise, R. J., *J. Chromatogr.*, 1990, **499**, 395.
23   Muñoz de la Peña, A., Ndou, T. T., Anigbogu, V. C., and Warner, I. M., *Anal. Chem.*, 1991, **63**, 1018.
24   Kano, K., Hashimoto, S., Imai, A., and Ogawa, T., *J. Inclusion Phenom.*, 1984, **2**, 737.
25   Muñoz de la Peña, A., Ndou, T. T., Zung, J. B., Greene, K. L., Live, D. H., and Warner, I. M., *J. Am. Chem. Soc.*, 1991, **113**, 1572.
26   Sanemasa, I., Koga, I., and Deguchi, T., *Anal. Sci.*, 1991, **7**, 641.
27   Sanemasa, I., Osajima, T., and Deguchi, T., *Bull. Chem. Soc. Jpn.*, 1990, **63**, 2814.
28   Osajima, T., Deguchi, T., and Sanemasa, I., *Bull. Chem. Soc. Jpn.*, 1991, **64**, 2705.
29   Wishnia, A., and Lappi, S. J., *J. Mol. Biol.*, 1974, **82**, 77.

Table 3 Parameter values obtained from data on solvent extraction of carbazole from cyclohexane into various aqueous DMSO solutions of CD

Value	Concentration of DMSO (% v/v)		
	30	40	50
Mean K_d for 8 measurements	0.126	0.365	1.07
RSD of K_d measurements (%)	2.9	4.4	2.6
Slope of D *versus* $[CD]_{a0}$ plot*/ dm³ mol⁻¹	8.69	9.99	22.3
Correlation coefficient for the plot*	0.8794	0.7755	0.6656
K_f (slope/K_d)/dm³ mol⁻¹	68.9	27.4	20.9

* Linear regression analysis was applied to 40 data points in the $[CD]_{a0}$ range 0–6 mol m⁻³ in the plot.

Fig. 4   Correlation between the apparent K_f value for a 1 : 1 carbazole–CD complex present in water–DMSO medium and the K_d value for carbazole on extraction from (○) heptane, (□) dodecane and (△) cyclohexane into the medium.

Sequential Injection Analysis Technique for the Concentration, Stoichiometry and Formation Constant Studies of Promethazine Hydrochloride Complexed With Palladium(II) in Hydrochloric Acid

Salah M. Sultan* and Nabeel I. Desai

The Chemistry Department, King Fahd University of Petroleum and Minerals, KFUPM, P.O. Box 2026, Dhahran 31261, Saudi Arabia

The sequential injection analysis (SIA) technique was successfully applied to the determination of promethazine hydrochloride in drug formulations. The chemical system is based on the complexation reaction of promethazine hydrochloride with Pd^{II} in 8.0×10^{-4} mol dm^{-3} HCl and measurement of the absorbance at 504 nm. Promethazine was determined in the range 50–400 ppm using 1.0×10^{-3} mol dm^{-3} Pd^{II} with an aspiration volume of 147.5 µl. The SIA technique was utilized for the determination of the concentration, stoichiometry and formation constant of the complexation reaction. The technique was found to be superior to flow injection analysis. The SIA method was statistically compared with the official British Pharmacopoeia method and showed comparable accuracy, but with the advantages of selectivity, simplicity, speed and amounts of reagents consumed.

Keywords: Sequential injection analysis; promethazine–palladium(II) complexation; stoichiometry

Promethazine hydrochloride, dimethyl[1-methyl-2-(phenothiazine-1-yl)ethyl]amine hydrochloride, is widely used for its antihistamine action and for various post-operative conditions. The available analytical methods have been reviewed,[1] and include two examples using flow injection analysis (FIA) that are relevant to this paper.[1,2] Both methods depend on the spectrophotometric determination of a red oxidized derivative of the drug, believed to be a dication radical, generated, respectively, by metavanadate[1] and cerium(IV).[2] The British Pharmacopoeia (BP) method[3] for promethazine uses Pd^{II} to generate a purple derivative, suitable for spectrophotometry.

Similar reactions between Pd^{II} and other phenothiazines have been investigated[4–6] and used as the basis of a sequential injection analysis (SIA) method.[7]

The present work describes an SIA method for promethazine based on its reaction with Pd^{II}.

Experimental

Reagents and Stock Solutions

Pd^{II}. A stock solution of 0.025 mol dm^{-3} Pd^{II} in 0.02 mol dm^{-3} hydrochloric acid was prepared by dissolving 0.4440 g of anhydrous $PdCl_2$ (Fluka, Buchs, Switzerland) in 50 cm^3 of 0.04 mol dm^{-3} hydrochloric acid. The mixture was heated at 80 °C until all the solid had dissolved, then cooled to room temperature and made up to 100 cm^3 with water to form a clear brownish yellow solution.

A stock solution containing a hydrochloric acid concentration lower than 0.02 mol dm^{-3} could not be prepared as Pd^{II} does not dissolve in less acidic solutions even after prolonged heating.

The molar absorptivity of the absorbing species is such that at the optimum pH of approximately 4 the optimum Pd^{II} concentration range over which Beer's law applied is $10^{-3}–10^{-4}$ mol dm^{-3}.

Hydrochloric acid. A stock solution of 10 mol dm^{-3} HCl was prepared by diluting AnalaR concentrated acid (Merck, Poole, Dorset, UK).

Promethazine. The stock solution was 1500 ppm (4.674×10^{-3} mol dm^{-3}) $C_{17}H_{20}N_2S \cdot HCl$ (Rhone-Poulenc, Dagenham, Essex, UK, Batch No. W3021), prepared by dissolving 0.15 g of the drug in 100 cm^3 of de-ionized water.

Pure drugs. The drugs studied together with the names of the suppliers and other relevant information are given in Table 1.

Table 1 Statistical comparison of the results for the determination of promethazine hydrochloride in commercial formulations by the proposed method with those obtained by the official BP method[3]

Formulation	Active ingredient	Recovery $\pm s$ (%)*		t-value[†]
		SIA	BP	
Phenergen tablets (Specia, France)	Promethazine hydrochloride, 25 mg	99.72 ± 0.6	99.31 ± 0.5	1.53
Phenergen syrup (Specia, France)	Promethazine hydrochloride, 666.67 ppm	99.9 ± 0.7	99.8 ± 0.3	0.32
Phenergen syrup Expectorant (Specia, France)	Promethazine hydrochloride, 666.67 ppm	99.4 ± 1.0	99.9 ± 0.6	1.12
Cigan Elixir (Cimabrex, Denmark)	Promethazine hydrochloride, 1000 ppm	100.1 ± 0.8	99.8 ± 0.4	0.84

* Standard deviation (s) for five determinations based on label claim.   [†] Theoretical t-value = 2.78 ($p = 0.05$).

Stock solutions of 1000 ppm of each of the drugs were prepared by dissolving the drug in water or dilute acid solution at room temperature.

Syrups and elixir. Test solutions were prepared by diluting a pipetted amount of the syrup or elixir directly with water or dilute acid solution in a calibrated flask.

Working solutions for calibration, Job's plot, molar ratio and all other studies were prepared by appropriate dilutions of the stock solutions.

Apparatus

Sequential injection analyser

The sequential injection analyser (Fig. 1) was constructed from the following components: A peristaltic pump (C4V, Alitea, Medina, WA, USA) featuring eight stainless-steel rollers on individual bearings was employed to propel the solutions. A Valco 10-port selector valve (Cheminert, Valco Instruments, Houston, TX, USA) was used to select the flows. Upchurch fittings (Upchurch, Oak Harbor, WA, USA) were used to lock unused ports. The holding and reaction coil tubing and also the tubing connecting the different units was made of PTFE (0.8 mm id). Teflon nuts and ferrules (Upchurch) were used to assemble the manifold. The pump tubing was Phar Med 1.02 mm id tubing (Upchurch), and was held on the pump rollers by FIA peristaltic pump tubing adapters (Upchurch). A reactor module consisting of 0.5 mm id PTFE tubing (Thermoplastic Scientific, NY, USA) of different lengths was used for mixing the solutions. Absorbance measurements were made with a Spectronic Mini-20 spectrophotometer (Milton Roy, Rochester, NY, USA), equipped with a grating monochromator detector and a Unovic ultra-micro-flow-through cell (Unovic Instruments, NY, USA) (20 µl) with a pathlength of 1.0 mm. A personal computer (Austin Computer Systems, Austin, TX, USA) equipped with a 120 Mbyte hard disk, 4 Mbyte RAM and VGA graphics was used to monitor the pump and valve. Communication between the computer and the external devices was effected with a general-purpose I/O board (Model ADA-110, Real Time Devices, State College, PA, USA). The computer was also used to collect the data; alternatively, the data were recorded by a Model 0555 single-channel strip-chart recorder (Cole-Parmer, Chicago, IL, USA).
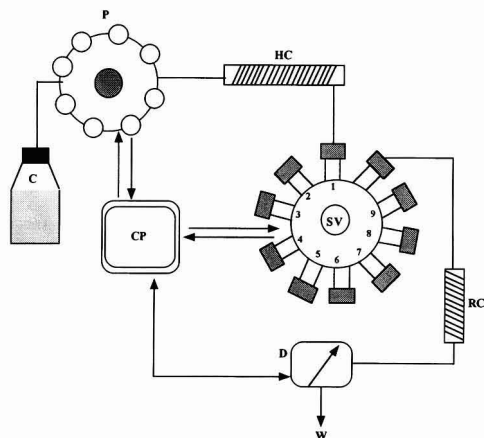
Fig. 1 SIA manifold: C, carrier; P, peristaltic pump; HC, holding coil; SV; selector valve; RC, reaction coil; D, detector; CP, computer; and W, waste.

A Perkin-Elmer (Norwalk, CT, USA) Lambda 5 UV/visible spectrophotometer equipped with 10.0 mm cells was used for preliminary investigations.

Software Packages

Microsoft windows 3.10 with DOS 6.20 was utilized to run the following software: FIA Lab 2.0 (beta release) (Alitea) was used to program the SIA system. Sigmaplot, version 1.02 (Jandel Scientific, Erkrath, Germany) was employed for data handling calculations and constructing graphs. Microsoft Word, version 6.0 (Microsoft Corporation, USA) was used for constructing tables and writing text.

Procedure

Fig. 1 shows the SIA manifold used. Fixed amounts of reagent, sample and carrier (wash) solutions were sequentially aspirated into the lines from the ports by means of the selector valve (SV). In each case, the excess solution introduced into the holding coil (HC) was expelled through port 7 to the auxiliary waste. The remaining steps of the procedure, which were controlled by the computer, were as follows: 1, The carrier solution was pumped through port 1, by setting the pump in the forward direction, for 25–45 in order to flush the system (holding coil, reactor and detector) with the carrier solution. 2, A pre-determined volume of the reagent solution was aspirated through port 2 into the holding coil (HC) in the reverse direction. The remaining reagents were aspirated into the holding coil *via* ports 3–8, as appropriate. 3, The drug solution was aspirated into the holding coil from port 9. The last two steps were achieved by setting the pump in the reverse mode.

Finally, the composite zone was propelled by the carrier solution through port 1 to the reaction coil and then the detector. When the mixing chamber was used instead of the reactor coil, the reagent(s) and the sample were initially injected into the mixing chamber. At fixed intervals, aliquots of the solution in the mixing chamber were withdrawn into the holding coil and then pushed to the detector using the carrier by forward pumping. The data were acquired by the computer and transferred to plotting software for further calculations.

In each of the above steps the volume of the solutions aspirated was determined from the time of aspiration and the volumetric flow rate of the pump (using the relationship, volume = flow rate × time), which was 29.5 µl s^{-1} in this study.

Determination of Flow Rate

The pump speed can be altered by changing the rev min^{-1} setting on the peristaltic pump. The rate of flow of the reagent inside the pump tubes was determined by withdrawing liquid (distilled water) at one end of the tube and collecting it at the other end in a measuring cylinder. The volume of liquid collected at a certain time gives the flow rate in ml min^{-1} at a particular rev min^{-1} value. This process was repeated for different rev min^{-1} values, giving different values of flow rate. A graph of flow rate *versus* pump speed (rev min^{-1}) was then plotted. A straight line described by the following equation was obtained:

Flow rate = 0.73644 + 0.05726 × (pump speed/rev min^{-1})

Therefore, for a pump speed of 500 rev min^{-1}, which was used in this work, the flow rate will be 1.77 ml min^{-1} or 29.5 µl s^{-1}.

Stoichiometry

For stoichiometric studies, the SIA system (Fig. 1), including all the tubes attached to the selector valve, was flushed with de-

ionized water (carrier) flowing at a rate of 29.5 µl s⁻¹. The following operations were then conducted:

1. Equimolar solutions of Pd^II and promethazine were connected to the selector valve through ports 2 and 3, respectively. About 80 µl of each reagent were introduced sequentially into the holding coil in the reverse mode for 3.0 s; the excess, together with some carrier, was transferred to the auxiliary waste through valve 7 in the forward mode for 8.0 s.

2. In Job's method of continuous variation, different aliquots of equimolar solutions of Pd^II and promethazine were taken and mixed in the holding coil so as to give solutions of identical total concentration (Pd^II + drug) but different mole fractions; the solution was then pushed for 40.0 s to the detector for signal monitoring. The volume of each reagent aspirated was varied between 14.8 µl (0.5 s) and 147.5 µl (5.0 s). The total volume aspirated was maintained constant at 162.0 µl by adjusting the aspiration times. This step was repeated while varying the aspiration time between 14.8 µl (0.5 s) and 280.3 µl (9.5 s).

3. In the molar ratio method, the total concentration of the ligand (promethazine) was maintained constant by aspirating 147.5 µl (5.0 s) of solution into the holding coil by flow reversal, while the Pd^II solution volume was varied between 14.8 µl (0.5 s) and 192.0 µl (6.5 s). This step was repeated except that the total concentration of the metal was held constant by fixing the flow reversal for 147.5 µl (5.0 s), while the volume of drug solution was varied between 14.8 µl (0.5 s) and 192.0 µl (6.5 s).

Ideally, in the molar ratio method, two straight lines with different slopes are obtained when the absorbance is plotted against the Pd^II-to-drug ratio, and the point of intersection of these two lines corresponds to the stoichiometric ratio on interpolation to the molar ratio axis.

Steps 2 and 3 were repeated but using 8.0×10^{-4} mol dm⁻³ hydrochloric acid as the carrier instead of water. There was no significant difference in the absorbance values obtained using either acid or water as carrier.

Results and Discussion

Chemical System

Prior to using the SIA technique, preliminary investigations were made in which the maximum absorbance (λ_{max}) over a wide range of pH values from 8.0×10^{-5} to 0.01 mol dm⁻³ was determined.

The optimum absorbance conditions as a function of pH were established by measurements on solutions of Pd^II (10 mol dm⁻³) and promethazine (150 ppm) at 28 increments of pH between 2.0 and 4.1. Both the wavelength of maximum absorbance and the absorbance itself increased from pH 2 (496.2 nm and 0.303, respectively) to pH 3.12 (503.9 nm and 0.369) before decreasing at pH 4.1 (502.2 nm and 0.279). The optimum pH for this work was selected as 3.1.

The stability of the complexes formed favoured this method over previous methods involving oxidation with stronger oxidizing agents than Pd^II in which a highly unstable radical product is monitored for quantification.[1,2,8,9]

The nature of the interaction between Pd^II and promethazine in the pH range 4.1–3.0 is believed to involve protonation of the drug followed by hydrogen bonding between the protonated nitrogen and one of the chlorine atoms of $PdCl_2$.[4–6,10] Complexes of the type ML_2X_2 and MLX_3 have also been reported,[10] where M = Pd, L = promethazine ligand and X = Cl.

An investigation of the type, stoichiometry and formation constant of such a complex was carried out by the Job's plot[11] and molar ratio[11,12] methods as described below.

Job's Plot Method

In Job's method of continuous variation, different aliquots of equimolar solutions of Pd^II and promethazine were mixed to give solutions of identical total concentration (Pd^II + drug) but different mole fractions. A volume of carrier solution was then aspirated; the carrier volume was selected to allow optimum mixing on flow reversal towards the detector. Analysis of the Job's plot was used to determine the stoichiometry of the complexation of Pd^II with promethazine in hydrochloric acid medium.

A typical Job's plot, illustrated in Fig. 2, was obtained by the SIA procedure using 8×10^{-4} mol dm⁻³ hydrochloric acid and an ionic strength of 0.20 mol dm⁻³, which was maintained by using lithium perchlorate. Water (de-ionized) was used as a carrier for analysis, but the experiment was also repeated several times with hydrochloric acid as carrier and also with mixing of the reactants in the holding coil. It was found that there was no significant difference when water or acid was used as a carrier, even if the mixing steps were included in the SIA program. The total volume of the two reagents for each run was kept constant at 295.1 and 162.3 µl.

It is worth noting that both reagents, *viz.*, Pd^II and promethazine, were injected, thus consuming minimal amounts of reagent compared with the manual procedure.

It is clear that the curves $A = f(X_{drug})$ exhibit a maximum for mole fractions of 0.5, indicating that the ratio of Pd^II : drug in the complex is 1 : 1. Only 10 min are needed to generate the Job's plot using SIA and less than 10 ml of the drug is sufficient to repeat the procedure many times.

Attempts to apply the molar ratio method[12,13] failed because the Pd^II concentration was a greater effect on the system, resulting in the formation of a mixed complex together with the oxidized form of the drug at higher concentrations of Pd^II, which makes the method unsatisfactory. This is in agreement with previous work, which indicated that various complex forms are possible.[7]

Overall, the Job's plot method is the more reliable and it has clearly shown that the molar ratio of the Pd^II–promethazine complex is 1 : 1.
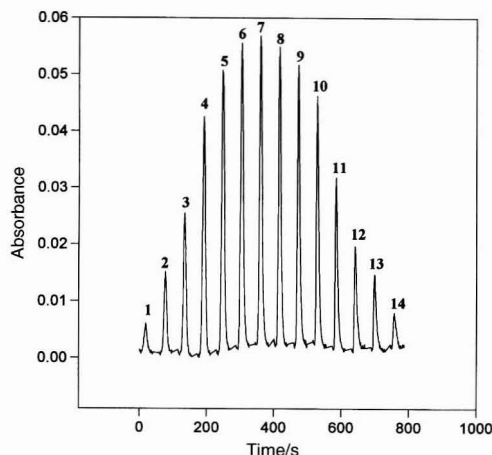
Fig. 2 Typical SIA trace representing a Job's plot for the promethazine system: [Pd^II] = [promethazine] = 1×10^{-3} mol dm⁻³ in 8×10^{-4} mol dm⁻³ hydrochloric acid; ionic strength = 0.20 mol dm⁻³. The total aspiration volume is equivalent to 295 µl and aspiration volumes were varied between 14.8 µl and 280.3 µl. Mole fraction of the drug: (1) 0; (2) 0.05; (3) 0.10; (4) 0.20; (5) 0.30; (6) 0.40; (7) 0.50; (8) 0.60; (9) 0.70; (10) 0.80; (11) 0.90; (12) 0.95; (13) 0.975; and (14) 0.10 µl.

Formation Constant

The formation constant and the composition of the Pd^{II}–promethazine complex were also investigated by numerical methods.[14,15] The JOBCON[16,17] program was used to analyse the continuous variation data. The program was modified by the authors and re-written in C-language and applied on a PC/AT computer. The calculations are based on fitting a function $f(x, \beta)$ to a set of experimental data, using a least-squares method. Unknown parameters are estimated by minimizing U, the sum of squares of residuals, defined by the following equation:

$$U = \sum_{i=1}^{n} (A_{exp} - A_{calc})^2$$

where n represents the number of experimental points, A_{exp} the experimental absorbance, and $A_{calc} = f(x, \beta)$, the absorbance calculated by the program from formation constants and stoichiometric ratios. Therefore, various experimental models could be fitted to the experimental data iteratively by varying the values of the formation constant and stoichiometric ratio.

The JOBCON program was used to calculate the formation constant from the continuous variation data for the Pd^{II}–promethazine complex. A 1 : 1 metal-to-ligand ratio was found to be the most probable, with a relative error of 14.99%, resulting in a value for the logarithm of the formation constant (log K_f) of 4.349. Other metal-to-ligand ratios ($m : n$) appeared to be improbable, giving high relative errors, particularly those where $m : n > 2$.

The value of log K_f reported[10] previously for promethazine was 5.52, which is close to the value obtained in the present work for the 1 : 1 Pd^{II}–promethazine complex. It was also observed that the stoichiometry and the value of the formation constant are independent of the total concentration of the metal ion and the ligand.

Calibration Graph

A series of standard solutions of promethazine hydrochloride were run in triplicate; a graph of absorbance *versus* concentration was found to be linear in the range 50–400 ppm. The calibration equation was:

$$A = 0.008654 + 0.000110\,C$$

where A is absorbance and C is concentration in ppm; the correlation coefficient (r^2) was 0.997.

The peak width at the baseline was measured to be 18 s, thus giving a throughput of 200 samples h^{-1}. The peak width was also determined at 60% peak height and found to be 2.4 s, indicating minimal dispersion. An average relative standard deviation (RSD) of 0.92% was obtained for six replicate determinations of 250 ppm of promethazine, indicating excellent reproducibility.

Application

The method was applied to the determination of promethazine hydrochloride in several commercial formulations, namely, Phenergen tablets, Phenergen promethazine, Phenergen Expectorant and Cigan Elixir. All drug formulations contained starch and glucose as excipients. The same formulations were also analysed by the BP method[3] and the results were statistically compared by calculating the percentage recoveries, standard deviations and the Student's *t*-test values. The results are shown in Table 1.

The accuracy of the proposed method was comparable to that of the BP method. The results also show that common excipients do not interfere with the determination.

The proposed method is simpler and more selective than the BP and previous methods. The utilization of Pd^{II} avoided oxidation of the drug during the analysis.

Conclusion

The proposed SIA method for the determination of promethazine was validated by complexation of the drug with Pd^{II} in dilute hydrochloric acid medium and was found to be superior to earlier FIA methods. The method developed was applied to the determination of promethazine in commercial formulations and was found to be superior to the official BP method, with a wide dynamic range (50–400 ppm), excellent reproducibility and an RSD of less than 0.96%. The capacity of the SIA technique was demonstrated by its application to the determination of concentrations, stoichiometries and formation constants of complexation reactions. A large number of experimental trials were performed utilizing relatively small amounts of reagents.

References

1   Sultan, S. M., *Analyst*, 1991, **116**, 177.
2   Sultan, S. M., and Suliman, F. O., *Anal. Sci.*, 1992, **8**, 841.
3   *British Pharmacopoeia*, HM Stationery Office, London, 5th edn., 1988, pp. 749 and 995.
4   Pellizzetti, E., *J. Chem. Soc., Dalton Trans.*, 1980, 484.
5   Geary, W. J., Mason, N. J., Nowell, I. W., and Nixon, L. A., *J. Chem. Soc., Chem. Commun.*, 1984, 1064.
6   Duddell, D. A., Goggin, P. L., Goodfellow, R. J., Norton, M. G., and Smith, J. G., *J. Chem. Soc. A*, 1970, 546.
7   Sultan, S. M., Suliman, F. O., and Bahruddin, B. S., *Analyst*, 1995, **120**, 561.
8   Sultan, S. M., *Microchem. J.*, 1991, **44**, 304.
9   Sultan, S. M., and Abdennabi, A. M., *Microchem. J.*, 1993, **48**, 343.
10 Geary, W. J., Mason, N. J., Nowell, I. W., and Nixon, L. A., *J. Chem. Soc., Dalton Trans.*, 1982, 1103.
11 Job, P., *Ann. Chim.*, 1928, **9**, 113.
12 Momoki, K., Sekino, J., Sato, H., and Yamaguchi, N., *Anal. Chem.*, 1969, **41**, 1286.
13 Yoe, J. H., and Jones, A. L., *Ind. Eng. Chem. Anal. Ed.*, 1944, **64**, 111.
14 Sabatini, A., Vacca, A., and Gans, P., *Coord. Chem. Rev.*, 1992, **120**, 289.
15 Sultan, S. M., *Anal. Lett.*, 1991, **24**, 1785.
16 Likussar, W., *Anal. Chem.*, 1973, **45**, 1926.
17 Meloun, M., and Javurek, M., *Talanta*, 1984, **31**, 1083.

Determination of Selenium by Atomic Absorption Spectrometry With Simultaneous Retention of Selenium(IV) and Tetrahydroborate(III) on an Anion-exchange Resin Followed by Flow Injection Hydride Generation From the Solid Phase

Pablo E. Carrero[†] and Julian F. Tyson*

Department of Chemistry, Box 34510, University of Massachusetts, Amherst, MA 01003-4510, USA

Selenium(IV) and tetrahydroborate(III) (borohydride) were simultaneously retained on a strong anion-exchange resin in a packed column. Hydrogen selenide was generated by passage of an injected zone of hydrochloric acid with subsequent detection by AAS with quartz tube atomization. The limits of detection, defined as the concentration giving a signal equal to 3s of the blank, were 0.24, 0.15 and 0.12 µg l^{-1} of Se for 1, 2 and 3 min preconcentration at a sample flow rate of 3 ml min^{-1}, respectively. The precision of the procedure, expressed as the RSD of 10 successive determinations of 5, 10, and 20 µg l^{-1} of Se, varied from 0.41 to 1.32, 0.24 to 0.81 and 0.18 to 0.61% for 1, 2 and 3 min preconcentration, respectively. The system was used for the determination of selenium in river, lake and tap water matrices. No appreciable matrix effects were observed and the system was calibrated with aqueous solutions of a pure selenium salt (Na$_2$SeO$_3$). The recoveries of spikes (0.5, 2, and 10 µg l^{-1} of Se) added to the water samples ranged from 96.0 to 102.0, 96.0 to 107.0 and 98.9 to 108% for river, lake and tap water, respectively.

***Keywords:** Selenium(IV); ion-exchange preconcentration; solid-phase hydride generation; water analysis; flow injection*

There are significant advantages in the use of hydride generation (HG) with AAS or other atomic spectrometric detection methods for the determination of elements which form volatile hydrides. Hydride generation has become one of the most powerful and well established techniques for the determination of arsenic, antimony, bismuth, germanium, lead, selenium, tellurium, tin, indium, and thallium. A variety of reactions have been used to convert the analyte in solution into the hydride.[1–8] There are also several reports of electrochemical hydride generation[9–11] and of thermochemical gas-phase hydride generation.[12] In the case of solution reactions, a metal–acid combination, or more commonly reaction with borohydride is employed for hydride generation. In early applications of the technique, the March reaction, based on a metal–acid system such as Zn–HCl producing nascent hydrogen which reacted with the analyte to form the hydride, was used.[3] The more commonly used reaction for hydride formation is the BH_4^-–acid reaction.[13]

Although some precursors are hydrated cations in the appropriate oxidation state, as for example with Pb^{IV}; for most analytes the precursor may well exist as an oxo-anion which is reduced prior to the final hydride transfer reaction, as would be the case with Se^{IV}. Initial applications used NaBH$_4$ pellets, but an aqueous solution stabilized by potassium or sodium hydroxide[4] may be conveniently used and is currently the most popular reagent. Other forms of borohydride have been used. Borohydride bound to a stationary phase in a column has been used for hydride generation of arsenic[5,6] and selenium.[7,8] However, the only advantage reported over the use of an aqueous solution of BH$_4^-$ was the suppression of some matrix interferences.

In our current work on hydride generation with in-atomizer trapping for determination of low concentrations of selenium by ETAAS,[14] we have found that detection limits are governed by impurities in the borohydride reagent. We considered that the immobilization of borohydride on an anion-exchange resin might result in a purer reagent and hence improved detection limits.

In the course of this study, we found that selenium was retained on the anion-exchange resin and that hydrogen selenide could be generated from the resin by the passage of acid when both selenium and borohydride were co-immobilized. In this paper, we report on the analytical performance of a system for the determination of selenium based on this method of generation of hydrogen selenide.

Experimental

Reagents

Apparatus

The detection unit used was a Perkin-Elmer (Norwalk, CT, USA) Model 3100 atomic absorption spectrometer. The atomizer was a flame-heated quartz T-shaped tube. The quartz tube was cleaned weekly with acid following the procedure described by Hatfield.[15] A hollow-cathode lamp (Perkin-Elmer) was used as a light source. The wavelength for Se was 196.0 nm. The spectral bandpass was 0.7 nm.

Manifold

The manifold, shown schematically in Fig. 1, was constructed from 0.8 mm id PTFE tubing, except the tubing between the argon confluence point, the gas–liquid separator and quartz tube, which was PTFE tubing of 1.5 mm id. The gas–liquid separator consisted of a 25 ml separating funnel with a two-holed rubber cap. The column consisted of a glass tube of 150 mm length and 4 mm id. Two PTFE reducing unions of $1/4 \times 1/8$ in (Cole-Parmer, Chicago, IL, USA), fitted at either end of the column, were used to connect it to the manifold.

A slurry of anion-exchange resin was introduced into the column with the aid of a syringe. A small amount of glass-wool was placed at the ends of the column to prevent loss of the resin. The column was ready for use after washing several times alternately with borohydride and hydrochloric acid solutions. Two six-port PTFE Rheodyne rotary valves (Supelco, Bellefonte, PA, USA) were used. The ion-exchange column was located in the injection loop of one and the other was used to introduce a discrete volume (500 µl) of acid. Two Ismatec SA MS-Reglo Model 7331-10 peristaltic pumps (from Cole-Palmer) were used, one for the carrier line and the other for the acid, sample, and borohydride lines. The waste from the gas–liquid separator was pumped with a Lachat Instruments (Milwaukee, WI, USA) Model 1200-000 peristaltic pump. The flows of reagents were regulated by using Tygon pump tubing (Cole-Parmer) of different internal diameters and by control of the pump head rotation speed.

Recommended Procedure

All the experiments were carried out using the manifold shown in Fig. 1. In the load position, Fig. 1(a), the sample of selenite (SeO_3^{2-}) and the borohydride were mixed and pumped through the column for a period of 1, 2 or 3 min, resulting in the simultaneous retention of both anions (SeO_3^{2-}, or possibly Se^{2-}, and BH_4^-). At the same time, the loop of valve 1 was filled with acid, while the de-ionized water carrier was pumped constantly through the system. In the injection position, Fig. 1(b), valve 2 was switched and the column was washed for a period of 20 s with carrier solution. Valve 1 was then switched and the acid was carried through the column generating

Fig. 1 Schematic diagram of the manifold for selenium preconcentration and hydride generation. (a) load position and (b) injection position. $V_{1,2}$, six-port valves; $P_{1,2,3}$, peristaltic pumps; QAC, quartz atomization cell; GLS, gas–liquid separator; CL, column packing with strong anion-exchange resin; L, 500 µl loop; CS, carrier solution, distilled, deionized 18 MΩ E-pure water (14 ml min^{-1}); AS, 4 mol l^{-1} HCl (1.5 ml min^{-1}); RS, 0.05% m/v NaBH$_4$ in 0.01% m/v NaOH (3.0 ml min^{-1}); S, sample (3.0 ml min^{-1}); and W, waste.

hydrogen selenide. The column was cleaned between samples and standards by passing 4% m/v borohydride in 0.5% m/v NaOH for 30 s followed by an injection of acid. The cleaning step was not needed between replicate injections of the same sample or standard.

Method Development

Determination of arsenic

Initial experiments involved repeating the procedures described by Tesfalidet and Irgum[5] and Narasaki *et al.*[6] for the determination of arsenic. In these procedures, the borohydride was first loaded on to the anion-exchange column and, after washing, the acidified analyte solution was passed through the column generating arsine and hydrogen. These experiments are not described in detail here. The detailed experimental work concerns the development of the new procedure for the determination of selenium.

Gas–liquid separation

Two types of gas–liquid separator were used, namely the Perkin-Elmer device from the FIAS unit (this was the empty plastic vessel) and a device constructed in-house from a 25 ml separating funnel. In neither case was any additional device used to reduce the transfer of water vapor or droplets to the atomizer. The drains from both these devices were pumped. In the case of the separating funnel device the drain pump rate was such that there was always 1–2 ml of liquid in the funnel.

Column dimensions

Two different strongly basic resins, Amberlite IRA-410 and Amberlyst A26, were packed in columns of various dimensions. Four different lengths (50, 100, 150 and 200 cm) and two different internal diameters (2 and 4 mm) were used in all possible combinations. Both resins have styrene–divinyl-benzene skeletal structures; however, Amberlite IRA-410 is a gel-type resin and Amberlyst A26 is a porous or macroreticular resin. The resulting columns were tested for selenium retention and subsequent hydride generation for six replicate measurements at two concentrations of selenium, 10 and 25 µg l^{-1}.

Parameter optimization

The multi-cycle alternating variable search optimization method[16,17] was used for the optimization of the following parameters: borohydride concentration, HCl concentration, carrier flow rate and stripping gas flow rate. The figure of merit for the optimization process was maximum net peak height sensitivity (*i.e.*, signal minus blank). Other parameters that were studied include the dimensions of the column, nature of the anion-exchange resin, oxidation state of the selenium and the flow rates of the sample and borohydride solutions.

Parameter optimization was carried out with a 1 min preconcentration (at 3 ml min^{-1} sample and borohydride flow rates), using a column size of 150×4 mm id packed with Amberlite IRA-410 anion-exchange resin. The optimization of the borohydride and HCl concentrations was carried out using sample solutions of 0, 10 and 25 µg l^{-1} of Se. The effect of such reagents was studied by varying these concentrations within the ranges 0.01–2% m/v NaBH$_4$ in 0.01% m/v NaOH, and 0.1–2 mol l^{-1} HCl. Samples of 10 and 25 µg l^{-1} were used in the studies of the effects of the argon stripping gas flow rate and the carrier flow rate, *i.e.*, the speed at which the acid passed through the column. The argon flow rates were varied between 50 and

1000 ml min^{-1}. The carrier flow rate was varied between 4 and 15 ml min^{-1}.

Analytical Performance

Using the optimal experimental conditions (given in Table 1), calibration graphs with 0, 5, 10, 15, 20, and 25 µg l^{-1} of Se for 1, 2 and 3 min of preconcentration were made. The precision of the system was evaluated as the RSD of 10 successive determinations of 5, 10 and 20 µg l^{-1} of Se for 1, 2 and 3 min of preconcentration, respectively. The accuracy was evaluated by means of the recovery of 0.5, 2 and 10 µg l^{-1} of Se spiked in river, lake and tap water.

The effect of the sample matrix was evaluated by the method of standard additions. Equal volumes of river, lake and tap water (45 ml) were taken, all but one were separately spiked with different amounts of selenium and then all were diluted to equal volumes (50 ml) to obtain three series of solutions with final concentrations added of 0, 5, 10, 15, 20 and 25 µg l^{-1} of Se. Signals were obtained under the optimal experimental conditions (Table 1) for a 3 min preconcentration time. All calibrations were obtained by an unweighted least-squares procedure.

Results and Discussion

Determination of Arsenic

The results reported previously[5,6] for the determination of arsenic were confirmed. Signals were obtained for both As^{III} and As^{V}. For a sample volume of 835 µl, the linear ranges for As^{III} and As^{V} were 0.6–40 and 0.9–50 µg l^{-1}, respectively. The precisions, expressed as RSD for five replicate determinations of 20 µg l^{-1}, were between 1.8% and 3.2% for As^{III} and between 2.4% and 4.1% for As^{V}.

Gas–Liquid Separator

The device based on the 25 ml separating funnel was used, rather than the smaller internal volume Perkin-Elmer device, to avoid the carry-over of liquid which tends to occur with certain combinations of argon gas flow rate and borohydride concentration with devices having small internal volumes. As the optimization studies required that these parameters be varied, the use of a more robust gas–liquid separator decreased the down-time spent cleaning and regenerating the surface of the quartz cell. However, for an FI-based procedure the gas–liquid separator will affect the peak height sensitivity by virtue of a contribution to the overall dispersion and it is likely that the device used here is sub-optimal with respect to this characteristic.

Column Dimensions and Resin Type

The best results were observed with larger column sizes (lengths and id) with both resins, *i.e.*, when the amount of resin was increased. However, lengths above 150 mm for the same internal diameter did not produce any improvement in the signal. The Amberlite IRA-410 gel-type resin produced better results than the Amberlyst A26 macroreticular resin. Therefore, a 150 × 4 mm id column packed with Amberlite IRA-410 gel-type resin was chosen for further experiments.

Parameter Optimization

The optimum conditions are given in Table 1. No signals were obtained from solutions of Se^{VI}. To achieve the best sensitivity, three cycles of the optimization process were necessary. The results of the third cycle for each parameter are discussed below. The effect of the concentration of borohydride is shown in Fig. 2. There was a steady increase in the blank signal as the concentration of borohydride increased from 0.01 to 1.0% m/v, with a slower increase from 1.0 to 2.0% m/v. For both samples (10 and 25 µg l^{-1} of Se) a sharp increase in the signal was observed as the borohydride concentration increased from 0.01 to 0.05% m/v NaBH$_4$, followed by a sharp decrease from 0.5 to 1.0% m/v. No signal was obtained in the absence of borohydride. The 0.05% m/v concentration produced the optimum net signal. This concentration of borohydride is considerably lower than that used in typical flow injection and typical batch procedures.

The effect of the concentration of HCl is shown in Fig. 3. As can be seen, the signals from the samples and the blank increased as the HCl concentration increased to 0.5 mol l^{-1}, but changed little thereafter. Therefore, 4 mol l^{-1} was chosen for further experiments.

The effect of carrier flow rate is shown in Fig. 4. Carrier flow rates between 12 and 15 ml min^{-1} resulted in the best net absorbance signal. A carrier flow rate of 14 ml min^{-1} was used in further experiments. The effect of the stripping gas flow rate is shown in Fig. 5. The most favorable rate was found to be 180 ml min^{-1}, hence this value was chosen for further experiments.

Table 1 Optimum operation conditions

Atomic absorption spectrometer—

Wavelength	196 nm
Slit width	0.7 nm
Lamp current	16 mA
Quartz cell temperature	900 °C
Background correction	On

On-line preconcentration and hydride generation—

HCl concentration	4 mol l^{-1}
NaBH$_4$ concentration	0.05% m/v
Sample flow rate	3.0 ml min^{-1}
NaBH$_4$ flow rate	3.0 ml min^{-1}
Carrier flow rate	14.0 ml min^{-1}
Argon flow rate	100 ml min^{-1}
Column size (length × id)	150 × 4 mm
Resin	Amberlite IRA-410

Fig. 2 Effect of concentration of NaBH$_4$ solution on the signal peak height (absorbance). A, no Se; B, 10 µg l^{-1} of Se; and C, 25 µg l^{-1} of Se. The error bars represent the standard deviation for five replicate measurements.

Analytical Performance

The calibration equations and the other performance figures of merit are summarized in Table 2. The system responded linearly from the detection limit up to 180, 120 and 80 µg l^{-1} of Se for
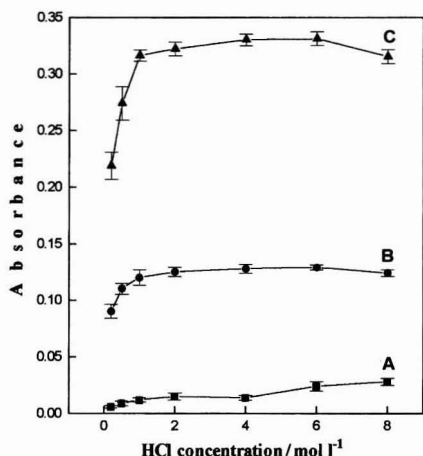
Fig. 3 Effect of concentration of HCl solution on the signal peak height (absorbance). A, no Se; B, 10 µg l^{-1} of Se; and C, 25 µg l^{-1} of Se. The error bars represent the standard deviation for five replicate measurements.
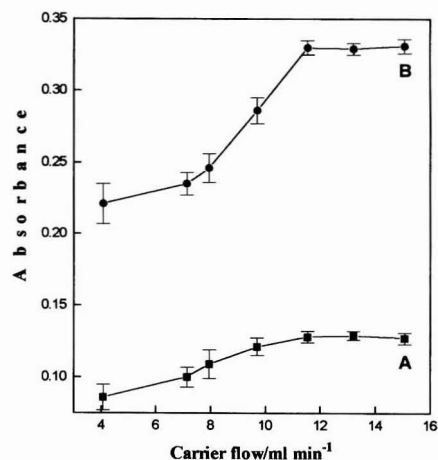
Fig. 4 Effect of the carrier solution flow on the net signal peak height (absorbance). A, 10 µg l^{-1} of Se; and B, 25 µg l^{-1} of Se. The error bars represent the standard deviation for five replicate measurements.

1, 2 and 3 min preconcentration, respectively. The precision of the procedure as a function of concentration, expressed as RSD, varied from 0.41 to 1.32, 0.24 to 0.81 and 0.18 to 0.61% for 1, 2 and 3 min preconcentration, respectively. The precision of the system improved with preconcentration time, but degraded severely if the residual sample and borohydride were not washed from the column. Carry-over between samples and standards was prevented by flushing residual selenium from the column with the 4% borohydride wash. The limits of detection, defined as the concentration giving a signal equal to three times the standard deviation of the blank signal, were 0.24, 0.15 and 0.12 µg l^{-1} of Se for 1, 2 and 3 min preconcentration, respectively. The sample throughput was 21 h^{-1} for 1 min preconcentration.

The results of the standard additions to the water sample matrices were compared with those for the same concentrations in distilled water. The characteristics of the regression lines are summarized in Table 3. The 95% confidence interval about the slope of the calibration in the distilled water matrix contains the slopes of the calibrations in the other matrices, *i.e.*, the confidence intervals of the slopes overlap in all cases and there is no significant difference between the slopes for the different matrices. As no appreciable matrix effect was observed, the analyses of the test samples were performed by calibration with aqueous solutions of a pure selenium salt (Na$_2$SeO$_3$).

The recoveries (and standard deviations) of spikes added to the water samples are given in Table 4 and ranged from 96 ± 4 to 102 ± 6, 96 ± 4 to 107 ± 6 and 99 ± 4 to 108 ± 6%, depending on the concentration, for river, lake and tap water, respectively. These values indicate that selenium can be quantitatively determined in such samples.
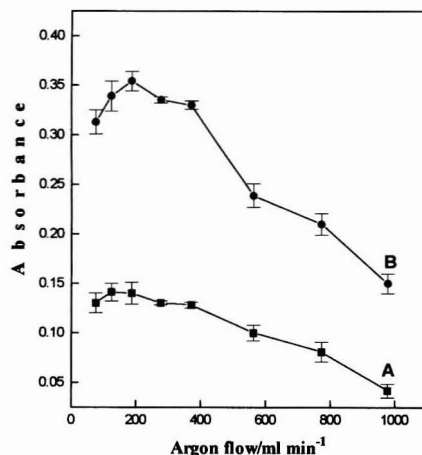
Fig. 5 Effect of stripping gas (argon) flow rate on the net signal peak height (absorbance). A, 10 µg l^{-1} of Se; and B, 25 µg l^{-1} of Se. The error bars represent the standard deviation for five replicate measurements.

Table 2 Analytical performance of the system

Time*/ (min)	Regression equation: $A = b + mC$[†]	r[‡]	LOD (3s)[§]/ µg l^{-1}	RSD (%)[¶]		
				5 µg l^{-1}	10 µg l^{-1}	20 µg l^{-1}
1	$A = 0.011 + 0.0123C$	0.9996	0.24	1.32	0.83	0.41
2	$A = 0.022 + 0.0197C$	0.9997	0.15	0.81	0.46	0.24
3	$A = 0.035 + 0.0256C$	0.9997	0.12	0.61	0.36	0.18

* Time of passage of sample through the column at 3 ml min^{-1}. † A is absorbance, b is intercept, m is slope and C is concentration of Se in µg l^{-1}. ‡ Regression coefficient. § LOD (3s) is the detection limit, calculated for $3s/m$, where s is the within-run standard deviation of a blank determination ($n = 10$). ¶ RSD for 5, 10 and 20 µg l^{-1} of Se ($n = 10$).

Determination of Se[IV] in Water

The results of the application of the proposed method to the determination of selenium in river, lake and tap water are given in Table 4 for a sample volume of 9 ml (3 min preconcentration time). The concentration of selenium in the river water sample was 0.14 ± 0.01 µg l^{-1}. The concentrations of selenium in the lake and tap water samples analyzed were below the detection limit of 0.12 µg l^{-1}. It is known that the concentration of SeO_3^{2-} in natural water[18-20] is usually very low and that selenium is present in water in various oxidation states and chemicals forms, including organic species.[18,21,22]

Conclusions

The co-immobilization of selenium and borohydride on an anion-exchange resin followed by passage of acid forms the basis of a viable method for the determination of selenium by HGAAS and quantitative recovery of selenium from water samples can be achieved. The procedure could be fully automated *via* a system of computer-controlled valves and pumps and can be used with any atomic spectrometric detection system. Work is in progress to implement the procedure on a Perkin-Elmer FIAS unit. The preconcentration of the analyte on the anion-exchange column allows the potential for improved sensitivity over conventional flow injection hydride generation techniques and the possibility of the separation of the analyte from cation interferences. Current development of the procedure is focused on overcoming such matrix interferences as it may be possible to immobilize the sample and the borohydride successively.

Table 3 Standard additions of selenium to water samples

		Regression line characteristics				
Matrix	Slope	s_{slope}	Confidence limits*	Intercept	s_{int}	$r^\dagger$
Distilled water	0.0257	0.00048	0.0013	0.032	0.0073	0.9995
River water	0.0249	0.00045	0.0012	0.039	0.0067	0.9998
Lake water	0.0251	0.00045	0.0012	0.035	0.0069	0.9998
Tap water	0.0248	0.00043	0.0012	0.034	0.0061	0.9999

* Confidence limits for the slope, given by ts; the t-value was taken at the 95% confidence level and $n - 2$ degrees of freedom. † Correlation coefficient.

Table 4 Analytical results for various water samples

Sample	Selenium added/ µg l^{-1}	Selenium found/ µg l^{-1}	Recovery (%)
River water			
(Fort river, Amherst)	0	0.14 ± 0.01	—
	0.5	0.65 ± 0.03	102 ± 6
	2.0	2.06 ± 0.07	96 ± 4
	10.0	10.05 ± 0.39	99 ± 4
Lake water			
(Puffers Pond, Sunderland)	0	<DL*	—
	0.5	0.48 ± 0.02	96 ± 4
	2.0	2.05 ± 0.05	103 ± 3
	10.0	10.70 ± 0.56	107 ± 6
Tap water			
(Amherst)	0	<DL*	—
	0.5	0.54 ± 0.03	108 ± 6
	2.0	2.01 ± 0.05	101 ± 3
	10.0	9.89 ± 0.43	99 ± 4

* Detection limit, 0.12 µg l^{-1} of Se.

References

1 Nakahara, T., *Spectrochim. Acta Rev.*, 1991, **14**, 95.
2 Godden, R. G., and Thomerson, D. R., *Analyst*, 1980, **105**, 1137.
3 Branch, C. H., and Hutchison, D., *Analyst*, 1985, **110**, 163.
4 Agterdenbos, J., and Bax, D., *Fresenius' Z. Anal. Chem.*, 1986, **323**, 783.
5 Tesfalidet, S., and Irgum, K., *Anal. Chem.*, 1989, **61**, 2079.
6 Narasaki, H., Kato, Y., and Kimura, H., *Anal. Sci.*, 1992, **8**, 893.
7 Cao, J.Y., and Narasaki, H., *Bunseki Kagaku*, 1994, **43**,169.
8 Tesfalidet, S., and Irgum, K., *Fresenius' J. Anal. Chem.*, 1991, **341**, 532.
9 Brockmann, A., Nonn, C., and Golloch, A., *J. Anal. At. Spectrom.*, 1993, **8**, 397.
10 Lin, Y., Wang, X., Yuan, D., Yang, P., Huang, B., and Zhuang, Z., *J. Anal. At. Spectrom.*, 1992, **7**, 287.
11 Ding, W.-W., and Sturgeon, R. E., *J. Anal. At. Spectrom.*, 1996, **11**, 225.
12 Blais, J. S., Momplaisir, G. M., and Marshall, W. D., *Anal. Chem.*, 1990, **62**, 1161.
13 Howard, A. G., *J. Anal. At. Spectrom.*, 1997, **12**, 267.
14 Tyson, J. F., Sundin, N. G., Hanna, C. P., and McIntosh, S. A., *Spectrochim. Acta Part B*, in the press.
15 Hatfield, D. B., *Anal. Chem.*, 1987, **59**, 1887.
16 Greenfield, S., Salman, M. S., Thomsen, M., and Tyson, J. F., *J. Anal. At. Spectrom.*, 1989, **4**, 55.
17 Miller, J. C., and Miller, J. N., *Statistics for Analytical Chemistry*, 3rd edn, Ellis Horwood, Chichester, 1993, pp. 185–187.
18 Cutter, G. A., *Anal. Chim. Acta*, 1978, **98**, 59.
19 Measures, C. I., and Burton, J. D., *Nature (London)*, 1978, **273**, 293.
20 Yu, Q., Liu, G. Q., and Jin, Q., *Talanta*, 1983, **30**, 265.
21 Cutter, G. A., *Anal. Chim. Acta*, 1983, **149**, 391.
22 Robberecht, H., and Van Grieken, R., *Talanta*, 1982, **29**, 823.

Evaluation of a Direct Solid Sampling Atomic Absorption Spectrometer for the Trace Determination of Mercury in Geological Samples

Gwendy E. M. Hall and Pierre Pelchat

Geological Survey of Canada, 601 Booth Street, Ottawa, Ontario, Canada K1A 0E8

This paper reports the evaluation of a new cold vapour atomic absorption spectrometer applied to the direct determination of Hg in geological materials. The AMA-254 is based on thermal decomposition of the sample and collection of the evolved Hg vapour on a gold amalgamator. A suite of 33 reference materials, including rocks, soils, sediments and coal, was analysed in duplicate, using sample masses ranging from *ca.* 30 to 300 mg. Agreement with recommended values was good for all but one sample, TILL-1, where this method produced high results of 145 µg kg^{-1} Hg compared to a proposed value of 92 µg kg^{-1} obtained by HCl–HNO$_3$ digestion. Precision, over the range of Hg in these samples of 4 to 6250 µg kg^{-1}, was shown to be 10% (±5% RSD). Cycle time was 5 min per sample.

Keywords: Mercury; direct determination; cold vapour atomic absorption spectrometry; geological

Cold vapour atomic absorption spectrometry (CVAAS) has been the method of choice for Hg determination since the classic paper by Hatch and Ott in 1968.[1] Most instrumental configurations are based on reduction of Hg^{2+} ions, present in an acidic medium, to Hg^0 vapour by addition of a reducing agent such as sodium tetrahydroborate or tin(II) chloride. Mercury vapour is then separated from solution prior to analysis by a gas–liquid separator accompanied in some schemes by a drying membrane. Such methods have been reviewed and improved upon recently through optimisation of the flow injection or continuous flow procedure.[2,3] Instead of measurement of the vapour by AAS, alternative techniques of AFS and ICP-AES have also been employed.[4] Amalgamation on gold is often used to preconcentrate Hg^0 (and/or other gaseous species such as CH$_3$HgCl and HgCl$_2$) formed from acidic solution[5] or present in air.[6,7]

Aqua regia (3 + 1 HCl–HNO$_3$) digestion (or its inverse counterpart) is commonly employed for the determination of total Hg in geological samples, the main mineral being cinnabar (HgS) which is only partially soluble in HNO$_3$ alone.[8–10] Care must be taken to avoid losses of organomercury compounds *via* volatilisation during open digestion[9] and oxidants such as KMnO$_4$ or K$_2$Cr$_2$O$_7$ are sometimes added to maintain Hg in solution as Hg^{2+} prior to analysis. These oxidants are also used to provide additional oxidising power in digesting samples high in organic content such as biological materials, sludges and vegetation.[11] Clearly, avoidance of a digestion step for Hg would obviate concerns such as (1) loss through volatilisation, precipitation or poor decomposition and (2) contamination from reagents, equipment and the environment in which digestion is carried out.

Recently Milestone (Sorisole, Italy) introduced a commercial AA spectrometer, known as the AMA-254, based on the former TMA-254 (trace mercury analyser) designed at the Technical University of Prague.[12] This sole purpose instrument is dedicated to the *direct* determination of Hg in solid media. The

performance of similar, custom-built instrumentation has been reported previously but, perhaps surprisingly, that success did not lead to commercialisation of this product.[13–15] In an application of the AMA-254 to the analysis of a variety of foodstuffs (*e.g.*, flour, corn, milk powder, oyster tissue), an accuracy of better than ±8% and a detection limit of 0.5 µg kg^{-1} were obtained.[16] Precision was in the range 1.6–6.7% RSD, the masses taken for analysis being in the range 100–300 mg. This paper reports the results of application of this instrument to the analysis of 33 geological reference materials (GRMs) of widely variable matrix. A recent paper by Terashima[17] also presented results for Hg in GRMs using direct combustion–amalgamation–AAS with the Nippon Jarrell-Ash Model AA-855 spectrometer equipped with a Model AMD mercury detector accessory.

Instrumentation

A schematic diagram of the AMA-254 is shown in Fig. 1. The weighed sample (≤350 mg) is placed in a nickel (or platinum) boat which is then introduced automatically into a quartz tube. Two ovens surround the quartz tube: the first is where sample decomposition occurs; and the second, held at a temperature of 750 °C, contains a Mn$_3$O$_4$ and CaO based catalyst which is employed to remove oxides of nitrogen and sulfur as well as halogens from the gas train. The sample is initially dried at 125 °C and then thermally decomposed at a temperature of 550 °C whereupon the evolved gases are swept in a flow of ultra-pure oxygen (Hg-free, scrubbed by passing through a charcoal trap if
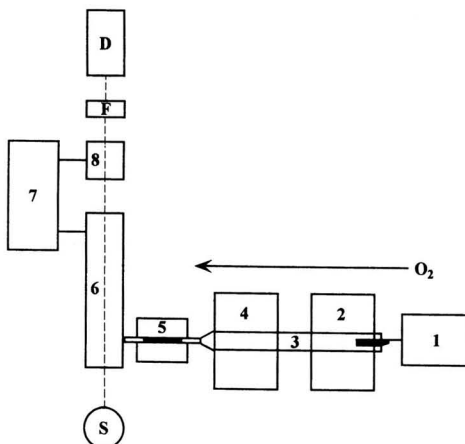
Fig. 1 Schematic of the AMA-254: 1, sample introduction by motorised system; 2, decomposition oven; 3, quartz tube; 4, catalytic oven; 5, gold amalgamator; 6, first measurement cell (1 cm x 7.5 cm); 7, delay flask; 8, second measurement cell (1 cm×1 cm); S, Hg vapour source lamp; F, interference filter; D, detector.

necessary) at a flow-rate of 200 ml min^{-1} through the second oven. Mercury vapour is then trapped on the gold amalgamator situated inside a third oven. The trap is then heated rapidly to release the Hg which is swept by the oxygen flow to the longer of two measurement cells located in a unit maintained at 120 °C to avoid vapour condensation. Both this cell and the second, at 1/10th the length of the first, are situated in the light path between a low pressure Hg vapour source lamp and an interference filter (to isolate the 253.65 nm Hg atomic resonance line, 9 nm bandwidth) and silicon UV detector. After the first absorption reading is acquired, Hg is carried into the delay flask and then to the short cell used for measurement at higher levels of Hg. The volume of the delay flask is larger than that of the first measurement cell (7) to ensure that all gaseous Hg has left this cell before entering the second (8). In this manner, the dynamic range is extended to about 600 ng of Hg. After release of Hg vapour to the measurement cell, a cooling pump is activated to cool down the amalgamator for more rapid cycling. Parameters such as drying time (9–999 s), decomposition time (1–999 s), and oxygen flow-rate are under computer control (PC). The temperatures used in the drying and decomposition stages are fixed and not programmable. Typically one sample can be processed every 5 min. This instrument differs markedly from the modular unit used by Terashima[17] where the single measurement cell limits the dynamic range to about 50 ng of Hg (*cf.* 600 ng). Furthermore, the latter instrumentation requires far more manual intervention such as insertion of the boat and frequent repacking of the combustion tube with Na_2CO_3 used to eliminate interference from halogens and sulfur species.
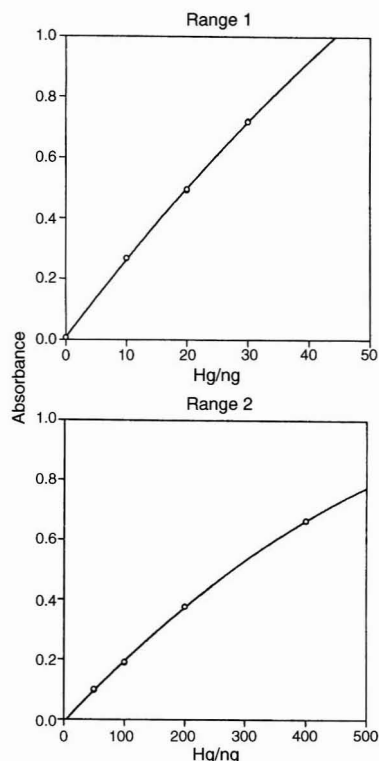
Fig. 2   Calibration curves for each measurement cell, range 1 being for cell 6 in Fig. 1 and range 2 for cell 8.

It is possible to programme this instrument to allow repeat dosing of the sample. For example, about 300 mg of sample would be introduced and thermally treated so that Hg is trapped on the amalgamator. Another 300 mg could then be introduced and decomposed, and so on, to a limit of 10 subsamples (*i.e.*, equivalent to 3 g of sample), after which all Hg would be released from the amalgamator and measured. Thus, a sample very low in Hg content (< 1 µg kg^{-1}) could be analysed, though at the expense of productivity.

Experimental

The instrument is allowed 30 min to stabilise prior to use, so that the ovens are at their respective temperatures. Drying and

Table 1 Results for Hg in 33 GRMs using the AMA-254 analyser. (Some samples show several sets of results from different bottles)

GRM	Hg/µg kg^{-1}	Literature value/µg kg^{-1}
Canadian Certified Reference Materials Project (CCRMP)*—		
SO-1 (soil)	18.3, 18.3	21 ± 3
SO-1 (second bottle)	18.6, 18.9	
SO-2 (soil)	86, 86	82 ± 12
SO-2 (second bottle)	90, 88	
SO-2 (third bottle)	87, 87	
SO-3 (soil)	8.9, 9.1	17 ± 7
SO-4 (soil)	29, 29	32 ± 10
LKSD-1 (lake sediment)	119, 115	110 ± 15
LKSD-2 (lake sediment)	171, 164	160 ± 19
LKSD-3 (lake sediment)	289, 291	290 ± 36
LKSD-4 (lake sediment)	203, 203	190 ± 17
LKSD-4 (second bottle)	187, 185	
TILL-1 (soil, B + C horizons)	145, 144	92 ± 11
TILL-2	69, 69	74 ± 13
TILL-2 (soil, B + C horizons)	122, 123	107 ± 15
TILL-4 (till)	29, 29	39 ± 12
Institute of Geophysical and Geochemical Prospecting (IGGE)†—		
GSD-2 (stream sediment)	34, 35	40
GSD-4 (stream sediment)	42, 41	44
GSD-6 (stream sediment)	45, 53	45
GSD-8 (stream sediment)	40, 42	42
GSD-10 (stream sediment)	276, 286	280
GSD-12 (stream sediment)	52, 55	56
GSR-2 (andesite)	7.0, 7.4	12
GSR-5 (shale)	8.7, 8.8	10
National Institute for Standards and Technology (NIST)‡—		
SRM 1630 (coal)	109, 105	130 ± 30
SRM 1633a (coal fly ash)	164, 159	160 ± 0
SRM 1633a (second bottle)	166, 162	
SRM 1645 (river sediment)	967, 942	1110 ± 500
SRM 1646 (estuarine sediment)	78, 78	63 ± 12
SRM 2709 (soil)	1438, 1371	1400 ± 80
SRM 2711 (contaminated soil)	5803, 6339	6250 ± 190
Miscellaneous§—		
MAG-1 (marine mud, USGS)	61, 61	N/A¶
JB-1a (basalt, GSJ)	6.5, 5.7	5.3–9 (*n* = 3)
JG-1a (granodiorite, GSJ)	4.2, 4.0	3.5–5 (*n* = 3)
BCSS-1 (marine sediment, NRCC)	194, 195	N/A
BCR-40 (coal)	378, 387	350 ± 60
SARM-20 (coal)	248, 238	250 ± 180
GN01 (barite, GSC)	83, 82	81 ± 5

* Literature values for: SO series are taken from ref. 18; LKSD from ref. 19; and the TILL series from ref. 20.   † Literature values from ref. 21.   ‡ Literature values from Certificates of Analysis.   § Literature values for: JB-1a and JG-1a from ref. 22; BCR-40 and SARM-20 from Certificates of Analysis; GN01 from the GSC database.   ¶ N/A, Not available. Underlined figures signify recommended operation values; others indicate proposed values.

decomposition times of 50 and 160 s, respectively, were selected. A delay of 45 s was employed to allow combustion products to be swept out of the instrument prior to rapid release of the Hg from the amalgamator. Two Ni boats were used; both were cleaned initially by applying a typical analysis cycle twice. Calibration was carried out using serial dilution of a 1000 mg l^{-1} Hg standard, maintained in 10% HNO$_3$ (CLHG4-2Y from SPEX Chemicals, Metuchen, NJ, USA). A constant volume of 100 µl of standard solution (including an HNO$_3$ blank) was used to construct both calibration curves. Standard solutions of 0, 0.1, 0.2 and 0.3 (equivalent to 30 ng) mg l^{-1} Hg were employed for the lower range and 0.5, 1, 2 and 4 mg l^{-1} Hg for the upper calibration curve (using the second measurement cell). Two readings were taken for each standard (*i.e.*, 10 min per standard). Such a complete calibration is not required daily; in fact, the change in slope of both curves over a period of one month was less than 2%. Our daily practice is to run two blanks followed by a solution standard as primary calibration. To assess quality control, a well characterised solid standard is included at a rate of 1 in 20 samples.

A suite of 33 GRMs, ranging from 4 to 6250 µg kg^{-1} in Hg, were analysed in duplicate (*i.e.*, two separate weighings and analysis of each sample). Where more than one bottle of the GRM was available in the laboratory, it too was sampled in duplicate. Samples were weighed to the nearest 0.1 mg, and varied from about 38 to 318 mg, higher masses being used for GRMs known to be low in Hg content (< 20 µg kg^{-1}). After every batch of 10 samples, a blank and a solid GRM were run to check for instrument drift. A blank was also run following a sample registering greater than 400 ng of Hg as absorbance values greater than 0.005 were otherwise encountered as carryover.

Results and Discussion

Calibration curves for the two ranges of Hg are given in Fig. 2. At Hg levels above about 35 ng, the upper range is used for measurement and here the degree of curvature above 0.8 absorbance units suggests that samples producing more than about 400 ng of Hg be reanalysed at a lower mass.

Results for Hg in the 33 GRMs are given in Table 1; also shown are the affiliations of these GRMs. The convention used by Govindaraju[21] to reflect the degree of confidence in the 'literature value' has been used here: those underlined signify recommended or accepted values while the others indicate

AMA 254 Hg analysis

Fig. 3 'Thompson and Howarth' plot for precision estimation, using the 38 sets of duplicate data taken from Table 1.

proposed values (with less certainty). For the CCRMP series analysed, data derived by the AMA-254 method agree well (within the given uncertainties) with the recommended or proposed values, with the exception of the results for SO-3 (a proposed value of 9 *vs.* 17 µg kg^{-1}) and TILL-1. The result for SO-3 of 9 µg kg^{-1} is in excellent agreement with the value of 10 ± 1 µg kg^{-1} obtained at the GSC by *aqua regia* digestion (*n* = 3) and CVICP-MS. Furthermore, Terashima[17] reports a value of 11 ± 1 µg kg^{-1} Hg in SO-3 by a combustion CVAAS method. The mean results of 203 and 186 µg kg^{-1} Hg in LKSD-4, with the excellent precision demonstrated by the replicate analyses, suggest that a difference in Hg content dependent on bottle may exist. The recommended values for Hg in the LKSD and TILL series[19, 20] are each based on 31–45 analyses from 4 to 7 laboratories using a mixture of concentrated HNO$_3$ and concentrated HCl for digestion. The much higher values obtained for TILL-1 by this direct method are interesting and suggest that further investigation is required into whether some Hg is in a form not amenable to this acid digestion.

Of the IGGE sediment and rock series examined, only the result for the andesite GSR-2 seems questionable, at 7.2 ± 0.2 µg kg^{-1} Hg compared to 12 µg kg^{-1}. In the absence of the standard deviation associated with this recommended value, it is difficult to assess the degree of accuracy here. The close agreement in the replicate results suggests that heterogeneity, with sampling at 220–280 mg, is not a problem. Excellent results are evident for the NIST SRMs analysed, though one value of 5803 µg kg^{-1} for SRM 2711 seems rather low (*cf.* 6250 ± 190 µg kg^{-1}). This result corresponds to a sample mass of only 45 mg. *Aqua regia* digestion of 500 mg aliquots of this GRM and measurement by CVICP-MS produced a mean value of 6166 ± 90 µg kg^{-1} Hg (*n* = 3). There is no recommended or proposed value for Hg in MAG-1, available from the United States Geological Survey, but the concentration found of 61 µg kg^{-1} is in good agreement with that obtained by Terashima,[17] 59 ± 3 µg kg^{-1}. For GRMs JB-1a and JG-1a, only three values are reported by the Geological Survey of Japan (GSJ) but the concentrations found by this method (6.1 ± 0.4 and 4.1 ± 0.1 µg kg^{-1} Hg, respectively) lie within these ranges. Results for the coal GRMs, BCR-40 (from the Community Bureau of Reference, Brussels) and SARM-20 (from the National Institute of Metallurgy, South Africa), also match well with values given with the Certificates of Analysis.

The data shown in Table 1 clearly demonstrate excellent reproducibility. These 38 sets of results were used to evaluate precision according to the method pioneered by Thompson and Howarth.[23] In this approach, the absolute difference between the duplicate pair is plotted against their mean on a log–log scale and a 95th percentile line for a selected precision (twice the RSD) is then drawn. Thus, the 95th percentile for the selected precision on each graph is an upper confidence limit (*i.e.*, the 'worst' case precision value) above which no more than 5% of the points should lie. Such a plot is shown in Fig. 3. Thus, these results indicate that a precison of 10% (±5%) can be expected in the range 4–6000 µg kg^{-1} Hg.

This instrument is a valuable addition for those concerned with the determination of Hg, particularly at low levels and in matrices where acid decomposition could create problems of volatilisation loss or contamination. Although a sample can be processed every 5 min, productivity should be improved by automation of sample introduction which would then make the instrument essentially operator free.

References

1   Hatch, W. R., and Ott, W. L., *Anal. Chem.*, 1968, **40**, 2085.
2   Hanna, C. P., Haigh, P. E., Tyson, J. F., and McIntosh, S., *J. Anal. At. Spectrom.*, 1993, **8**, 585.
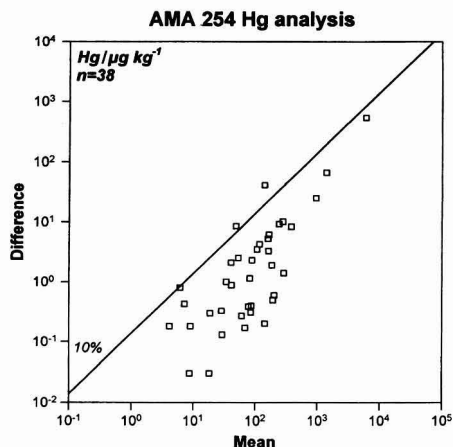
3   Fernandez, B. A., Fernandez de la Campa, M. R., and Sanz-Medel, A., *J. Anal. At. Spectrom.*, 1993, **8**, 1097.

4   Saouter, E., and Blattmann, B., *Anal. Chem.*, 1994, **66**, 2031.

5   Liang, L., and Bloom, N. S., *J. Anal. At. Spectrom.*, 1993, **8**, 591.

6   Frech, W., Baxter, D. C., Dyvik, G., and Dybdahl, B., *J. Anal. At. Spectrom.*, 1995, **10**, 769.

7   Temmerman, E., Vandecasteele, C., Vermeir, G., Leyman, R., and Dams, R., *Anal. Chim. Acta,* 1990, **236**, 371.

8   Jonasson, I. R., Lynch, J. J., and Trip, L. J., *Geol. Surv. Can. Pap. 73–21,* 1973, 19pp.

9   Van Delft, W., and Vos, G., *Anal. Chim. Acta*, 1988, **209**, 147.

10 Mudroch, A., and Kokotich, E., *Analyst*, 1987, **112**, 709.

11 Landi, S., and Fagioli, F., *Anal. Chim. Acta*, 1994, **298**, 363.

12 Stresko, V., Polakovicova, J., and Kubova, J., *J. Anal. At. Spectrom.*, 1994, **9**, 1173.

13 Vaughn, W. W., and McCarthy, J. H., *U. S. Geol. Surv. Prof. Pap.*, 1964, **501-D**, D123.

14 Wittmann, Zs., *Talanta*, 1981, **28**, 271.

15 Dumarey, R., and Dams, R., *Mikrochim. Acta,* 1984, **III/3-4**, 191.

16 Salvato, N., and Pirola, C., *Mikrochim. Acta*, 1996, **123**, 63.

17 Terashima, S., *Geostand. Newsl.*, 1994, **18**, 199.

18 Gladney, E. S., and Roelandts, I., *Geostand. Newsl.*, 1989, **13**, 217.

19 Lynch, J. J., *Geostand. Newsl.*, 1990, **14**, 153.

20 Lynch, J. J., *Geostand. Newsl.*, 1996, **20**, 277.

21 Govindaraju, K., *Geostand. Newsl.*, 1994, **18**, 158.

22 Imai, N., Terashima, S., Itoh, S., and Ando, A., *Geostand. Newsl.*, 1995, **19**, 135.

23 Thompson, M., and Howarth, R. J., *J. Geochem. Explor.*, 1978, **9**, 23.

Application of Derivative Variable-angle Synchronous Scanning Phosphorimetry in a Microemulsion Medium for the Simultaneous Determination of 2-Naphthoxyacetic Acid and 1-Naphthalenacetamide

Antonio Segura Carretero, Carmen Cruces Blanco* and Alberto Fernández Gutiérrez

Department of Analytical Chemistry, Faculty of Sciences, University of Granada, C/Fuentenueva s/n, 18071 Granada, Spain. E-mail: mruces@goliat.ugr.es

The applicability of derivative variable-angle synchronous scanning (DVASS) microemulsion phosphorimetry at room temperature (ME-RTP) was demonstrated for the simultaneous determination of the plant growth regulators 2-naphthoxyacetic acid and 1-naphthalenacetamide in soil samples. This technique permits linear or non-linear paths to be scanned at preselected angles through the excitation–emission phosphorescence matrix in order to obtain the highest signal values and interference-free bands. The phosphorescence emission of the two compounds was obtained using sodium sulfite as an O_2 scavenger and thallium nitrate as an external heavy atom salt perturbed in sodium docecyl sulfate microemulsion aqueous solutions. A statistical model of the central composite design type to obtain the optimum phosphorescence responses was applied. The increased selectivity afforded by the DVASS technique permitted the demonstration of its applicability to the simultaneous determination of phosphorescence signals of these two compounds obtained in a microemulsion medium which show closely overlapped profiles giving mean recoveries of 89.0% ($n = 5$) for 1-naphthalenacetamide and 103.5% ($n = 5$) for 2-naphthoxyacetic acid, with an RSD of 7.35 and 5.90%, respectively, in real samples.

Keywords: Derivative variable-angle synchronous scanning phosphorimetry; phytohormones; room temperature phosphorescence; microemulsion; experimental design

Because of the overlap of the broad-band spectra observed when carrying out multicomponent analysis of real samples by luminescence techniques, many types of time-consuming separation techniques are always required. Synchronous spectrometry (SS), a method first used by Lloyd[1] to identify a number of fluorescent PAHs, involves simultaneous scanning of the excitation and emission monochromators synchronized in such a fashion that a well defined relationship is maintained between the two wavelengths. This technique has the limitation of exploring only those sections of the excitation–emission matrix (EEM) located at 45°. This problem was overcome by Kubic *et. al*,[2] who introduced a modification of conventional synchronous scanning called variable-angle synchronous scanning[3–5] (VASS), which permits the relative scan speeds of each monochromator to be varied digitally[3] or by a microcomputer[6–9] and any zones of the EEM to be explored, avoiding the limitation mentioned above.

The VASS technique does not require highly sophisticated equipment but its application was not extended until computer systems became part of most equipment. Most of these applications are related to the analysis of fluorescent compounds,[4,10–18] with only one application to the resolution of mixtures of phosphorescent compounds.[6,19]

The true advantage of VASS over SS is not related to the band-narrowing effect but to the capacity to go throughout maximum intensity peaks (which circumvents overlapping spectral areas), giving great flexibility in choosing the scan paths to pass as near as possible to the spectral maxima of different compounds, which is a valuable advantage in the resolution of compounds in multicomponent analyses of real samples over SS or derivative synchronous techniques.

In this work, the use of VASS was extended to the application of derivative scanning of the corresponding VASS spectra obtained from the detailed inspection of the EEM where less interference from one analyte to the other is obtained. The better results obtained with this derivative variable-angle synchronous scanning spectroscopic (DVASS) technique applied to the resolution of a mixture of two phosphorescent compounds at room temperature in solution was demonstrated in the simultaneous determination of the phytohormones 1-naphthaleneacetamide (NAD) and 2-naphthoxyacetic acid (NOA), which are usually applied to prevent fruit fall, so fruit composition has to be specially regulated in each country.

Despite the native fluorescence of NAD,[20,21] the possibility of applying phosphorescence detection has not previously been considered. With respect to NOA, only a few phosphorimetric methods have been proposed, mainly at low temperature,[22–24] with only two using room temperature with a solid support[25,26] or micellar[27] or organized media.[28]

As the derivative method permits the division of total luminescence spectra into positive and negative parts, better resolution for simultaneous quantification can be achieved by comparison of the derivative variable-angle phosphorescent emission–excitation matrices of both compounds, allowing one to find zones where quantification can be carried out without interferences from other compounds in the mixture.

In this paper, we present the first application of DVASS with phosphorescence detection to the simultaneous determination of NAD and NOA in soil samples, with very satisfactory results.

Experimental

Reagents

The solvents used, dichloromethane and butan-1-ol, the surfactant sodium dodecyl sulfate (SDS), analytical-reagent grade thallium(I) nitrate and anhydrous sodium sulfite (all from Sigma, St. Louis, MO, USA) were used as received. Aqueous solutions were prepared with doubly distilled water. The sodium sulfite solutions were prepared daily and kept in tightly stoppered containers.

NAD and NOA (Sigma) were used without further purification. Microemulsion stock standard solutions were prepared by dissolving 10 mg of NAD or NOA in 1 ml of dichloromethane and 1 ml of butan-1-ol and diluting to 100 ml with 0.5 mol l^{-1} SDS.

All experiments were performed with analytical-reagent grade chemicals and pure solvents. Doubly distilled, demineralized water was used throughout.

Instrumentation and Software

All recordings of uncorrected luminescence spectra and measurements of micelle-stabilized roon temperature phosphorescence (MS-RTP) intensities were carried out with an Aminco Bowman (Rochester, NY, USA) Series 2 luminescence spectrometer equipped with a 7 W pulsed xenon lamp and a thermostated cell holder. The system was controlled with a personal computer with a 40 MB hard disk, 4 MB of RAM, a 3.5 in 1.44 MB floppy disk drive, a VGA color monitor with VGA graphics adapter card, a serial two-button mouse, DOS 6.0, OS/2 version 2.0 and a GPIB(IEEE-488) interface card for computer instrument communication. An Ultrasons ultrasonic bath (Selecta, Barcelona, Spain) was used for sample sonication.

The software package used to carry out the experimental design was STATGRAPHICS, Statistical Institution Edition Version 6.0 (Statistical Graphics, Rockville, MD, USA).

General Procedure

A 30 or 200 μl aliquot of NAD or NOA microemulsion, respectively, 0.730 or 0.560 ml of 0.5 mol l^{-1} SDS, respectively, 1.00 ml of 0.25 mol l^{-1} thallium(I) nitrate and 0.25 ml of 0.8 mol l^{-1} sodium sulfite were introduced into a 10 ml calibrated flask and diluted to volume with water. If a precipitate appeared after the addition of the thallium(I) nitrate, the flask was warmed until the precipitate disappeared, before the other reagents were added. After thorough mixing, the flask was placed in a water-bath at 25 ± 1 °C for 10 min. Standard 10 mm fused-silica cells were filled with this analyte solution.

The relative phosphorescence intensities of the samples and the blank were measured at $\lambda_{ex}/\lambda_{em}$ 280/478 nm for NAD and $\lambda_{ex}/\lambda_{em}$ 336/501 nm for NOA. The gate time (t_g) was kept constant at 200 μs for both compounds and the delay time (t_d) was 200 μs for NAD and 100 μs for NOA. Excitation and emission slits of 16 nm were used throughout.

Phosphorescence signals at the fixed wavelengths were used to construct the corresponding calibration graphs.

Procedure for Soil Sample Analysis

The method was applied to soil samples from Gójar village (Granada, Spain). Certain amounts of NAD and NOA were added to 10 g of sample in such a way that the final concentration was included in the range of the calibration graph. The samples were extracted twice with a mixture of 20 ml of dichloromethane and 20 ml of butan-1-ol, filtering under vacuum, and washing the dry residue with 40 ml of the same mixture. Both extracts were mixed and evaporated to dryness in a rotary evaporator at 60 °C.

The residue was diluted to 10 ml with the above mixture and 2 ml were taken and diluted with 100 ml of 0.5 mol l^{-1} SDS. The basic procedure was applied to this solution.

Caution: thallium(I) salts and dichloromethane are very toxic.

Results and Discussion

Experimental Variables

MS-RTP suffers from a limitation due to the slow dissolution of hydrophobic analytes. To avoid this problem in analyses for compounds such as NAD and NOA, an aqueous microemulsion of the analytes in apolar solvents was used. A microemulsion is a stable, optically transparent monodisperse system of 10–20 mm diameter droplets intermediate in size between an emulsion and a micelle. Microemulsions are formed spontaneously when appropriate amounts of water, an apolar solvent, a surfactant and a co-surfactant are mixed.

To form oil-in-water (o/w) microemulsions containing a hydrocarbon core, critical concentrations of the surfactant SDS and of the apolar solvent and the alcohol should be carefully selected to create a microenvironment where the two phytohormones should be protected from collisional deactivation that can cause phosphorescent quenching.

For this reason, different proportions of the apolar solvent dichloromethane and the alcohol butan-1-ol were tested between 0.5 and 6% v/v. The best results were obtained when using 2% dichloromethane and butan-1-ol, and this proportion was selected for the rest of the experimental work, while the concentrations of dichloromethane and butan-1-ol in the final solution were 0.02%, respectively.

Together with the selection of these concentrations, an external heavy atom addition with deoxygenation carried out by sodium sulfite is decisive in obtaining intense RTP signals. Hence studies of the effects of each of these experimental variables and their interactions have to be carried out. The simplest way to do this is to use a three-variable, composite cube-star design.[29] The variables used in this multivariate optimization were SDS, TlNO$_3$ and Na$_2$SO$_3$ concentrations. The maximum response was obtained with [SDS] = 3.80×10^{-2} mol l^{-1}, [TlNO$_3$] = 2.50×10^{-2} mol l^{-1} and [Na$_2$SO$_3$] = 2.00×10^{-2} mol l^{-1} and these concentrations were used in the rest of the experimental work.

The different instrumental parameters that could affect the phosphorescence response, such as wavelength maxima, scanning speed, delay time, gate time and detector sensitivity, were conveniently selected (see Table 1).

In order to avoid possible phosphorescence signal modifications, a thermostatically controlled water-bath at 25 ± 1 °C was adopted for the rest of the experimental work. At this temperature and after waiting 5 min before making measurements, the phosphorescence signals remain stable for at least 1h.

Phosphorescence Spectral Characteristics

The object of this work was to extend the interesting characteristics of the derivative technique, previously demonstrated in applications to normal excitation and emission spectra, and to synchronous spectra in luminescence analysis, to their application to the spectra obtained after variable-angle synchronous scanning spectrometry.

As can be seen from Fig. 1, the simultaneous determination of NAD and NOA by normal fluorescence spectrometry is not possible, owing to their great spectral overlap.

Based on the possibility in this work of obtaining the phosphorescence signal of both compounds using a microemulsion medium, a careful examination of the phosphorescence spectra of these two compounds was carried out.

The extent of the possible phosphorescence spectral overlap can be usefully examined by interfacing a microcomputer to the spectrometer to obtain the total phosphorimetric information

Table 1 Instrumental parameters

Parameter	NAD	NOA
Excitation/emission wavelength/nm	280/478	336/501
Excitation/emission slits/nm	16/16	16/16
Minimum period pulse/ms	5	5
Scanning speed/nm s^{-1}	2	2
Delay time/μs	100	200
Gas time/μs	200	200
Detector sensitivity/V	1100	1100

available in the EEM. With suitable computer programs, the three-dimensional (3-D) spectra can be obtained and presented as an isometric projection, where the emission spectra at stepped increments of the excitation wavelength are recorded and plotted. Also, the 3-D spectra can be effectively transformed into a 2-D plot with iso-lines of equal intensity as a function of excitation and emission wavelengths [see Fig. 2(*a*) and (*a'*)].

The 2-D representation is of great interest as it yields information about the most suitable route to follow in the excitation–emission matrix to obtain the variable-angle phosphorescence spectra, which could allow their simultaneous determination.
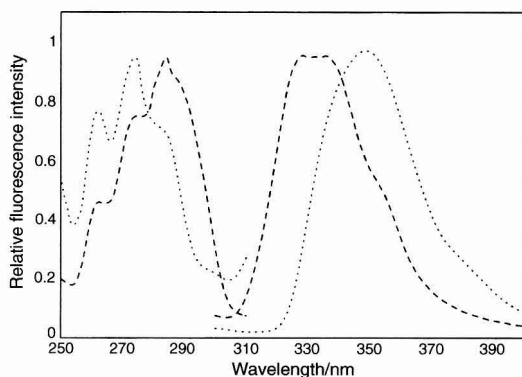
Fig. 1 Normal excitation–emission fluorescence spectra of 0.30 µg ml^{-1} of NAD (dashed lines) and 1.0 µg ml^{-1} of NOA (dotted lines). Detector sensitivity, 700 V. [SDS] = 3.80×10^{-2} mol l^{-1}.

Although high resolution is always demonstrated in the application of VASS to fluorescence or phosphorescence EEM, the similarity of the chemical structures of the present two analytes impedes their direct determination.

Because once a VASS spectrum has been obtained it could be manipulated by a suitable computer program, the possibility of applying the derivative technique to these spectra was considered. These DVASS spectra consist of positive [Fig. 2(*b*) and (*b'*)] and negative [Fig. 2(*c*) and (*c'*)] parts, which increased the possibilities of resolution.

The individual derivative contour plots for NAD and NOA showed that the main peaks with interference-free bands were centred on their respective wavelength excitation–emission pairs $\lambda_{ex}/\lambda_{em}$ 280/478 and 336/501 nm for NAD and NOA, respectively, using the positive and negative parts of the contour plots of the corresponding derivatives for both compounds.

One of the most important merits of contour plots is that sections through them give very useful information. The application of DVASS has made it possible to explore those areas of this contour plot where the highest signal values with interference-free bands are present.

Because phosphorescence measurement works with two additional parameters (t_d and t_g) compared with fluorescence, we used them as another selectivity parameter.

As can be seen in Fig. 2, there is partial overlap between NAD and NOA under the NAD measurement conditions. For this reason, we made use of the differences between the t_d values of the two compounds. On varying the t_d value from 100 to 200 µs, a marked decrease in the phosphorescence signal of the NOA was observed whereas maximum phosphorescence response was obtained for NAD at 200 µs.

To measure the VASS spectra, no special equipment was required. The excitation/emission monochromators were changed manually and 30 points of each EEM route section were selected to measure the phosphorescence signals under the
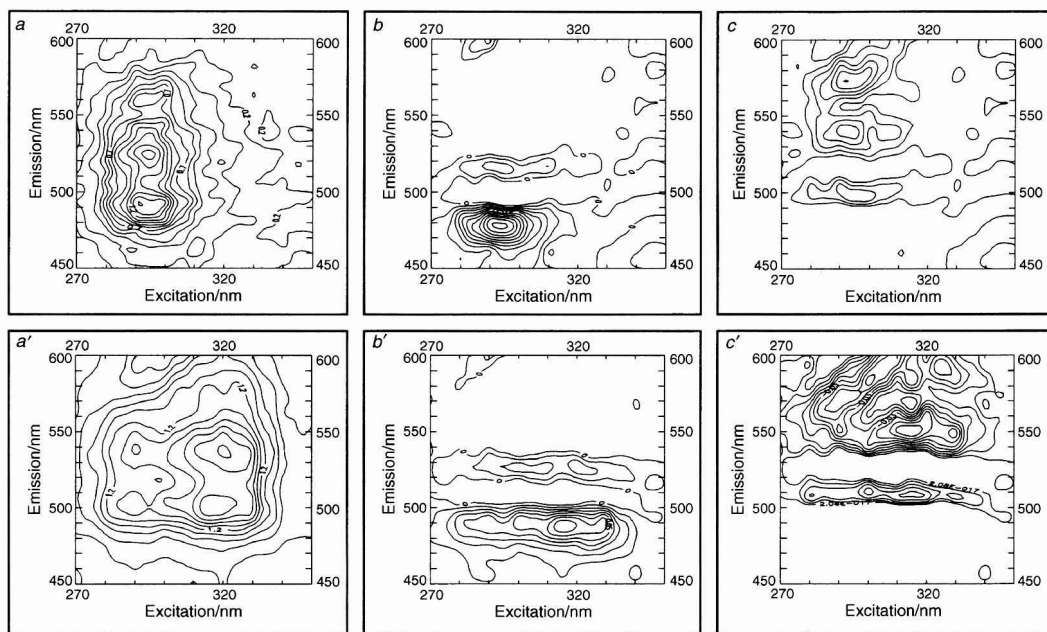
Fig. 2 Two-dimensional image plot of total luminescence spectra (*a* and *a'*) and positive (*b* and *b'*) and negative (*c* and *c'*) part of the corresponding derivative spectra for NAD and ANOA, respectively. *a*, *b* and *c*, NAD 0.30 µg ml^{-1}; and *a'*, *b'* and *c'*, NOA 2.0 µg ml^{-1}. t_d 200 µs for NAD and 100 µs for NOA; t_g, 200 µs, detector sensitivity 1100 V. [SDS] = 3.80×10^{-2} mol l^{-1}; [TlNO$_3$] = 2.50×10^{-2} mol l^{-1}; [Na$_2$SO$_3$] = 2.00×10^{-2} mol l^{-1}.

instrumental conditions previously selected. The phosphorescent signals obtained were then treated in a software graph package to construct the spectra.

The variable-angle scanning route was carefully determined by trial and error to traverse those parts of the 3-D spectral zones with the least overlap. The scan was selected to transverse those parts of the 3-D data matrix with the least overlap and the closest approach of the maximum peaks. In spite of the fact that losses in sensitivity occur because no maximum peaks are traversed, interference-free signals of the two components may be obtained from the chosen routes that scan the 3-D zones by skirting the slopes of the peak and avoiding the areas of interference between the two compounds. Fig. 3 shows a 3-D variable-angle scanning spectrum for a binary mixture.

The technique used to choose suitable wavelengths to take measurements proportional to NAD and NOA concentrations for the preparation of calibration graphs was the 'zero contributions' method. As Fig. 4 shows, the measurements of the relative phosphorescence intensity for a mixture of these phytohormones at $\lambda_{ex}/\lambda_{em}$ 280/478 nm is a function of NAD concentration only and at 336 and 501 nm is a function of NOA concentration only. Consistently these wavelength values were selected to construct the calibration graphs.
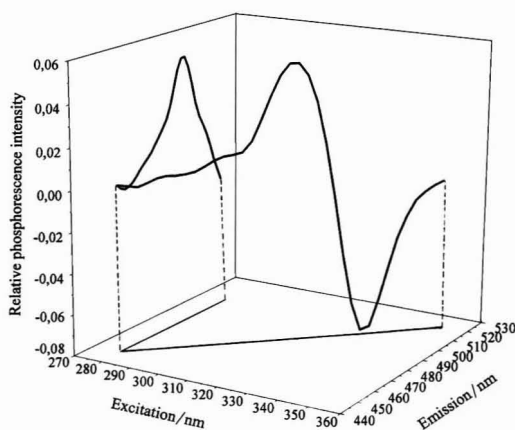
Analytical Parameters

In order to test the mutual independence of the analytical signals of NAD and NOA from the corresponding concentration of the other compound at the wavelengths selected, the following calibrations were performed.

The technique used to choose suitable wavelengths to take measurements proportional to the two phytohormones for the preparation of calibration graphs was the 'zero contribution' method. As can be seen in Fig. 5, the measurements of the phosphorescence intensity for a mixture of these phytohormones at $\lambda_{ex}/\lambda_{em}$ 280/478 and 336/501 nm are functions of NAD and NOA concentrations, respectively, and were used to establish the corresponding calibration graphs. It can be seen that increasing the concentration of each compound in turn had no effect on the measurement wavelength of the other compound.

These calibration graphs were constructed for standard solutions containing between 0.15 and 0.60 µg ml^{-1} of NAD and 1 and 4 µg ml^{-1} of NOA. The more important analytical parameters[30] for the two compounds are summarized in Table 2.

The repeatability of the proposed method was determined. The precision was measured for phytohormone concentrations of 0.30 µg ml^{-1} of NAD and 2 µg ml^{-1} of NOA with seven independent determinations. The RSDs were 3.50 and 3.64% for NAD and NOA, respectively.

The VASS phosphorimetric method was also applied to the analysis of several synthetic mixtures of the two compounds in different ratios using the same tolerance criteria as indicated previously. The results are summarized in Table 3; very good recoveries were always obtained.

Fig. 3 Three-dimensional spectra of a mixture of NAD and NOA. Conditions as in Fig. 2.
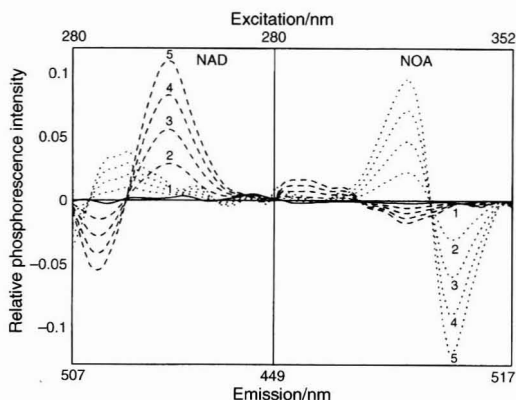
Fig. 5 Two-dimensional projections of the calibration graphs established for (dashed line) NAD [(1) 0, (2) 0.15, (3) 0.30, (4) 0.45 and (5) 0.60 µg ml^{-1}] and (dotted lines) NOA [(1) 0, (2) 1.0, (3) 2.0, (4) 3.0 and (5) 4.0 µg ml^{-1}]. t_d, 200 µs for NAD and 100 µs for NOA; t_g, 200 µs; detector sensitivity, 1100 V. [SDS] = 3.80×10^{-2} mol l^{-1}; [TINO$_3$] = 2.50×10^{-2} mol l^{-1}; [Na$_2$SO$_3$] = 2.00×10^{-2} mol l^{-1}.

Fig. 4 Two-dimensional projection of: (dashed line) NAD, (dotted line) NOA and (solid line) a binary mixture. Conditions as in Fig. 2.

Table 2 Analytical parameters

Parameter	NAD	NOA
Linearity [1 − RSD (b)%]*	97.99	97.88
Analytical sensitivity/µg ml^{-1}	0.0165	0.1108
Detection limit/µg ml^{-1}	0.036	0.243
Quantification limit/µg ml^{-1}	0.121	0.809
Linear dynamic range/µg ml^{-1}	0.036–0.6	0.243–4.0

* See ref. 30.

Table 3 Study of phytohormone recoveries in synthetic mixtures

Concentration added/µg ml^{-1}		Concentration found/µg ml^{-1}		Recovery (%)	
NAD	NOA	NAD	NOA	NAD	NOA
0.30	2.00	0.263	2.05	87.7	102.4
0.30	1.00	0.273	1.90	91.0	94.5
0.15	1.00	0.141	1.03	94.2	102.9
0.45	2.00	0.341	2.34	75.8	116.9
0.45	1.00	0.425	1.06	94.5	106.1

Applications

A soil sample from Gójar village (Granada, Spain) was spiked with NAD and NOA by adding appropriate volumes of a standard solution. Different recovery experiments were performed on the spiked soil samples. Samples of soil containing 30 µg ml^{-1} of NAD and 2 µg ml^{-1} of NOA were analysed. Mean values of 89.0% ($n = 5$) for NAD and 103.5% ($n = 5$) for NOA, with RSDs of 7.35% and 5.90%, respectively, were obtained.

References

1   Lloyd, J. B. F., *Nature (London)*, 1971, **231**, 64.
2   Kubic, T. A., Kanabrocki, T., and Dwyer, J., paper presented at the 32nd Annual Congress of the American Academy of Forensic Sciences, 1980.
3   Miller, J. N., *Analyst*, 1984, **109**, 191.
4   García Sánchez, F., Ramos Rubio, A. L., Cerdá, V., and Oms, M. T., *Anal. Chim. Acta*, 1990, **228**, 293.
5   Clark, B. F., Frei, A. F., Milne, K. T., Pattle, D. M. G., and Williams, M. H., *Anal. Chim. Acta*, 1985, **170**, 35.
6   Cabaniss, S. E., *Anal. Chem.*, 1991, **63**, 1323.
7   Clark, B. J., Fell, A. F., Aitchison, I. E., Pattie, D. M. G., Williams, M. H., and Miller, J. N., *Spectrochim. Acta, Part B*, 1983, **38**, 61.
8   Om, M. T., Cerdá, V., García Sánchez, F., and Ramos Rubio, A. L., *Talanta*, 1988, **35**, 671.
9   García Sánchez, F., Ramos Rubio, A. L., Cerdá, V., and Oms, M. T., *Talanta*, 1988, **35**, 335.
10 Clark, B. J., Fell, A. F. Milne, K. T., Pattie, D. G., and Williams, H., *Anal. Chim. Acta*, 1985, **170**, 35.
11 Oms, M. T., Forteza, R., Cerdá, V., Maspoch, S., Coello, J., and Blanco, M., *Anal. Chim. Acta*, 1990, **233**, 159.
12 Lee, Y. Q., Huang, X. Z., Xu, J. G., and Chen, G. Z., *Chin. Chem. Lett.*, 1991, **2**, 23.
13 Li, Y., Huang, X., Xu, J., and Chen, G., *Fenxi Huaxue*, 1991, **19**, 538.
14 Li, Y., Cai, D., Huang, X., and Xu, J., *Fenxi Huaxue*, 1993, **21**, 1420.
15 Li, Y. Q., Huang, X. Z., Xu, J. G., and Chen, G. Z., *Talanta*, 1994, **41**, 695.
16 García Sánchez, F., Fernández Gutiérrez, A., and Cruces Blanco, C., *Anal. Chim. Acta*, 1995, **306**, 313.
17 Capitán-Vallvey, L. F., del Olmo, M., Avidad, R., Navaln, A., de Orbe, I., and Vílchez, J. L., *Anal. Chim. Acta*, 1995, **302**, 193.
18 García Sánchez, F., Cedazo, M., Lovillo, J., and Navas Díaz, A., *Talanta*, 1996, **43**, 1377.
19 Segura Carretero, A., Cruces Blanco, C., and Fernández Gutiérrez, A., *Anal. Chim. Acta*, 1996, **329**, 165.
20 Cochrane, W. P., Lanouette, M., and Grant, R. J., *J. Assoc. Off. Anal. Chem.*, 1988, **63**, 145.
21 García Sánchez, F., and Cruces Blanco, C., *Quim. Anal.*, 1988, **7**, 299.
22 Sanders, L. B., and Winefordner, J. D., *J. Agric. Food Chem.*, 1972, **20**, 166.
23 Trautwein, N. L., and Guyon, J. C., *Mikrochim. Acta*, 1979, **1**, 413.
24 Aaron, J. J., Kaleel, E. M., and Winefordner, J. D., *J. Agric. Food Chem.*, 1979, **27**, 1233.
25 Roth, M., *J. Chromatogr.*, 1967, **30**, 276.
26 Aaron, J. J., and Winefordner, J. D., *Analusis*, 1979, **7**, 168.
27 Segura Carretero, A., Cruces Blanco, C., and Fernández Gutiérrez, A., *Talanta*, 1996, **43**, 1001.
28 Muñoz de la Peña, A., and Durán-Merás, I., *Talanta*, 1993, **40**, 1657.
29 Box, G. E. P., Hunter, W. G., and Hunter, J. S., *Statistics for Experiments*, Wiley, New York, 1978, ch. 15.
30 Cuadros Rodríguez, L., García Campaña, A. M., Jiménez Linares, C., and Román Ceba, M., *Anal. Lett.*, 1993, **26**, 1243.

Effect of the Substituent Group at the Isothiocyanate Moiety of Edman Reagents on the Racemization and Fluorescence Intensity of Amino Acids Derivatized With 2,1,3-Benzoxadiazolyl Isothiocyanates

Hirokazu Matsunaga, Tomofumi Santa, Takayuki Iida, Takeshi Fukushima, Hiroshi Homma and Kazuhiro Imai*

Faculty of Pharmaceutical Sciences, University of Tokyo, 7-3-1 Hongo, Bunkyo-ku, Tokyo 113, Japan

It is shown that an electron-withdrawing or -donating group at the *para*-position of aromatic isothiocyanate significantly affects the racemization of 2,1,3-benzoxadiazolylthiazolinone (TZ) derivatives of amino acids, derivatized with newly synthesized benzoxadiazolyl isothiocyanates in Edman sequence analysis. A linear relationship between the logarithms of the TZ-amino acid enantiomer ratio and the *para*-substituent constants (σ_p) for the isothiocyanate moiety was obtained, and the D/L configuration of the amino acid residue was retained with an isothiocyanate containing an electron-donating group at the *para*-position. The *para*-substitution effect on the racemization of phenylhydantoin (PTH) amino acids was also confirmed by several *para*-substituted phenylisothiocyanate (PITC) reagents, including nitro-PITC, chloro-PITC, PITC, methyl-PITC and methoxy-PITC. The relationship between the fluorescence intensity of the 2,1,3-benzoxadiazolyl TZ amino acid and σ_p was also demonstrated. When the isothiocyanate containing an electron-donating group was used, the fluorescence intensity of the TZ-amino acid decreased while retaining the D/L configuration of the amino acid residues.

Keywords: N-*Terminal amino acid sequence;* D/L *configuration analysis; substituent effect; racemization; fluorescence intensity;* β-*cyclodextrin column; phenylisothiocyanate*

Since a method for amino acid sequence analysis using phenylisothiocyanate (PITC) was reported by Edman,[1] various techniques have been introduced to improve the detection limit[2–4] or automate the sequencer.[5–7] As new peptides containing D-amino acids are being found, an amino acid sequencing method capable of determining the D/L-amino acid configuration is also becoming necessary. However, only a few papers have described the determination of the D/L-amino acid configuration with the Edman method.

Previously, the racemization mechanism at the cyclization/cleavage stage was investigated with the use of 7-*N,N*-dimethylaminosulfonyl-4-(2,1,3-benzoxadiazolyl) isothiocyanate (DBD-NCS)[8] and it was shown that a proton located at the α-carbon atom was replaced by a surrounding proton in the protic acid during the cyclization/cleavage reaction, resulting in racemization. The reactivity of an isothiocyanate group at the cyclization/cleavage stage was thought to be associated with the racemization of thiazolinone (TZ)-amino acid with no reactivity dependent upon the electron-withdrawing or -donating ability of the *para*-substituent group. In this study, 2,1,3-benzoxadiazolyl isothiocyanate derivatives with different electron

densities at the *para*-substituent group were used and the effect on the racemization and fluorescence intensity of TZ-amino acid residues was investigated. We also confirmed the effect of the electron-withdrawing or -donating activity on the racemization of PTH-amino acids using several *para*-substituent PITC.

Experimental

Materials

The following materials were employed: dipeptides (L-Ala–Gly, L-Leu–Gly) (Sigma, St. Louis, MO, USA), HPLC-grade acetonitrile, methanol and 4-nitro-PITC and sequencer-grade pyridine (Kanto Chemical, Tokyo, Japan), sequencer-grade trifluoroacetic acid (TFA) and PITC (Wako, Osaka, Japan), 4-chloro-PITC (Tokyo Chemical Industry, Tokyo, Japan) and 4-methyl-PITC and 4-methoxy-PITC (Merck-Schuchardt, Darmstadt, Germany). Water was purified using a Milli-Q system (Millipore, Bedford, MA, USA). All other reagents were of analytical- or guaranteed-reagent grade and used without further purification.

2,1,3-Benzoxadiazolyl isothiocyanate

Five isothiocyanate reagents were synthesized as outlined below with their structures confirmed on the basis of chemical and physico-chemical evidence. 7-Aminosulfonyl-4-(2,1,3-benzoxadiazolyl) isothiocyanate (ABD-NCS) and DBD-NCS were synthesized as described previously.[9]

4-N,N-*Dimethylamino-7-nitro-2,1,3-benzoxadiazole*

NBD-Cl (200 mg) was dissolved in 15 ml of methanol. After the addition of 0.5 ml of a dimethylamine solution, the mixture was stirred for 30 min and 190 mg of NBD-NMe$_2$ were obtained as orange crystals, m.p. 220–222 °C. ^{1}H NMR(CDCl$_3$): δ 8.50 (1 H, d, J = 8.0 Hz), 6.21 (1 H, d, J = 8.0 Hz), 3.65 (6 H, s). Elemental analysis: calculated for C$_8$H$_8$N$_4$O$_3$ C, 46.16; H, 3.87; N, 26.91; found: C, 45.84; H, 3.62; N, 26.64%. Atmospheric pressure chemical ionization mass spectrometry (APCI-MS): *m/z* 209 ([M + H]$^+$).

4-N,N-*Dimethylamino-7-amino-2,1,3-benzoxadiazole*

4-*N,N*-Dimethylamino-7-nitro-2,1,3-benzoxadiazole (130 mg) was dissolved in a mixture of 15 ml of methylene chloride, 5 ml of methanol and 3 ml of concentrated hydrochloric acid. After addition of 300 mg of iron powder, the mixture was vigorously stirred for 30 min. The reaction mixture was poured into 100 ml of a 1 M NaOH solution and extracted with 100 ml of methylene chloride. The organic layer was dried with anhydrous Na$_2$SO$_4$ and concentrated *in vacuo*. The residue was chromatographed on silica gel (ethyl acetate–hexane) to afford 100 mg of amine

as a brown powder. ^{1}H NMR (CDCl$_3$): δ 6.32(1 H, d, J = 8.0 Hz), 6.12 (1 H, d, J = 8.0 Hz), 4.03 (2 H, s, br), 3.08 (6 H, s). Elemental analysis: calculated for C$_8$H$_{10}$N$_4$O C, 53.92; H, 5.66; N, 31.44; found C, 53.69; H, 5.38; N, 31.22%. APCI-MS: m/z = 179 ([M + H]$^+$).

7-N,N-*Dimethylamino-4-(2,1,3-benzoxadiazolyl) isothiocyanate (DABD-NCS)*

4-*N,N*-Dimethylamino-7-amino-2,1,3-benzoxadiazole (39 mg) was dissolved in 5 ml of acetonitrile and 50 mg of thiophosgene in 0.3 ml of benzene were added slowly. The mixture was refluxed for 30 min. The reaction mixture was evaporated to dryness *in vacuo* and the residue was chromatographed on silica gel (hexane–ethyl acetate) to afford 24 mg of isocyanate as an orange powder, m.p. 108–111 °C. ^{1}H NMR (CDCl$_3$): δ 7.07 (1 H, d, J = 8.0 Hz), 5.92 (1 H, d, J = 8.0 Hz), 3.38 (6 H, s). Elemental analysis: calculated for C$_9$H$_8$N$_4$OS C, 49.08; H, 3.66; N, 25.44%; found C, 49.17; H, 3.58; N, 25.45%. APCI-MS: m/z = 221 ([M + H]$^+$).

4-*Methoxy-7-nitro-2,1,3-benzoxadiazole*

NBD-Cl (200 mg) was dissolved in 30 ml of methanol. After the addition of 0.3 ml of triethylamine, the mixture was refluxed for 8 h. The reaction mixture was evaporated to dryness under reduced pressure and the residue was chromatographed on silica gel (50% methylene chloride in hexane) to afford 150 mg of NBD-OMe as red–orange crystals. m.p. 113–114 °C. ^{1}H NMR (CDCl$_3$): δ 8.56 (1 H, d, J = 8.0 Hz), 6.69 (1 H, d, J = 8.0 Hz), 4.24 (3 H, s). Elemental analysis: calculated for C$_7$H$_5$N$_3$O$_4$ C, 43.09; H, 2.58; N, 21.53; found C, 43.26; H, 2.45; N, 21.26%. APCI-MS: m/z = 196 ([M + H]$^+$).

4-*Methoxy-7-amino-2,1,3-benzoxadiazole*

4-Methoxy-7-nitro-2,1,3-benzoxadiazole (100 mg) was dissolved in a mixture of 8 ml of methanol and 2 ml of concentrated hydrochloric acid. After the addition of 300 mg of iron powder, the mixture was vigorously stirred for 30 min. The reaction mixture was poured into 200 ml of a 1 M NaOH solution and extracted with 100 ml of methylene chloride. The organic layer was dried with anhydrous Na$_2$SO$_4$ and concentrated *in vacuo*. The residue was chromatographed on silica gel (hexane–CH$_2$Cl$_2$) to afford 45 mg of the corresponding amine as red–orange crystals, m.p. 158–160 °C. ^{1}H NMR (CDCl$_3$): δ 6.39 (1 H, d, J = 8.0 Hz), 6.28 (1 H, d, J = 8.0 Hz), 4.14 (2 H, s, br), 3.96 (3 H, s). Elemental analysis: calculated for C$_7$H$_7$N$_3$O$_2$ C, 50.91; H, 4.27; N, 25.44; found C, 50.65; H, 4.11; N, 25.43%. APCI-MS: m/z = 166 ([M + H]$^+$).

7-*Methoxy-4-(2,1,3-benzoxadiazolyl) isothiocyanate (MBD-NCS)*

4-Methoxy-7-amino-2,1,3-benzoxadiazole (80 mg) was dissolved in 5 ml of acetonitrile and 80 mg of thiophosgene in 0.3 ml of benzene were added slowly. The mixture was refluxed for 2 h. The reaction mixture was evaporated to dryness *in vacuo* and the residue was chromatographed on silica gel (methylene chloride–hexane) to afford 45 mg of isothiocyanate as yellow crystals, m.p. 130–131 °C. ^{1}H NMR (CDCl$_3$): δ 7.10 (1 H, d, J = 8.0 Hz), 6.47 (1 H, d, J = 8.0 Hz), 4.07 (3 H, s). Elemental analysis: calculated for C$_9$H$_8$N$_4$OS C, 46.37; H, 2.43; N, 20.28; found: C, 46.22; H, 2.20; N, 20.12%. APCI-MS: m/z = 207 (M$^+$).

4-*Amino-7-chloro-2,1,3-benzoxadiazole*

NBD-Cl (400 mg) was dissolved in a mixture of 8 ml of methanol and 2 ml of concentrated hydrochloric acid. After the

addition of 400 mg of iron powder, the reaction mixture was stirred for 30 min, poured into 100 ml of 1 M NaOH solution and extracted with 100 ml of methylene chloride. The organic layer was dried with anhydrous Na$_2$SO$_4$ and concentrated *in vacuo*. The residue was chromatographed on silica gel (methylene chloride–hexane) to afford 180 mg of amine as a yellow powder, m.p. 164-165 °C. ^{1}H NMR (CDCl$_3$): δ 7.20 (1 H, d, J = 8.0 Hz), 6.29 (1 H, d, J = 8.0 Hz), 4.62 (2 H, s, br). Elemental analysis: calculated for C$_6$H$_4$N$_3$OCl C, 42.75; H, 2.39; N, 24.93; found C, 42.47; H, 2.19; N, 24.66%. APCI-MS: m/z = 168 (M$^-$).

7-*Chloro-4-(2,1,3-benzoxadiazolyl) isothiocyanate (CBD–NCS)*

4-Amino-7-chloro-2,1,3-benzoxadiazole (80 mg) was dissolved in 6 ml of acetonitrile and 80 mg of thiophosgene in 0.3 ml of benzene was added slowly. The mixture was refluxed for 4 h. The reaction mixture was evaporated to dryness *in vacuo* and the residue was chromatographed on silica gel (methylene chloride–hexane) to afford 70 mg of isothiocyanate, m.p. 141–142 °C. ^{1}H NMR (CDCl$_3$): δ 7.38 (1 H, d, J = 8.0 Hz), 7.08 (1 H, d, J =8.0 Hz). Elemental analysis: calculated for C$_7$H$_2$N$_3$OSCl C, 39.73; H, 0.95; N, 19.86; found C, 39.79; H, 0.73, N, 19.59%. APCI-MS: m/z = 211 (M$^+$).

Preparation of 2,1,3-benzoxadiazolyl-TZ-amino acids

A 10 μl volume of L-Leu–Gly (25 mM) dissolved in 50% v/v pyridine in water and 20 mM Edman reagent (DBD-NCS, ABD-NCS, CBD-NCS, MBD-NCS or DABD-NCS) in 50% pyridine (10 μl) were vortex mixed and heated at 50 °C for 20 min. After the coupling reaction, the mixture was washed three times with 100 μl of heptane containing 20% dichloromethane. The aqueous phase was evaporated to dryness using a centrifugal evaporator (SPE-200, Shimadzu, Kyoto, Japan) at 50 °C for 15 min, and 30 μl of trifluoroacetic acid (TFA) were added to the residue. The mixture was heated at 50 °C for 5 min and dried under a stream of nitrogen (cleavage/cyclization reaction). The resulting residue was dissolved in the HPLC mobile phase and immediately chromatographed.

Preparation of PTH-amino acids

A 10 μl volume of L-Ala–Gly (25 mM) dissolved in 50% v/v pyridine in water and 90 μl of the Edman reagent solution [ethanol–pyridine–water (6 + 1 + 1 v/v) dissolved in the Edman reagent] were mixed and heated at 50 °C for 20 min. PITC, nitro-PITC, chloro- PITC, methyl-PITC or methoxy-PITC were used as Edman reagents. After the coupling reaction, the mixture was washed three times with 100 μl of heptane. The aqueous phase was evaporated to dryness using a centrifugal evaporator at 50 °C for 15 min and 30 μl of TFA were added to the residue. The mixture was heated at 50 °C for 5 min and dried under a stream of nitrogen (cleavage/ cyclization reaction). The resulting residue was dissolved in 100 μl of water containing 50% v/v TFA and heated at 50 °C for 10 min. After the recyclization reaction, the sample solution was dried under a stream of nitrogen, dissolved in the HPLC mobile phase and immediately chromatographed.

Apparatus

Apparatus used for the identification of reagents was as follows. Melting-points were measured on a Yanagimoto (Tokyo, Japan) micro melting-point apparatus and were uncorrected. Proton nuclear magnetic resonance (^{1}H NMR) spectra were obtained on a JEOL GSX-400 spectrometer (Tokyo, Japan) with tetramethylsilane as the internal standard (abbreviations used: s,

singlet; d, doublet). Mass spectra were measured on a Hitachi (Tokyo, Japan) M-1200 mass spectrometer with an APCI system.

HPLC was carried out using an L-7100 pump (Hitachi) equipped with a Rheodyne (Cotati, CA, USA) 20 injector (Model 7125, 20 μL injection loop), an L-4200 UV detector (Hitachi) and a D-7500 chromatointegrator (Hitachi).

Determination of the Enantiomer Ratio of 2,1,3-Benzoxadiazolyl-TZ-amino Acids

2,1,3-Benzoxadiazolyl-TZ-amino acids were prepared from L-Leu–Gly as described above and TZ amino acids (CBD-TZ-Leu, DBD-TZ-Leu, ABD-TZ-Leu, MBD-TZ-Leu and DABD-TZ-Leu) were first collected by reversed-phase (RP) HPLC on an ODS column (YMC J'shere ODS H-80, 150 × 4.6 mm id, spherical, 5 μm, 80 Å; YMC, Kyoto, Japan). Gradient elution was employed for TZ-amino acids using eluent A [acetonitrile–water (3 + 7, v/v) containing 10 mM formic acid] and eluent B (acetonitrile containing 10 mM formic acid). The linear gradient program was from 0% B (0 min) to 80% B (30 min) at a flow rate of 1.0 ml min⁻¹. For the determination of the D/L configuration, an ES-phCD column (150 × 6.0 mm id, 5 μm, Shinwa Chemical Industries, Kyoto, Japan) was used (separation of TH or TZ amino acid enantiomers). The ES-phCD column was packed with a fully phenylcarbamoylated β-cyclodextrin. Elution was carried out at a flow rate of 0.5 ml min⁻¹ using water–methanol (CBD-TZ-Leu, 2 + 8 v/v; DBD-TZ-Leu and ABD-TZ-Leu, 3 + 7, MBD-TZ-Leu and DABD-TZ-Leu, 4 + 6) containing 10 mM formic acid and 50 mM urea. The absorbance of 2,1,3-benzoxadiazolyl TZ-Leu was measured at 254 nm.

Determination of the Enantiomer Ratio of PTH-amino Acids

PTH amino acids were prepared from L-Ala–Gly as described above, separated using an ODS column and collected in a manner similar to that described for the determination of the enantiomer ratio of 2,1,3-benzoxadiazolyl-TZ-amino acids. For the determination of the D/L configuration of PTH- Ala, an ES-1/2phCD column (150 × 6.0 mm id, 5 μm; Shinwa Chemical Industries) was used. The ES- 1/2phCD column was packed

with 50% phenylcarbamoylated β-cyclodextrin. Elution was carried out at a flow rate of 0.8 ml min⁻¹ using water–methanol (65 + 35 v/v) containing 10 mM acetic acid, except for PTH-Ala, which was prepared from PITC, for which water–methanol (85 + 15) containing 10 mM acetic acid was used. PTH-Ala was detected with the UV/VIS detector at 269 nm.

The chromatographic details of the separation of the enantiomers are summarized in Table 1.

Physical Properties of 2,1,3-Benzoxadiazolyl-TZ-amino Acids

2,1,3-Benzoxadiazolyl-TZ-Leu prepared as described above was collected by RP-HPLC, and the fluorescence intensity and UV absorption of TZ-Leu in the HPLC eluate were measured with a fluorescence detector (F-4010; Hitachi) and a UV/VIS spectrophotometer (Ubest 50; JASCO, Tokyo, Japan), respectively. A portion of the collected 2,1,3-benzoxadiazolyl TZ amino acid solution was also subjected to LC–MS (M-1200H LC–APCI-MS system; Hitachi), which was connected to a pump (L-6200; Hitachi) equipped with a 20 μL Rheodyne Model 7125 injector. The mass spectrometer was operated in the APCI mode with the drift, focus and multiplier voltage set at 20, 120 and 1800 V, respectively. The temperature of the vaporizer and desolvation regions was set at 180 and 400 °C, respectively. The flow injection analysis (FIA) mode was used at a flow rate of 1.0 ml min⁻¹ in the isocratic mode using acetonitrile.

Results and Discussion

Determination of the Enantiomer Ratio of 2,1,3-Benzoxadiazolyl-TZ-amino Acids

In a previous study,[8] the racemization mechanism of the cyclization/cleavage reaction was investigated, and the *N*-terminal Pro dipeptide was significantly racemized at the intermediate stage, in addition to the TZ-amino acid. The degree of racemization observed for both the intermediate and TZ amino acid was dependent on the rate of the cyclization/cleavage reaction.[10] To demonstrate the effect of an electron-withdrawing group on the racemization of TZ-amino acids, the *para*-substituted 2,1,3-benzoxadiazolyl isothiocyanates synthe-

Table 1 Chromatographic conditions employed for the enantiomeric separation of the amino acid derivatives

Derivative	Mobile phase	Flow rate/ ml min⁻¹	Column	Wavelength*/ nm
DBD-TZ-Leu	Methanol–water (7 + 3 v/v) containing 10 mM formic acid and 50 mM urea	0.5	ES-phCD	254
ABD-TZ-Leu	Methanol–water (7 + 3 v/v) containing 10 mM formic acid and 50 mM urea	0.5	ES-phCD	254
CBD-TZ-Leu	Methanol–water (8 + 2 v/v) containing 10 mM formic acid and 50 mM urea	0.5	ES-phCD	254
MBD-TZ-Leu	Methanol–water (6 + 4 v/v) containing 10 mM formic acid and 50 mM urea	0.5	ES-phCD	254
DABD-TZ-Leu	Methanol–water (6 + 4 v/v) containing 10 mM formic acid and 50 mM urea	0.5	ES-phCD	254
nitro-PTH-Ala	Methanol–water (35 + 65 v/v) containing 10 mM acetic acid	0.8	ES-1/2phCD	269
chloro-PTH-Ala	Methanol–water (35 + 65 v/v) containing 10 mM acetic acid	0.8	ES-1/2phCD	269
PTH-Ala	Methanol–water (15 + 85 v/v) containing 10 mM acetic acid	0.8	ES-1/2phCD	269
Methyl-PTH-Ala	Methanol–water (35 + 65 v/v) containing 10 mM acetic acid	0.8	ES-1/2phCD	269
Methoxy-PTH-Ala	Methanol–water (35 + 65 v/v) containing 10 mM acetic acid	0.8	ES-1/2phCD	269

* Detected with a UV detector.

sized were used to examine racemization at the cyclization/cleavage reaction stage (Scheme 1). 2,1,3-Benzoxadiazolyl-TZ-amino acid was also used for the determination of the D/L configuration since the determination by TZ-amino acids omitting the conversion stage was thought to be simple for clarifying the racemization mechanism.[8]

For the enantiomeric separation of D/L-2,1,3-benzoxadiazolyl-TZ-amino acids, urea was added to the HPLC eluent as it was known that the addition of urea dramatically enhanced the enantioselectivity of β-CD by capillary zone electrophoresis.[11] Fig. 1 shows chromatograms for the separation of enantiomers of *para*-substituted 2,1,3-benzoxadiazolyl-TZ-Leu on a phenylcarbamoylated β-cyclodextrin column with the mobile phase containing 50 mM urea, and the enantiomer ratios [D/(D + L)] were 47.0% (DBD-TZ-D-Leu), 38.0% (ABD-TZ-D-Leu), 26.0% (CBD-TZ-D-Leu), 13.7% (MBD-TZ-D-Leu) and 9.8% (DABD-TZ-D-Leu).

To clarify the contribution of the electron density at the *para*-position, the Hammett substituent constant (σ) was adopted as the electron-withdrawing parameter.[12] σ was expressed as follows:

$$\sigma = \log K - \log K_0 \quad (1)$$

$$\sigma = a\sigma_m + b\sigma_p + \varepsilon \quad (2)$$

where K_0 is the ionization constant (K) of the unsubstituted acid or base, σ_m and σ_p are the *meta*- and *para*-substituent constants, respectively, and the coefficients a, b and ε are evaluated *via* the least-squares method. Fig. 2 shows the relationship between σ_p of the isothiocyanate reagents and the logarithms of the enantiomer ratios [D/(D + L)]. It should be noted that a reasonably linear relationship between σ_p and the logarithms of the enantiomer ratios of 2,1,3-benzoxadiazolyl TZ-Leu was obtained. This clearly demonstrates that electron-withdrawing or -donating activity at the *para*-substituent has an effect on the extent of racemization of TZ amino acids, with an isothiocyanate containing an electron-donating group resulting in greater retention of the original configuration.

Determination of the Enantiomer Ratio of PTH-amino Acids

The effects of an electron-withdrawing group on the racemization of PTH-amino acids and several *para*-substituted PITCs (nitro-PITC, chloro-PITC, PITC, methyl-PITC and methoxy-PITC) used for the formation of PTH-amino acids were also investigated. The PTH-amino acid enantiomers were separated on the 50% phenylcarbamoylated cyclodextrin column as described previously for D/L configuration sequence analysis.[13]

Fig. 3 shows the three PTH-Ala differing in electron densities at the *para*-position and the enantiomer ratios [D/(D + L)] were
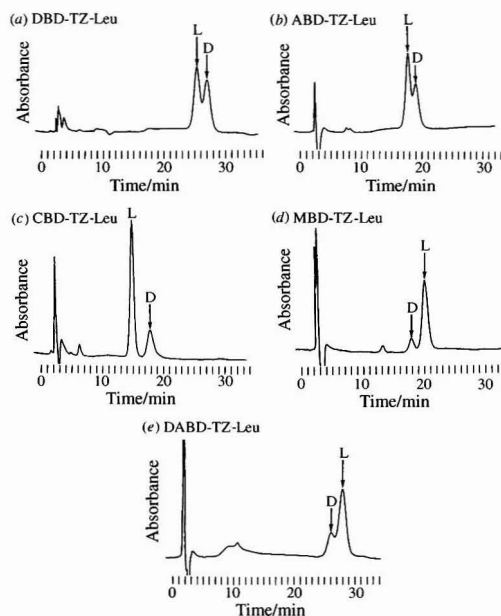
Fig. 1 Chromatograms of (*a*) DBD-TZ-Leu, (*b*) ABD-TZ-Leu, (*c*) CBD-TZ-Leu, (*d*) MBD-TZ-Leu and (*e*) DABD-TZ-Leu. A phenylcarbamoylated β-cyclodextrin column (ES-phCD; 150 × 6.0 mm id, 5 µm; Shinwa Chemical Industries) was used for the determination of the D/L configuration of 2,1,3-benzoxadiazolyl-TZ-Leu. 2,1,3-Benzoxadiazolyl-TZ-Leu was detected by the UV/VIS at measurement 254 nm. DBD-TZ-Leu, 7-*N*,*N*-dimethylaminosulfonyl-4-(2,1,3-benzoxadiazolyl)-TZ-Leu; ABD-TZ-Leu, 7-aminosulfonyl-4-(2,1,3-benzoxadiazolyl)-TZ-Leu; CBD-TZ-Leu, 7-chloro-4-(2,1,3-benzoxadiazolyl)-TZ-Leu; MBD-TZ-Leu, 7-methoxy-4-(2,1,3-benzoxadiazolyl)-TZ-Leu; DABD-TZ-Leu, 7-*N*,*N*-dimethylamino-4-(2,1,3-benzoxadiazolyl)-TZ-Leu.

Scheme 1 Structures of *para*-substituted 2,1,3-benzoxadiazolyl isothiocyanates. DBD-NCS; 7-*N*,*N*-dimethylaminosulfonyl-4-(2,1,3-benzoxadiazolyl) isothiocyanate; ABD-NCS, 7-aminosulfonyl-4-(2,1,3-benzoxadiazolyl) isothiocyanate; CBD-NCS, 7-chloro-4-(2,1,3-benzoxadiazolyl) isothiocyanate; MBD-NCS, 7-methoxy-4-(2,1,3-benzoxadiazolyl) isothiocyanate; DABD-NCS, 7-*N*,*N*-dimethylamino-4-(2,1,3-benzoxadiazolyl) isothiocyanate.
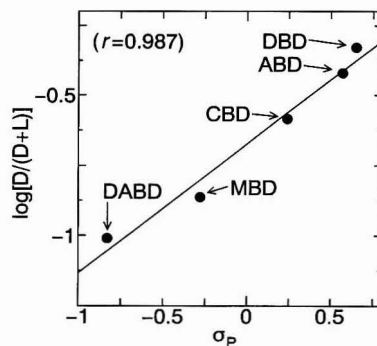
Fig. 2 Relationship between the Hammett *para*-substituent constants (σ_p) of *para*-substituted 2,1,3-benzoxadiazolyl-TZ-Leu and the the logarithms of the enantiomer ratios. σ_p values of the *para*- substituent groups are from ref. 12.

28.4% (nitro-PTH-D-Ala), 24.2% (chloro-PTH-D-Ala), 18.5% (PTH-D- Ala), 15.5% (methyl-PTH-D-Ala) and 4.9% (methoxy-PTH-D-Ala). Fig. 4 shows the relationship between σ_p of the isothiocyanate reagents and the logarithms of the enantiomer ratios [D/(D + L)]. The extent of racemization of PTH-amino acids seemed to be enhanced by the electron-withdrawing groups, although a linear regression between σ_p and logarithms of D/(D + L) was not obtained owing to the further racemization during the conversion step to PTH.

Physical Properties of 2,1,3-Benzoxadiazolyl-TZ-amino Acids

Fig. 5 shows a chromatogram of five 2,1,3-benzoxadiazolyl-TZ-amino acids, which were separated by RP-HPLC. The

(a) Nitro-PTH-Ala

(b) Chloro-PTH-Ala
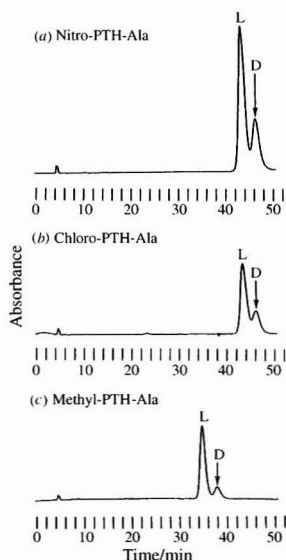
(c) Methyl-PTH-Ala

Fig. 3 Typical chromatograms of (a) nitro-PTH-Ala, (b) chloro-PTH-Ala and (c) methyl-PTH-Ala. An ES-1/2phCD column (150 × 6.0 mm id, 5 μm; Shinwa Chemical Industries) was used for the determination of the D/L configuration determination of PTH-Ala. PTH-amino acids were detected by UV/VIS measurement at 269 nm. nitro-PTH-Ala, 4-nitrophenylth-iohydantoin-Ala; chloro-PTH-Ala, 4-chlorophenylthiohydantoin-Ala; methyl-PTH-Ala, 4-methylphenylthiohydantoin-Ala.
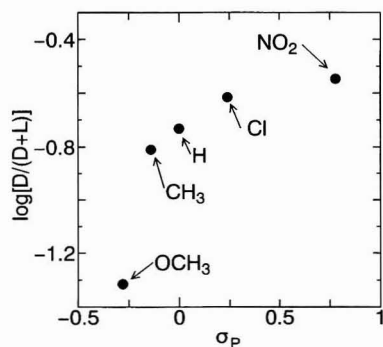
Fig. 4 Relationship between the Hammett *para*-substituent constants (σ_p) of *para*-substituted PTH-Ala and the logarithms of the enantiomer ratios. σ_p values of the *para*-substituent groups are from ref. 12.

2,1,3-benzoxadiazolyl TZ-Leu fractions were collected and fluorescence spectra, UV absorption and molecular mass were measured (Table 2). The fluorescence of MBD-TZ-Leu and DABD-TZ-Leu could hardly be detected, and it was obvious that MBD-NCS and DABD-NCS were isothiocyanate reagents with an electron-donating group at the *para*-position. We then investigated the effect of the *para*-substituent on the fluorescence intensity of the other TZ-Leu derivatives, using the electron-withdrawing parameter (σ_p).[12] To evaluate the relationship between the *para*-substitutent of the 2,1,3-benzoxadiazolyl moiety and fluorescence intensity, we used the ratio $F(at\ \lambda_{em})/A(at\ \lambda_{max})$, which was obtained as follows:

$$F = KI_0\phi abc \tag{3}$$

$$A = -\log I/I_0 = abc \tag{4}$$

$$F(at\ \lambda_{em})/A(at\ \lambda_{max}) = KI_0\phi \tag{5}$$
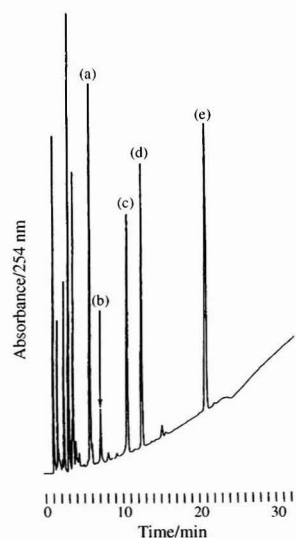
Fig. 5 Chromatogram of TZ-amino acids. The peaks correspond to (a) ABD-TZ-Leu, (b) DABD-TZ-Leu, (c) MBD-TZ-Leu, (d) DBD- TZ-Leu and (e) CBD-TZ-Leu. Gradient elution was employed for TZ-amino acids using eluent A [acetonitrile–water (3 + 7 v/v) containing 10 mM formic acid] and eluent B (acetonitrile containing 10 mM formic acid). The linear gradient program was from 0% B (0 min) to 80% B (30 min) at a flow rate of 1.0 ml/min. TZ-amino acids were separated using an ODS column (YMC J'shere ODS H-80, 150 × 4.6 mm id, spherical, 5 μm, 80 Å; YMC). TZ-amino acids were detected by UV/VIS measurement at 254 nm. ABD-TZ-Leu, 7-aminosulfonyl-4-(2,1,3-benzoxadiazolyl)-TZ-Leu; DABD-TZ-Leu, 7-*N,N*-dimethylamino-4-(2,1,3-benzoxadiazolyl)-TZ-Leu; MBD-TZ-Leu, 7-methoxy-4-(2,1,3-benzoxadiazolyl)-TZ-Leu; DBD-TZ-Leu, 7-*N,N*-di-methylaminosulfonyl-4-(2,1,3-benzoxadiazolyl)-TZ-Leu; CBD-TZ-Leu, 7-chloro-4-(2,1,3-benzoxadiazolyl)-TZ-Leu.

Table 2 Characteristics of 2,1,3-benzoxadiazolylthiazolinone derivatives of amino acids

Derivative	m/z^*	λ_{max}/nm	λ_{em}/nm	Ratio[†]
DBD-TZ-Leu	398	386	513	19.9
ABD-TZ-Leu	370	386	519	8.6
CBD-TZ-Leu	325	389	522	1.7
MBD-TZ-Leu	321	374	—	—
DABD-TZ-Leu	334	453	—	—

* Data were measured in the APCI mode. [†] Ratio = fluorescence intensity (λ_{em})/UV absorption (λ_{max}).

where F, ϕ, I, I_0, A, a, b and c correspond to fluorescence intensity, fluorescence quantum yield, intensity of the incident beam, intensity of the reflection beam, absorbance, absorption coefficient, cell length and concentration of the 2,1,3-benzoxadiazolyl-TZ-amino acid, respectively. K is a constant which is dependent on the instrument. The ratio is the intrinsic value concerning the fluorescence intensity of the 2,1,3-benzoxadiazolyl-TZ-amino acid. Fig. 6 shows the relationship between σ_p and the logarithms of the ratios. These results suggest that the electron density of the *para*-substituent also affects the fluorescence intensity of 2,1,3-benzoxadiazolyl-TZ-amino acids.

Considering the results described above, an isothiocyanate reagent which contained an electron-withdrawing group at the *para*-position caused the racemization of TZ-amino acids during sequence analysis, although the fluorescence intensity of TZ amino acid was increased. DBD-NCS, which was the reagent having the most electron-withdrawing group at the *para*-position in this study, could be used successfully to analyze the sequence of 25 pmol of Leu[5]-enkephalin.[10]

Concerning the retention of the original configuration of TZ-amino acid, we have already reported that the cyclization/

cleavage reaction by a Lewis acid, boron trifluoride (BF_3), was the most effective, and TZ amino acid was scarcely racemized during sequence analysis.[14] Consequently, further study on the combination of an isothiocyanate with a strong electron-withdrawing group at the *para*-position, such as DBD-NCS, and the use of a Lewis acid in sequence analysis will lead to a more sensitive and accurate method for the determination of D/L-amino acid configuration. A stronger electron-withdrawing group at the *para*-position than DBD-NCS will lead to a more sensitive method for sequence analysis such as 7-nitro-4-(2,1,3-benzoxadiazolyl) isothiocyanate (NBD-NCS), and is now in process of being synthesized.

References

1   Edman, P., *Acta Chem. Scand.*, 1956, **10**, 761.
2   Muramoto, K., Norihara, K., Ueda, A., and Kamiya, H., *Biosci., Biotechnol. Biochem.*, 1994, **58**, 300.
3   Miyano, H., Nakajima, T., and Imai, K., *Biomed. Chromatogr.*, 1987, **2**, 139.
4   Haniu, M., and Shively, J., *Anal. Biochem.*, 1988, **173**, 196.
5   Bidlingmeyer, B. A., Cohen, S. A., and Tarvin, T. L., *J. Chromatogr.*, 1984, **336**, 93.
6   Matsudaira, P., *J. Biol. Chem.*, 1987, **262**, 10035.
7   Hewick, R. M., Hankapiler, M. W., Hood, L. E., and Dreyer, W. J., *J. Biol. Chem.*, 1981, **256**, 7990.
8   Matsunaga, H., Iida, T., Santa, T., Fukushima,T., Homma, H., and Imai, K., *Anal. Chem.*, 1996, **68**, 2850.
9   Imai, K., Uzu, S., Nakashima, K., and Akiyama, S., *Biomed. Chromatogr.*, 1993, **7**, 56.
10 Matsunaga, H., Santa, T., Hagiwara, H., Homma, H., Imai, K., Uzu, S., Nakashima, K., and Akiyama, S., *Anal. Chem.*, 1995, **67**, 4276.
11 Yoshinaga, M., and Tanaka, M., *J. Chromatogr. A*, 1994, **679**, 359.
12 Hansch, C., Leo, A., and Taft, R. W., *Chem. Rev.*, 1991, **91**, 165.
13 Imai, K., Matsunaga, H., Santa, T., and Homma, H., *Biomed. Chromatogr.*, 1995, **9**, 195.
14 Matsunaga, H., Iida, T., Fukushima, T., Santa, T., Homma, H., and Imai, K., *Biomed. Chromatogr.*, 1996, **10**, 95.
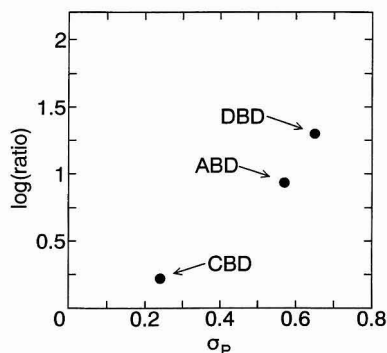
Fig. 6 Relationship between the Hammett *para*-substituent constants (σ_p) of 2,1,3-benzoxadiazolyl-TZ-Leu and the logarithms of the ratios, F(at λ_{em})/A(at λ_{max}). σ_p values of the *para*-substituent groups are from ref. 12.

Application of a Novel Fluorescence Probe in the Determination of Nucleic Acids

Qing-Zhi Zhu, Fang Li, Xiang-Qun Guo, Jin-Gou Xu* and Wen-You Li

The Research Laboratory of SEDC of Analytical Science for Material and Life Chemistry, Department of Chemistry, Xiamen University, Xiamen 361005, China. E-mail: jgxu@xmu.edu.cn

A novel fluorimetric method has been developed for rapid determination of DNA and RNA with hypocrellin A (HA) as a fluorescence probe, based on the fluorescence enhancement of HA in the presence of DNA or RNA. Maximum fluorescence is produced in the pH range 3.4–4.0, with maximum excitation and emission wavelengths at 470 and 600 nm, respectively. Under optimal conditions, the calibration graphs are linear over the range 0–200.0 ng cm^{-3} for calf thymus DNA and 13.0–200.0 ng cm^{-3} for yeast RNA, respectively. The corresponding detection limits are 5.0 ng cm^{-3} for calf thymus DNA and 13.0 ng cm^{-3} for yeast RNA. The relative standard deviation of six replicate measurements is 4.5% for 100 ng cm^{-3} calf thymus DNA. DNA could be determined in the presence of 20% m/m yeast RNA. The mechanism for the binding of HA to DNA is also studied.

Keywords: Spectrofluorimetric determination; hypocrellin A; deoxyribonucleic acid; ribonucleic acid

The quantitative analysis of nucleic acids is of interest since it is often used as a reference for measurements of other components in biological samples. Generally, direct use of the natural fluorescence emission properties of nucleic acids for their structural and dynamic studies, and fluorimetric determinations has been limited[1,2] due to the low fluorescence quantum yield of native DNA ($\phi_f = 4 \times 10^{-5}$),[3] so an extrinsic probe must be employed. Up to now, a number of fluorimetric methods for the determination of nucleic acids have been established,[4–8] several of the most widely used involve staining with a dye such as ethidium bromide;[4] however, the sensitivity is poor due to background emission. In recent years, the interest in trivalent lanthanide cations[9–12] and dimeric asymmetric cyanine dyes[13,14] as fluorescence probes for the biological properties of nucleic acids has increased markedly due to their long wavelength emission and high sensitivity. However, the main disadvantage of these methods is that the lanthanide metals (such as Eu^{3+} and Tb^{3+}) and cyanine dyes (such as TOTO, YOYO, *etc.*) are very expensive.

Hypocrellin A (HA), a new derivative of perylenequinone, is a traditional Chinese medicinal herb ingredient[15] and displays strong fluorescence emission at 600 nm with maximum excitation at 470 nm, the structure of which is shown in Fig. 1. Jiang[16,17] has reviewed its general chemical properties. Recently, HA has received most attention because it is found to be a new efficient singlet oxygen ($^1O_2$) generator[18–20] and has been successfully employed in the clinical photodynamic therapy treatment of a number of skin diseases, such as white lesions of vulva, keloid, vitiligo, psoriasis, tinea capitis and lichen amyloidosis *etc.*[21] To our knowledge, however, the use of HA as a fluorescence probe for determination of nucleic acids has not been reported so far. HA emits at long wavelength with a large Stoke's shift and its fluorescence is significantly enhanced in the presence of nucleic acids in a weak acid medium. Therefore, HA has been employed as a fluorescence probe and a sensitive fluorimetric method has been developed for the determination of nucleic acids. The use of HA as a fluorescence probe leads to a particularly inexpensive, simple and sensitive system, permitting a limit of detection of 5.0 ng cm^{-3} calf thymus (CT) DNA and 13.0 ng cm^{-3} RNA, respectively. The mechanism for the binding of HA to DNA is also studied.

Experimental

Apparatus

A Hitachi (Tokyo, Japan) 650-10S spectrofluorimeter equipped with a plotter unit and a 1 cm quartz cell was used for recording and making fluorescence measurements. The absorption spectrum was performed on a Shimadzu (Kyoto, Japan) UV-240 UV/VIS spectrophotometer. All the pH measurements were made with a digital pH and temperature meter Model 631 (Extech, Boston, MA, USA).

Reagents

All chemicals were of analytical reagent grade or highest available purity. All aqueous solutions were made up in distilled, deionized water.

Commercially prepared calf thymus DNA and yeast RNA, obtained from Sino-American Biotechnology (Shanghai, China), were directly dissolved in water at a final concentration of 100 µg cm^{-3} and stored at 4 °C. These solutions were diluted to 1.0 µg cm^{-3} with water as working solutions. A HA stock
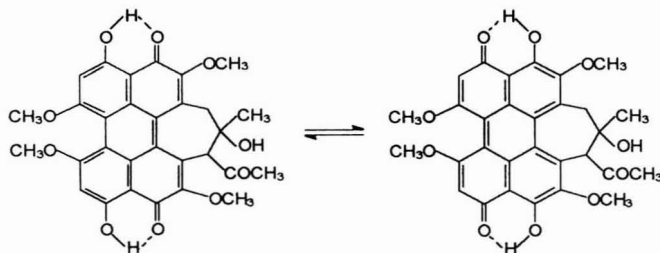
Fig. 1 Structure of HA.

solution (1.0×10^{-4} mol dm^{-3}) was prepared by dissolving the appropriate mass of HA (Yunnan Microbe Institute, Kunming, China) into 100 cm^3 of ethanol and stored in the dark. This solution was diluted to 1.0×10^{-5} mol dm^{-3} with water as working solution. A pH 3.6 acetate buffer solution was prepared by mixing 46.3 cm^3 of 0.2 mol dm^{-3} HAc and 3.7 cm^3 ml of 0.2 mol dm^{-3} NaAc.

Procedure

Transfer into a 10 cm^3 standard flask 0.8 cm^3 of buffer solution (pH 3.6), 1.0 cm^3 of HA solution (1.0×10^{-5} mol dm^{-3}). Add a known volume of CT DNA (or RNA) standard solution. Dilute to the volume with water and mix. Measure the relative fluorescence intensity at 600 nm with excitation at 470 nm. Background fluorescence has been subtracted for each value reported except for excitation and emission spectra.

Results and Discussion

Spectral Characteristics of Fluorescence

HA is a new derivative of perylenequinone, which is not soluble in water, but can easily dissolve in some organic solvents, such as ethanol, chloroform, *etc.* It shows two isomers in solution, and there is an equilibrium of isomerization.[16]

The uncorrected excitation and emission spectra of HA are shown in Fig. 2. In a weakly acidic medium, HA displays three excitation bands located at 350, 470 and 550 nm, respectively. The maximum excitation peak is at 470 nm, which may be assigned to a π–π^* transition, while the longer wavelength band results from intramolecular proton transfer.[22] The fluorescence spectrum of HA consists of two emission bands, located at 600 and 650 nm (shoulder peak). The shorter wavelength band is due to π–π^* transition, and the other band can be attributed to intramolecular proton transfer.[22] Diwu *et al.*[23] reported the effects of the concentration of HA, solvents, acid, bases and temperature on the fluorescence spectra of HA, the results showed that the intramolecular proton transfer of the excited HA is weakened at low temperature and the emission bands of HA shifted slightly to long wavelength with increasing concentration of HA, furthermore, the intensity ratio of the two emission bands changed dramatically. In addition, they also indicated that the fluorescence properties of HA are related to the characteristics of solvents, and this may allow HA to act as a new kind of fluorescence probe to study the biological macromolecular system.

In our research, it was found out that the excitation and emission maxima of the HA–CT DNA system are similar to that

of HA, but the fluorescence intensity is significantly enhanced. On the other hand, RNA can similarly enhance the fluorescence of HA, however, its enhancement ability is lower than that of DNA. These results indicated that HA can be used as a new fluorescence probe for sensitive determination of DNA. In this paper, the maximum excitation peak at 470 nm and the emission peak at 600 nm were used for fluorescence intensity measurements.

As described above, the fluorescence spectral maximum remains unchanged at 600 nm. This result is in contradistinction from the observed large red shifts in the fluorescence maxima when the compounds intercalate into the helix.[24] This suggests that HA binds to the double helix in a non-intercalative way.

Optimization of the General Procedure

The experimental results indicate that the maximum and constant fluorescence intensity occurred when the HA concentration was in the range 8.0×10^{-7}–2.4×10^{-6} mol dm^{-3}. In this work, a HA concentration of 1.0×10^{-6} mol dm^{-3} was recommended. The effect of pH on the fluorescence enhancement of the system was studied. The fluorescence intensity reached a maximum over the pH range 3.4–4.0 and decreased outside this pH range. A pH of 3.6 was recommended for use, by addition of 0.8 cm^3 of buffer solution in 10 cm^3 of final solution. The influence of incubation time on fluorescence intensity was also investigated. The results showed that the maximum fluorescence intensity was reached immediately when the solutions were mixed, and remained constant for 30 min. When the incubation time was longer than 30 min, the fluorescence intensity began to decrease. Therefore, a 5 min incubation time was adopted in this work. For RNA, the optimum conditions were similar to that of the DNA system.

Interaction of HA With DNA

In Fig. 3 the absorption spectra of HA in the presence of various concentrations of CT DNA are shown. It can be seen that the absorbance of HA shows a slight increase with increasing amounts of DNA. However, the absorption maximum at 465 nm remains unchanged, even in the presence of an excess of CT DNA. These results are in contrast to the observed large red shifts in absorption maxima[25] and strong hypochromism when the dye intercalates into the base stack.[26] Therefore, it is suspected that the minor changes observed with HA could be due to the dye interacting with the double helix in a non-intercalative way.
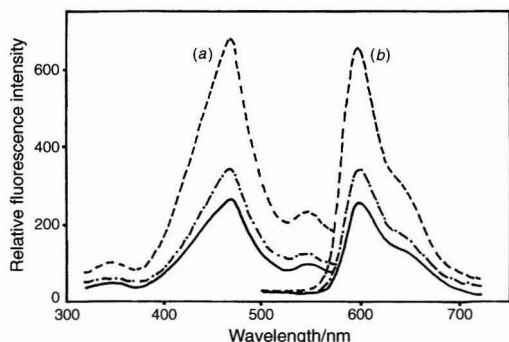
Fig. 2 Excitation (*a*) and emission (*b*) spectra of free HA (solid curves) and in the presence of CT DNA (dashed curves) and RNA (dot-dashed curves). HA: 1.0×10^{-6} mol dm^{-3}; CT DNA: 100 ng cm^{-3}; RNA: 100 ng cm^{-3}.
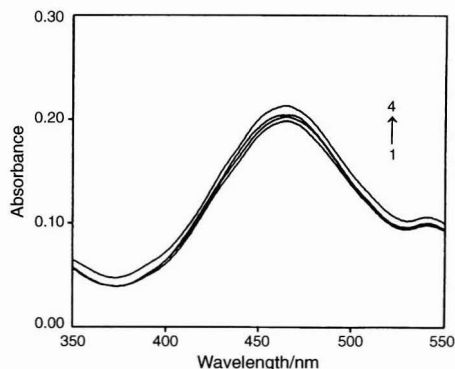
Fig. 3 Absorption spectra of HA with increasing concentrations of CT DNA: (1) 0 µg cm^{-3}, (2) 1.0 µg cm^{-3}, (3) 5.0 µg cm^{-3} and (4) 10.0 µg cm^{-3}. HA: 1.0×10^{-6} mol dm^{-3}.

In order to further establish the DNA binding affinity of HA, the iodide quenching and salt effect on HA in the presence and absence of CT DNA has been examined. The fluorescence quenching data were plotted according to the Stern–Volmer equation:

$$F_0/F = 1 + K_{sv} [Q]$$

where F_0 and F are the fluorescence intensities in the absence and in the presence of KI, respectively; K_{sv} is the Stern–Volmer quenching constant; and [Q] is the concentration of the quencher (KI). If HA is intercalated into the base stack, it should be protected from the anion quencher, owing to the base pairs above and below the intercalator, so the magnitude of K_{sv} of the free HA should be higher than that of the bound HA; in contrast, the magnitude of K_{sv} of the free HA should be lower than that of the bound HA.[27] In aqueous solutions, iodide quenched the fluorescence of HA very efficiently. Addition of potassium iodide to a mixture of HA and CT DNA resulted in extensive quenching of the fluorescence intensity (Fig. 4). The quenching constants for the free HA and the bound HA with CT DNA were 71 and 255 dm^3 mol^{-1}, respectively. These results indicate that HA may bind to DNA in a non-intercalative way.

The effect of the ionic strength on the fluorescence intensity of HA was investigated by the addition of NaCl, the results are shown in Fig. 5. It is obvious that in the absence of CT DNA, the addition of NaCl to the free probe had little effect on the fluorescence yield of the dye; the Stern–Volmer quenching constant is 15 dm^3 mol^{-1}. However, in the presence of CT DNA, a greater quenching effect was observed when NaCl was
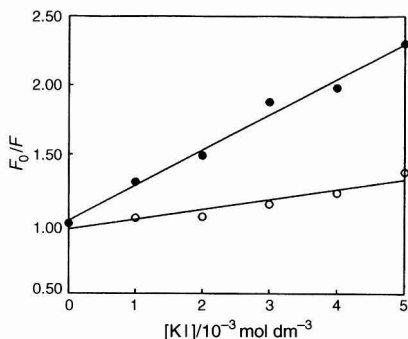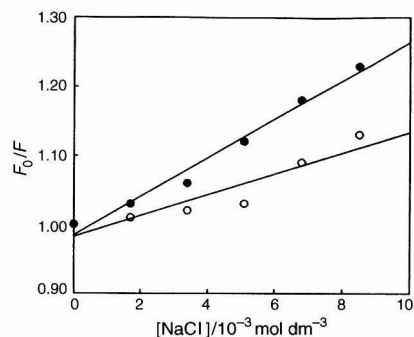
added, and the estimated K_{sv} value with NaCl was 28 dm^3 mol^{-1}. Since the fluorescence of the free HA was only slightly quenched by the salt, it is evident that the quenching in the presence of DNA was due to the release of the probe from the helix into the bulk aqueous solution. The quenching constant with NaCl was less than that with KI (K_{sv} = 255 dm^3 mol^{-1}) because iodide is a more effective quencher of the fluorescence than chloride. The strong dependence of the binding on the ionic strength clearly indicates that HA binding to DNA is non-intercalative rather than intercalation into the helix.

Calibration Graphs

The calibration graphs for the determination of DNA (or RNA) were constructed under the optimal conditions. The results are shown in Fig. 6. There are good linear relationships between the fluorescence enhancement and the concentrations of CT DNA (or RNA). All the analytical parameters are presented in Table 1. From Table 1 it can be seen that the sensitivity for the determination of CT DNA is higher than that for RNA. The limit of detection (LOD) is given by the equation, LOD = Ks_0/ S, where K is a numerical factor chosen according to the confidence level desired, s_0 is the standard deviation of the blank measurements (n = 7) and S is the sensitivity of the calibration graph. Here a value of 3 for K was used.

Comparison of the Methods

Some characteristics of the proposed method and other methods for nucleic acid determinations are summarized in Table 2. Compared to classical dyes like ethidium and Hoechst, the proposed method has higher sensitivity, larger Stoke's shift and longer emission wavelength. In addition, it is more sensitive and rapid than methods that use lanthanide cations as fluorescence probes. However, the proposed method seems to be less precise and has a narrow linear range. Methods using the cyanine dyes, such as TOTO, YOYO, etc., are more sensitive than the HA method, but they show shorter Stoke's shift and longer incubation time. In addition, these dyes are very expensive.

Fig. 4   Quenching of HA fluorescence by KI in the presence of CT DNA (filled circles) and in the absence of CT DNA (open circles). HA: 1.0 × 10^{-6} mol dm^{-3}; CT DNA: 100 ng cm^{-3}.

Fig. 5   Effect of NaCl solutions on HA fluorescence in the presence of CT DNA (filled circles) and in the absence of CT DNA (open circles). HA: 1.0 × 10^{-6} mol dm^{-3}; CT DNA: 100 ng cm^{-3}.
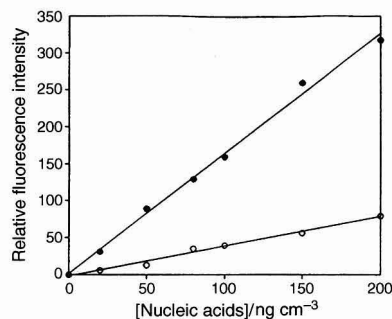
Fig. 6   Calibration curves for CT DNA (filled circles) and yeast RNA (open circles). Conditions given under Procedure.

Table 1 Analytical parameters for the determination of nucleic acids

Nucleic acid	Linear range/ ng cm^{-3}	Linear regression equation*	LOD/ ng cm^{-3}	r
Calf thymus DNA	0–200	F = 1.62 c + 1.69	5.0	0.9976
Yeast RNA	13.0–200	F = 0.40 c − 1.64	13.0	0.9927

* c in ng cm^{-3}.

Table 2 Comparison of methods for determination of DNA

Methods	$\lambda_{ex}/\lambda_{em}$*	Incubation time/min	LOD/ ng cm^{-3}	Linear range/ µg cm^{-3}	RSD (%)
Ethidium bromide[4]	546/590	—	10	—	—
Hoechst 33258[5]	356/492	—	10	0–15	—
Tb^{3+}-phenanthroline[11]	298/543.5	20–30	100	0.4–15	3.0
Eu^{3+}-tetracycline[12]	398/615	—	10	0.02–1.0	3.0
TOTO[14]	488/535	20–30	0.5	0.0005–0.1	—
YOYO[14]	470/510	20–30	0.5	0.0005–0.1	—
This method	470/600	5	5	0–0.2	4.5

* Excitation/emission wavelength in nm.

Table 3 Determination of CT DNA in synthetic samples

Sample no.	Composition of samples/ ng cm^{-3}	Recovery of DNA* (%)	RSD (%)
1	DNA (50)	100	2.9
2	DNA (100)	98.7	4.5
3	DNA(100) + RNA(5)	99.9	4.2
4	DNA(100) + RNA(10)	96.2	3.1
5	DNA(100) + RNA(20)	103.5	4.0
6	DNA(100) + RNA(50)	124.0	5.0

* Average of six determinations.

Table 4 Determination of yeast RNA in synthetic samples

Sample no.	Composition of samples/ ng cm^{-3}	Recovery of RNA* (%)	RSD (%)
1	RNA (50)	97.6	4.5
2	RNA (100)	101.7	2.9
3	RNA(100) + DNA(5)	129.0	2.0
4	RNA(100) + DNA(10)	179.0	3.4

* Average of six determinations.

Determination of Nucleic Acids in Synthetic Samples

As described above, the sensitivity of the fluorescence determination of CT DNA is higher than that of RNA: DNA has a much greater ability to enhance the fluorescence yield of HA. It is, therefore, expected that DNA could be measured in the presence of RNA. The determination of DNA in synthetic samples, which contained various concentrations of RNA, were carried out according to the experimental procedure. The results are shown in Table 3. It can be observed that CT DNA could be determined in the presence of up to 20% RNA with satisfactory results.

The above procedure was also applied to the determination of RNA in two synthetic samples (Table 4). Table 4 shows that the presence of DNA seriously interferes with the determination of RNA even when the concentration ratio of DNA to RNA in the samples is 5%.

Conclusions

The proposed fluorescence method has high sensitivity for the determination of nucleic acids with HA as a new fluorescence probe. In weak acid medium, the fluorescence of HA is significantly enhanced by nucleic acids due to the binding of the probe to DNA (or RNA) in a non-intercalative way. In addition to its sensitivity, other advantages of this method include its non-toxicity, simplicity, rapidity, large Stoke's shift and long emission wavelength. The only operation is the mixing of two solutions before fluorescence measurements. Furthermore, the large Stoke's shift and long wavelength emission may allow the proposed method to avoid the interference of the background efficiently in biological systems.

References

1   Udenfriend, S., and Zaltzman, P., *Anal. Biochem.*, 1962, **3**, 49.
2   Borresen, H. C., *Acta Chem. Scand.*, 1963, **17**, 921.
3   Lakowicz, J. R., *Fluorescence Spectroscopy, Vol 3: Biochemical Applications*, Plenum Press, New York, 1992, pp. 137.
4   Le Pecq, J.-B., and Paoletli, C., *Anal. Biochem.*, 1966, **17**, 100.
5   Kapuscinski, J., and Skoczylas, B., *Anal. Biochem.*, 1977, **83**, 252.
6   Labarca, C., and Paigen, K., *Anal. Biochem.*, 1980, **102**, 344.
7   Topal, M. D., and Fresco, J. R., *Biochemistry*, 1980, **19**, 5531.
8   Al-Hakeem, M., and Sommer, S. S., *Anal. Biochem.*, 1987, **163**, 433.
9   Pavlick, D., and Formoso, C., *Biochemistry*, 1978, **17**, 1537.
10 Ringer, D. P., Howell, B. A., and Kizer, D. E., *Anal. Biochem.*, 1980, **103**, 337.
11 Ci, Y. X., Li, Y. Z., and Chang, W. B., *Anal. Chim. Acta*, 1991, **248**, 589.
12 Ci, Y. X., Li, Y. Z., and Liu, X. J., *Anal. Chem.*, 1995, **67**, 1785.
13 Rye, H. S., Yue, S., Wemmer, D. E., Quesada, M. A., Haugland, R. P., Mathies, R. A., and Glazer, A. N., *Nucleic Acids Res.*, 1992, **20**, 2803.
14 Rye, H. S., Dabora, J. M., Quesada, M. A., Mathies, R. A., and Glazer, A. N., *Anal. Biochem.*, 1993, **208**, 144.
15 Wan, X. Y., and Cheng, Y. T., *Chinese Sci. Bull.*, 1980, **25**, 1148.
16 Jiang, L. J., *Chinese Sci. Bull.*, 1990, **35**, 1608.
17 Jiang, L. J., *Chinese Sci. Bull.*, 1990, **35**, 1681.
18 Diwu, Z. J., and Lown, J. W., *J. Photochem. Photobiol. A: Chem.*, 1992, **64**, 273.
19 Diwu, Z. J., and Lown, J. W., *J. Photochem. Photobiol. A: Chem.*, 1992, **69**, 191.
20 Diwu, Z. J., Zhang, C., and Lown, J. W., *J. Photochem. Photobiol. A: Chem.*, 1992, **66**, 99.
21 Diwu, Z. J., and Lown, J. W., *Photochem. Photobiol.*, 1990, **52**, 609.
22 Diwu, Z. J., Jiang, L. J., and Zhang, M. H., *Sci. Sin., Ser. B (Engl. Ed.)*, 1989, **33**, 18.
23 Diwu, Z. J., Jiang, L. J., and Zhang, M. H., *Acta Phys. Chem. Sin.*, 1989, **5**, 250.
24 Le Pecq, J.-B., and Paoletti, C., *C. R. Acad. Sci. Paris*, 1964, **259**, 1786.
25 Wilson, W. D., Tanious, F. A., Watson, R. A., Barton, H. J., Strekowska, A., Harden, D. B., and Strekowski, L., *Biochemistry*, 1989, **28**, 1984.
26 Cantor, C., and Schimmel, P. R., *Biophysical Chemistry*, Freeman, San Francisco, 1980, vol. 2, pp. 398.
27 Kumar, C. V. Turner, R. S., and Asuncion, E. H., *J. Photochem. Photobiol. A: Chem.*, 1993, **74**, 231.

Surface-enhanced Raman Scattering Observations on Bipyridine, Phthalimide, Phenylethylamine and Theobromine by Using a Fine Silver Particle-doped Cellulose Gel Film

Youichi Kurokawa[*a], **Yoshika Imai**[b] **and Yuko Tamai**[a]

[a] *Department of Material Chemistry, Faculty of Engineering, Tohoku University, Aoba-ku Sendai 980-77, Japan*
[b] *Department of Basic Science, Ishinomaki Senshu University, Ishinomaki 986, Japan*

A surface-enhanced Raman scattering (SERS)-active Ag particle-doped cellulose gel film was prepared reproducibly by the counter diffusion method. In the literature, SER spectra of 2,2'-bipyridine and phthalimide were similar to those adsorbed on Ag sol. This doped film permits the SERS of a vital functional substance such as a theobromine to be obtained at concentrations down to 10^{-3}–10^{-7} M.

Keywords: Surface-enhanced Raman scattering: fine silver particles; cellulose; gel; film

Raman enhancement by molecules adsorbed on an Ag electrode has been the subject of considerable interest.[1,2] Surface-enhanced Raman scattering (SERS) also can be observed for other substrates, such as a vaporized Ag film,[3] Ag-coated filter-paper,[4,5] Ag flake[6] and colloidal Ag particles.[7] Much has been reported on SERS using Ag sol as an active substrate.[7] Although the procedure for preparing an Ag sol is simple, many factors, such as pH, ionic strength, temperature and amount of adsorbate, affect the aggregation of the sol and cause intensity variations of the SER spectra. Hence much effort has been devoted to developing Ag substrates for trace analysis. It seems that Ag-coated filter-paper is adequate in practice for observing SERS because this substrate provides an Ag particle morphology which is uniform on the submicrometer scale necessary for enhancement.[4] However, it seems that it needs an intimate surface structure of the Ag particles and the cellulose on a scale of a few tens of nanometers for additional enhancement. Here, we prepared an Ag particle-doped SERS-active cellulose film substrate which is uniform on the nanometer scale and which can be prepared easily with good reproducibility.

Experimental

All chemicals were commercially available. The preparation of the finely porous cellulose acetate (CA) film used was as described previously.[8] The method is essentially the same as in the preparation of reverse-osmosis cellulose gel film. The casting solution was prepared by mixing CA (acetyl content 39.8%) (Wako, Osaka, Japan), formamide and acetone in a ratio of 25 : 35 : 40 by mass. The solution was spread on a glass plate at room temperature using a casting knife. After evaporation for 30 min, the cast film was gelled by immersing it (film + glass plate) in ice-cold water for 2 h. The doping of the Ag particles into the CA film was performed in an acrylate box-type cell into which the CA film could be clamped, such that one half of the cell was separated from the other half-cell by the film. We refer to it as a counter-diffusion method, which involves diffusing 0.1 M NaOH solution and 0.1 M AgNO₃ solution from opposite

sides of the CA film. Fig. 1 shows an illustration of the method. The solutes from the cell compartments diffuse into the CA film and interact with the consequent formation of hydrous Ag₂O particles. The doped film was next immersed in a reducing solution, *i.e.*, 5% formalin, 0.05 M NaBH₄ or 10% hydrazine solutions. The Ag₂O particles were thus reduced to Ag particles. The Ag particle-doped film was dipped into an analyte solution for 1 h. After removal from the solution, the film was washed with distilled water and then dried at a room atmosphere. SER spectra were obtained using a Spex 1403 spectrometer equipped with an argon ion laser (Spectra-Physics, San Jose, CA, USA). All spectra were obtained using 514.5 nm radiation as an excitation source. X-ray diffraction (XRD) was carried out using Cu Kα irradiation with an Ni filter. Electron microscopy was performed with a Hitachi (Tokyo, Japan) H-800 instrument. The sample was adjusted by dissolving the doped film in pyridine.

Results and Discussion

The doped CA film looks like a solid solution. Substrate CA gel films without doping contain 20–30% water depending on the preparation conditions. Water in the gel film constitutes hydrophilic microdomains in which particle formation and growth proceed. The domains prevent the particles from growing beyond a definite size which depends on the casting solution. We used the composition described previously, taking into account the ease of casting of the solution on a glass plate (viscosity is critical) at room temperature. The doped film is a sort of intimate mixture of CA and Ag particles on a nanometer scale, because in appearance it is a homogeneous composite gel.

Ag colloids have a typical absorption around 380–410 nm due to plasmon excitations. Fig. 2 shows the absorption spectra of doped films treated by the reducing agents formalin, NaBH₄

CA gel film

Counter Diffusion Method
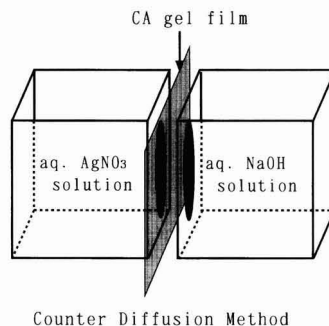
Fig. 1 Illustration of the counter-diffusion method.

and hydrazine solutions. NaBH$_4$ gives relatively sharp spectra indicative of monodispersed particles, hydrazine gives broad spectra and formalin gives broader spectra indicative of polydispersed particles. This difference may be due to the differences in the action of the reducing agents, namely, vigorous reaction with nascent H$_2$ in hydrazine solution, reaction with nascent H$_2$ in NaBH$_4$ and slow reducing action of aldehyde in formalin. As the Ag particles aggregate, the spectra change from a single sharp band to a broad band. Further aggregation gives rise to precipitation. As shown in Fig. 2, an aggregate state can be fixed in the gel film. This is favorable for preparing a doped film compatible with the wavelength of the laser source. It seems that the doped film treated with formalin solution is suitable in near-infrared enhanced Raman scattering.

Fig. 3 shows the XRD patterns of doped films. These are similar in position line-by-line to each other. The doped film has a slightly larger diffraction plane (200) than bulk Ag. The peak of the doped film is broad, indicating fine particle character. The approximate size can be estimated from XRD by using Scherrer's equation. The particle size obtained is 24 nm for formalin treatment, 15 nm for NaBH$_4$ solution treatment and 20 nm for hydrazine treatment. Fig. 4 shows the scanning electron micrograph of a doped film dissolved in pyridine. It illustrates that particles are not monodispersed but polydispersed, as shown in the spectra in Fig. 2. It is known that the parameters that affect SERS are the surface roughness of the electrode and weak aggregation of particles in a sol. Surface roughness and particle sizes ranging from several to a few tens of nanometers provide strong surface enhancement. This doping procedure

Fig. 2 Absorption spectra of Ag particle-doped CA films: A, formalin treatment; B, NaBH$_4$ solution treatment; and C, hydrazine treatment.

Fig. 3 X-ray diffraction patterns of films doped with fine Ag particles: A, formalin treatment; B, NaBH$_4$ solution treatment; and C, hydrazine treatment.

gives the substrate the surface roughness convenient for observing SERS. We used the doped film for SERS observations because it gives a broad plasmon spectrum for the aggregated particles and less decomposition of cellulose by the laser.

Fig. 5(*a*) shows the SER spectrum of phthalimide. Its vibrational assignments have been made for the Ag sol substrate.[9] The band at 213 cm^{-1} is probably due to the Ag–N stretching vibration. The bands at 582 and 678 cm^{-1} are due to ring deformation. The strongest band is observed at 1005 cm^{-1}, which is a totally symmetric vibration. For the other bands, that at 1143 cm^{-1} may be due to ring stretching, 1161 cm^{-1} to C–H bending and 1374 cm^{-1} to ring stretching. This spectrum is similar to that of phthalimide adsorbed on an Ag sol. The most noticeable difference between the spectrum of the solid state of phthalimide and those of Ag sol and doped film is the presence of the C=O stretching vibration (1706–1756 cm^{-1}), which is absent in the Ag sol and doped film. The intensity loss of this band is probably due to a strong interaction of the molecule with the solvent through the oxygen of the C=O, which increases the polarity of the C=O bond. However, the doped film is in the dry state without solvent. The cellulose acetate support does have an acetyl and, more likely, hydroxyl groups which can interact similarly with the C=O bond. Therefore, these in the doped film may play the same role as the solvent in the Ag sol.

Fig. 5(*b*) shows the SER spectrum of 2,2'-bipyridine. Our SER spectrum compares most closely to that of bipyridine adsorbed on Ag sol at pH 8.5 and that in 0.1 м KCl on an Ag electrode.[10–12] It gives rise to a most prominent band at 1012 cm^{-1}, which is the breathing vibration of the pyridine skeleton. In the region where there is C=C and C=N stretching, bands at 1483, 1570 and 1587 cm^{-1} are observed. The strong band at 248 cm^{-1} is probably due to the Ag–N stretching vibration. For pyridine adsorbed on Ag sol, the Ag–N stretching vibration has been observed at 220 cm^{-1}.[13] Overall, our results are consistent with the previous interpretation of 2,2'-bipyridine in a *cis* conformation. The molecule interacts with the Ag sol surface (or Ag electrode) via σ donation from both 2-position nitrogens in a chelating fashion. The molecule sits perpendicular to the surface.

The major limitation in the use of Raman spectra for pharmaceutical agents has been interference from the fluorescence present in the agent which obscures the Raman signal. Generally, the adsorption on the solid is acccompanied by
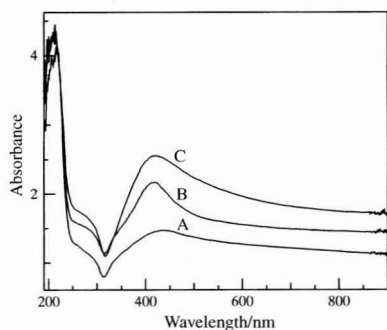
Fig. 4 Scanning electron micrograph of the doped film.
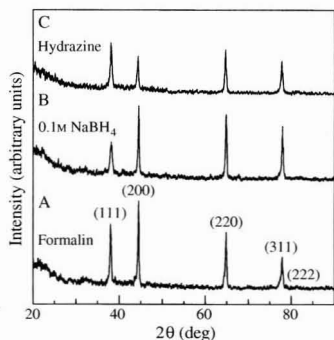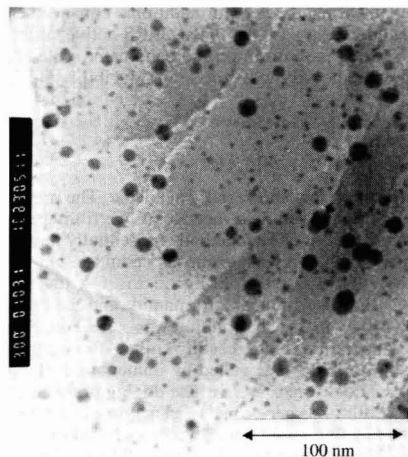
strong quenching of fluorescence. As can be seen from the Ag–N band in Fig. 5(*a*) and (*b*), the doped film shows stronger adsorption to the analyte compared with Ag sol. We tested phenylethylamine as a model substance of a stimulant, methamphetamine (the most abused drug in Japan), and a diuretic, theobromine. These substances in blood and urine are indirectly detected by HPLC or GC–MS after pre-treatment. The former structure resembles phenylpropanolamine, which is an ingredient of a cold remedy.[13] Because of limited reported vibrational data, vibrational assignments are inadequate. The SER spectrum of phenylethylamine is shown in Fig. 5(*c*). It is in the form of an HCl adduct because it is not otherwise soluble in water. Methamphetamine is also abused in the form of the HCl adduct by the addition of HCl solution. A strong Ag–N or Ag–Cl band at 246 cm^{-1} appears. It has been reported that this band is enhanced in the presence of Cl^{-}.[14] Because the Ag particle is positively charged, this bond may be enhanced more through Cl^{-} adsorbed on Ag. Intense bands at 1005 and 1604 cm^{-1} are observed. The former band is assigned to the phenyl ring breathing and the latter may be due to a ring stretching vibration
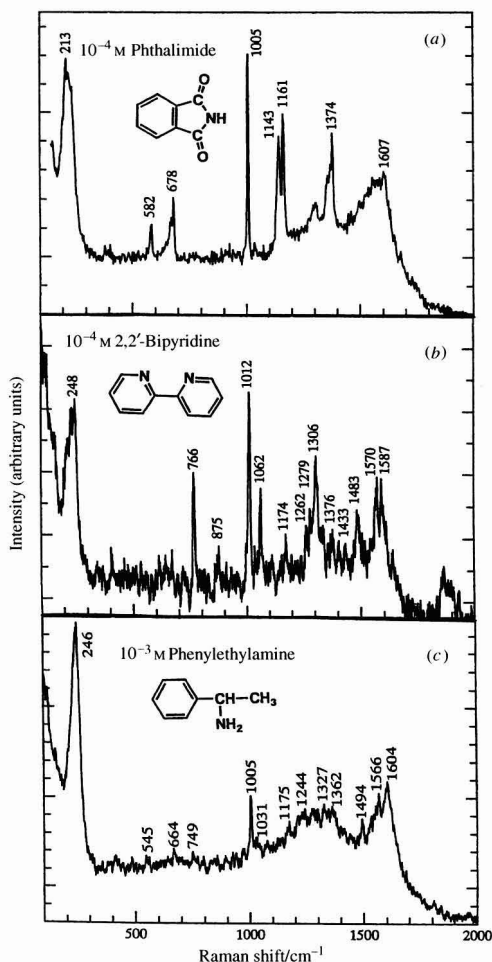
Fig. 6 SER spectrum of theobromine with analyte concentration 10^{-3} M.
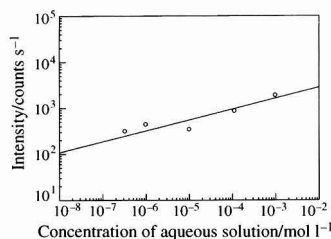
Fig. 7 Logarithmic calibration plot for theobromine.

or NH$_3^+$ group deformation. As can be seen from Fig. 5(*c*), it appears that 1200–1600 cm^{-1} bands are superimposed on a broad background band, which may be due to a product of the decomposition of the adsorbate or the cellulose by the laser. Similar behaviour can be seen in Fig. 5(*a*) and (*b*). It has been reported that 2-pyrazinecarboxylic acid is photodecomposed into graphitic carbon, and that disordered graphite gives two broad bands centred at approximately 1350 and 1530 cm^{-1}.[15]

The SER spectrum of theobromine is shown in Fig. 6. In this case also, the carbon bands can be recognized underlying the SERS bands. The band at 641 cm^{-1} may be due to ring breathing, those at 1200–1400 cm^{-1} to ring stretching and those at 1607 cm^{-1} to C–C and C–N stretching. These bands can be detected down to the 10^{-6} M level. In Fig. 7, a logarithmic calibration plot for this substance is shown. The data were obtained from the 1310 cm^{-1} band. The plot is linear over nearly four orders of magnitude.

Conclusion

We have developed a SERS-active substrate–cellulose gel film doped with Ag fine particles by a counter diffusion method. It can be successfully used for the determination of N-containing substances and drugs. The advantages of this procedure are the simplicity of substrate preparation, low cost and ease of handling.

References

1 Otto, A., Mrozek, I., Grabhorn, H., and Akermann, W., *J. Phys. Condens. Matter*, 1992, **4**, 1143.
2 Nabier, I., Chourpa, I., and Manfair, M., *J. Raman Spectrosc.*, 1994, **25**, 13.

Fig. 5 SER spectra of (*a*) phthalimide with analyte concentration 10^{-4} M, (*b*) 2,2'-bipyridine with analyte concentration 10^{-4} M and (*c*) phenyl-ethylamine (HCl adduct) with analyte concentration 10^{-3} M.

3   Moody, R. L., Vo-Dinh, T., and Fletcher, W. H., *Appl. Spectrosc.*, 1987, **41**, 966.
4   Sutherland, W. S., and Winefordner, J. D., *J. Raman Spectrosc.*, 1991, **22**, 549.
5   Lee Arthur, S. L., and Li, Y.-S., *J. Raman Spectrosc.*, 1994, **25**, 209.
6   Hudson, M., and Waters, D. N., *Spectrochim. Acta, Part A*, 1991, **47**, 1467.
7   References cited in ref. 2.
8   Kurokawa, Y., *J. Membr. Sci.*, 1996, **114**, 1.
9   Aroca, R., and Clarijo, R. E., *Spectrochim. Acta, Part A*, 1988, **49**, 171.
10 Cooney, R. P., Mahoney, M. R., Howard, M. W., and Spink, J. A., *Langmuir*, 1985, **1**, 273.
11 Kim, M., and Itoh, K., *J. Phys. Chem.*, 1987, **91**, 126.
12 Strekas, T. C., and Diamondopoulos, P. S., *J. Phys. Chem.*, 1990, **94**, 1986.
13 Li, Y.-S., Lee, A., and Wang, Y., *J. Raman Spectrosc.*, 1991, **22**, 191.
14 Liarg, E. J., Engert, C., and Kiefer, W., *Vib. Spectrosc.*, 1995, **8**, 431.
15 Suh, J. S., Moskovitz, M., and Shakhesemampour, J., *J. Phys. Chem.*, 1993, **97**, 1678.

Determination of Trace Amounts of Oil in Water by Adsorption Filtration

Part 1. Infrared Method

Huiling Zou[a], Qingli Jiang[b], Weian Liang[*c], Zhenyu Zhang[c], and Shifu Zou[c]

[a] *Shandong Supervision and Inspection Institute for Production Quality, Shandong, China*
[b] *Shandong Polytechnic University, Shandong, China*
[c] *Chemical Department, Shandong University, Jinan 250100, China*

Silicon carbide was examined as an adsorbent on which oil can be easily adsorbed and subsequently eluted. A method for the determination of trace amounts of oil in water was developed. A water sample was filtered through a funnel containing silicon carbide and the adsorbed oil was then eluted and measured by infrared spectrometry or other methods. The amount of organic solvent used in this method was much less than that in an extraction method, the enrichment efficiency was greatly increased and the method is superior to liquid–liquid extraction. The method was applied to synthetic samples and effluent samples from an oil refinery and the experimental results were satisfactory. The detection limit in a water sample is 0.002 ppm, the recovery is more than 90%, the average error is 1.8% and the average deviation is 6.1%.

Keywords: Adsorption filtration; silicon carbide adsorbent; oil determination; water; infrared spectrometry

For the determination of trace amounts of oil in water, not many simple and convenient methods are available.[1–3] Most of the reported methods have low sensitivity and are not satisfactory for the present requirements. Although fluorescence methods have high sensitivity, their application is limited because the results are greatly affected by different sources of oil. Hence there is an urgent need to increase the sensitivity of analysis. With regard to the properties of oil (saturated hydrocarbons), we considered that increasing the enrichment efficiency is probably the most effective approach. To increase the enrichment efficiency, a larger amount of water sample or a smaller volume of organic solvent (*e.g.*, CCl$_4$) is generally used. Both of these are difficult to accomplish by extraction, but easily by adsorption.[4] Up to now only a few adsorbents have been reported for analyses to determine oil,[4–8] and there are several problems with such adsorbents. For example, some adsorbents have a low affinity for oil and adsorb too much water simultaneously; some adsorbents themselves are weakly soluble in organic solvents and produce interferences. We have found that an adsorbent made from industrial silicon carbide can easily adsorb oil with subsequent easy elution. This adsorbent does not have the above defects and has the advantages of high mechanical intensity and heat resistance and resistance to strong acids and weak bases.

The adsorbent was contained in an oil-trap funnel though which water samples were filtered. The adsorbed oil was eluted with a small amount of an organic solvent and measured by an infrared (or ultraviolet or fluorescence) method. The recovery of crude or heavy diesel oil in water samples was ≥90%. The enrichment efficiency was at least eight times greater than an extraction method. In order to enhance the above advantages, to make the volume of water sample greater and the sensitivity higher, we intend to join the oil-trap funnel to a sampler and

make a combined device for automatic sampling. When the device is put into a water body, sampling and oil trapping would be accomplished in a single step. The problem of taking samples back to the laboratory would therefore be avoided.

This paper introduces the infrared method for measuring trace amounts of oil in water after adsorption and separation.

Experimental

Apparatus and Reagents

A Model IR 408 infrared spectometer (Shimadzu, Kyoto, Japan) was used. The quartz cells and the shelf were assembled in the laboratory.

Microsyringes (10 µl). Experiments showed that the microsyringes were not suitable for viscous oil (heavy diesel oil, *etc.*) but were suitable for diluting oil solution in CCl$_4$ or other solvents.

Oil-trap funnel. This was blown from glass with different shapes and sizes according to need. A generally used funnel is shown in Fig. 1. The funnel contained 8 g of adsorbent (100–120 mesh).

Carbon tetrachloride, analytical-reagent grade. Its transmittance near 2960 cm^{-1} was >90%.

Standard oil solution. Accurately weigh a suitable quantity of commercial heavy oil and dilute it with CCl$_4$ to the volumes required to give concentrations of 50 and 10 g l^{-1}.

Synthetic water sample. The procedure for making 400 ml of a 1 ppm oil-containing water sample is given as an example. Place 400 ml of water in a 500 ml reagent bottle and inject 8 µl of standard oil solution (50 g l^{-1}) centrally above the water
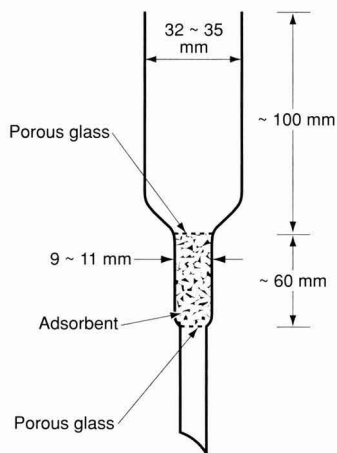
Fig. 1   Oil-trap funnel.

surface. Touch the syringe tip slightly on the inner wall of the bottle several times in order to remove the remaining liquid. Tighten the stopper and shake the bottle vigorously for 2 min. According to the measured results, the concentration did not change for at least 8 h and the solution was apparently clear.

Calibration

In a series of 10 ml Nessler tubes place 0, 2, 4, 6, 8 and 10 μl of standard oil solution (50 g l^{-1}), add 10 ml of CCl_4 to each tube and mix well. Transfer the solutions one by one into a 20 mm quartz cell and scan the infrared spectrum (3500–2500 cm^{-1}). Read the transmittance at the peak 2960 cm^{-1}, deduct the reagent blank and convert the result into absorbance. Plot the absorbance *versus* concentration in mg of oil per 10 ml of CCl_4. The resulting calibration graph was a straight line passing through the origin.

Analysis of Water Samples

Install the oil-trap funnel on a vacuum unit and pump the funnel until it is dry. Wash the funnel with small amounts of CCl_4 and soak for about 2 min, then pump it dry. Wash the funnel three times with distilled water.

Take a suitable volume of water sample (containing 0.1–1.0 mg of oil), and 5 g of NaCl and 2 ml of HCl (1 + 1) per 1000 ml of sample and mix well. Filter the solution by suction with a filtration rate of about 50–100 ml min^{-1}. Wash the sample bottle and funnel three times with small amounts of 5% NaCl solution. Aspirate continuously for 5–6 min to remove the remaining water in the funnel. Lay the sample bottle aside in order to recover any adsorbed oil if necessary.

Remove the funnel and discard the filtrate. Place a dry tube in the filtration flask to receive eluate, then reconnect the funnel. Wash the funnel with 10 ml of CCl_4 and soak for about 2 min. Suck the CCl_4 down into the tube, remove the tube, add CCl_4 to the 10 ml mark, add 3 g anhydrous Na_2SO_4 and shake to dry. Transfer the supernatant into a quartz cell and scan the infrared spectrum as above.

If necessary, recover the oil adsorbed on the sample bottle. Wash the bottle with another 10 ml of CCl_4, then measure the eluate.

Results and Discussion

Pre-treatment of Water Samples

Without pre-treatment, the results for the analyses of synthetic samples prepared from distilled water and tap water were low. Only after pre-treatment were the results satisfactory. The pre-treatment method was similar to extraction.[1-3] The experimental results are given in Table 1.

Effect of Granularity of Adsorbent

The funnel was the same as in Fig. 1 except that the granularity and amount of adsorbent were different. The amount of adsorbent was decreased to 5 g in order to make the effect of granularity on recovery more obvious. The results are given in Table 2.

It can be seen that the smaller the granularity, the higher was the recovery. As further reductions in the granule size would make the filtration rate too slow, 100–120 mesh was selected.

Effect of Amount Adsorbent

The funnel structure is shown in Fig. 1. Different amounts of 100–120 mesh adsorbent were tested. The filtration rate for each test was adjusted to the same range by controlling the negative pressure. The results are given in Table 3.

It can be seen that the recovery was enhanced on increasing the amount of adsorbent. However, when the amount of adsorbent added was > 6 g, further improvement in the recovery was not distinct. In order to obtain a faster filtration rate, 8 g of adsorbent was selected.

Effect of Filtration Rate

The filtration rate was related to several factors, such as funnel structure and amount and granularity of the adsorbent. We varied the filtration rate by adjusting the intensity of suction while other factors were kept fixed. The results are given in Table 4.

It can be seen that the recovery was not affected by the filtration rate between 10 and 130 ml min^{-1}. This result represents a very important advantage of the adsorption method, because only by filtering a large volume of water sample in a shorter time can the enrichment efficiency be substantially enhanced. This is demonstrated by the following data, where V_w and V_o are the volume of water sample and organic phase, respectively, and V_w/V_o is the enrichment efficiency:

V_w/ml	500	1000	5000
Extraction method:			
$\dfrac{V_w}{V_o}$ (V_o/ml)	10 (50)	13.3 (75)	–
Adsorption method:			
$\dfrac{V_w}{V_o}$ (V_o/ml)	50 (10)	100 (10)	500 (10)

V_o values for the extraction method were taken from the approximate value normally used for V_o of the adsorption method in our experiments. It can be seen that when the volume of water sample was increased, the enrichment efficiency was greatly enhanced in the adsorption method and is much superior than the extraction method.

Table 1 Effect of pre-treatment on recovery (400 ml water sample containing 1 ppm of oil). Conditions: filtration rate 13–18 min per 400 ml; 6 g of adsorbent (100–120 mesh)

Pre-treating agent		Recovery (%)	
NaCl/g	H_2SO_4/ml	Single results	Average
0	0	72.0, 69.4, 71.0	70.5
0	0	81.9, 79.6, 83.3	81.6*
1	0	88.5, 84.0, 82.0	84.4
2	0	92.0, 88.8, 89.5	90.1
2	1	89.6, 89.8	89.7
2	2	89.4, 90.6	90.0
3	0	90.1, 92.1, 90.9	91.0
4	2	90.6, 91.1, 90.1	90.6

* Water sample prepared from tap water.

Table 2 Effect of granularity of adsorbent on recovery (400 ml water sample containing 1 ppm of oil). Filtration rate: 14–23 min per 400 ml

	Recovery (%)	
Size (mesh)	Single results	Average
40–60	69.0, 70.0, 69.5	69.5
60–80	69.8, 78.4, 72.8	73.6
80–100	82.4, 84.0, 84.6	83.6
100–120	90.1, 88.6, 91.3	90.0
100–120*	90.1, 90.6	90.4

* The funnel had been used over 100 times.

Table 3 Effect of amount of adsorbent on recovery (400 ml water sample containing 1 ppm of oil)

Adsorbent		Filtration rate/min per 400 ml	Recovery (%)	
Amount/ g	Thickness/ cm		Single values	Average
4	2	18–23	82.2, 84.4, 81.0	82.5
6	3	16–22	93.1, 85.9, 91.5	90.2
8	4	18–23	89.8, 91.0, 89.2	90.0
10	5	22–25	95.0, 90.8, 89.6	91.8

Table 4 Effect of filtration rate on recovery

	Water sample 400 ml, oil 1 ppm		
Filtration rate—			
ml min^{-1}	40, 36	25, 23	10, 12
min per 400 ml	10, 11	16, 17	40, 33
Recovery (%)			
Single	91.1, 86.5	94.8, 86.6	89.2, 90.6
Average	88.8	90.2	89.9
	Water sample 1000 ml, oil 0.5 ppm		
Filtration rate—			
ml min^{-1}	113, 118	66, 63	25, 22
min per 400 ml	15, 17	30, 32	80, 92
Recovery (%)			
Single	92.0, 87.8	87.5, 89.8	92.0, 91.0
Average	89.9	88.9	91.5
	Water sample 5000 ml, oil 0.05 ppm		
Filtration rate—			
ml min^{-1}	8, 9	7, 8	4, 7
min per 400 ml	56	64	106
Recovery (%)			
Single	107.4	94.1	93.4
Average		98.2	

Table 5 Comparison between extraction and adsorption methods (500 ml synthetic water sample containing 0.50 mg of oil)

Method	Found/mg per 500 ml					Recovery (%)
	Single results				Average	
Extraction	0.475	0.490	0.482	0.493	0.480	96.1
Adsorption—						
Funnel	0.478	0.424	0.490	0.432	0.456	91.5
Bottle	~0.02	~0.02	~0.02	~0.02		~3

Comparison With Extraction Method

Conditions for comparison were selected by the requirements of the extraction method. For example, a smaller volume of water sample and a higher concentration of oil were used. The advantage of the adsorption method was not taken into consideration here.

Analysis of a synthetic water sample

A water sample of 400 ml containing 1.25 ppm of oil was prepared and pre-treated. For extraction,[1] the sample was prepared directly in a separating funnel, then extracted twice with CCl_4 (20 + 10 ml). The extracts were combined and analysed. For adsorption, the sample was prepared in a reagent bottle. After filtration, the funnel and water sample bottle were washed with 10 ml of CCl_4 separately and each of the eluates was analysed. The results are given in Table 5.

Table 6 Comparison between extraction and adsorption methods (actual water sample, 400 ml)

Method	Found/mg l^{-1}					Average
	Single values					
Extraction	7.63	8.56	7.48	8.22	6.80	7.44
	(1)*	(3)	(5)	(7)	(9)	
Adsorption—						
a (funnel)	7.88	8.80	8.10	8.00	8.14	8.18
	(2)*	(4)	(6)	(8)	(10)	
b (bottle)	0.34	0.26	0.22	0.28	0.25	0.29
a + b	8.22	9.06	8.32	8.28	8.39	8.47

* Numbers in parentheses are the sample numbers.

In the last row in Table 5, because the amounts of oil were too small and the relative errors were too large, the data are given only as rough information. It was calculated that the recovery using the extraction method was higher by about 2% or 5% than that using the adsorption method according to whether the loss of oil adsorbed on the sample bottle was taken into account or not, respectively. It can be seen that the results obtained by the two methods were almost coincident.

Analysis of a real water sample

Twelve 400 ml samples of effluent water from a skimming pond in an oil refinery were taken from 30 cm below the water surface. According to the order of taking the samples, they were numbered odd for extraction and even for adsorption. The samples were slightly turbid with floating oil and brown–black flocculates in it.

In the extraction method, the boundary of the two phases was not clear. After standing for 30 min, the organic phase was still like a network structure. When the amount of NaCl was increased to 15 g and the sample was extracted three times with CCl_4 (30 + 20 + 10 ml), it was somewhat improved. When the organic phase flowed down, there was finally always a layer of brown emulsifiable concentrates, which was not dissolved by CCl_4 and had to be discarded after the third extraction. Three parts of the extract were combined and diluted to 60 ml, and after dewatering it was measured.

In the adsorption method, the oil-trap funnel was washed twice with CCl_4 (10 + 10 ml). The two eluates were combined and diluted to 60 ml and, after dewatering, it was measured in a 20 mm cell.

The results are given in Table 6. The concentration measured by adsorption was on average 0.73 mg l^{-1} more than that measured by extraction, i.e., about 9%. This was probably related to the brown emulsifiable concentrates discarded in the extraction process.

The proposed adsorption method is clearly superior to the extraction method. Under our experimental and instrumental conditions, i.e., a 5000 ml water sample, noise signal $A = 0.004$, the detection limit of oil in water is 0.002 ppm. The recovery is >90%, the average error is 1.8% and the average deviation is 6.1%.

References

1 Editorial Board of National Bureau of Environmental Protection, China, *Analytical Methods for the Monitoring of Water and Wastewater*, China Environmental Science Press, Beijing, 3rd edn., 1989, pp. 368–375.
2 *Specifications of Oceanographic Survey: Water Monitoring and Analysis (HY 003.4-91)*, National Bureau of Oceanography Press, Beijing, 1991, pp. 153–163.

3 American Public Health Association, American Water Works Association and Water Pollution Control Federation, *Standard Methods for the Examination of Water and Wastewater*, APHA Washington, 17th edn., 1988, pp. 5.41–5.46.
4 Green, D. R., and Pap, D. L., Anal. Chem., 1987, **59**, 699.
5 Gruenfeld, M., *Environ Sci. Technol.*, 1973, 7, 636.
6 Ahmed, S. M., Beasley, M. D., Efromson, A. C., and Ronald, A. H., *Anal. Chem.*, 1974, **46**, 1858.
7 Ducreux, J., Boulet, R., Petroff, N., and Roussel, J. C., *Int. J. Environ. Anal. Chem.*, 1982, **12**, 195.
8 Scalen, O., and Wicander, A. B., *Br. Pat.*, 1 402 825, 1973.

Capillary Electrophoresis Detector Using a Light Emitting Diode and Optical Fibres

Paul A. G. Butler[a], Brian Mills[b] and Peter C. Hauser*[a]

[a] Department of Chemistry, University of Basel, Spitalstrasse 51, 4056 Basel, Switzerland
[b] Department of Chemistry, University of Auckland, Private Bag 92019, Auckland, New Zealand

The construction of a simple absorption monitor for capillary electrophoresis, based on a bright blue-green light emitting diode as radiation source, is described. Fibre optic coupling between light source, capillary and photodiode detectors was employed. It was found that, owing to the use of a high intensity light emitting diode, no optical focusing elements were required. The performance of the device was found to be comparable to that of a commercial detector, and the versatility is demonstrated with methods for the determination of transition metal ions by complexation with 4-(2-pyridylazo)resorcinol and the indirect detection of other inorganic cations and anions using organic dyes.

Keywords: Capillary electrophoresis; optical absorption detector; light emitting diode; fibre optic

The most frequently used form of detection with capillary electrophoresis (CE) is direct or indirect optical absorption in the UV or visible region of the spectrum. For commercially available instruments, often detectors from high-performance liquid chromatography (HPLC) have been adapted in order to be used with capillaries. These typically incorporate a deuterium or tungsten lamp, a monochromator and a photomultiplier tube. This then represents the most complicated item of a basically very simple system.

The use of light emitting diodes (LEDs) as nearly monochromatic light sources coupled to photodiodes may provide a more simple alternative, as has been the case for many other photometric instruments, detectors and sensors in analytical chemistry.[1–3] Reports on the use of LEDs in CE have been limited, however. Liu *et al.*[4] have described the design of a detector cell for special capillaries of rectangular cross-section incorporating an LED and photodiodes, but no results for electrophoresis have been given. Tong and Yeung[5] have presented a system in which a camera lens and a pair of ball lenses were used to focus the light from an LED through a capillary. A microscope lens was employed to concentrate the light into a reference beam and two photodiodes were used as signal and reference detectors. The two signals were processed numerically on a computer to form the ratio in order to remove noise. The indirect detection of several inorganic anions using permanganate as absorbing dye in the running buffer was demonstrated. A different approach to focusing the light from an LED through a capillary has been described by Bruno *et al.*[6] Gradient index (GRIN) lenses were butted directly to an LED and a photodiode and these were incorporated in an absorption cell incorporating a capillary fitted with apertures on either side. No details on its performance in CE were given either, however.

Macka *et al.*[7] have described the use of LEDs fitted into a commercial CE detector in place of the standard light source. They demonstrated the determination of Mg, Ca, Sr and Ba *via* the complexes with Arsenazo I using green and yellow LEDs. A comparison of noise, stray light and linearity with that of conventional light sources showed a favourable performance for LEDs. Boring and Dasgupta[8] have presented the design of a

purpose-made detector for CE. This cell is fitted with an aperture, can hold optical filters for wavelength selection and may be equipped with conventional light sources as well as LEDs. A comparative evaluation of performance in terms of baseline noise, stray light and linearity also showed that LEDs can be useful light sources for CE detectors.

The difficulty in the design of a photometric capillary detector is the requirement to pass light of adequate intensity through the core of the capillary with an internal diameter of 100 µm or less. Usually, an aperture of some kind needs to be provided in front of the capillary and perhaps on the backside also in order to restrict stray light from reaching the detector. The aperture, capillary and detector then have to be aligned carefully.

If the light from the source needs to be focused, in order to provide a sufficiently high intensity, a lens system has to be added to this assembly. To allow some flexibility for optimization of the alignment, some of these components ideally are mounted so that they can be moved with ease. The overall detector system then becomes fairly complex, and the resulting mechanical instability can be a major cause of signal fluctuations. In addition, it is very difficult to focus the light emanating from an LED in a wide angle into a spot of the dimensions required, and this is certainly not possible with a simple lens. However, in the course of our investigations it became apparent that some of the recently introduced bright LEDs provide sufficient intensity to allow detection on a capillary using a photodiode without requiring focusing.

Restriction of the light path to the core of the capillary was achieved by using optical fibres of a dimension close to the internal diameter of the capillary to carry the light to and from the capillary rather than using the conventional means of an aperture plate. The use of optical fibres to form an absorption cell around a capillary has been described previously, albeit not for LED-based systems.[9,10]

LEDs possess a long life and output that is stable compared with discharge lamps. The output does still vary slightly, however, especially with temperature. Temperature coefficients of output intensity of up to 1% per °C are found.[11,12] With the short pathlengths available with on-column capillary detection, the measured absorbances are very small, and even slight variations in the light level reaching the detector will decrease the signal-to-noise ratio for a detector, unless compensated for. This can be achieved by deriving a reference beam from the LED, in addition to the signal beam, and then processing the two resulting detector currents with a log-ratio amplifier.[1,13–15] Such a log-ratio amplifier not only allows for fluctuations of the source but also directly emulates Lambert–Beer's law and converts the signal into absorbance units (AU).

The device described here thus shows unprecedented simplicity for an optical detector for CE. This was achieved by the combination of LED light source and photodiode detectors, the absence of any focusing optics and the combination with simple signal processing electronics contained in a single integrated circuit. Its practical usefulness was demonstrated by its application to three groups of potential analytes. Firstly, the detection of transition metals as their complexes with 4-(2-pyr-

idylazo)resorcinol (PAR) was shown. Secondly, the indirect detection of alkali and alkaline earth metals ions and of inorganic anions was carried out by employing cationic or anionic indicator dyes, respectively, in the running buffer.

Experimental

Apparatus and Materials

A SpectraPhoresis 100 CE instrument (Thermo Separation Products, Fremont, CA, USA) using a Spectra 100 UV/VIS detector (Spectra-Physics, Mountainview, CA, USA) was used as a benchmark for performance comparison with the LED-based detector. A tungsten lamp, which had seen less than 100 h of service, was fitted to the unit. The detector reported here was tested using the SpectraPhoresis 100 power supply and injector modules, but was not specifically designed to be used only with this system. The high-intensity green LED (Type NSPG500S; λ_{max}: 525 nm, half-width: 30 nm) was obtained from Nichia Chemical Industries (Tokushima, Japan). Photodiodes with SMA connectors suitable for optical fibres (Stock No. 633-363) were obtained from RS Components (Corby, Northants, UK). Details of the log-ratio amplifier circuit can be found in earlier publications.[13–15] A MacLab 4s data acquisition system (ADI Instruments, Castle Hill, New South Wales, Australia), controlled by Chart software version 3.5.4/s (ADI Instruments) running on a 7200/90 Power Macintosh computer, was used for data acquisition. Data reduction utilized Peaks software version 1.3.4 (ADI Instruments), running on the same computer. The micropositioner stage possessing three degrees of movement (Stock No. A38, 528) used for the alignment of the LED with the optical fibres was obtained from Edmund Scientific (Barrington, NJ, USA). Optical fibres of 125 μm (FT-125-URT) and 200 μm (FT-200-URT), as well as all other optical fibre-related materials (polishing accessories, connectors, strippers, fibre scribe, *etc.*), were obtained through Thorlabs (Newton, NJ, USA). Uncoated silica capillaries of 360 μm outer diameter and different internal diameters were obtained from Polymicro Technologies (Phoenix, AZ, USA), while the coated CElect N capillary (100 μm, 363 μm od, neutral-coated, Part No. 8-52794) was sourced from Supelco (Bellefonte, PA, USA). Optical windows for detection were formed on the capillaries by stripping off the polyimide coating with hot concentrated sulfuric acid. All chemicals were of analytical-reagent grade (Fluka, Buchs, Switzerland), except for Chlorophenol Red (Merck, Darmstadt, Germany). Ultrapure water (18.2 MΩ cm) was used for all aqueous solutions (Millipore, Bedford, MA USA).

Procedures

The method for the determination of transition metal ions by complexation with PAR (Co^{2+}, Cu^{2+}, Fe^{2+} and Zn^{2+}) was adapted from ref. 16. *N*-[Tris(hydroxymethyl)methyl]-3-aminopropanesulfonic acid (TAPS) (10 mmol dm^{-3}, pH 8.40), containing PAR (0.1 mmol dm^{-3}) was used as the running buffer. The small concentration of PAR was included to help stabilize the more labile complexes (Cu–PAR and Zn–PAR), but did not significantly increase the background absorbance of the buffer. Analytes were pre-complexed before analysis in a solution containing PAR at 1.0 mmol dm^{-3} but otherwise being identical with the running buffer. It was found that the position of the Cu–PAR peak is highly pH-dependent, and resolution from the free PAR and Fe–PAR peaks requires strict control of the pH. A pH of 8.40 was used in this work, although the exact pH required varied slightly from column to column, depending on their history.

Indirect anion and cation determination was carried out by adaptation of methods described by Malá *et al.*[17] Tris(hydroxymethyl)methylamine (TRIS) (10 mmol dm^{-3}, pH 7.2), containing Chlorophenol Red (CPR) (0.25 mmol dm^{-3}) and adjusted with acetic acid was used as the running buffer for the anion determination. This buffer was also used as the matrix for sample injection. Although λ_{max} for CPR is at 572 nm, the absorbance at 525 nm is still 90% of this value. This permitted us to use the high-intensity 525 nm LED for this method. Pyronine Y (λ_{max} = 548 nm) was employed for the indirect determination of cations, instead of the Methyl Green used by Malá *et al.*. Pyronine Y has an acceptable spectral match with the LED, and a lower molecular mass than Methyl Green. This is important for the resolution of species analysed by indirect methods, as any discrepancy in mobility between the analyte and the absorbing molecule affects peak shape. The same buffer as above was used, but containing 0.15 mmol dm^{-3} Pyronine Y at a pH of 4.01. Again, the running buffer was used as the matrix for sample injection.

Before use, the fused-silica capillaries were flushed with 1 mol dm^{-3} sodium hydroxide for 5 min, by suction, followed by ultrapure water for 10 min, and finally, the appropriate background electrolyte for 10 min. They were then allowed to equilibrate overnight and the buffer was replaced. The coated capillary (used for the anion determination) was flushed with ultrapure water for 10 min, followed by the appropriate background electrolyte for 10 min. It was then also allowed to equilibrate overnight and the buffer replaced. After this equilibration procedure, several blank electrophoretic runs were performed to stabilize the baseline. To avoid buffer precipitation, the capillaries were normally filled with ultrapure water for storage. To maintain a stable baseline, it was found necessary to flush the capillary with background electrolyte between runs. Immediately prior to use, all solutions were de-gassed under vacuum, with ultrasonic agitation, then filtered through a 0.22 μm membrane filter.

Construction of the Detector

The overall scheme is given in Fig. 1. The light from the LED is picked up by two optical fibres, one of which leads to the detector cell itself and then onto the signal photodiode, the other directly to the reference photodiode. The photocurrents from the two photodiodes are processed by the log-ratio amplifier. This is a simple but powerful design based on a single integrated circuit and has been described previously.[13–15] The fibre ends leading onto the photodiodes were fitted with SMA connectors and all ends were polished by standard means. Both light collecting fibres are clamped closely together in a purpose-made holder opposite the LED which is mounted on a small three-axis micromanipulator. The LED used comes in a standard package and had its dome removed and was polished in order to allow close access to the active part. The micromanipulator allowed the light intensity coupled into the cell to be maximized by finding the region of highest intensity on the LED surface. For this purpose, the photodiodes were temporarily connected to operational amplifiers in the current follower configuration, which gives an output voltage directly proportional to the photocurrent. After alignment, the LED and
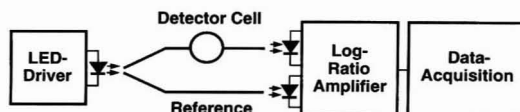
Fig. 1 Overall schematic diagram of the detector system.

fibre ends can be glued together permanently and the micro-manipulator removed.

A schematic diagram of the detection cell is given in Fig. 2. The design relies on the use of three capillaries with identical outer but different internal diameters. The light guides passing the radiation to and from the separation tube are inserted into two capillaries with bores appropriate for the fibres. Easy alignment that maintains concentricity is achieved by placing the three tubes into two identical grooves machined in the form of a cross on a PVC substrate. To our knowledge, this arrangement has not been described previously. The fibre used for guiding the radiation to the cell has an active diameter of 125 µm in order to match closely the internal diameter (100 µm) of the separation capillary used, while the fibre connecting the cell to the signal photodiode has an active diameter of 200 µm. Immersion oil, as used in microscopy, was placed on the intersection between the capillaries in order to minimize refraction and reflective losses.

The cell body consists of two blocks 50 mm square and 10 mm thick, held together, resulting in an overall size of 50 × 50 × 20 mm. The blocks consist of grey PVC, which has the advantages of being opaque, thereby eliminating exogenous and reducing indigenous scattered light, and of being slightly compliant, reducing the possibility of damage to the capillaries. The mating surfaces are machined as smooth as possible, and two perpendicular V-shaped grooves are machined across the face of one of the blocks. These grooves are made exactly the same depth, which is calculated to leave a standard, 360 µm capillary lying in these grooves with its top surface approximately 25 µm proud of the surface of the block. Under these conditions, any capillaries that are concentric in construction, and possess the same outside diameter, will have their bores lying co-planar when clamped by the second block, whose surface is left flat. The two blocks are held together with 12 lightly tightened screws placed in a pattern about the two grooves. This arrangement was chosen to allow the application of an even pressure to maximize rigidity and reduce the possibility of damage to the relatively brittle capillaries.

The ends of the optical fibres were stripped of their protective cladding before insertion into the capillaries (50 mm long). A clearance of 10 µm between fibre and capillary bore was found to be adequate. The fibres were glued into the capillaries with epoxy adhesive in order to provide a permanent and rigid assembly and the ends polished. Heat-shrink tubing was applied to reinforce the assembly where the capillaries with the fitted fibres exit the cell.
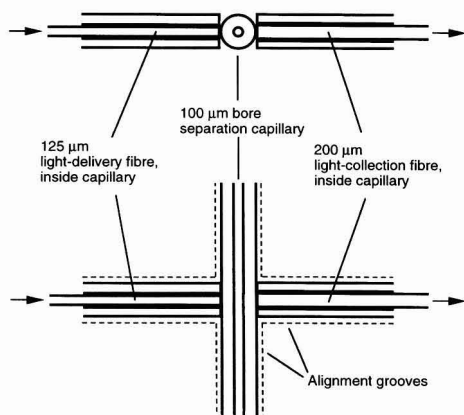
Results and Discussion

Detector Characteristics

Perhaps the most critical issue for a small-scale detector that does not utilize any focusing elements for concentrating the radiation is the available intensity. This has to be evaluated by measuring the current obtained on the detector photodiode and comparing this value with the minimum required by the electronic components for adequate processing. A photocurrent of typically 600 nA was measured (by connecting the photodiode to an operational amplifier in the current follower configuration) for a capillary filled with water. This is well removed from the dark current of the photodiode and the minimum required current for the log-ratio amplifier. Owing to the short optical pathlength for capillaries only small absorbance values are measured, and thus the photocurrent will never be much lower than this value even when absorbing species are present in the capillary. The intensity obtained is therefore adequate. The green (525 nm) LED employed has one of the highest intensities (luminous intensity: 5 Cd, luminous output: 2 mW) available for any LED. However, LEDs of similar intensity have recently become available for the blue and yellow to red range of the spectrum. An exception might be the wavelength of 565 nm at which conventional green LEDs emit.

A further important criterion of a detector for CE is its stability as, again, owing to the short optical pathlength, small absorbance differences need to be resolved. The baseline recorded for the detector, with de-gassed, high-purity water in the capillary, without application of a separation voltage is presented in Fig. 3A. Also given is the baseline obtained for the commercial detector employed in our laboratory (Fig. 3B) fitted with the same capillary as used for the test with the LED. The peak-to-peak noise level for the LED-based detector is approximately 30 µAU (absorbance units), while that of the commercial detector was approximately 90 µAU. The LED detector therefore shows a better performance in terms of baseline noise. This is believed to be related to the inherent relative stability of the light source. It should be noted, however, that it was necessary to assure a high rigidity of all optical fibre connections in order to eliminate any fluctuations in transmission efficiency due to movements.

By referring back to Fig. 2, it is evident that the design of the detector allows some light from the source fibre (considering that the light will emanate as a cone) to reach the collection fibre through the separation capillary but without passing through the core. The amount of this stray light was determined (by comparing the photocurrents for water and black ink in the capillary) as 3%. This value is perhaps surprisingly low. However, it has to be considered that not all of the actually present stray light is picked up by the collection fibre. Also, the intensity distribution through the different escape angles from the source fibre may not be even. In any case, stray light is not

Fig. 2 Cross-sectional schematic view from two angles of the detector cell. Dimensions are approximately to scale.

Labels in Fig. 2: 100 µm bore separation capillary; 125 µm light-delivery fibre, inside capillary; 200 µm light-collection fibre, inside capillary; Alignment grooves
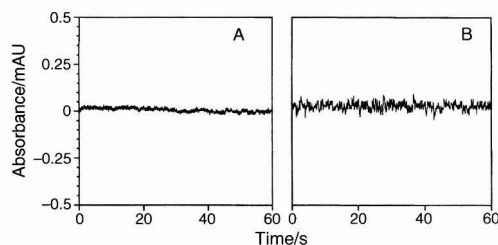
Fig. 3 Baseline noise recorded under static conditions: A, LED-based detector; B, commercial detector. 100 µm id plain fused-silica capillary filled with water.

a major concern when small absorbances are being measured (as long as its intensity remains constant). For the range of absorbances expected (up to about 10 mAU) a level of 3% stray light causes a deviation of 3% from the true absorbance value. However, in practice this is compensated for when carrying out a calibration with standard solutions.

Detector Performance

To demonstrate the performance of the detector under practical conditions, the separation of PAR complexes of Co, Cu, Fe and Zn ions was carried out for the LED-based detector as well as the conventional detector. The results are shown in Fig. 4A and B for the LED-based and commercial detectors, respectively. The same capillary was used for the experiments with both detectors. It can be seen that the results are very similar. The baseline noise under run conditions was found to be only slightly higher (about 50%) than the values reported above for both detectors. The average number of theoretical plates observed was almost identical for both detectors, *i.e.,* 180 800 for the LED-based detector and 179 600 for the commercial detector, indicating that the intrinsic resolution of the LED-based detector is at least as good as that of the commercial detector. Regan *et al.*[16] obtained an average of 74 800 theoretical plates, using a commercial detector and similar experimental conditions, but used a 50 μm id capillary. Where excessive current is not the limiting factor in the application of separation voltage, larger capillaries display greater detection sensitivity, both due to the greater pathlength and the larger amount of sample that can be loaded, and the resolution attainable is not dependent primarily on the capillary size.[18]

The peak heights relative to each other show some variation between the two detectors. This is presumed to be caused by the different spectral characteristics of the light sources. A linear calibration graph (r^2 = 0.9996) was obtained for Co standards as an example, for concentrations between 2.5×10^{-6} and 2.5×10^{-4} mol dm^{-3}. Seven concentrations were used in total and the peak area response (mAU $\times$ s) was employed. Although the response due to a given concentration of complexed ions is 10–15% greater for the commercial detector, equal detection limits of approximately 5×10^{-7} mol dm^{-3} were determined for both devices.

It is demonstrated with Fig. 5 that it is also possible to determine alkali and alkaline earth metal ions *via* indirect detection using the LED-based device. Note that the input from the indirect measurements has been inverted to provide 'positive' peaks in the electropherograms. The method was adapted from Malá *et al.*,[17] but the dye Pyronine Y was substituted for Methyl Green in order to match better the

emission wavelength of the LED used. As is evident from Fig. 5 the baseline is less stable than for the PAR work. However, this is not intrinsic to the detector but a feature of indirect detection as also reported by other workers.[5]

Also tested was a method for the indirect determination of inorganic anions. Tong and Yeung[5] reported the use of permanganate as the visualizing anionic species. Our attempts to use permanganate for anion detection were hampered by the precipitation of manganese dioxide on the walls of the column, despite the use of filtered, high-purity reagents and water. It was decided to follow the method used by Malá *et al.*,[17] using CPR, for visualizing anions. The corresponding electropherogram is shown in Fig. 6. The performance in terms of baseline stability and separation is similar to that obtained for the indirect cation detection. Note that it was found not to be possible to separate nitrate and sulfate under the experimental conditions used, but, as evidenced from Fig. 4A and B, this is not due to a lack of detector resolution, this being the equal of the commercial detector.

Conclusion

The simple detector based on a LED showed a performance equal to that of a conventional detector. By adapting different
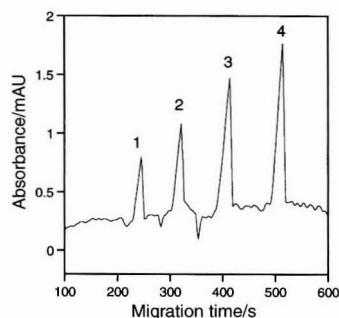
Fig. 5 Electropherogram of the indirect detection of cations using a plain fused-silica capillary of 100 μm id, 59 cm total length (40 cm to detector). Running buffer: 1 mmol dm^{-3} TRIS (pH 4.01) containing 0.15 mmol dm^{-3} Pyronine G. Peaks: 1 = K$^+$; 2 = Ca^{2+}; 3 = Na$^+$; 4 = Li$^+$. All 10^{-3} mol dm^{-3}, except for K$^+$, 2×10^{-3} mol dm^{-3}. Separation voltage: 15 kV. Electrokinetic injection of ions in running buffer: 10 kV, 2 s.
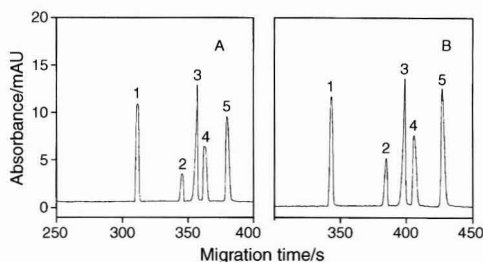
Fig. 4 Electropherograms of metal–PAR chelate separation using a plain fused-silica capillary of 100 μm id, 98 cm total length (70 cm to detector): A, LED-based detector; B, commercial detector. Running buffer: 10 mmol dm^{-3} TAPS (pH 8.40) containing 0.1 mmol dm^{-3} PAR. Peaks: 1 = Co^{2+}; 2 = free PAR; 3 = Cu^{2+}; 4 = Fe^{2+}; 5 = Zn^{2+}, all metals 2.5×10^{-5} mol dm^{-3}. Separation voltage: 30 kV. Electrokinetic injection of ions in running buffer with elevated PAR concentration: 10 kV, 8 s.
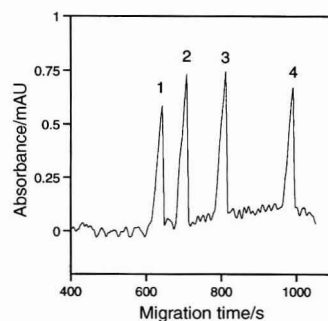
Fig. 6 Electropherogram of the indirect detection of anions using a neutral-coated fused-silica capillary of 100 μm id, 96 cm total length (68 cm to detector). Running buffer: 10 mmol dm^{-3} TRIS (pH 7.2), containing 0.25 mmol dm^{-3} CPR. Peaks: 1 = Cl$^-$; 2 = SO$_4{}^{2-}$; 3 = ClO$_3{}^-$; 4 = F$^-$. All 10^{-3} mmol dm^{-3}, except for SO$_4{}^{2-}$, 5×10^{-4} mmol dm^{-3}. Separation voltage: 15 kV. Electrokinetic injection of ions in running buffer: 10 kV, 4 s.

methods it was found possible to determine three classes of analytes by using direct as well as indirect detection. The use of visible light is a departure from the commonly used near-UV wavelengths but did not prove to be an obstacle. On the contrary, it has been stated that the use of visible light is of advantage as the likelihood of spectral interference from the sample matrix is reduced.[17] It was also found possible to adapt the methods so that they could all be performed with the same LED and a change of light source was not necessary. On the other hand, the present detector cell should also work well with light sources other than LEDs, if adequate intensity can be coupled into the optical fibre serving for radiation delivery. It could also be adapted to fluorescence detection. The utility lies in its simplicity, the integrity of its alignment, and its modular nature. In its present form, it could also be used for applications other than CE such as supercritical fluid chromatography, capillary liquid chromatography, or capillary flow injection analysis. Its simplicity arises from the fact that no costly and complex optical elements such as GRIN lenses, ball lenses or any other focusing elements were required. However, the separation capillaries used were all of 100 µm internal diameter. For certain applications it may be preferable to use smaller diameters. This will make efficient coupling of sufficient light without the use of a lens more challenging.

References

1 Dasgupta, P. K., Bellamy, H. S., Liu, H., Lopez, J. L., Loree, E. L., Morris, K., Petersen, K., and Mir, K. A., *Talanta*, 1993, **40**, 53.

2 Trojanowicz, M., Worsfold, P. J., and Clinch, J. R., *Trends Anal. Chem.*, 1988, **7**, 301.

3 Taib, M. N., and Narayanaswamy, R., *Analyst*, 1995, **120**, 1617.

4 Liu, H., Dasgupta, P. K., and Zheng, H. J., *Talanta*, 1993, **40**, 1331.

5 Tong, W., and Yeung, E. S., *J. Chromatogr. A*, 1995, **718**, 177.

6 Bruno A. E., Maystre, F., Krattiger, B., Nussbaum, P., and Gassmann, E., *Trends Anal. Chem.*, 1994, **13**, 190.

7 Macka, M., Andersson, P., and Haddad, P. R., *Electrophoresis*, 1996, **17**, 1898.

8 Boring, C. B., and Dasgupta, P. K., *Anal. Chim. Acta*, 1997, **342**, 123.

9 Foret, F., Deml, M., Kahle, V., and Bocek, P., *Electrophoresis*, 1986, **7**, 430.

10 Bruno, A. E., Gassmann, E., Pereclès, N., and Anton, K., *Anal. Chem.*, 1989, **61**, 876.

11 Gage, S., Hodapp, M., Evans, D., and Sorensen, H., *Hewlett-Packard Optoelectronics Applications Manual*, McGraw-Hill, New York, 1977.

12 Nunley, W., and Bechtel, J. S., *Infrared Optoelectronics*, Marcel Dekker, New York, 1987.

13 Hauser, P. C., and Litten, J. C., *Anal. Chim. Acta*, 1994, **294**, 49.

14 Hauser, P. C., Rupasinghe, T. W. T., and Cates, N. E., *Talanta*, 1995, **42**, 605.

15 Hauser, P. C., Rupasinghe, T. W. T., Lucas, C. C., and McClure, A., *Analyst*, 1995, **120**, 2635.

16 Regan, F. B., Meaney, M. P., and Lunte, S. M., *J. Chromatogr. B*, 1994, **657**, 409.

17 Malá, Z., Vespalec, R., and Bocek, P., *Electrophoresis*, 1994, **15**, 1526.

18 Yin, H., Keely-Templin, C., and McManigill, D., *J. Chromatogr. A*, 1996, **744**, 45.

On-line Derivatisation in Combined High-performance Liquid Chromatography–Gas Chromatography–Mass Spectrometry

Colin G. Chappell[†a], Colin S. Creaser[*a] and Martin J. Shepherd[b]

[a] *Department of Chemistry and Physics, Nottingham Trent University, Clifton Lane, Nottingham, UK NG11 8NS*
[b] *CSL Food Science Laboratory, Norwich Research Park, Colney, Norwich, UK NR4 7UQ*

Procedures are reported for the combined HPLC–GC and HPLC–GC–MS analysis of involatile analytes using on-line derivatisation. Derivatisation was carried out between the HPLC and the GC separation stages using two approaches; pre-mixing of the derivatisation reagent and the analytes in the HPLC effluent ahead of the GC pre-column, and independent reagent delivery after deposition of the desolvated analytes in the GC pre-column. The derivatisation of the stilbene hormones, quinoxaline-2-carboxylic acid, sulfamethazine and 2-naphthoic acid with silylation, methylation and acetylation reagents was investigated. Derivatisation efficiencies in the range 84–100% were achieved for the stilbene hormones and acidic compounds. The HPLC–derivatisation–GC procedure was demonstrated for the determination of the stilbene hormones in processed meats with detection limits between 0.17 and 0.47 µg kg^{-1} and RSDs in the range 2.3–4.9% for HPLC–GC with electron ionization quadrupole ion trap MS detection.

Keywords: High-performance liquid chromatography–gas chromatography–mass spectrometry; on-line derivatisation; veterinary drugs; stilbene hormones; involatile analytes

The derivatisation of analyte functional groups, to increase volatility and improve thermal stability, is a requirement for the analysis of many compounds by GC. In on-line HPLC–GC,[1–6] the analyte may therefore have to be derivatised prior to the GC separation step. Derivatisation can be performed off-line, before the sample is introduced into the HPLC systems, but for convenience an on-line approach is desirable. Since HPLC–GC has evolved as an advance towards high-resolution sample clean-up and assay automation, it is necessary to incorporate any time-consuming derivatisation step as part of an integrated system. On-line derivatisation in HPLC–GC has, however, received little attention. Raglione and Hartwick[7] described a system for the on-line derivatisation of triglycerides, to yield the free fatty acid methyl esters, using an acid catalyst fixed bed reactor positioned between the HPLC column and the GC system. Although the application demonstrated the on-line derivatisation principle, the reaction kinetics were too slow for the procedure to be a viable assay. Wessels *et al.*[8] reported the application of a loop-type interface for on-line derivatisation in the elucidation of the structures of drug degradation products and carboxylic acids by LC–GC–MS.[8]

A related area which has received greater attention is the automated extraction of analytes from aqueous samples, with on-line derivatisation coupled to GC. Ballesteros *et al.*[9] developed a system for the continuous extraction and simul-taneous derivatisation of phenols and *N*-methylcarbamates in aqueous samples using an on-line system, which incorporated a PTFE membrane phase separator. Goosens *et al.*[10] reported a system for determining propionic acid and 2,6-difluorobenzoic acid in aqueous samples, and also chlorinated anilines, using on-line reaction in a segmented stream, followed by extraction using a sandwich membrane phase separator on-line to a gas chromatograph.

Pentachlorophenol determination with derivatisation performed on the GC pre-column has been carried out using diazomethane and acetic anhydride,[11] and the use of trimethylanilinium hydroxide and similar reagents for methylation within the hot GC injector is a well established method for on-line derivatisation in GC.[12] Surfactants have been derivatised quantitatively to their butyl esters in a similar manner, following ion-pair formation with the tetrabutylammonium ion.[13] On-column derivatisation with silylation reagents for GC,[14–16] including flash derivatisation of the stilbene hormones with bis(trimethylsilyl)trifluoroacetamide (BSTFA)[17] has been investigated, and a pre-column reactor[18] and a pre-column trap[19] have also been used with silylation reagents in combination with GC.

Reaction GC, where a microreactor filled with catalysts is positioned either before or after the GC column, has been reported for the determination of carbon skeletons and for functional group analysis.[12,20,21] Pyrolysis–GC combined with on-line methylation has also been described.[22] Post-column derivatisation with GC–MS has been used with on-line catalysts to perform hydrogenation and oxidation type conversions,[23–25] and an olefin 'scrubber' has been used with multi-dimensional GC for hydrocarbon analysis.[26,27] Amphetamine and methamphetamine have been derivatised on-line to their trifluoroacetate derivatives in a GC–MS system by introduction of *N*-methylbis(trifluoroacetamide) (MBTFA) vapour into the GC injector and column inlet[28] and post-column vapour-phase derivatisation in GC–MS has been investigated by Ligon and Grade.[29]

In this paper, we report the development of on-line derivatisation for HPLC–GC and HPLC–GC–MS using procedures to bring about derivatisation within the GC pre-column. Reagents for silylation, methylation and acylation were investigated for the derivatisation of some representative veterinary drugs and other model compounds (Fig. 1). The methodology is demonstrated for the determination of the stilbene hormones[30] in processed meats, using HPLC–GC–MS, with on-line derivatisation to yield the trimethylsilyl ethers. Sub-µg kg^{-1} detection limits were easily achieved.

Experimental

Reagents and Chemicals

Methanol (HPLC grade) and pentane (Distol grade) were obtained from Fisons (Loughborough, Leicestershire, UK). Dichloromethane (pesticide residue analysis grade) was pur-

chased from BDH (Poole, Dorset, UK). Acetic anhydride (AA), BSTFA and sodium aluminosilicate 10 Å molecular sieve over which the dichloromethane and pentane were stored were purchased from Sigma (Poole, Dorset, UK). *N*-Methyl-*N*-(*tert*-butyldimethylsilyl)trifluoroacetamide (MTBSTFA), Methelute reagent [0.2 M trimethylanilinium hydroxide (TMAH) in methanol] and *N*-methyl-*N*-trimethylsilyltrifluoroacetamide (MSTFA) were obtained from Pierce and Warriner (UK) (Chester, UK). Triethylamine (TEA), HPLC-grade *N,N*-dimethylformamide (DMF) and dimethylformamide dimethyl acetal (DMFDMA) were purchased from Aldrich (Gillingham, Dorset, UK). Stock standard solutions of the stilbene hormones (Sigma) were prepared at 1 mg ml^{-1} in both dichloromethane and methanol. Stock solutions of quinoxaline-2-carboxylic acid (QCA) and 2-naphthoic acid (NA) (Aldrich) were prepared at 1 mg ml^{-1} in DMF. A stock standard solution of sulfamethazine (SM) was prepared in methanol at 1 mg ml^{-1}.

Instrumentation of On-line Derivatisation

The HPLC–GC instrumentation incorporating an on-column interface with a mass flow valve, as described previously,[4] was further modified for the on-line derivatisation experiments (Fig. 2). The HPLC column was replaced by a length of PTFE tubing in preliminary investigations. Sample injections were made to the HPLC injection valve, and the fraction containing the analyte(s) was diverted to the GC system *via* the on-column interface.

Two approaches were used for on-line derivatisation. In the first, analytes were diverted to the GC pre-column and deposited on the interior surface, with the solvent removed by fully concurrent evaporation. Reagent was then introduced to derivatise the analytes *in situ*. The second approach allowed the pre-mixing of the analyte(s) and reagent in the LC effluent stream, such that they both entered the inlet of the GC pre-column together. To determine the extent of reaction which took place on-line, the flame ionization detector (FID) responses for each analyte studied were compared with an equivalent amount

derivatised to completion off-line. The HPLC–GC system was interfaced to a quadrupole ion trap mass spectrometer (Finnigan, ITMS, Hemel Hempstead, Hertfordshire, UK) to confirm the identities of the derivatives.

Independent Introduction of Analyte and Reagent to GC Pre-column

A 2 × 3 port switching valve [Rheodyne (Cotati, CA, USA) Model 7030] was connected to the 10-port valve of the on-column interface, as shown in Fig. 3. Reagent was delivered *via* a syringe pump [Razel A-99, Semat Technical (UK) St. Albans, Hertfordshire, UK]. The valves were operated independently, such that the sample was first delivered to the gas chromatograph [Fig. 3(*a*)], the transfer line then was backflushed with carrier gas [Fig. 3(*b*)], and finally reagent was introduced into the gas chromatograph to derivatise the analyte [Fig. 3(*c*)]. Excess of reagent was backflushed from the transfer line by returning the valves to the arrangement shown in Fig. 3(*b*). The early vapour exit (EVE) was kept open during delivery of both sample and reagent to the GC pre-column to allow the venting of vapours. Following reagent delivery, the GC oven temperature was increased and the EVE (Fig. 2) closed at an appropriate temperature before loss of the derivatised analytes, to allow the quantitative trapping of the derivatives within the cryogenic cold trap. When transfer from the pre-column to the cold trap was complete, the mid-point split was closed, the EVE re-opened and the cryogenic trap turned off to allow the analysis to proceed on the analytical GC column (35 m × 0.25 mm id, 0.25 μm film thickness of RSL200), with detection by FID (280 °C) or MS. The GC injector port was maintained at 90 °C.

Introduction of Pre-mixed Analyte and Reagent to GC Pre-column

A syringe pump directly connected to the Valco (Houston, TX, USA) C10W valve was used for reagent delivery (Fig. 4). In one switching position [Fig. 4(*a*)], reagent from the syringe pump was mixed with the LC effluent stream *via* a T-piece upstream of the valve. In the alternative switching position [Fig. 4(*b*)], the transfer line was backflushed with carrier gas. Transfer of the derivatised analytes to the GC column was carried out as described above. Independent on/off control of the syringe
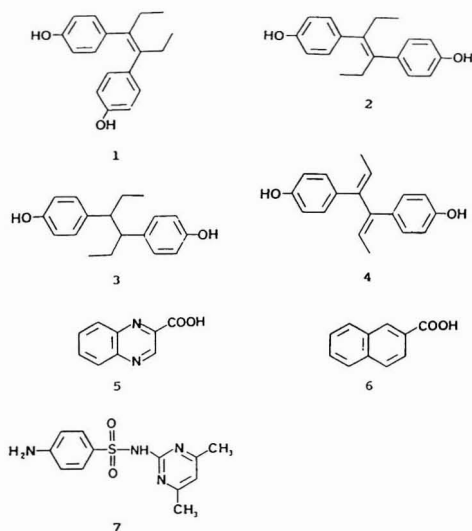
Fig. 1 Structures of the compounds studied: (1) *cis*-Diethylstilbestrol (*cis*-DES); (2) *trans*-diethylstilbestrol (*trans*-DES); (3) hexestrol (HES); (4) dienestrol (DIE); (5) quinoxaline-2-carboxylic acid (QCA); (6) 2-naphthoic acid (NA); (7) sulfamethazine (SM).
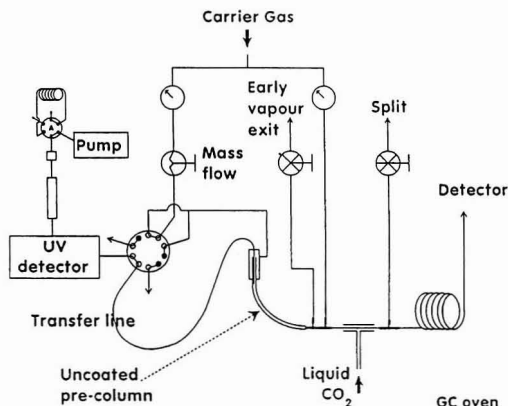
Fig. 2 Schematic illustration of the normal-phase HPLC–GC instrumentation showing the switching position for loading a fraction from the HPLC to the GC column.

pump enabled sample fractions to be sent to the gas chromatograph without derivatising reagent if necessary.

Silylation of the Stilbene Hormones

Silylation experiments were carried out using the independent introduction of sample and reagent. Experiments were performed on diethylstilbestrol using a 9 m × 0.53 mm id uncoated GC pre-column (SGE UK, Milton Keynes, UK) connected to a 2 m × 0.53 mm id coated section (1.5 μm film of DB5, J&W Scientific, Folsom, CA, USA) at the outlet end. The analytes in dichloromethane were injected using the HPLC injection valve and transferred to the GC pre-column using dichloromethane at 200 μl min^{-1}. The solvent was eliminated by fully concurrent evaporation. The GC temperature programme was 65 °C (held for 4 min) 20 °C min^{-1} ramp to 100 °C (held for 5 min), then at 20 °C min^{-1} to 240 °C (held for 9 min), and was started when the analytes were injected. Following delivery of the analytes to the GC system at 65 °C, the reagent mixture (22% v/v BSTFA–pentane or 22% v/v MSTFA–pentane) was introduced to the GC pre-column at a flow rate of 140 μl min^{-1} for 2.5 min, when the oven temperature reached 100 °C. The cryogenic cold trap was turned on at 160 °C, the EVE closed at 200 °C and the mid-point split closed after 1.5 min at 240 °C. The EVE was re-opened and the cold trap turned off after 2 min at 240 °C. Off-line silylation of standards was performed using neat BSTFA or MSTFA.[20]
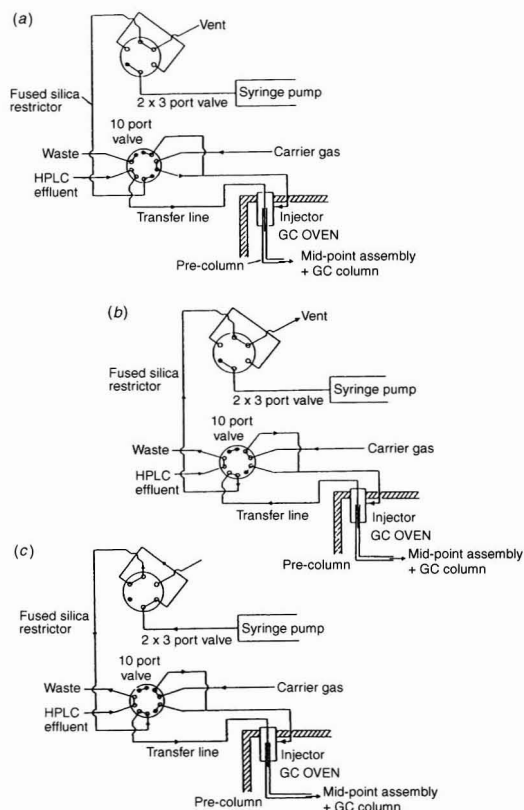
Silylation of Carboxylic Acids

Dilutions of the QCA and NA in DMF stock solutions were prepared in methanol. Injections were made to the pre-column and additions of reagent were carried out as described for the stilbene hormones. The GC column was programmed from 65 °C (held for 5 min) at 20 °C min^{-1} to 100 °C (held for 5 min), then at 20 °C min^{-1} to 190 °C (held for 9 min). The analytes were introduced at 65 °C and the reagent at 100 °C as described for the stilbenes. The cryogenic cold trap was turned on at 120 °C, the EVE closed at 150 °C and the mid-point split closed at 180 °C. The cold trap was turned off and the EVE re-opened at 190 °C. The pre-column was later replaced with a coated capillary (10 m × 0.53 mm id, 1.5 μm film thickness of DB5), MTBSTFA in pentane (20% v/v) used as reagent and pentane as the mobile phase. The GC column was programmed from 65 °C (held for 4 min) at 20 °C min^{-1} to 130 °C, then at 20 °C min^{-1} to 220 °C (held for 12 min). The reagent was introduced for up to 2.5 min at 140 μl min^{-1} at 130 °C. The cryogenic cold trap was turned on at the end of the 130 °C period, the EVE closed at 150 °C and the mid-point split closed after 4.5 min at 220 °C. The cold trap was turned off and the EVE re-opened after 5 min at 220 °C. Derivatisations *via* the HPLC injection valve route were also performed. Standards (up to 10 μg) were derivatised off-line as for the stilbenes.

Methylation of the Stilbene Hormones

Alkylation reactions were performed using pre-mixing of analyte and reagent before introduction into a coated pre-column. Hexestrol was selected for methylation, with TMAH as the methylation reagent. The analyte was injected into the HPLC system with pentane as mobile phase at a flow rate of 70–100 μl min^{-1}. The reagent (0.2 M TMAH in methanol) was diluted five-fold with methanol to give 40 mM TMAH, and was

Fig. 3 Schematic illustration of the on-line derivatisation system for the independent delivery of sample and reagent. (*a*) Loading of sample from HPLC to GC pre-column; (*b*) transfer line backflushed with carrier gas; (*c*) reagent delivery to GC pre-column.
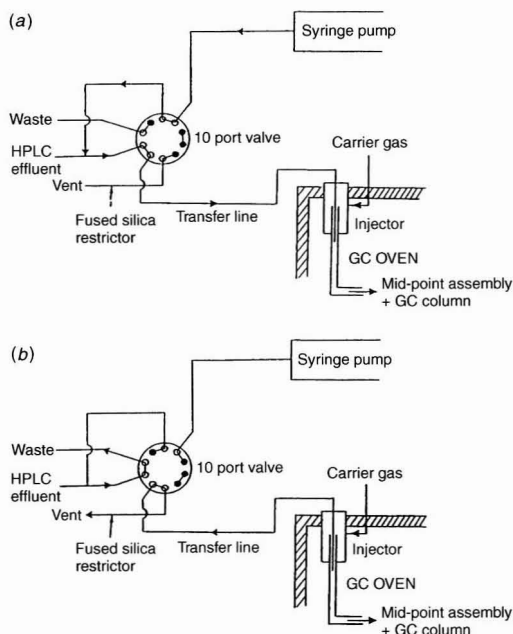
Fig. 4 Schematic illustration of the on-line derivatisation system for the pre-mixing of HPLC effluent with reagent, ahead of the GC pre-column. (*a*) Loading of sample and reagent to GC pre-column; (*b*) backflush of transfer line with carrier gas.

introduced by the syringe pump to the effluent stream at 50 µl min⁻¹. The GC column was programmed from 130 °C (held for 3 min) at 20 °C min⁻¹ to 220 °C (held for 15 min), then at 20 °C min⁻¹ to 300 °C. Introduction of analyte and reagent was effected at 130 °C for 3 min. The solvent was eliminated by fully concurrent evaporation. The cold trap was turned on at 190 °C, the EVE closed at 220 °C and the mid-point split closed after 6.5 min at 220 °C. The cold trap was turned off and the EVE re-opened after 7 min at 220 °C. Off-line standards were prepared as described previously.[6]

Methylation of Sulfamethazine

TMAH and DMFDMA were used for methylation. In both instances, the analyte was introduced into the HPLC injection valve after pre-mixing with reagent. The mobile phase was pentane at 70 µl min⁻¹. TMAH (0.2 M in methanol) and DMFDMA were both used undiluted. For the TMAH experiments, the GC column was programmed from 200 °C (held for 5 min) at 20 °C min⁻¹ to 300 °C (held for 10 min). The mid-point split was closed after 1.5 min at 300 °C, with the cold trap turned off and the EVE re-opened 30 s later. For the DMFDMA experiments, the same temperature programme was used except that the final temperature (300 °C) was held for 20 min. In both instances, analyte and reagent introduction into the GC system was effected at 200 °C, the cryogenic cold trap was turned on at the end of the 200 °C period and the EVE closed at 220 °C.

Methylation of Carboxylic Acids

Experiments with QCA and NA were performed using neat DMFDMA reagent (up to 10 µl), introduced with the analyte(s) into the HPLC injection valve. The mobile phase was pentane or methanol–pentane (10 + 90) at 100 µl min⁻¹, and was evaporated by fully concurrent evaporation. The GC column was programmed from 100 °C (held for 5 min) at 20 °C min⁻¹ to 185 °C (held for 16 min). The analyte and reagent were introduced into the GC system at 100 °C. The cryogenic cold trap was turned on at 130 °C, the EVE closed at 150 °C and the mid-point split closed after 7.5 min at 185 °C. The EVE was re-opened and the cold trap turned off after 8 min at 185 °C. Off-line standard derivatives were prepared in neat DMFDMA reagent at 65 °C.

Acylation Reaction Conditions

Acylation was investigated using diethylstilbestrol, with analyte and reagent introduction *via* the HPLC injection valve. Injections of the analyte were made with 10 µl of 2% triethylamine in acetic anhydride. The mobile phase was pentane at 100 µl min⁻¹ and was evaporated by fully concurrent evaporation. The GC column was programmed from 100 °C (held for 7 min) at 30 °C min⁻¹ to 240 °C (held for 24 min). Sample and reagent introduction was effected at 100 °C into a 10 m DB5-coated pre-column. The cryogenic cold trap was turned on at 220 °C, the EVE closed at 240 °C and the mid-point split closed after 13.5 min at 240 °C. The cold trap was turned off and the EVE re-opened after 14 min at 240 °C. Off-line standard derivatives were also prepared, using 2% triethylamine in acetic anhydride at 65 °C for 1 h.

HPLC–GC–MS With On-line Derivatisation of Stilbene Hormones in Processed Meats

Samples of garlic sausage (5 g) and Danish salami (5 g) were extracted using the initial stage of the Verbeke procedure.[6] The final extract was, however, re-constituted in 100 µl methanol–pentane (15 + 85), for HPLC–GC–MS analysis using a quadrupole ion trap mass spectrometer. The HPLC pump [LKB

(Stockholm, Sweden) Model 2150], injector (Negretti–Zambra 20 µl loop) and UV detector [Waters (Milford, MA, USA) Model 455] were used in conjunction with a 25 cm × 2.1 mm id 5 µm LiChrosorb Diol HPLC column (Hichrom, Reading, Berkshire, UK) which was eluted with methanol–pentane (15 + 85) mobile phase. Following injection of standards or extract (20 µl) into the HPLC system, two fractions (about 10.5–11.3 and 12.0–16.0 min) were diverted to the GC system *via* the on-column interface, and the solvent was eliminated by fully concurrent evaporation. The GC system was fitted with a 10 m coated pre-column as described earlier. The GC column programme, which was started on introduction of sample to the HPLC, was 100 °C (held for 22 min) at 20 °C min⁻¹ to 240 °C (held for 16 min), then at 20 °C min⁻¹ to 300 °C. Two minutes after the delivery of the second HPLC fraction is complete, reagent from the syringe pump (22% BSTFA in pentane) was diverted to the GC pre-column (oven at 100 °C) at 140 µl min⁻¹ for 2.8 min. The arrangement for reagent introduction was as illustrated in Fig. 3. Following the delivery of reagent, the cold trap was turned on at 180 °C, the EVE closed at 220 °C and the mid-point split closed after 7.5 min at 240 °C. The EVE was re-opened, the cold trap turned off and acquisition by the mass spectrometer started 30 s later. Data were acquired using either full scanning electron ionization (EI) over the range *m/z* 50–450, selected ion monitoring EI using the mass ranges *m/z* 205–220 and *m/z* 375–415 or multiple scan monitoring (MSM),[31] to scan the EI and methane chemical ionization (CI) spectra alternately.

Results and Discussion

Two approaches were investigated for on-line derivatisation following HPLC separation in combined HPLC–GC. The first involved analyte derivatisation by pre-mixing of the reagent with the HPLC effluent immediately prior to introduction into the GC pre-column, whilst the second employed independent delivery of the HPLC effluent into the GC pre-column followed by reagent addition after deposition of the analytes by evaporation of the mobile phase. An advantage of both of these procedures for on-line derivatisation between HPLC and GC is that only the part of the initial crude extract containing the analyte(s) needs to be exposed to the derivatising reagent, hence depletion of the reagent by matrix material and the formation of potentially interfering derivatised co-extractants are reduced. In addition, the elevated temperatures which may be required for derivatisation reactions to be carried out quickly enough for on-line use, can easily be achieved in the GC pre-column. Since HPLC separation of the derivatives from excess of reagent and associated by-products is not possible, there is the potential for interference in the GC system, especially if a non-specific detector such as an FID is used. The HPLC–GC interface was therefore configured to exclude much of the reagent from the analytical GC column. The reagents used for the on-line derivatisation experiments and the derivatisation efficiencies for the analytes studied using a variety of reagents are summarised in Table 1.

Silylation

On-line silylation experiments employed independent delivery of analyte and reagent (Fig. 3). The analytes were first introduced into the GC pre-column from the HPLC system *via* the switching valve and the solvent was removed by fully concurrent evaporation, leaving the analytes deposited on the inner surface of the pre-column. Derivatisation was achieved by independent delivery of the reagent from the syringe pump into the pre-column, allowing contact between analyte and reagent

at a temperature governed by the GC oven. Silylation experiments were carried out using BSTFA and MSTFA for the preparation of trimethylsilyl (TMS) derivatives, and MTBSTFA for the preparation of *tert*-butyldimethylsilyl (tBDMS) derivatives. The TMS ethers were readily produced for the phenolic compounds diethylstilbestrol (DES) and hexestrol (HES), but, MTBSTFA was found to be a more suitable reagent for the silylation of the acids NA and QCA because of the greater stability of the tBDMS esters.

DES was silylated on-line using BSTFA and MSTFA, with the reaction reaching completion in both cases. It was observed, however, that the relative proportions of *cis*- and *trans*-DES varied depending on whether the derivatisation was performed on- or off-line. In both cases, the amount of *cis*-DES increased owing to *trans* to *cis* conversion, a phenomenon which has been observed before during silylation,[32] but this conversion was more pronounced for the on-line process. This can be seen in Fig. 5 which shows the GC–FID traces obtained for 60 ng injections of DES, silylated off-line [Fig. 5(*a*)] and on-line [Fig. 5(*b*)]. This emphasises the importance of measuring both isomers when determining DES. A linear response was observed for the sum of the *cis* and *trans* isomers (correlation coefficient 0.998) for the on-line derivatisation of diethyl-stilbestrol over the range 10–100 ng, with reagent delivery *via* the syringe pump.

Initial investigations into the on-line silylation of the stilbene hormones were performed using an uncoated pre-column. However, it was found that losses of the derivatised analytes occurred through the EVE if the oven temperature was allowed to exceed 120 °C. Incorporation of a 2 m section of coated column at the end of the pre-column enabled the oven temperature to be increased to 200 °C, before closure of the EVE, without sample loss. A large excess of reagent was required to achieve complete derivatisation on-line [equivalent to 77 µl of neat BSTFA (209 µmol), for a maximum of 0.75 nmol of analyte]. Derivatisation efficiencies in excess of 90% could be achieved if the amount of reagent was reduced *ca.* 10-fold, but the approach described was required where it was necessary to ensure that absolutely no underivatised analyte remained on the pre-column. If the dichloromethane mobile phase was not freshly prepared each day, the UV baseline steadily increased and the GC response obtained for a DES standard derivatised on-line diminished. This was possibly caused by the accumulation of moisture in the solvent on standing, causing re-activation of the pre-column, leading to adsorptivity problems and hydrolysis of the trimethylsilyl group

of the derivative. If the solvent was replaced with dichloro-methane stored over a molecular sieve and freshly filtered, the expected response was restored.

On-line trimethylsilylation experiments with NA and QCA were performed initially under the same derivatisation conditions as those for DES, using an uncoated pre-column with a coated end section. It was found from these on-line derivatisation experiments that both QCA and NA showed a poor trimethylsilylation efficiency (*ca.* 10%) with BSTFA and MSTFA using dichloromethane as the mobile phase. Experiments performed with MTBSTFA reagent with the uncoated pre-column and dichloromethane mobile phase gave derivatisation efficiencies of up to 59% for NA.

To address the potential causes of these poor derivatisation efficiencies, the pre-column was replaced with a length of DB5 column (10 m × 0.53 mm id 1.5 µm film thickness) to reduce the potential for binding to active sites on the silica surface. MTBSTFA in pentane (20% v/v solution) was used as the silylating reagent to yield the tBDMS derivatives, with pentane as the mobile phase to eliminate the problems observed with dichloromethane. The silylation of the carboxylic acids was considerably improved by these changes to the method. Complete derivatisation was achieved for NA, and nearly complete derivatisation for QCA (96%), if a large excess of reagent was used (*ca.* 297 µmol of reagent to derivatise up to *ca.* 4.6 nmol of analyte). A temperature of 130 °C was required owing to the higher boiling point of MTBSTFA (168–170 °C) compared with BSTFA and MSTFA. which allowed successful derivatisation, but the closure of the early vapour exit at 150 °C, which was necessary to prevent losses of the derivative, prevented the total elimination of reagent matrix material from the analytical column. No derivatisation was observed if the concentration of the reagent delivered from the syringe pump was decreased to 8%, even on extended exposure. This reflected the observations made for the silylation of the stilbenes with BSTFA and MSTFA. Conversely, if the concentration was raised to about 40%, too much reagent-derived material reached the analytical GC column and so 20% MTBSTFA in pentane was chosen as a suitable concentration.

Table 1 Efficiencies for on-line derivatisation of model compounds in combined HPLC–GC–MS

Compound	Reagent*	Derivatisation efficiency (%)†	Derivatisation method‡
DES	BSTFA	100	ID
DES	MSTFA	100	ID
DES	AA/TEA	84	PM
HES	TMAH	100	PM
NA	BSTFA	10	ID
NA	MTBSTFA	100	ID
NA	DMFDMA	94	PM
QCA	BSTFA	< 2	ID
QCA	MTBSTFA	96	ID
SM	TMAH	—	PM
SM	DMFDMA	—	PM

* See Experimental section for identification. † On-line efficiency determined relative to the analyte response for off-line derivatisation taken to completion. ‡ ID = independent reagent delivery after deposition of the desolvated analytes in GC pre-column; PM = pre-mixing of analytes and reagent ahead of GC pre-column.
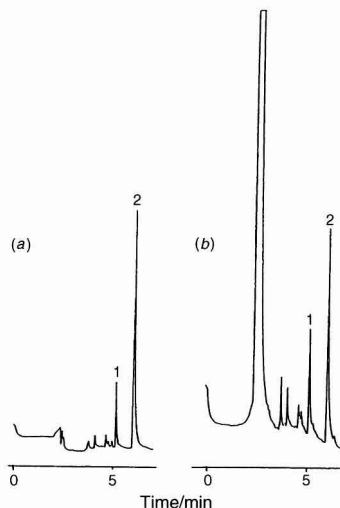
Fig. 5 GC–FID traces illustrating the trimethylsilyl derivatives of (1) *cis*- and (2) *trans*-diethylstilbestrol. (*a*) 60 ng of DES derivatised off-line; (*b*) 60 ng of DES derivatised on-line with 22% BSTFA in pentane from the syringe pump. FID attenuation, 32. GC column, 35 m × 0.25 mm id, 0.25 µm film thickness of RSL200. Separation performed at 240 °C.

Alkylation

Alkylation experiments were performed using methanolic TMAH and DMFDMA with pre-mixing of the HLPC effluent and reagent ahead of the GC pre-column (Fig. 4). HES, NA and SM were the analytes studied. Hexestrol was successfully methylated using TMAH, with the reaction going to completion. NA was methylated using DMFDMA, with efficient derivatisation achieved. SM was derivatised using both TMAH and DMFDMA.

Initial experiments on HES were performed using neat TMAH reagent (200 mM in methanol) delivered by the syringe pump, but this caused an accumulation of excessive reagent-derived material on the pre-column which was not vented *via* the EVE. Consequently, unacceptable interferences obscured the analytical separation. By diluting the reagent five-fold in methanol to give 40 mM TMAH, it was possible to achieve complete derivatisation, with an acceptable level of matrix background. As with silylation, a large excess of reagent was required to achieve efficient derivatisation (6 μmol for 0.75 nmol of HES). Although the selection of higher temperatures is desirable to increase the speed of reaction (200–280 °C typically for on-column methylation in GC), a compromise was necessary depending on the volatility of the derivative, since the EVE remained open during the derivatisation process. Reducing the on-line derivatisation temperature to 100 °C resulted in an excessive accumulation of reagent-derived matrix material.

Methylation experiments with SM were performed using both TMAH and DMFDMA, with the analyte and reagent being mixed immediately prior to introduction to the injection valve. Methylation would be expected to occur at the N^1- and N^4-positions with TMAH, but DMFDMA forms a dimethylaminomethylene derivative at the N^4-position.[12] These two derivatives were assigned to peaks with retention times of 4.84 and 6.33 min, respectively, under identical GC conditions.

Adsorption of SM within the system caused problems, since it was necessary to inject relatively large amounts (0.5–1.0 μg) in order to see any derivatised GC peak. Large excesses of TMAH and DMFDMA were required (about 3.8 and 157 μmol, respectively, for 3.6 nmol of SM). It was also necessary to use a high initial oven temperature (200 °C) to obtain a derivatised analyte peak, and this itself caused evaporation of solvent within the transfer line inside the GC injector, rather than in the pre-column. Consequently, deposits quickly accumulated within the transfer line. These cumulative problems prevented any satisfactory estimation of derivatisation efficiency. In contrast to SM, alkylation of 2-NA was readily achieved, with DMFDMA reagent giving a derivatisation efficiency of 94%.

Acylation

Acylation was investigated using DES as the analyte, and 2% triethylamine in acetic anhydride as the reagent (about 109 μmol for up to 0.74 nmol of analyte). The reagent and analyte were pre-mixed ahead of the GC pre-column. The retention times of acetylated *cis*- and *trans*-DES (7.19 and 8.40 min, respectively) were more than 2 min longer than for the respective silylated derivatives at the same oven temperature. A derivatisation efficiency of 84% was achieved on-line.

HPLC–GC–MS With On-line Dervatisation of Stilbene Hormones in Processed Meats

The effect of sample matrix on the derivatisation was investigated for the HPLC–GC analysis of processed meat extracts spiked with the stilbene hormones, using on-line silylation and quadrupole ion trap MS detection. HPLC separation of the underivatised stilbene hormones was carried out on a LiChrosorb Diol column with methanol–pentane (15 + 85) as mobile phase. Under these conditions, HES, DIE and *trans*-DES co-

eluted at a retention time of *ca.* 13.50 min ($k' = 3.5$), and *cis*-DES eluted at 10.75 min ($k' = 2.6$). Fig. 6 shows the separation achieved for extracts of garlic sausage and Danish salami with the stilbene-containing fractions transferred to the pre-column indicated. The chromatograms illustrate the degree of clean-up of the stilbene hormones and their separation from matrix components afforded by HPLC.

Standards and extracts were analysed by HPLC–GC–MS with on-line silylation, using either EI or multiple scan monitoring (MSM)[31] of alternate EI and positive ion CI mass spectra with methane as reagent gas. For the EI experiments, the full m/z 50–450 mass range or the selected mass ranges m/z 205–220 and 375–415 were scanned. In the MSM experiments, spectra were recorded over the mass range m/z 50–450. Fig. 7 shows the single ion chromatograms for the trimethylsilylated stilbenes obtained by MSM, following HPLC–on-line derivatisation–GC analysis of Danish salami spiked at 6 μg kg^{-1} with each of the stilbenes. The chromatograms obtained under EI conditions showed no interferences for any of the ions. The chromatograms obtained under CI conditions, however, showed an interference in the HES channel that broadened the HES peak, preventing accurate determination. DIE and *trans*-DES
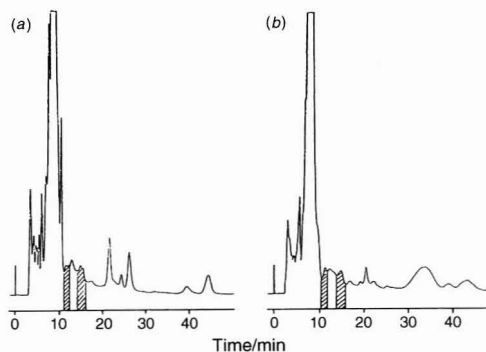
Fig. 6 HPLC traces with UV detection (254 nm, AUFS = 2.56) for the separations obtained for extracts from (*a*) garlic sausage and (*b*) Danish salami.
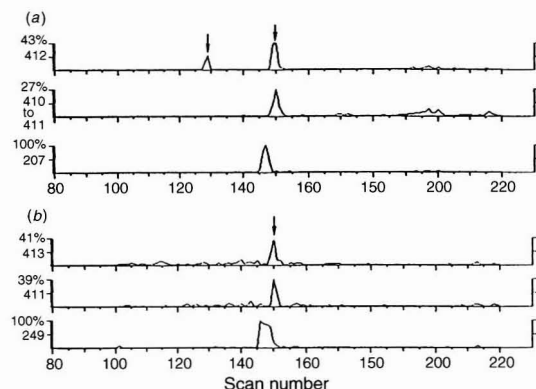
Fig. 7 Ion chromatograms for trimethylsilylated stilbenes in extract of Danish salami, spiked equivalent to 6 μg kg^{-1}, using multiple scan monitoring to alternately scan EI and positive ion CI spectra during the same run, following introduction from the HPLC–GC system, with on-line derivatisation. (*a*) EI ion chromatograms for *cis*- and *trans*-DES at m/z 412; DIE at m/z 410–411; HES at m/z 207. (*b*) CI ion chromatograms for *cis*- and *trans*-DES at m/z 413; DIE at m/z 411; HES at m/z 249.

peaks were free from interference, but *cis*-DES was of insufficient intensity at the spiked level to be observed at *m/z* 413. The detection limit for DES in extracts from the processed meats under EI conditions was 0.47 µg kg⁻¹ total DES to detect *cis*-DES and 0.17 µg kg⁻¹ total DES to detect *trans*-DES, based on the molecular ion of the TMS derivative at *m/z* 412. For HES (*m/z* 207) and DIE (*m/z* 410), the detection limits were 0.33 and 1.20 µg kg⁻¹, respectively. However, for DIE, the detection limit based on the summed ions at *m/z* 410 and 411 was 0.38 µg kg⁻¹. This improved detection limit was a reflection of the formation of the protonated [M + H]⁺ ion (*m/z* 411) by a matrix-CI process under the EI conditions of the quadrupole ion trap. The RSD for on-line silylation following replicate analyses (*n* = 5) of underivatised stilbene hormone standards (7.5 ng each) by HPLC–GC–MS with on-line silyliation was calculated to be 4.9, 4.0, 3.2 and 2.3% for *cis* and *trans*-DES, HES and DIE, respectively. The detection limit for DES under CI conditions was 4.90 µg kg⁻¹ using the [M + H − CH₄]⁺ ion of *cis*-DES (*m/z* 397) and 2.64 µg kg⁻¹ to detect the [M + H]⁺ ion of *trans*-DES (*m/z* 413). For DIE (*m/z* 411), the detection limit was 1.64 µg kg⁻¹ and for HES (*m/z* 249) the detection limit had to be estimated at 0.31 µg kg⁻¹ (S/N = 3 : 1) because of the interference observed at *m/z* 249. Overall, positive ion CI gave poorer detection limits for both the standards and for the processed meat extracts except for HES, where the detection limits for standards were slightly better under CI conditions.

Conclusion

The potential of on-line derivatisation in HPLC–GC has been demonstrated for the silylation, alkylation and acylation of phenolic compounds and the silylation and alkylation of carboxylic acids. Preliminary investigations for the on-line derivatisation of sulfamethazine were also carried out. The methodology was applied to the determination of stilbene hormones in processed meats using quadrupole ion trap MS detection, demonstrating the potential of the approach for trace analysis in a complex matrix.

Derivatisation was carried out successfully using both pre-mixing and independent delivery of reagent and analyte. The pre-mixing approach is limited by reagent–mobile phase compatibility, but this is not a problem using independent delivery of reagent and analyte. The latter approach may be prone to adsorption problems with certain basic or acidic compounds unless a fully coated pre-column is used. In addition, large excesses of reagent were needed to ensure complete derivatisation in order to eliminate carryover between analyses, and this highlighted the advantage of a selective detection system to cope with reagent-derived interferences. A further advantage of on-line analysis is that the temperatures required for rapid derivatisation are easily achieved in the GC oven.

References

1 Davies, I. L., Markides, K. E., Lee, M. L., Raynor, M. W., and Bartle, K. D., *J. High Resolut. Chromatogr.*, 1989, **12**, 193.

2 Cortes, H. J., in *Multidimensional Chromatography: Techniques and Applications*, ed. Cortes, H. J., Marcel Dekker, New York, 1990, p. 251.

3 Grob, K., *On-Line Coupled LC–GC*, Hüthig, Heidelberg, 1991.

4 Chappell, C. G., Creaser, C. S., and Shepherd, M. J., *J. Chromatogr*, 1992, **626**, 223.

5 Chappell, C. G., Creaser, C. S., Shepherd, M. J., and Stygall, J. W., *Biol. Mass Spectrom.*, 1992, **21**, 688.

6 Chappell, C. G., Creaser, C. S., and Shepherd, M. J., *J. High Resolut. Chromatogr. Chromatogr. Commun.*, 1993, **16**, 479.

7 Raglione, T. V., and Hartwick, R. A., *J. Chromatogr.*, 1988, **454**, 157.

8 Wessels, P., Ogorka, J., and Schwinger, G., *J. High Resolut. Chromatogr. Chromatogr. Commun.*, 1993, **16**, 708.

9 Ballesteros, E., Gallego, M., and Valcáre, L. M., *J. Chromatogr.*, 1993, **633**, 169.

10 Goosens, E. C., Broekman, M. H., Wolters, M. H., Strijker, R. E., de Jong, D., de Jong, G. J., and Brinkman, U. A. Th., *J. High Resolut. Chromatogr.*, 1992, **15**, 242.

11 Grob, K., and Neukom, H. P., *J. Chromatogr.*, 1984, **295**, 49.

12 *Handbook of Derivatives for Chromatography*, ed. Blau, K., and King, G. S., Heyden, London, 1979.

13 Field, J. A., Miller, D. J., Field, T. M., Hawthorne, S. B., and Giger, W., *Anal. Chem.*, 1992, **64**, 3161.

14 Horning, E. C., Horning, M. G., Ikekawa, N., Chambaz, E. M., Jaakonmaki, P. I., and Brooks, C. J. W., *J. Gas Chromatogr.*, 1967, **5**, 283.

15 Esposito, G. G., *Anal. Chem.*, 1968, **40**, 1902.

16 Rasmussen, K. E., *J. Chromatogr.*, 1976, **120**, 491.

17 Covey, T. R., Silvestre, D., Hoffman, M. K., and Henion, J. D., *Biol. Environ. Mass Spectrom.*, 1988, **15**, 45.

18 Weisse, P. M., and Hanson, R. H., *Anal. Chem.*, 1972, **44**, 2393.

19 McCugan, W. A., and Howsam, S. G., *J. Chromatogr.*, 1973, **82**, 370.

20 Beroza, M., and Inscoe M. N., in *Ancillary Techniques of Gas Chromatography*, ed. Ettre, L. S., and McFadden, W. H., Wiley, New York, 1969, p. 89.

21 Berezkin, V. G., *Chemical Methods in Gas Chromatography*, Elsevier, Amsterdam, 1983.

22 Ishida, Y., Isomura, S., Tsuge, S., Oktani, H., Sekino, T., Nakanishi, M., and Kimeto, T., *Analyst*, 1996, **121**, 853.

23 Teeter, R. M., Spencer, C. F., Green, J. W., and Smithson, L. H., *J. Am. Oil Chem. Soc.*, 1966, **43**, 82.

24 Mikaya, A. I., Zaikin, V. G., Ushakov, N. V., and Vdovin, V. M., *Mass Spectrom. Rev.*, 1990, **9**, 115.

25 Chaffee, A. L., and Liepa, L., *Anal. Chem.*, 1985, **57**, 2429.

26 Di Sanzo, F. P., Uden, P. C., and Siggia, S., *Anal. Chem.*, 1979, **51**, 1529.

27 Di Sanzo, F. P., Lane, J. L., and Yoder, R. E., *J. Chromatogr. Sci.*, 1988, **26**, 206.

28 Tsuchihashi, H., Nakajima, K., Nishikawa, M., Shiomi, K., and Takahashi, S., *J. Chromatogr.*, 1989, **467**, 227.

29 Ligon, W. V., Jr., and Grade, H., *Anal. Chem.*, 1991, **63**, 255.

30 Shepherd, M. J., in *Food Contaminants: Sources and Surveillance*, ed. Creaser, C. S., and Purchase, R., Royal Society of Chemistry, Cambridge, 1991, pp. 109–176.

31 Creaser, C. S., Mitchell, D. S., O'Neill, K. E., and Trier, K. T., *Rapid Commun. Mass Spectrom.*, 1990, **4**, 217.

32 Derks, H. J. G., Freudenthal, J., Litjens, J. L. M., Klaassen, R., Gramberg, L. G., and Borrias van Tongeren, V., *Biomed. Mass Spectrom.*, 1983, **10**, 209.

Determination of Dimetridazole in Poultry Tissues and Eggs Using Liquid Chromatography–Thermospray Mass Spectrometry

Andrew Cannavan and D. Glenn Kennedy*

Veterinary Sciences Division, Department of Agriculture for Northern Ireland, Stormont, Belfast, UK BT4 3SD. E-mail: kennedyg@dani.gov.uk

A method is presented for the determination of the nitroimidazole drug dimetridazole (DMZ) in poultry tissues and eggs by liquid chromatography (LC)–thermospray mass spectrometry (MS). Deuteriated DMZ was employed as an internal standard. Samples were extracted with dichloromethane (muscle) or toluene (liver, egg) and applied to silica gel cartridges. Dimetridazole was eluted with acetone and the eluate evaporated to dryness at 40 °C under nitrogen. The residue was redissolved in methanol–water (1 + 1, v/v) and washed with hexane before LC–MS analysis. Quantification was by the ratios of the positive [M + H]+ ions at m/z 142 and 145 for DMZ and the internal standard, respectively. Internal standard corrected recoveries were between 93 and 102% with RSDs between 1.2 and 7.7% for liver spiked at 5, 10 and 20 ng g^{-1} and muscle and eggs spiked at 5 ng g^{-1}. Absolute recoveries were approximately 80%. The method is suitable for statutory residue testing and was used to measure DMZ residues in eggs from chickens fed a diet containing DMZ at 10 mg kg^{-1}.

Keywords: Dimetridazole; nitroimidazoles; liquid chromatography–mass spectrometry; residues

Dimetridazole (DMZ, 1,2-dimethyl-5-nitroimidazole) is a nitroimidazole drug used in veterinary medicine to control infection of turkey flocks with the protozoal flagellate *Histomonas meleagridis*, which causes histomoniasis (or 'blackhead'), a disease which has been responsible for large losses in the turkey industry. It is also effective against coccidiosis in poultry, and has been used in swine feed for the prevention and treatment of swine dysentery and trichonomiasis.

DMZ has been reported to be mutagenic and carcinogenic.[1] In the European Union (EU), Commission Regulation 1798/95[2] placed DMZ in Annex IV of Council Regulation (EC) 2377/90.[3] Therefore, marketing authorisations were withdrawn on July 31, 1996, for veterinary medicines containing DMZ for use in food producing animals other than game birds. Any residues found in broiler chickens are therefore in violation of the regulations. However, there is currently a DMZ product available for use in turkey feed under the Feed Additives Directive 70/524 EEC.[4] DMZ residues may therefore occur in turkey tissues, where the previously approved maximum residue level (MRL) of 10 ng g^{-1} still apparently applies.[5] DMZ residues may also occur in the tissues of broiler/layer hens or in eggs as a result of accidental feed contamination or improper use of the drug.[6] Under similar circumstances, residues of the ionophore lasalocid in eggs due to carry-over from medicated to non-medicated feed during manufacture have been reported.[7] Sensitive and reproducible methods are therefore required by the EU[8] to test for DMZ residues in poultry tissues and eggs.

Various analytical techniques have been used for the determination of DMZ and/or its metabolites in tissues and eggs. Methods published include high-performance liquid chromatography (HPLC) with UV or diode-array detection,[9–12] HPLC with electrochemical detection[13] and gas chromatography with electron-capture detection.[14] Sample clean-up may be by multiple liquid–liquid extraction or by solid-phase extraction using silica or octadecyl (C$_{18}$) bonded phases. A gas chromatography–mass spectrometry method for DMZ and ipronidazole in swine feed has been described.[15] Mass spectrometry is the preferred technique for confirmatory residue analyses[16] because of the specificity provided by mass-related data. It has been shown[17,18] that liquid chromatography–mass spectrometry (LC–MS) can provide quantitative data for residue analysis using relatively simple extraction and clean-up steps.

This paper describes a method for the determination of DMZ in poultry meat and liver and in eggs by LC–MS after solvent extraction and solid phase clean-up on a silica cartridge. The limit of determination of the method, that is, the lowest level at which it has been validated, is 5 ng g^{-1}, or half the MRL, in accordance with EC criteria for compounds with an established MRL.[19] The limit of detection, based on a signal-to-noise ratio of 3 : 1, is < 1 ng g^{-1}. The method was used to measure DMZ levels in eggs from chickens fed a diet formulated to approximate to 10% contamination of DMZ-free meal with DMZ medicated meal, and to test for DMZ residues in tissues from these birds slaughtered 1 d after withdrawal.

Experimental

Materials

All solvents were of HPLC-grade and other chemicals were of analytical-reagent grade. DMZ was obtained from Sigma (Poole, Dorset, UK). The internal standard, deuteriated DMZ [D$_3$-DMZ, 1,2-dimethyl-(1-methyl-D$_3$)-5-nitroimidazole] was obtained from RIVM (Bilthoven, The Netherlands). Stock standard solutions of DMZ (1.0 mg ml^{-1}) and D$_3$-DMZ (100 µg ml^{-1}) were prepared in methanol and were stable for at least 3 months when stored at 4 °C in amber-coloured vials. Dilute standard solutions (10 and 1 µg ml^{-1}) were prepared by dilution of the stock standards with methanol and were stable for at least 1 month when stored at 4 °C in amber-coloured vials. A working standard solution (1 µg ml^{-1}) containing both DMZ and D$_3$-DMZ was prepared monthly by dilution of the 10 µg ml^{-1} standards in methanol–water (1 + 1, v/v) and was stored as above. The LC mobile phase was methanol-water (1 + 1, v/v) containing ammonium acetate (0.05 mol l^{-1}).

Equipment

The HPLC system consisted of a Hewlett-Packard (Stockport, Cheshire, UK) Series 1050 pump and autosampler and a Partisil 5 ODS 3 (250 × 4 mm id) column (Whatman, Clifton, NJ, USA). The mass spectrometer was a Hewlett-Packard 5989A MS Engine with a thermospray LC–MS interface and MS ChemStation. The instrument was tuned daily using the system

software and the HP poly(propylene glycol) tuning solution according to the manufacturer's instructions. The instrument was operated in positive-ion mode with filament-initiated chemical ionisation. The vaporiser probe stem temperature was maintained at 95% of the take-off temperature. The ion source and quadrupole were set to 250 and 100 °C, respectively. The electron multiplier voltage was set to 2008 V and the high-energy dynode was set to 8000 V. Scan mode was employed to obtain spectra over the range m/z 50–350 350 for DMZ and the internal standard. For sample analysis, the instrument was operated in selected-ion monitoring (SIM) mode with a dwell time of 500 ms and with low mass resolution enabled. Peak area data were obtained for the ions at m/z 142 (DMZ) and 145 (internal standard). Bakerbond Silica disposable extraction columns (3 ml, J. T. Baker, Phillipsburg, NJ, USA) were washed immediately before use with toluene (5 ml) and were not allowed to dry out before application of the sample. The columns were used in conjunction with a Vac-Elut vacuum manifold fitted with stainless steel Luer stop-cocks (Varian, Harbour City, CA, USA). Glass centrifuge tubes (110×25 and 100×12 mm) to be used in the extraction and clean-up were siliconized using Surfasil siliconizing fluid (Pierce, Rockford, IL, USA).

Incurred Eggs

Feed containing approximately 10 mg kg^{-1} DMZ was prepared by mixing commercial turkey finisher pellets containing 100 mg kg^{-1} DMZ with a DMZ-free feed (1 + 9, m/m). To facilitate mixing, the pellets were milled to a similar consistency as the DMZ-free meal. Six layer hens, approximately 18 weeks of age, were individually housed in wire cages. Each morning for 7 d each bird received approximately 120 g of the feed described above. The birds had free access to fresh water. Eggs were collected once a day, homogenized using a domestic food blender and stored at −20 °C. On day 8 the birds were killed by asphyxiation with carbon dioxide and samples of breast muscle and liver were minced using a food blender and stored at −20 °C pending analysis.

Sample Extraction

Aliquots of minced liver or muscle or egg homogenate (4 g) were weighed into 110×25 mm id siliconized centrifuge tubes. Internal standard was added (10 µg ml^{-1}, 20 µl) and fortified samples were prepared by adding an appropriate amount of DMZ standard solution. The samples were allowed to stand for 15 min before extraction.

Liver

Toluene (12 ml) was added and the samples were homogenized for 1 min using a Silverson homogenizer. The tubes were centrifuged (2000 rev min^{-1}, 4 °C, 10 min) and the supernatants decanted into clean siliconized tubes. A further aliquot of toluene (10 ml) was added to the tissue pellet in each tube, the tubes were capped, shaken for 1 min, centrifuged and the supernatants combined with the initial extracts.

Eggs

Egg samples were extracted as described for liver samples except that the initial extraction was performed by gently shaking the egg homogenate with toluene rather than using a homogenizer.

Muscle

Dichloromethane (12 ml) was added and the samples were homogenized for 1 min as for liver samples. The tubes were

centrifuged (600 *g*, 4 °C, 10 min). The tissue pellets were displaced with a spatula and the lower (dichloromethane) layers were carefully transferred into clean siliconized tubes. Each tissue pellet was re-extracted by shaking with a further aliquot (10 ml) of dichloromethane, the tubes centrifuged and the dichloromethane layers combined with the initial extracts.

Clean-up

The toluene or dichloromethane extracts were applied to silica columns prepared as described above. The columns were washed with dichloromethane (5 ml, for toluene extracts) or toluene (5 ml, for dichloromethane extracts) then hexane (5 ml) and allowed to dry under vacuum for 10 min. DMZ was eluted into siliconized 100×12 mm tubes with acetone (2 ml). The eluates were evaporated to dryness at 40 °C under nitrogen and the residues vortex-mixed with methanol (100 µl) to facilitate dissolution. Water (100 µl) was added and the tubes were again vortex-mixed. Hexane (1 ml) was added and the tubes were capped and shaken for 40 s to partition any fats precipitated on addition of the water. The tubes were centrifuged (600 *g*, 4 °C, 5 min) and the hexane layers discarded. The extracts were then transferred into microvials for analysis.

LC–MS Analysis

Mobile phase was pumped through the column at a flow rate of 1 ml min^{-1} for 10 min to equilibrate the system prior to the first injection. Aliquots (25 µl) of the mixed DMZ–D$_3$-DMZ working standard solution were injected until reproducible peak areas were obtained. Aliquots of sample extracts (25 µl) were then injected, with a standard injection after every four samples. Peak areas for the ions at m/z 142 and 145 were recorded. Results were calculated using the ratios of m/z 142/145.

Results and Discussion

The structure and positive-ion thermospray mass spectrum of DMZ, run using the methanol–ammonium acetate mobile phase described above, are shown in Fig. 1. Typically, for positive-ion LC-MS, the main peak is the molecular ion $[M + H]^+$ at m/z 142 and there are no significant fragment ions. For D$_3$-DMZ, the spectrum (not shown) is similar, with the peak corresponding to the molecular ion shifted to m/z 145. A secondary ion is present at m/z 174 (or 177 in D$_3$-DMZ), at approximately 10% of the
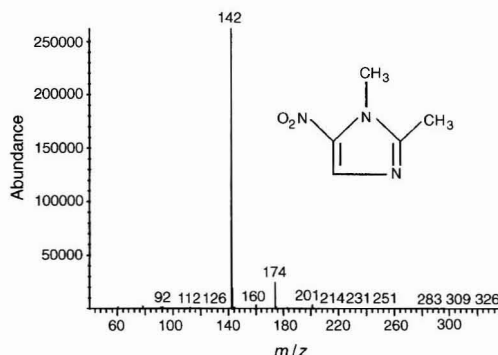
Fig. 1 Chemical structure and filament-assisted positive-ion LC–thermospray mass spectrum of DMZ.

abundance of the base peak. This probably corresponds to a methanol adduct. At low levels in SIM mode, the ion at m/z 174 was not sufficiently abundant to be used as a second confirmatory ion.

Initially, a mobile phase containing acetonitrile rather than methanol was used. This also gave the $[M + H]^+$ ion, but with a secondary ion at m/z 183, corresponding to an acetonitrile adduct, at approximately 70% of the abundance of the base peak. When run in SIM mode, however, the acetonitrile-containing mobile phase produced a very high background for the molecular ion (m/z 142), so only the acetonitrile adduct could usefully be monitored. The method was therefore optimized using the methanol-containing mobile phase. However, if required, further confirmation of the presence of DMZ in a sample could be provided by re-analysing that sample using the acetonitrile-containing mobile phase and monitoring the ion at m/z 183.

Fig. 2 shows SIM chromatograms at m/z 142 and 145 for a DMZ standard, a negative egg extract and an extract of an incurred egg sample containing 16.1 ng g^{-1} DMZ. At the retention time of DMZ the chromatograms are free from interfering peaks. Thermospray mass spectrometry is very compound-specific. As a consequence, it has been our experience that interfering peaks are comparatively rare. The absence of any interference at the retention time of DMZ shown in Fig. 2 confirms this view, and demonstrates the specificity of this technique. Chromatograms for muscle and liver (not shown) were similar.

The linearity of the instrument was assessed by analysing a series of standard solutions of DMZ, in the absence of internal standard, at concentrations ranging from 0 to 4 µg ml^{-1} (equivalent to 0–200 ng g^{-1} in tissue and egg; Fig. 3). Linear regression analysis of the data gave a linearity coefficient of 0.999, the curve being described by the equation $y = 3.2 \times 10^6 x + 7.5 \times 10^4$ (y = peak area; x = concentration in µg ml^{-1}).

Dichloromethane and toluene were found to be equally efficient as extractants for DMZ, giving approximately 80% absolute recovery for the method. Dichloromethane gave a cleaner initial extract for chicken muscle. When centrifuged, the muscle tissue formed a clean pellet which could be displaced with a spatula, allowing the lower dichloromethane layer to be poured off. For liver, toluene gave a cleaner homogenate, leaving the homogenizer head free from tissue debris. On centrifugation, the liver tissue formed a pellet at the bottom of the tube, allowing the toluene layer to be decanted. Egg samples were homogenized prior to extraction, then extracted by shaking gently with toluene, thus avoiding emulsion formation. Toluene is also more suitable for egg samples because it does not extract the yolk pigments to the same extent as does dichloromethane, giving a cleaner final extract.

A silica gel clean-up, as used by Ramos *et al.*,[11] was chosen because the extracts could be applied directly to silica cartridges without any evaporation/concentration step. This minimised the loss of DMZ which was found to occur at evaporation stages and also improved the turn-round time of the method. Acetone was used as the eluent so that the final evaporation step could be carried out quickly at 40 °C under nitrogen, again minimizing loss of DMZ. It was also found that siliconizing the glassware used in the assay increased absolute recoveries from approximately 70 to > 80%. The use of a deuterated internal standard with quantification by ion ratios gives corrected recoveries of approximately 100%.

The method was validated for chicken liver, muscle and egg samples. Inter- and intra-assay reproducibility were assessed by extracting and analysing five replicates of blank chicken liver, spiked at 5 ng g^{-1} (half the MRL), on three separate occasions. The results are presented in Table 1. Intra-assay validation was also carried out on five replicates of liver spiked at 10 and 20 ng g^{-1} (the MRL and twice the MRL) and on muscle and egg spiked at 5 ng g^{-1}. The results are presented in Table 2.

Measurable DMZ residues were found in eggs taken 1 d after commencement of the DMZ diet and in all eggs taken thereafter. The mean concentration of DMZ in eggs taken after 7 d was 21.6 ng g^{-1}. This is in agreement with the results of Posyniak *et al.*,[6] who found residues in the eggs of birds on the second day of administration of oral doses (50 mg kg^{-1}) of DMZ and thereafter until several days after the final administration of the drug. This represents a potential pathway for DMZ to enter the human food chain at levels greater than the MRL set for turkey tissues. Further studies are in progress to characterise DMZ carry-over into eggs. No residues of DMZ were found in muscle
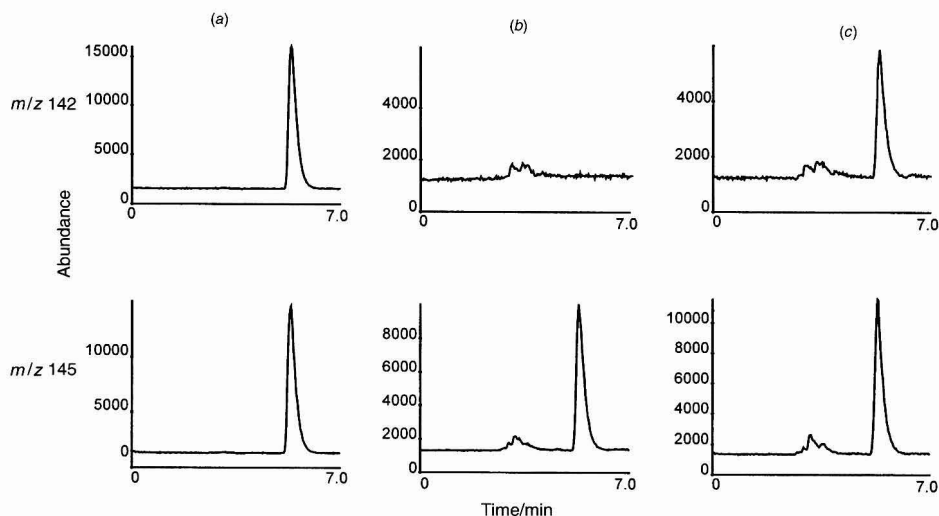
Fig. 2 SIM chromatograms of (*a*) a DMZ standard (equivalent to 50 ng g^{-1}), (*b*) a known negative egg extract and (*c*) an incurred egg extract containing 16.1 ng g^{-1} DMZ. Upper panel (m/z 142) is the $[M + H]^+$ ion for DMZ and the lower panel (m/z 145) the $[M + H]^+$ ion for D$_3$-DMZ.

or liver samples from the birds that were slaughtered 1 d after withdrawal from the DMZ diet. This is in keeping with the known pharmacokinetics of the drug.[19]
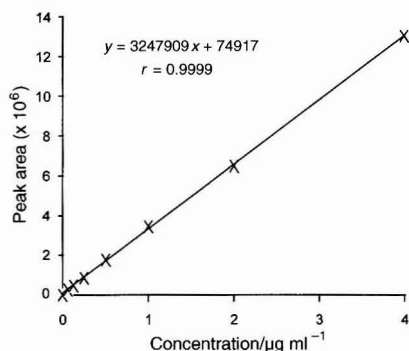
Fig. 3   Linearity of LC–MS for DMZ. Standards are equivalent to 0–200 ng g^{-1} in tissues.

Table 1 Inter- and intra-assay reproducibility and recovery for dimetridazole in chicken liver spiked at 5 ng g^{-1}

Sample	Parameter	Day 1	Day 2	Day 3	Overall
Liver	Mean/ng g^{-1}	4.8	4.7	5.1	4.8
	s/ng g^{-1}	0.210	0.361	0.090	0.297
	RSD (%)	4.4	7.7	1.8	6.1
	Mean recovery (%)	95.7	93.1	101.5	96.8
	n	5	5	5	15

Table 2 Intra-assay precision and recovery of the method for chicken liver spiked at 10 and 20 ng g^{-1} and for muscle and egg spiked at 5 ng g^{-1}

Parameter	Liver	Liver	Muscle	Egg
Spike level/ng g^{-1}	10	20	5	5
Mean/ng g^{-1}	9.6	19.2	5.1	4.9
s/ng g^{-1}	0.154	0.236	0.086	0.087
RSD (%)	1.6	1.2	1.7	1.8
Mean recovery (%)	96.2	95.8	101.8	97.2
n	5	5	5	5

Conclusions

The method described can be used to detect and quantify DMZ residues in turkey tissues to ensure that the current MRL of 10 ng g^{-1} is not exceeded, and to monitor poultry tissues and eggs for residues caused by contaminated feed or illegal use of DMZ. The application of LC–thermospray MS provides mass-related data which are desirable for confirmatory methods. The assay is simple and rapid, enabling 15–20 samples to be analysed in one working day.

References

1   Voogd, C. E., Van der Stel, J. J., and Jacobs, J. J. J. A. A., *Mutat. Res.*, 1979, **26**, 483.
2   Commission Regulation 1798/95, 25 July, 1995, *Off. J. Eur. Comm.*, 1995, **L174**, 20.
3   Council Regulation 2377/90, 26 June, 1990, *Off. J. Eur. Comm.*, 1990, **L224**, 1.
4   Council Directive 70/524/EEC, 23 November, 1970, *Off. J. Eur. Comm.*, 1970, **L270**, 1.
5   Council Regulation 675/92, 18 March, 1992, *Off. J. Eur. Comm.*, 1992, **L73**, 8.
6   Posyniak, S., Semeniuk, S., Zmudski, J., Niedzielska, J., and Biernacki, B., *Vet. Res. Commun.*, 1996, **20**, 167.
7   Kennedy, D. G., Blanchflower, J. B., Hughes, P. J., and McCaughey, W. J., *Food Addit. Contam.*, 1996, **13**, 787.
8   Council Directive 96/23/EC, 29 April, 1996, *Off. J. Eur. Comm.*, 1996, **L125**, 10.
9   Hobson-Frohock, A., and Reader, J. A., *Analyst*, 1983, **108**, 1091.
10   Mallinson, E. T., Henry, A. C., and Rowe, L., *J. Assoc. Off. Anal. Chem.*, 1992, **75**, 790.
11   Ramos, M., Aranda, A., Reuvers, T., and Jimenez, R., *Anal. Chim. Acta*, 1993, **275**, 317.
12   Semeniuk, S., Posyniak, S., Niedzielska, J., and Zmudski, J., *Biomed. Chromatogr.*, 1995, **9**, 238.
13   Carignan, G., Skakum, W., and Sved, S., *J. Assoc. Off. Anal. Chem.*, 1988, **71**, 1141.
14   Newkirk, D. R., Righter, H. F., Schenck, F. J., Okrasinski, J. L., and Barnes, C. J., *J. Assoc. Off. Anal. Chem.*, 1990, **73**, 702.
15   Morris, W. J., Nandrea, G. J., Roybal, J. E., Munns, R. K., Shimoda, W., and Skinner, H. R., *J. Assoc. Off. Anal. Chem.*, 1987, **70**, 630.
16   Commission Decision 93/256/EEC, 14 April, 1993, *Off. J. Europ. Commun.*, 1993, **L118**, 64.
17   Blanchflower, W. J., Cannavan, A., and Kennedy, D. G., *Analyst*, 1994, **119**, 1325.
18   Cannavan, A., Blanchflower, W. J., and Kennedy, D. G., *Analyst*, 1995, **120**, 331.
19   Law, G. L., Mansfield, G. P., Muggleton, D. F., and Parnell, E. W., *Nature (London)*, 1963, **197**, 1024.

Determination of Thyreostats in Thyroid and Urine Using High-performance Liquid Chromatography–Atmospheric Pressure Chemical Ionisation Mass Spectrometry

W. John Blanchflower, Peter J. Hughes, Andrew Cannavan, Maurice A. McCoy and D. Glenn Kennedy*

Veterinary Sciences Division, Department of Agriculture for Northern Ireland, Stormont, Belfast, UK BT4 3SD. E-mail: kennedyg@dani.gov.uk

A method using liquid chromatography–atmospheric pressure ionisation mass spectrometry is described for the determination of five thyreostats in urine and thyroid tissue. Samples were extracted with ethyl acetate and the extracts were cleaned up on silica solid-phase cartridges. They were then concentrated and injected into the LC–MS system, monitoring the [M + H]+ ions for each compound. Additional fragment ions for confirmation purposes could be obtained by increasing the cone voltage on the LC–MS system. Detection limits were in the region of 25 ng g^{-1} and recoveries ranged from 41% for the more hydrophilic compounds such as thiouracil to above 100% for the more hydrophobic compounds such as propyl- or phenylthiouracil.

Keywords: Thyreostats; tapazole; thiouracils; mercaptobenzimidazole; liquid chromatography–mass spectrometry; atmospheric pressure chemical ionisation

Thyreostats, also referred to as 'anti-hormones,' are a group of compounds which increase the mass of animals by enhancing the water retention in tissues. Their use as has been banned throughout the European Union, but it is known that they have been used illegally in cattle to obtain enhanced premiums when animals are presented for slaughter. It has been alleged that consumption of meat containing illegal thyreostat residues may have caused an increased incidence in Spain of aplasia cutis, a characteristic scalp defect.[1] In order to facilitate the elimination of thyreostat abuse, Member States are required to develop confirmatory tests to detect thyreostats in animal tissues and fluids.

Older published methods for determination of thyreostat residues have involved TLC[2,3] or HPLC,[3,4] both of which may present problems with specificity and sensitivity. More recently, Schilt *et al.*[5] described a method that used gas chromatography (GC) with either nitrogen–phosphorus detection or mass spectrometry (MS). This method was highly specific but was only applicable to urine and required the preparation of mercurated affinity columns for clean-up. It also required the formation of derivatives for GC or GC–MS. DeBrabander and co-workers used HPTLC clean-up and GC–MS confirmation for the determination of thyreostats in thyroid and muscle,[6] and recently described the use of mercurated affinity columns and GC–MS–MS for the detection of thyreostats in urine.[7]

We have recently shown that modern LC–MS is an excellent technique for the detection of residues of veterinary drugs such as ionophores,[8] furazolidone[9] and levamisole[10] in biological samples, requiring no derivatisation and using simple clean-up steps. In this paper, we describe the application of LC–MS, using atmospheric pressure chemical ionisation (APCI), to the determination of thyreostats in urine and thyroid tissue. The method is suitable for the determination of tapazole (TAP,

methimazole), thiouracil (TU), methylthiouracil (MTU), propylthiouracil (PrTU) and phenylthiouracil (PhTU).

Samples are extracted into ethyl acetate and anhydrous sodium sulfate is used to improve the partition of the more polar analytes such as TAP, TU and MTU into the organic solvent. Mercaptoethanol is added to reduce binding to protein and improve recoveries. The extracts are cleaned up using silica solid-phase extraction, concentrated and injected into the LC–APCI–MS system. Single ion monitoring is used to detect the [M + H]+ ion for each thyreostat. Additional fragment ions can also be obtained for confirmation purposes by re-running the samples using a higher cone voltage on the LC–MS source.

Experimental

Materials

All solvents were of HPLC grade and other chemicals were of analytical-reagent grade. TAP, TU, MTU, PrTU and PhTU were obtained from Sigma (Poole, Dorset, UK). Stock standard solutions of each (1 mg ml^{-1}) were prepared in methanol. These were stable for 2 weeks when stored in a brown bottle at 4 °C. A mixed dilute standard (2 µg ml^{-1}) was prepared as required by dilution of the stock standard solutions with 25% v/v methanol–water.

Mobile phase A consisted of de-ionised water containing 0.1% v/v heptafluorobutyric acid. Mobile phase B consisted of 55% v/v methanol–water also containing 0.1% v/v heptafluorobutyric acid. Both solutions were filtered and degassed using an HPLC solvent filter unit (Millipore–Waters, Watford, UK) fitted with a 0.45 µm HVLP filter. The flow rate was set at 1 ml min^{-1} and the gradient profile was as follows: 0 min, 5% B; 8–13 min, 95% B; 15–21 min, 5% B. The total run time was 21 min.

Equipment

The binary gradient HPLC equipment consisted of a Merck–Hitachi L6200A intelligent pump, an L6000 pump and AS2000 autosampler (Merck, Poole, Dorset). The HPLC column was a Prodigy ODS3 reversed-phase column, 150 × 4.6 mm id (Phenomenex, Macclesfield, Cheshire, UK). An on-column prefilter unit fitted with a 2 µm filter was used to prevent particulates from contaminating the column.

The HPLC column was coupled to the APCI probe of a Platform LC–MS system (Micromass, Altrincham, Cheshire, UK). The source of the instrument was maintained at 150 °C. The APCI probe temperature was 450 °C and the flow rates of the sheath and drying gases were 50 and 200 l h^{-1}, respectively. The instrument was operated in the positive ion mode with a cone voltage of either 10 or 35 V (see later). Full scan data were collected in order to obtain spectra from standards and single-ion monitoring (SIM) data (dwell time 0.5 s for each ion) were collected when analysing samples.

Sample Extraction

Thyroid tissue

Thyroid tissue was either analysed fresh or stored at -20 °C until analysis. Aliquots (3 g) were weighed into 100×27 mm glass centrifuge tubes. Assay recoveries were also set up at this stage by spiking portions of negative tissue with solutions of the thyreostats, allowing them to stand for 10 min and then treating them as for normal samples. The tubes were placed in a fume cupboard and diammonium ethylenediaminetetraacetate (EDTA, 50 μl, 0.1 mol l^{-1}) and 2-mercaptoethanol (25 μl) were added to each. The samples were then extracted by homogenisation for 1 min with ethyl acetate (10 ml) and anhydrous sodium sulfate (1 g) using a Silverson homogeniser (Silverson Machines, Chesham, UK). Any residues adhering to the outside of the homogeniser blades were scraped into the tubes using a spatula and the tubes were placed in an ultrasonic bath for 10 min and centrifuged at 600 *g* for a further 10 min.

Urine

Aliquots of urine (1 ml) were placed in 100×15 mm Quickfit tubes. Assay recoveries were also set up by spiking negative urine samples with small volumes of standard solutions. The tubes were placed in a fume cupboard and EDTA (10 μl, 0.1 mol l^{-1}) and 2-mercaptoethanol (10 μl) were added to each. Each sample was extracted by shaking vigorously for 30 s with ethyl acetate (5 ml). Granular anhydrous sodium sulfate (4 g) was immediately added and the sample was again shaken vigorously for a further 30 s, breaking up the sodium sulfate clump if necessary using a small spatula. The tubes were then placed in an ultrasonic bath for 10 min and centrifuged at 600 *g* for a further 10 min.

Sample Clean-up

Aliquots of the ethyl acetate extracts (4 ml for tissue or 3.5 ml for urine) were transferred in to 100×15 mm tubes and evaporated to dryness at 60 °C under nitrogen. The residues were dissolved in chloroform (3 ml) by sonicating for 10 min. Silica Sep-Pak solid-phase extraction cartridges (Waters, Bedford, MA, USA) were prepared by washing with chloroform (4 ml). The sample extracts were applied, the cartridges were again washed with chloroform (4 ml) and any thyreostats present were eluted with methanol–chloroform (15 + 85 v/v, 2.5 ml) into 70 $\times$ 13 mm tubes. The chloroform eluates were evaporated to dryness under nitrogen at 50 °C and the residues were dissolved in 25% v/v methanol–water (200 μl) by sonicating for 10 min. They were then transferred to autosampler vials for analysis using LC–MS.

LC–MS Analysis

Samples were initially analysed at a cone voltage of 10 V for maximum sensitivity. Up to four ions could be monitored for each compound by re-running suspect samples using a cone voltage of 35 V (see below).

The system was equilibrated by running two aliquots of mixed standard (25 μl, 2 μg ml^{-1} of each of the thyreostats) through the system before sample analyses. Samples extracts (25 μl) were then injected followed by a standard after three samples. Peak area data were simultaneously collected in the positive ion mode for the [M + H]$^+$ ions at *m/z* 115, 129, 143, 171 and 205 for TAP, TU, MTU, PrTU and PhTU, respectively.

Calculations

Calculations were based on the peak areas of the [M + H]$^+$ ions using a cone voltage of 10 V. The 2 μg ml^{-1} mixed standard was equivalent to 0.333 μg g^{-1} of each of the thyreostats in thyroid tissue and 0.57 μg ml^{-1} in urine. The amounts present in the samples were determined with reference to the mean peak areas of the standard before and after each three sample extracts.

Results and Discussion

Fig. 1 shows the molecular structure of TU (upper left), and the full scan spectrum of a 2.5 μg injection of a TU standard, recorded using a cone voltage of 35 V (lower left). TU gives an [M + H]$^+$ ion at *m/z* 129, with a number of prominent fragment ions. The ion at *m/z* 112 corresponds to [M + H -17]$^+$, and probably results from loss of ammonia following ring opening. The ion at *m/z* 70 corresponds to [M + H -59]$^+$, and probably results from loss of SCNH following ring opening. A fourth ion was observed at *m/z* 84. However, for initial testing of samples, a cone voltage of 10 V was used. This maximised the sensitivity of the method, because at 10 V, only the [M + H]$^+$ ion at *m/z* 129 was observed. Fig. 1 also shows a SIM spectrum for a standard solution (2.0 μg ml^{-1}, equivalent to 0.333 μg g^{-1} thyroid) of TU (upper right). The spectrum has been normalised so that 100% is equal to an abundance of 4.00×10^5. A SIM spectrum for a known negative thyroid is shown in Fig. 1 (centre right). This spectrum has also been normalised to 4.00×10^5. No interfering peaks are visible at the retention time of TU. A SIM spectrum of a known negative thyroid, fortified with TU at a concentration of 0.2 μg g^{-1}, is shown at the lower right of Fig. 1. As previously, this spectrum has been normalised to 4.00×10^5. The recovery of TU in this sample was 55%. The limit of detection of the assay, based on a signal-to-noise ratio of 3 : 1, is estimated at approximately 0.025 μg g^{-1}. Similar spectra are obtained when urine was used as the matrix (data not shown).

Fig. 2 is laid out in a similar manner for MTU. Four ions may be detected using a cone voltage of 35 V. As for TU, the [M + H]$^+$ ion of MTU at *m/z* 143 is present. The fragment ion at *m/z* 126 probably corresponds to loss of ammonia and that at *m/z* 84 to loss of SCNH. A fourth ion is also present at *m/z* 98. All of the SIM spectra (*m/z* 143) are normalised to 7.00×10^5. The response of PhTU is shown in Fig. 3 and was similar to that of TU and MTU. Ions were detected corresponding to [M + H]$^+$ (*m/z* 205), [M + H -17]$^+$ (*m/z* 188), [M + H -59]$^+$ (*m/z* 146) and *m/z* 103. In this case all SIM spectra (*m/z* 205) have been normalised to 8.00×10^5. Fig. 4 shows the response of PrTU. This compound exhibited a fragmentation pattern that differed slightly from TU, MTU and PhTU. While ions corresponding to [M + H]$^+$, [M + H -17]$^+$ and [M + H -59]$^+$ were present (*m/z* 171, 154 and 112, respectively), there was no prominent fourth ion. All of the SIM spectra for PrTU (*m/z* 171) have been normalised to 8.00×10^5. Finally, the response of TAP is shown in Fig. 5. While an ion corresponding to [M + H]$^+$ (*m/z* 115) is present, the pattern of fragmentation is different for this compound. However, four fragment ions at *m/z* 115, 88, 83 and 57 may be detected. The SIM spectra for TAP (*m/z* 115) have all been normalised to 1.00×10^6.

Reproducibility and recovery values for the assay as applied to thyroid and urine are shown in Tables 1 and 2, respectively. The overall recoveries in tissue ranged from 50% for TU to 90% for PrTU. For urine, overall recoveries ranged from 42% for TU to 104% for PrTU. The generally lower recoveries for TAP, TU and MTU reflect the difficulties in extracting these polar compounds from aqueous solutions. In the initial stages of developing the assay we found the recoveries of some of the compounds to be as low as 20%. The addition of salt or the use of multiple extractions did not significantly improve the figures. It was found, however, that the addition of anhydrous sodium sulfate to remove water led to a marked improvement and the addition of 2-mercaptoethanol and EDTA further improved the figures. Previous studies have overcome some of the difficulties of extracting the polar thyreostats from urine into organic
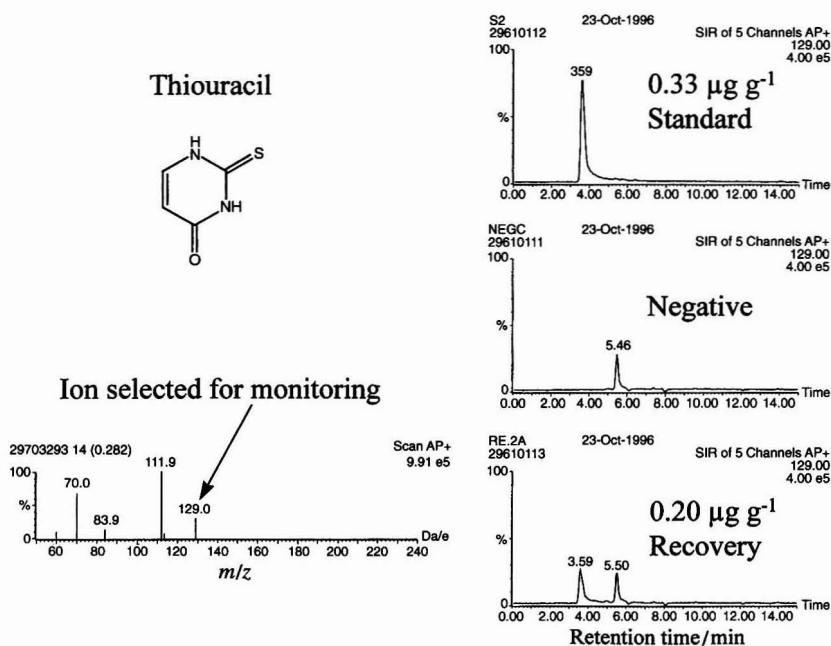
Fig. 1 LC–APCI-MS of thiouracil. Left: upper panel, structure of TU; lower panel, full scan spectrum of TU standard (2.5 µg) using a cone voltage of 35 V. Right: SIM spectra, cone voltage = 10 V, *m/z* 129, normalised to 4.00 × 10⁵. Upper panel, standard, equivalent to 0.33 µg TU per g thyroid; centre panel, known negative thyroid; lower panel, negative thyroid fortified with TU at 0.20 µg g⁻¹.
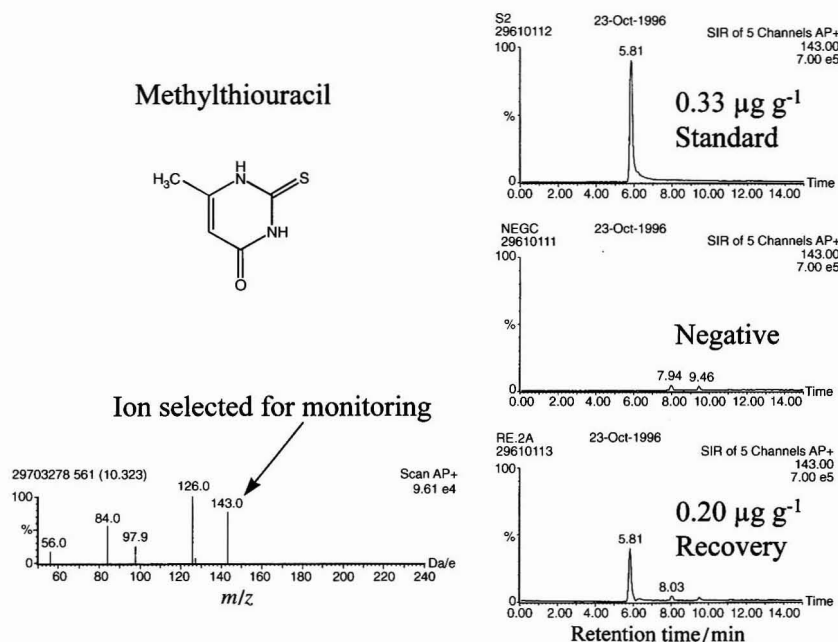
Fig. 2 LC–PCI-MS of methylthiouracil. Left: upper panel, structure of MTU; lower panel, full scan spectrum of MTU standard (2.5 µg) using a cone voltage of 35 V. Right: SIM spectra, cone voltage = 10 V, *m/z* 143, normalised to 7.00 × 10⁵. Upper panel, standard, equivalent to 0.33 µg MTU per g thyroid; centre panel, known negative thyroid; lower panel, negative thyroid fortified with MTU at 0.20 µg g⁻¹.
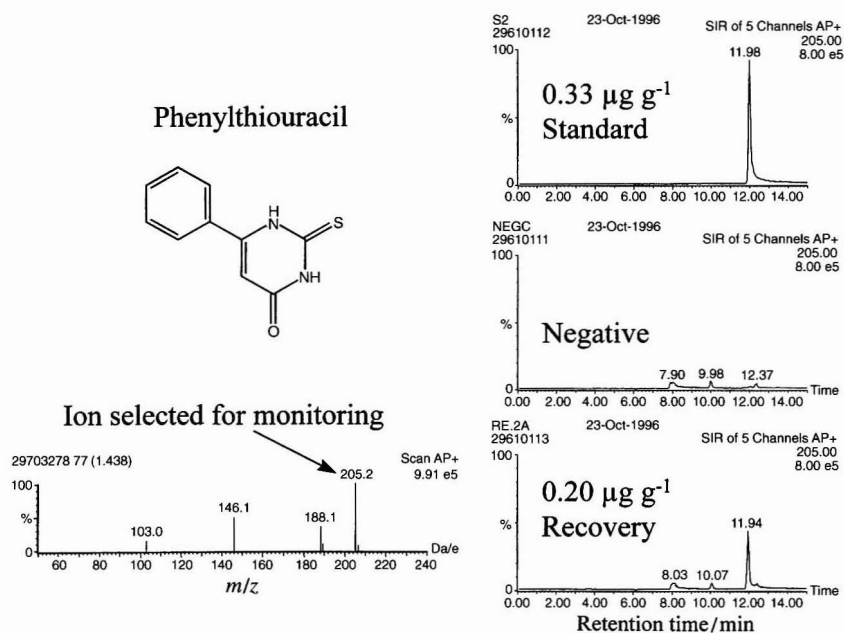
Fig. 3 LC–APCI-MS of phenylthiouracil. Left: upper panel, structure of PhTU; lower panel, full scan spectrum of PhTU standard (2.5 µg) using a cone voltage of 35 V. Right: SIM spectra, cone voltage = 10 V, *m/z* 205, normalised to 8.00×10^5. Upper panel, standard, equivalent to 0.33 µg PhTU per g thyroid; centre panel, known negative thyroid; lower panel, negative thyroid fortified with PhTU at 0.20 µg g^{-1}.
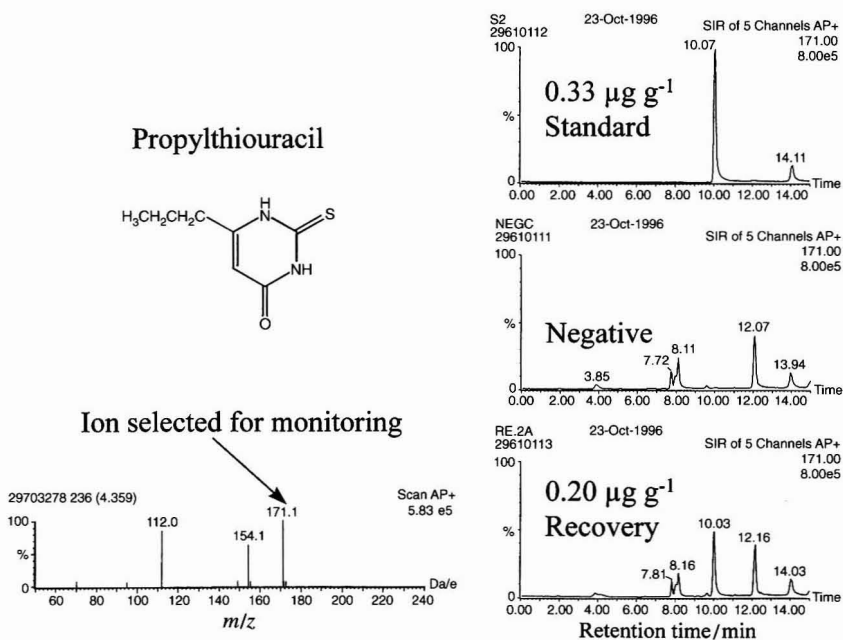
Fig. 4 LC–APCI-MS of propylthiouracil. Left: upper panel, structure of PrTU; lower panel, full scan spectrum of PrTU standard (2.5 µg) using a cone voltage of 35 V. Right: SIM spectra, cone voltage = 10 V, *m/z* 171, normalised to 8.00×10^5. Upper panel, standard, equivalent to 0.33 µg PrTU per g thyroid; centre panel, known negative thyroid; lower panel, negative thyroid fortified with PrTU at 0.20 µg g^{-1}.

solvents by applying samples directly to a mercurated affinity column.[5–7] One of these studies[5] reported recoveries of 95% for TU, MTU and PTU. However, TAP gave very low recoveries and PhTU was not included in the method. Their method was also applicable only to urine. DeBrabander's group developed a procedure that was capable of detecting thyreostats in urine using GC–MS. Samples were cleaned up using the mercurated

affinity columns prior to HPTLC. Suspect spots were scraped off, derivatised and injected into the GC–MS system.[6] Most recently, the same group developed a GC–MS–MS method for the determination of TAP in urine and tissues that had a detection limit of about 50 ng ml^{-1}.[7] The recovery of TAP was approximately 53%, similar to that achieved in the present study.
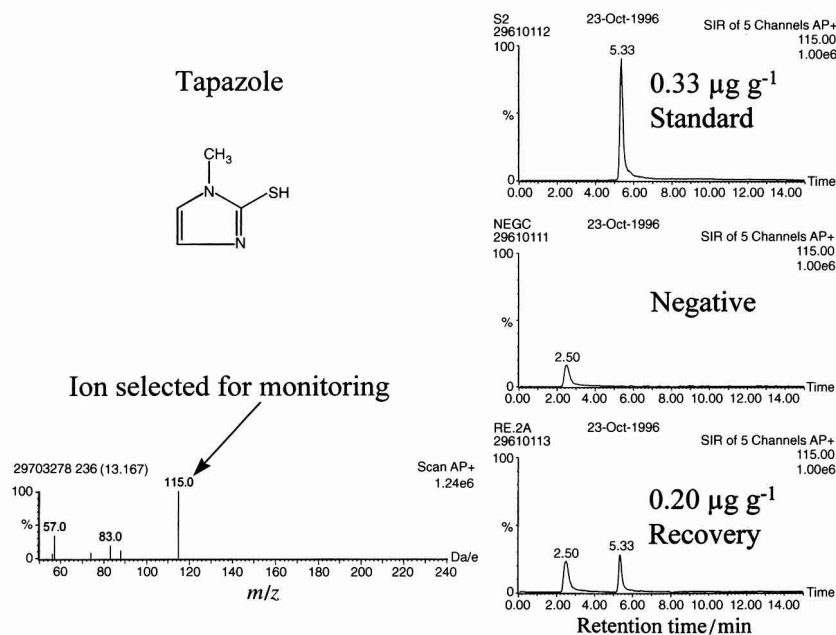
Fig. 5 LC–APCI-MS of tapazole. Left: upper panel, structure of TAP; lower panel, full scan spectrum of TAP standard (2.5 µg) using a cone voltage of 35 V. Right: SIM spectra, cone voltage = 10 V, m/z 115, normalised to 1.00×10^6. Upper panel, standard, equivalent to 0.33 µg TAP per g thyroid; centre panel, known negative thyroid; lower panel, negative thyroid fortified with TAP at 0.20 µg g^{-1}.

Table 1 Reproducibility and recovery values for the determination of thyreostats in thyroid tissue. Known negative samples were spiked with 0.2, 1.0 and 5.0 µg g^{-1} of each of the thyreostats. Five replicates were analysed on each of three days

Parameter	0.2 µg g^{-1} added					1.0 µg g^{-1} added					5.0 µg g^{-1} added				
	TAP	TU	MTU	PrTU	PhTU	TAP	TU	MTU	PrTU	PhTU	TAP	TU	MTU	PrTU	PhTU
Day 1—															
Found/µg g^{-1}	0.12	0.11	0.13	0.17	0.14	0.65	0.60	0.69	0.96	0.86	2.67	2.41	2.74	4.13	3.90
s/µg g^{-1}	0.013	0.014	0.014	0.014	0.017	0.044	0.032	0.043	0.058	0.054	0.177	0.113	0.121	0.230	0.255
RSD (%)	11.1	12.0	11.1	7.7	11.8	6.8	5.4	6.2	6.1	6.3	6.6	4.7	4.4	5.6	6.5
Recovery (%)	58.5	57.5	62.6	87.4	71.5	65.4	59.6	69.1	95.8	86.0	53.5	48.1	54.9	82.6	78.1
Day 2—															
Found/µg g^{-1}	0.12	0.12	0.13	0.17	0.15	0.63	0.59	0.64	0.90	0.75	2.58	2.54	2.48	4.06	3.53
s/µg g^{-1}	0.011	0.006	0.011	0.013	0.009	0.044	0.045	0.030	0.042	0.033	0.178	0.159	0.134	0.173	0.189
RSD (%)	9.4	5.1	8.2	7.7	6.0	7.0	7.6	4.7	4.7	4.4	6.9	6.2	5.4	4.4	5.4
Recovery (%)	60.7	59.1	67.2	87.2	74.2	63.1	58.9	64.2	89.6	75.4	51.6	50.9	49.6	81.2	70.6
Day 3—															
Found/µg g^{-1}	0.12	0.12	0.13	0.16	0.13	0.61	0.58	0.66	0.86	0.73	2.42	2.63	2.63	4.02	3.41
s/µg g^{-1}	0.012	0.008	0.009	0.014	0.007	0.028	0.030	0.049	0.061	0.041	0.053	0.094	0.045	0.139	0.176
RSD (%)	10.1	6.9	6.5	8.6	5.5	4.6	5.1	7.4	7.1	5.6	2.2	3.6	1.7	3.5	5.2
Recovery (%)	60.7	58.0	66.0	82.1	66.9	61.1	57.7	65.6	85.9	73.0	48.4	52.6	52.5	80.3	68.2
Overall—															
Found/µg g^{-1}	0.12	0.12	0.13	0.17	0.14	0.63	0.59	0.66	0.90	0.78	2.56	2.53	2.62	4.07	3.62
s/µg g^{-1}	0.012	0.011	0.012	0.013	0.011	0.042	0.035	0.043	0.067	0.067	0.176	0.150	0.150	0.178	0.292
RSD (%)	10.0	9.2	9.0	7.4	8.1	6.7	6.0	6.5	7.4	9.1	6.9	5.9	5.7	4.4	8.1
Recovery (%)	60.0	57.7	65.7	86.0	71.0	63.3	58.7	66.3	90.4	78.2	51.1	50.5	52.4	81.4	72.3

Table 2 Reproducibility and recovery values for the determination of thyreostats in urine. Known negative samples were fortified with 0.2, 1.0 and 5.0 µg ml^{-1} of each of the thyreostats. Five replicates were analysed on each of three days

Parameter	0.2 µg g^{-1} added					1.0 µg g^{-1} added					5.0 µg g^{-1} added				
	TAP	TU	MTU	PrTU	PhTU	TAP	TU	MTU	PrTU	PhTU	TAP	TU	MTU	PrTU	PhTU
Day 1—															
Found/µg g^{-1}	0.16	0.09	0.13	0.21	0.17	0.82	0.46	0.68	1.02	0.90	3.53	2.33	3.05	5.32	4.53
s/µg ml^{-1}	0.008	0.010	0.012	0.018	0.013	0.028	0.086	0.103	0.080	0.057	0.293	0.353	0.355	0.365	0.289
RSD (%)	4.9	11.3	9.4	8.3	7.9	3.4	18.7	15.1	7.9	6.3	8.3	15.1	11.7	6.9	6.4
Recovery (%)	78.1	43.3	65.3	106.5	83.0	82.0	46.1	68.5	101.8	90.0	70.6	46.7	61.10	106.4	90.7
Day 2—															
Found/µg g^{-1}	0.16	0.08	0.12	0.21	0.15	0.84	0.52	0.74	1.11	0.90	3.32	2.28	3.03	4.66	4.05
s/µg ml^{-1}	0.006	0.008	0.005	0.009	0.006	0.033	0.036	0.029	0.027	0.029	0.034	0.137	0.167	0.076	0.112
RSD (%)	4.0	9.8	3.7	4.0	3.9	3.9	6.9	4.0	2.4	3.2	1.0	6.0	5.5	1.6	2.8
Recovery (%)	79.6	42.1	61.5	106.4	77.0	84.2	52.5	73.8	111.2	89.7	66.4	45.7	60.6	93.3	80.9
Day 3—															
Found/µg ml^{-1}	0.18	0.08	0.13	0.19	0.17	0.82	0.48	0.70	0.99	0.91	3.30	2.44	3.10	4.57	3.92
s/µg ml^{-1}	0.006	0.012	0.015	0.014	0.011	0.045	0.094	0.101	0.107	0.082	0.149	0.120	0.132	0.134	0.167
RSD (%)	3.5	14.6	12.2	7.2	6.8	5.5	19.6	14.4	10.8	8.9	4.5	4.9	4.2	2.9	4.2
Recovery (%)	88.4	42.0	62.9	94.1	84.8	82.4	48.0	69.7	99.1	91.5	66.0	48.9	62.1	91.4	78.4
Overall—															
Found/µg ml^{-1}	0.16	0.08	0.13	0.21	0.16	0.83	0.49	0.71	1.05	0.90	3.38	2.35	3.06	4.85	4.17
s/µg ml^{-1}	0.012	0.011	0.011	0.016	0.013	0.034	0.074	0.080	0.089	0.053	0.208	0.223	0.405	0.405	0.333
RSD (%)	7.6	12.5	8.8	8.0	7.9	4.1	15.2	11.3	8.5	5.9	6.1	9.5	7.3	8.3	8.0
Recovery (%)	82.3	42.3	63.3	102.7	82.0	82.9	48.9	70.9	104.5	90.2	67.7	47.1	61.2	97.0	83.3

Commission Decision 93/256/EEC[11] lays down criteria for low resolution GC–MS methods for the detection of banned compounds, such as anabolic growth promoters and thyreostats. Monitoring of four ions in samples with ion ratios corresponding to those in standards to within ±10% is the preferred option for low resolution GC–MS analyses. There are no specific criteria for LC–MS analyses. However, the described LC–MS assay produces four ions for all of the thyreostats except PrTU. The method is simple to perform and requires no special reagents. Accordingly, it may prove suitable as a confirmatory method that meets the criteria suggested in Commission Decision 93/256/EEC. The use of thyreostats for fattening purposes is illegal within the EU. As a consequence, no maximum residue limits have been set and the confirmed presence of any concentration of a thyreostat in an animal constitutes a violation. The absolute accuracy of the assay is therefore not as critical as for medicines with an established maximum residue limit. However, the accuracy could be improved by the use of internal standards, labelled with stable isotopes. These are slowly becoming available for other compounds and, given sufficient demand, those for the thyreostats may follow.

The detection limits for the assay are dependent on a number of factors, including the sensitivity of the LC–MS instrument during a particular run and the efficacy of the clean-up steps towards individual samples. In general, however, the assay gave a detection limit of about 25 ng g^{-1} in tissue or 25 ng ml^{-1} in urine, at a signal-to-noise ratio of 3 : 1. This is comparable to previously published methods.

Mercaptobenzimidazole (2-benzimidazolethiol), another compound which can be used as a thyreostat, can also be determined using the described assay by monitoring its [M + H]$^+$ ion at *m/z* 151. It elutes from the HPLC column approximately 1 min after PrTU. Although it has not been included in the validation of this assay, recoveries and detection limits are similar to those of PrTU and PhTU.

In conclusion, the described assay has several advantages over previously published methods. It is applicable to a wide range of compounds, the extraction and clean-up steps are simple, no specialised reagents are required, no derivatisation prior to analysis is required and up to four ions can be readily produced for all compounds. LC–MS appears now to be at a sufficiently advanced stage of development to be considered as a mainstream technique for veterinary drug residue analysis.

References

1 Martinez-Frias, M. L., Cereijo, A., Rodriguez-Pinilla, E., and Urioste, M., *Lancet*, 1992, **339**, 742.
2 Pochard, M. F., Karageorgis, M., and Chevalier, M., *Analusis*, 1983, **11**, 499.
3 Blum, J., Venzin, I., and Lutz, H., *Schweiz. Arch. Tierheilk*, 1986, **128**, 419.
4 Hooijerink, H., and De Ruig, W. G., *J. Chromatogr.*, 1987, **394**, 403.
5 Schilt, R., Weseman, J. M., Hooijerink, H., Korbee, H. J., Traag, W. A., Van Steenbergen, M. J., and Haasnoot, W., *J. Chromatogr.*, 1989, **489**, 127.
6 DeBrabander, H., Batjoens, P., and Van Hoof, J., *J. Planar Chromatogr.*, 1992, **5**, 124.
7 Batjoens, P., DeBrabander, H., and DeWasch, K., *J. Chromatogr.*, 1996, **750**, 127.
8 Blanchflower, W. J., and Kennedy, D. G., *J. Chromatogr. B*, 1996, **675**, 225.
9 McCracken, R. J., Blanchflower, W. J., Rowan, C., McCoy, M. A., and Kennedy, D. G., *Analyst*, 1995, **120**, 2347.
10 Cannavan, A., Blanchflower, W. J., and Kennedy, D. G., *Analyst*, 1995, **120**, 331.
11 Commission Decision 93/256/EEC of 14th April 1993, *Off. J. Eur. Commun.*, 1993, **L118**, 64.

Determination of the Quaternary Ammonium Compounds Dequalinium and Cetylpyridinium Chlorides in Candy-based Lozenges by High-performance Liquid Chromatography

R. B. Taylor*, S. Toasaksiri, R. G. Reid and D. Wood

School of Pharmacy, The Robert Gordon University, Schoolhill, Aberdeen, UK AB10 1FR

The retention behaviour of the quaternary ammonium compounds benzalkonium chloride, cetylpyridinium chloride and dequalinium chloride on a 100 × 4.6 mm id cyanopropyl stationary phase column is reported as a function of organic modifier and ionic hydrophobic mobile phase additive concentrations. Optimum liquid chromatographic mobile phases using different mobile phase additives are reported which are suitable for the determination of cetylpyridinium chloride and dequalinium chloride in a variety of candy-based lozenge formulations. The quantitative aspects of assays based on the separation of active ingredients and formulation excipients were established. The generality of application of the assay methods was evaluated by determining the quaternary ammonium content of different lozenges and comparing the values obtained with the stated dose.

Keywords: High-performance liquid chromatography; quaternary ammonium compound; dequalinium chloride; cetylpyridinium chloride; lozenge formulations

Quaternary ammonium compounds (QACs) are widely used in lozenge formulations for their antimicrobial activity in the treatment of common infections of the mouth and throat. The candy-based lozenge has been shown[1] to be more effective than tablet formulations for QAC antibacterial activity. The most common compounds used are the cetylpyridinium and dequalinium chlorides although benzalkonium chloride is also used in some formulations. A study has been carried out to compare the antimicrobial activity of QACs against specified organisms.[2] During this work it was determined that no general assay method could be located in the literature for the determination of QACs in candy-based lozenge formulations.

The literature contains several non-chromatographic methods for the general assay of such QACs although these have not been established as being adequately specific for determination of these compounds in complex matrices. These methods include the compendial non-aqueous volumetric assay[3,4] and techniques based on the formation of ion-pair complexes with organic dyes such as Methyl Orange, Bromothymol Blue and Orange IV with subsequent extraction into organic solvents and spectrophotometric measurement.[5–9] Such ultraviolet/visible spectrophotometric methods lack specificity when applied to lozenge formulations which generally contain artificial colourings and the volumetric procedure is inadequately sensitive for unit dose determination. Other assays have involved the use of chromatographic methods for QACs. Among these is a GLC method for benzalkonium chlorides.[10] Benzalkonium chloride has been determined in ophthalmic solutions[11] by reversed-phase chromatography using a cyano stationary phase following solid-phase extraction to remove interfering polymeric material. Benzalkonium chloride has also been determined using various stationary phases.[12–18] A thin-layer method using densitometry

at 400 nm after reaction with potassium triiodide has been used to determine benzalkonium, cetylpyridinium and cetyltrimethy-lammonium chlorides[19] but no information on its specificity in complex matrices is provided. An LC method has been reported[20] for the determination of cetylpyridinium chloride in saliva. Cetylpyridinium chloride has also been determined in tablets containing benzocaine and dextromethorphan using C_{18} with a mobile phase of methanol–water containing 50% chloroform[21] and in mouthwash using a CN stationary phase.[22] No chromatographic methods could be located in the literature for the determination of dequalinium chloride.

The purpose of the present work is to report the rational development of LC methodology for the chromatography of these QACs and to assess the utility of this methodology for the determination of these compounds in candy-based lozenge formulations. This will require adequate specificity from the various colouring materials used and also from local anaesthetics such as benzocaine which is an additional active ingredient in some lozenges. It is intended that the procedure outlined will be of general use in the application of chromatography to the determination of these compounds in other matrices by describing the retention characteristics for the three QACs as a function of organic modifier and ionic and hydrophobic mobile phase additives.

Experimental

A modular LC system was used for the assay development consisting of a Jasco (PU 980) pump and ultraviolet absorbance detector (PU 975) (Jasco UK, Great Dunmow, Essex, UK) operated at 220 nm for benzalkonium chloride (BZK), 254 nm for cetylpyridinium chloride (CPC) and 240 nm for dequalinium chloride (DQC). The column was 100 × 4.6 mm id containing 5 μm cyanopropylsilica (Hypersil CPS) as stationary phase. The Shandon produced stationary phase (HETP, Macclesfield, Cheshire, UK) was slurry-packed in the laboratory at a pressure of 700 kPa using acetone and hexane and stepwise conditioned to a mobile phase of water–methanol (Rathburn Chemicals, Walkerburn, UK.) Manual injection was used *via* a Rheodyne 7125 (Cotati, CA, USA) six-port valve fitted with a 20 μl (CPC and DQC) or 100 μl (BZK) loop. Chromatograms were recorded using an ABB Goerz SE120 potentiometric recorder (Belmont Instruments, Glasgow, UK). For determination of lozenge content the method was run on a comparable Jasco HPLC system fitted with an AS-950 autosampler and the system controlled by LC-Net II data collection and Borwin software (Jasco UK). The optimum mobile phase was determined as 20 mM phosphate buffer (pH 2.5)–methanol (60 + 40) containing 30 mM cetyltrimethylammonium bromide (CTAB) for CPC ($k' = 4.38$) and 5 mM tetrabutylammonium bromide (TBA) for DQC ($k' = 3.92$).

BZK (BP-grade) was obtained from Thornton and Ross, Huddersfield, UK. CPC and DQC were obtained from Sigma-

Aldrich, Poole, Dorset, UK. The DQC used as standard was certified by the supplier to be 98.5% pure with respect to dried mass by non-aqueous titration. The CPC standard was greater than 99% pure. Liquid chromatography of the CPC standard showed a single peak with no evidence of related impurities. The DQC standard showed evidence of two related impurities. Peak area measurements indicated that the parent peak accounted for 94.6% of the material injected assuming equal response factors for the individual components. For quantitative measurements the volumetric purity of 98.5% was used.

Samples of candy-based lozenges containing the different QACs were obtained commercially through retail outlets. CTAB and TBA used as mobile phase additives were obtained from Merck, Poole, Dorset, UK, and Sigma-Aldrich, respectively. Phosphate buffer salts were also obtained from Merck. Water was purified by distillation and subsequent treatment by a Millipore Milli-Q system [Millipore (UK), Watford, Hertfordshire, UK].

For quantitative measurements, DQC used as standard was dried to constant mass at 100 °C. Residual water was determined by coulometric Karl Fischer reaction using a Mitsubishi CA-20 moisture meter (Anachem, Luton, Bedfordshire, UK) standardized by adding known masses of water directly to the reaction vessel. CPC was used as supplied after storage in a desiccator and determination of water content. In preparing standard solutions the purity of the dried material and the residual water content were allowed for in the calculation of the concentration.

Results and Discussion

Development of Chromatographic Separation

The structures of the three QACs are shown in Fig 1. There are considerable differences among the three compounds to be determined both in hydrophobicity and also in ionic charge particularly for DQC the structure of which incorporates two primary amine groups. All of the compounds are very hydrophobic as a result of the extended hydrocarbon chain and this, in spite of the quaternary nitrogens, resulted in long retention times when a C_{18} stationary phase was used. The

literature indicated that CPC could be successfully eluted from a cyanopropylsilica stationary phase.[20] The retention characteristics of the compounds were studied using this stationary phase in several aqueous mobile phases containing different concentrations of methanol as organic modifier. Plots of capacity factor (k') as a function of methanol concentration are shown in Fig. 2. It is evident from Fig. 2 that separation can be achieved among these three compounds using methanol–water eluents but that CPC produced inconveniently long retention times compared with DQC and BZK in eluents which allowed adequate resolution. One method of altering retention times selectively is to use hydrophobic and ionic mobile phase additives of appropriate charge to increase or decrease retention. Retention times may be increased by using an organic modifier at concentrations to produce relatively short retention times and to increase retention by the addition of an additive such as octane sulfonic acid of charge opposite to the analyte. This approach was used in the assay of BZK. The alternative approach of operating at low methanol concentration, buffering the solvent to low pH and adding a similarly charged, *i.e.,* cationic, hydrophobic ion such as cetrimide or tetrabutylammonium as the bromide was chosen. Inclusion of these additives was found to result in sharp symmetrical peaks and it was found that different additives resulted in different selectivities with respect to the lozenge matrix.

Fig. 3(*a*) shows the variation of capacity factor (k') with cetrimide concentration. This behaviour was also found to be general for TBA [Fig. 3(*b*)]. The processes involved are interpreted as adsorption of the hydrophobic additive onto the surface of the stationary phase, the surface concentration being determined by the mobile phase concentration. The associated like charge accumulated on the surface then acts to decrease retention by coulombic repulsion. At the same time any residual silanols deprotonated at this low pH are effectively masked by the adsorbed additive. Mobile phases were selected by chromatographing lozenge samples containing the appropriate QAC in order to minimize matrix interference. It was found that while similar mobile phases in terms of buffer concentration and buffer/organic modifier concentration could be used, different additives were required to optimize the specificity of CPC and DQC determination in respective lozenges.
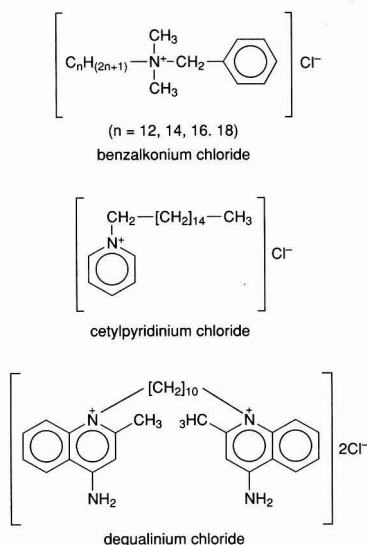
Fig. 1 Structures of the quaternary ammonium compounds.
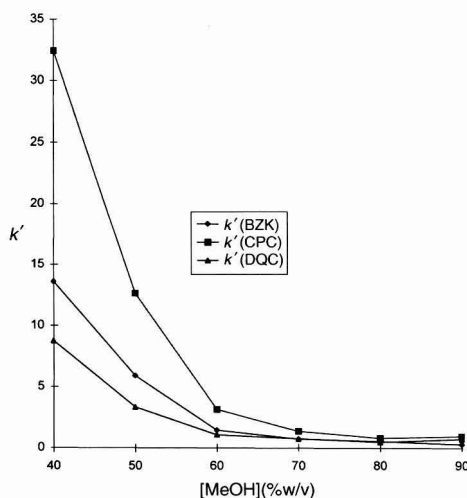
Fig. 2 Variation of capacity factor (k') with methanol concentration using a 100×4.6 mm id column packed with 5 µm cyanopropylsilica stationary phase.

Representative chromatograms of each compound in a lozenge are shown in Fig. 4(*a*) and (*b*).

Quantitative Methods

Linearity of detector response was established for each compound by preparing five standard solutions over the following concentration ranges: CPC, 10–50 μg cm^{-3}; and DQC, 5–25 μg cm^{-3}. The mean peak areas obtained at appropriate absorbance settings following five replicate injections of each standard were plotted as a function of concentration and the regression equations obtained. For both CPC and DQC it was found that adsorption occurred on the glass surfaces resulting in non-linear calibrations. The inclusion of 40% methanol in the solvent eliminated this effect and all standards and samples were subsequently prepared in the chromatographic mobile phase.

Within-day precision was determined by measuring the relative standard deviation (RSD) following replicate injections of a standard solution.

Limit of quantification was calculated by injecting successively more dilute solutions of each compound at decreasing absorbance ranges until a signal-to-noise ratio of 6 was obtained and the concentration recorded.

Sample preparation consisted of dissolving a single lozenge in the appropriate mobile phase by placing in an ultrasonic bath for 20 min and making up to 25 cm^3 with mobile phase. The resulting solution was filtered through a 0.2 μm membrane filter and the filtrate was injected directly into the chromatograph.
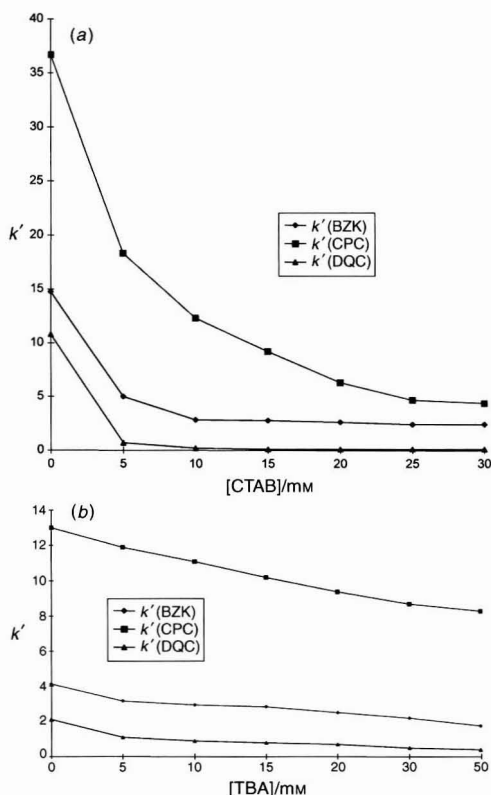
Following triplicate injections the concentration of the analyte in the solution was determined from the calibration equation and the mass in the lozenge calculated.

Absence of interference from matrix components was established as follows. Two aliquots (9 cm^3) of a lozenge solution prepared as described above were transferred into 10 cm^3 calibrated flasks. One flask was made up to volume with mobile phase, the other with a solution of the appropriate QAC at a known concentration. The concentration of QAC in each flask was determined by comparison with the standard calibration line and the recovery calculated as the difference expressed as a percentage of the amount added. Peak homogeneity was examined by ultraviolet diode-array spectrometry and also by reducing the organic modifier concentration. No evidence was found of any peak inhomogeneity which would result in inadequate specificity for the analyte and all detectable components of the lozenges were completely resolved from the QAC being determined.

Using the automated system the content of the appropriate QAC was determined in ten individual lozenges of three different lozenges from different manufacturers.

The regression equation and correlation coefficient of the linearity determination for each QAC are shown in Table 1. The intercepts of the regression calibration lines for all compounds were less than 0.5% of the peak area at the maximum analyte concentration and thus not significantly different from zero at the 95% confidence level. The mean within-day precisions,
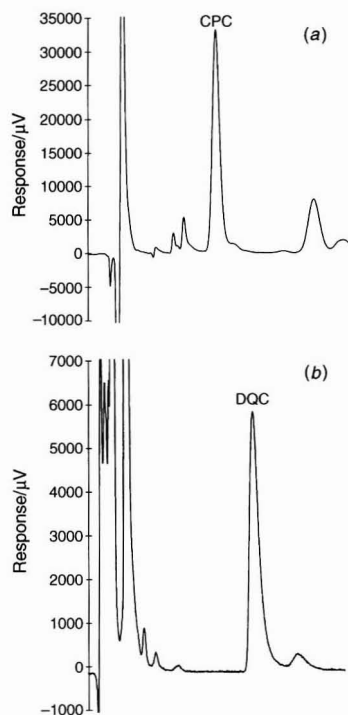
Fig. 4 (*a*) Chromatogram of Type 2 lozenge. Solvent consists of 40% methanol–60% 20 mM phosphate buffer pH 2.5 containing 30 mM CTAB. Column, 100 × 4.6 mm id, packed with 5 μm cyanopropylsilica. Flow rate, 1.5 cm^3 min^{-1}; wavelength, 254 nm. Retention time of CPC is 3.65 min. (*b*) Chromatogram of Type 4 lozenge. Solvent consists of 40% methanol–60% 20mM phosphate buffer pH 2.5 containing 5 mM TBA. Column, 100 × 4.6 mm id, packed with 5 μm cyanopropylsilica. Flow rate, 1.5 cm^3 min^{-1}; wavelength, 240 nm. Retention time of DQC is 5.55 min.

Fig. 3 Variation of capacity factor (*k*′) with (*a*) cetrimide concentration and (*b*) TBA concentration.

averaged over the calibration standards used for the different compounds (RSD), are seen from Table 1 to be 1.13 and 0.79%. Calibration graphs obtained on successive days showed no significant difference in their slopes. The limits of quantification are 5 and 1.5 µg cm^{-3} for CPC and DQC, respectively, which are adequate for the determination of all analytes in a single lozenge. Table 1 also lists the percentage recovery following the spiking of the lozenge matrix and the values obtained indicate the absence of matrix interference.

Table 2 shows details of the lozenges examined. Each of the ten lozenges chosen from each manufacturer were analysed in triplicate using the appropriate analytical procedure and the mean and standard deviation are shown.

The analytical variation among the triplicate determinations for individual lozenges for all lozenges analysed is in the region of 1% RSD. The values of content obtained for the CPC lozenges indicate 95.3, 92.8 and 92.9% of the stated dose, respectively, for the three lozenge types studied. This is within the limits for such preparations of 90–125% stated in the US

Pharmacopeia (ref. 3, p. 268). The method is also capable of showing the increased variability of Type 1 lozenges compared with Types 2 and 3. Types 4 and 5 DQC lozenges tested contain, on average, 119 and 118% of the labelled amount. Type 6, produced by a different manufacturer, yielded consistently higher contents at 132.2% of the stated dose. These DQC results also support the ability of the proposed method to distinguish between different preparations.

Table 1 Validation data for the determination of CPC and DQC including linearity of calibration, within-day precision, limit of quantification (LOQ) and recovery from spiked lozenge samples

Compound	Regression equation*	r^2	Mean within-day precision (RSD %)	LOQ/ µg cm^{-3}	Recovery from spiked lozenge (%)
CPC	$A = 2233\,C$ $+(-10)$	0.9983	1.13 ($n = 5$)	5.0	102.3
DQC	$A = 5027\,C$ $+1027$	0.9996	0.79 ($n = 5$)	1.5	99.7

* A = Peak area; C = concentration.

Table 2 Determination of CPC and DQC in different types of commercial candy-based lozenges

Commercial lozenge	QAC	Stated dose per lozenge/mg	Mean mass found ± s ($n = 10$)	Stated adjuvants and concentrations
Type 1	CPC	1.4	1.34 ± 0.15	Benzocaine (10 mg)
Type 2	CPC	1.4	1.29 ± 0.03	
Type 3	CPC	1.4	1.30 ± 0.05	Menthol (5 mg) Eucalyptol (3 mg)
Type 4	DQC	0.25	0.297 ± 0.004	Benzocaine (10 mg)
Type 5	DQC	0.25	0.296 ± 0.019	
Type 6	DQC	0.25	0.330 ± 0.017	

References

1 Richards, R. M. E., and Rochester, L. M., Proceedings of the 49th International Congress of Pharmaceutical Sciences of FIP, Elsevier, Amsterdam, 1989, vol. 20, p. 132.
2 Richards, R. M. E., and Xing, D. K. L., *J. Pharm. Sci.,* 1993, **82**, 1218.
3 United States Pharmacopeia, *National Formulatry XXII,* US Pharmacopeial Convention, Rockville, MD, 1990, pp. 268 and 1935.
4 *British Pharmacopoeia,* HM Stationery Office, London, 1993, pp. 200 and 201.
5 Chin, T. F., and Lach, J. L., *J. Am. Pharm. Assoc. Sci. Ed.,* 1965, **54**, 1550.
6 Chatten, L. G., and Okamura, K. O., *J. Pharm. Sci.,* 1973, **62**, 1328.
7 Lowry, J. B., *J. Pharm. Sci.,* 1979, **68**, 110.
8 Mohamed, H. A., *Anal. Lett.,* 1993, **26**, 2421.
9 Leung, C. P., and Kwan, S. Y., *Analyst,* 1979, **104**, 143
10 Suzuki, S., Nakamura, Y., Kaneko, M., Mori, K., and Watanabe, Y., *J. Chromatogr.,* 1989, **463**, 188.
11 Fan, T. Y., and Wall, M., *J. Pharm. Sci.,* 1993, **82**, 1172.
12 Heinig, K., Vogt, C., and Werner, G., *J. Chromatogr. A,* 1996, **745**, 281.
13 Marsh, D. F., and Takahashi, L. T., *J. Pharm. Sci.,* 1983, **72**, 521.
14 Elrod, L., Golich, T. G., and Morley, J. A., *J. Chromatogr.,* 1992, **625**, 362.
15 Parkin, J. E., *J. Chromatogr.,* 1993, **635**, 75.
16 Bleau, G., and Desaulriers, M., *J. Chromatogr.,* 1989, **487**, 221.
17 Santoni, G., Tonsini, A., Gratteri, P., Mura, P., Furlanetto, S., and Pinzauti, S., *Int. J. Pharm.,* 1993, **93**, 239.
18 Gomez-Gomar, A., Gonzalez-Aubert, M. M., Garces-Torrents, J., and Costa-Segarra, J., *J. Pharm. Biomed. Anal.,* 1990, **8**, 871.
19 Paesen, J., Quintens, I., Thoithi, G., Roets, E., Reybrouk, G., and Hoogmartins, J., *J. Chromatogr.,* 1994, **677**, 377.
20 Collins, A. E., and Deasy, P. B., *J. Pharm. Sci.,* 1990, **79**, 116.
21 Linares, P., Gutierrez, M. C., Lazaro, F., Luque De Castro, M. D., and Valcárcel, M., *J. Chromatogr.,* 1991, **558** 147.
22 Meyer, R. C., and Takahashi, L. T., *J. Chromatogr.,* 1983, **280**, 159.

Bixin and Norbixin in Human Plasma: Determination and Study of the Absorption of a Single Dose of Annatto Food Color

Luis W. Levy*[a], Edmundo Regalado[a], Scarly Navarrete[a] and Ruth H. Watkins[b]

[a] *Inexa, Industria Extractora CA, P.O. Box 17-03-4581, Quito, Ecuador*
[b] *North Carolina State University, Box 7624, Raleigh NC 27695, USA*

A procedure was developed for the detection and determination of bixin and norbixin in human plasma by reversed-phase HPLC with a sensitivity limit of 5 µg l⁻¹. A group of seven volunteers ingested a single dose of 1 ml of a commercial Annatto Food Color (16 mg of *cis*-bixin in soybean oil). The presence of bixin (*cis* and *trans*) and norbixin (*cis* and *trans*) was demonstrated in the plasma at average levels of 11.6, 10.1, 2.8 and 0 µg l⁻¹ of bixin and 48, 58, 53 and 29 µg l⁻¹ of norbixin after 2, 4, 6 and 8 h, respectively. Considerable individual variations were observed. Complete plasma clearance generally occurred for bixin by 8 h and for norbixin by 24 h after ingestion of *cis*-bixin.

Keywords: *Bixin; norbixin; carotenoids; intestinal absorption; human plasma; high-performance liquid chromatography*

Bixin is unique among the naturally occurring carotenoids because of its two carboxylic groups, one of which is a methyl ester. Bixin occurs mainly in the pericarp of the seed of the Annatto plant *Bixa orellana*. Extracts of the seed pericarp in different concentrations of bixin and of norbixin (the water-soluble, hydrolyzed derivative of bixin) are used commercially as Annatto Food Colors (E 160b). Annatto has been a normal ingredient of the diet of Latin America for many centuries. A recent review on the chemistry, extraction and uses of annatto was presented by Collins.[1]

The uptake of ingested bixin into the human bloodstream has not been reported previously, even though numerous studies on the determination of carotenoids in plasma and serum have been published.[2–5] Because most of these are based on liquid–liquid transfer of the carotenoids into hexane, none would show the presence of bixin or norbixin in plasma or serum because of the low solubility in hexane of these highly polar carotenoids. Another reason for the previous failure to detect bixin or norbixin in human blood may have been the fact that with the exception of Latin America and Spain, normal human intake of bixin and norbixin in most countries is very low (probably < 4 mg per day per person).[6] The low liposolubility of these carotenoids has even given rise to doubts about whether they are absorbed into the human bloodstream at all. This question is of practical importance because of the extensive use of Annatto Food Colors in human foods.

Experimental

We have developed a procedure for the sample preparation of human plasma based on liquid–liquid transfer of bixin and norbixin from plasma into chloroform. The addition of an internal standard with similar solubility characteristics (Sudan I) at the beginning of the procedure obviates the need for quantitative transfers of the chloroform phase. An additional advantage of the procedure is that centrifugation is not necessary at any stage because undissolved solids accumulate in the upper, aqueous phase and therefore do not contaminate the solution used for the final HPLC determination. The procedure involves (1) addition of an internal standard (Sudan I) to the plasma sample, (2) denaturation of proteins with ethanol and (3) subsequent liquid–liquid extraction of bixin, norbixin and internal standard with chloroform. The pooled chloroform phases are evaporated to dryness. The solvent-free residue is dissolved in methanol and injected into a reversed-phase HPLC column, based on the method of Scotter *et al.*[7] Results are calculated through the HPLC peak area ratio of bixin (or norbixin) to the internal standard.

Materials and Apparatus

Methanol, ethanol, chloroform, acetonitrile and acetic acid were of analytical-reagent grade. Laboratory equipment included a mini-separating funnel (30 ml), a rotary evaporator with the bath set at 50 °C and a Pasteur pipette.

For HPLC, a Spectra-Physics (San Jose, CA, USA) SP 8770 system was used with a flow rate of 1.5 ml min⁻¹ at 0.76 Kpsi. Injection of 10 µl were made *via* a Rheodyne (Cotati, CA, USA) loop into a Spherisorb S50DS1 column (Phase Separations, Queensferry, Clwyd, UK). The mobile phase was acetonitrile–2% aqueous acetic acid (70 + 30). The detector was set at 460 nm.

A 0.8 µg ml⁻¹ solution of the internal standard, Sudan I (Aldrich, Milwaukee, WI, USA) was prepared by dissolving 4 mg in 100 ml of methanol and diluting 1 ml to 50 ml with methanol.

Procedure

Draw blood samples (10 ml) by venipuncture into EDTA-containing tubes (Venosect II; Merck, Darmstadt, Germany). Prepare plasma by centrifugation in the usual way.

Transfer plasma (exactly 3 ml) into a mini-separating funnel, add Sudan I solution (exactly 1 ml) and then ethanol (6 ml). Shake well and let the mixture rest for 30 min. Add chloroform (3 ml) and shake vigorously for 1 min. Let the mixture stand for phase separation. Transfer a major part of the lower phase into the distillation flask of the rotary evaporator.

Repeat the extraction of material remaining in the separating funnel (containing some solids) by adding ethanol (3 ml) and then chloroform (6 ml). Shake well after each addition. Let the mixture stand for phase separation. Transfer the major part of the lower (chloroform) phase into the same distillation flask and repeat the extraction once more. Transfer the major part of the lower phase into the same distillation flask.

Evaporate the pooled chloroform solutions to dryness in the rotary evaporator (bath temperature 50 °C, vacuum). Mix the dry residue with methanol (1 ml) and aid the extraction of the residue by placing the flask in an ultrasonic bath. Separate the solution by means of a Pasteur pipette, leaving any undissolved material in the flask. Use this solution for injection into the HPLC system.

To verify that no bixin, norbixin or internal standard remained undissolved on the solids in the distillation flask, extract the residue with chloroform (1 ml) and inject the extract into the HPLC system. This chromatogram should not show any peaks of bixin, norbixin or internal standard.

Calculation of Results

To obtain the concentration of bixin in plasma in $\mu g\ l^{-1}$, add the peak areas of *cis*- and *trans*-bixin and then apply the equation.

$$\frac{\text{bixin areas}}{\text{area of int. std.}} \times \frac{\mu\text{g int. std.}}{\text{ml plasma}} \times \frac{1000}{5.62}$$

To obtain the concentration of norbixin in plasma in $\mu g\ l^{-1}$, add the peak areas of the norbixin isomers and then apply the equation

$$\frac{\text{norbixin areas}}{\text{area of int. std.}} \times \frac{\mu\text{g int. std.}}{\text{ml plasma}} \times \frac{1000}{5.62}$$

Discussion of the Procedure

Use of acetic acid in the mobile phase

This is necessary to ensure the solubility of bixin and norbixin as specified in the HPLC method of Scotter *et al.*[7] which was used in this work. In contrast to the other natural carotenoids, neither bixin nor norbixin is sensitive to acids.

Proof of correct identification of peaks

A typical chromatogram of plasma containing norbixin and bixin (Fig. 1) shows three peaks of norbixin isomers at retention times between 6 and 8 min, the peak of the internal standard at about 11 min and the peaks of *cis*- and *trans*-bixin at 16–18 min. A chromatogram of bixin- and norbixin-free plasma showed no peaks in the area of interest. The peaks of bixin and norbixin isomers in the plasma were identified through their electronic spectra as obtained with a photodiode-array detector (Fig. 2), which are the typical spectra of bixin and norbixin in the mobile phase. Further proof was obtained through spiking with authentic samples of *cis*-norbixin and *cis*-bixin, prepared in the laboratory.

Sum of the peak areas of the isomers

For the calculation of the results, the sum of the areas of the three norbixin peaks and the two bixin peaks are used to express the results as norbixin and bixin, respectively.

Solubilities of bixin, norbixin and internal standard

At the concentration levels in this procedure, the solubilities of bixin, norbixin and Sudan I in ethanol and chloroform are sufficiently similar to allow the addition of the Sudan I as an internal standard at the beginning of the procedure. Hence dilution factors and less than quantitative transfer during the procedure do not affect the calculation of the results.

Recovery and sensitivity limit

The recovery was tested by adding pure bixin (50 ng) to a sample of carotenoid-free plasma (10 ml), which was then subjected to the analytical procedure as described. The bixin to Sudan I absorbance ratio at 460 nm as found from the HPLC trace after the analytical procedure was better than 90% of that of a standard mixture of the same concentrations of bixin and Sudan I. The sensitivity limit was established as 5 $\mu g\ l^{-1}$ by applying the criterion of 'the lowest measurable concentration of the compound that generates a peak with a height equivalent to a threefold improvement over the baseline noise.'[5]

Optical absorption ratio of bixin and Sudan I

At equal concentrations in the mobile phase used, bixin and norbixin show an absorbance 5.62 times stronger than that of

Fig. 1 Typical HPLC trace for plasma after ingestion of Annatto Food Color. Peaks: 1–3, norbixin isomers; 4, internal standard; and 5 and 6, bixin isomers.
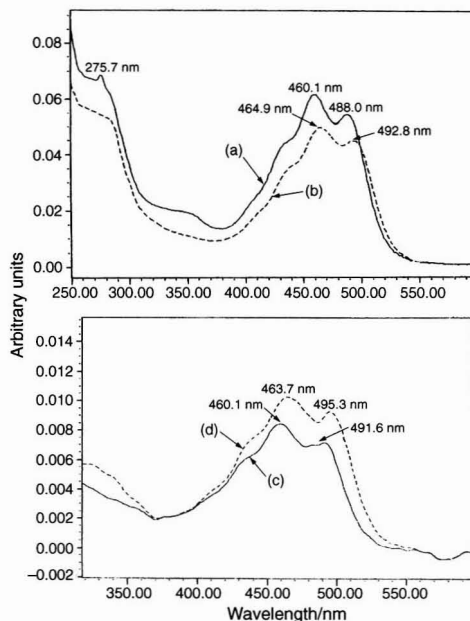
Fig. 2 Photodiode-array spectra: (a) peak 1; (b) peak 2; (c) peak 5; and (d) peak 6. See Fig. 1.

Sudan I at 460 nm. This factor is used in the equation for the calculation of results.

Results and Discussion

Bixin and Norbixin Levels in Human Plasma After Ingestion of a Single Dose of Annatto Food Color

We applied the procedure to the investigation of the intestinal absorption of bixin from a commercial Annatto Food Color ingested in a single dose by each of seven human volunteers on two separate occasions. The volunteers who participated in this controlled ingestion study were healthy adults of both sexes, recruited from the staff of Inexa (Quito, Ecuador). After a normal breakfast, each ingested 1 ml of a commercial Annatto Food Color containing 16 mg of bixin, followed by a glass of milk. We examined their plasma at regular time intervals after ingestion. HPLC of the ingested Annatto Food Color (1.6% bixin in soybean oil; Inexa) showed *cis*-bixin as the main peak (Fig. 3). In view of the subsequent plasma results, it is important to note that <0.3% norbixin was present in the ingested color.

Blood samples were drawn at time zero and at 2, 4, 6 and 8 h after ingestion. Some participants volunteered additional blood samples at 24 and 48 h after ingestion. No control of their diet was made after the sixth hour from the time of ingestion. In

some cases a rise in bixin level was found after 8 or 24 h from the time the controlled intake occurred, suggesting that some food colored with annatto (a common food additive in Ecuador) had been ingested after the initial 6 h. Subsequent questioning confirmed this suspicion.

The bixin and norbixin levels in the plasma of the volunteers are shown in Table 1. A typical sequence of plasma HPLC profiles at 0, 2 and 4 h is shown in Fig. 4. Significant bixin and norbixin levels were found starting at 2 h after ingestion of the Annatto Food Color. The bixin level reached a maximum 2 h after ingestion and that of norbixin at 4 h. Generally a rise in the norbixin level was found after 2 h, concurrent with a decrease of the bixin level. Plasma bixin levels returned to zero at 8 h from
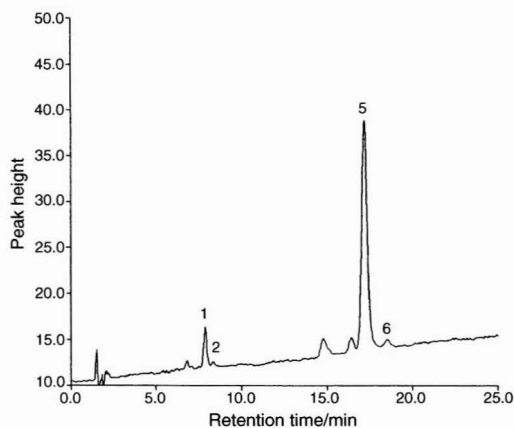
Fig. 3 HPLC of the Annatto Food Color used for ingestion. Peaks: 1, *cis*-norbixin; 2, *trans*-norbixin; 5, *cis*-bixin; and 6, *trans*-bixin.

Table 1 Plasma bixin and norbixin levels after ingestion of a single dose of Annatto Food Color (16 mg of bixin)*

Time after ingestion/h	Bixin/µg l^{-1}		Norbixin/µg l^{-1}	
	Average	Range	Average	Range
0 (baseline)	2.9†	0–11	10.5‡	0–32
2	11.6	0–18§	48.0	3–144
4	10.1	2–24	57.8	3–97
6	2.8	0–9	53.2	38–74
8	0.0	0–3	28.7	7–41
24	0.0	—	16.1¶	17–20¶

* Values below the sensitivity limit of 5 µg l^{-1} are shown when a peak was within the calibration range of the instrument. † (b) Baseline level zero in 7 of 11 cases. ‡ (c) Baseline level zero in 4 of 11 cases. § In one case a 4 h delay in the appearance of bixin was observed (same individual with zero at 2 h). ¶ Suspected additional uncontrolled ingestion of bixin after the 6 h through normal diet in 4 of 11 cases.
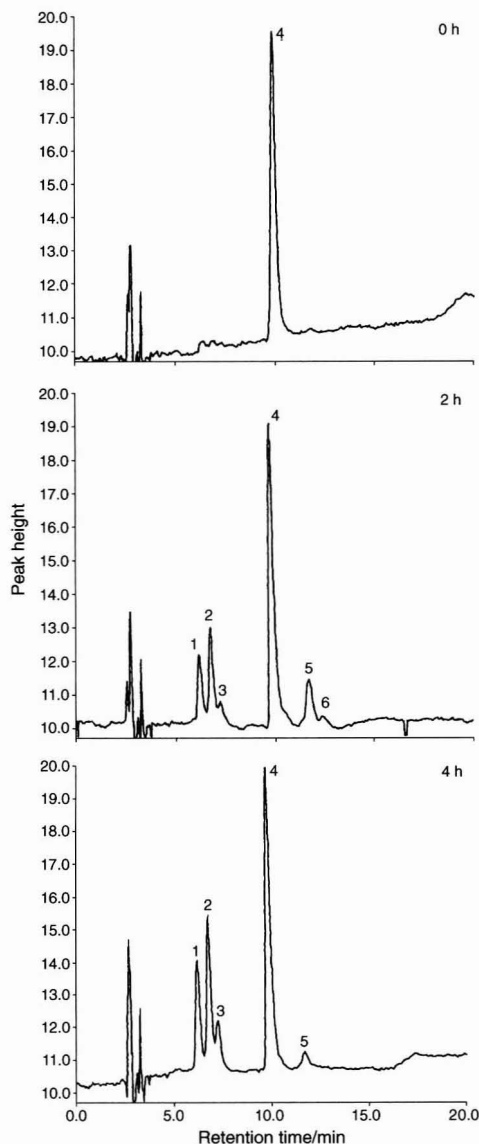
Fig. 4 Sequence of plasma HPLC at 0, 2 and 4 h after ingestion of Annatto Food Color. For identification of peaks, see Fig. 1.

the time of ingestion. The norbixin levels decreased more slowly. Even after 48 h some norbixin was found in some participants, but this may be explained by additional ingestion of annatto in this period through the normal diet.

Initial Absorption of Bixin and Subsequent Conversion to Norbixin

The Annatto Food Color ingested contained mainly bixin (16 mg) with very little norbixin (about 0.5 mg). Bixin appeared unchanged in the plasma initially, but subsequently decreased with a concurrent increase in norbixin, suggesting a conversion of bixin into norbixin in the blood. However, the norbixin levels found in the plasma at 4 h exceeded fivefold the bixin encountered 2 h before. This strong increase in norbixin suggests that a slow conversion of bixin to norbixin had occurred in the intestinal tract and was followed by absorption of the norbixin.

Conversion of cis to trans Isomers

Natural annatto contains mainly *cis*-bixin. Nevertheless, *trans* isomers appeared in the plasma together with the *cis* isomers, suggesting isomerization at some stage of the uptake. Such isomerizations after ingestion of a single isomer have been found with other carotenoids, such as β-carotene[8,9] and lycopene.[10,11]

Plasma Levels of Bixin and Norbixin

In these experiments, the maximum bixin and norbixin levels found in plasma after ingestion of a massive dose of Annatto Food Color were 24 and 144 µg l^{-1}, respectively. These are comparable to the ranges for other carotenoids normally found in plasma (*e.g.*, β-carotene 40–530, lutein 90–410 and lycopene 70–460 µg l^{-1}). Low levels of bixin and norbixin appear to be normal but occasional constituents of human plasma in Ecuador and probably other Latin American countries where annatto is a frequent constituent of the traditional diet, especially in soups and rice.

Possible Biological Action of Bixin

Among the natural carotenoids, bixin is one of the more effective biological singlet molecular-oxygen quenchers.[12] It is an antioxidant inhibitor of lipoxygenase activity.[13] Methylbixin has shown enhancement activity of gap junctional communication which is important in cancer prevention.[14] In view of the important biological actions and functions found in recent years for the carotenoids as anticarcinogens and in the prevention of

artherosclerosis and other diseases,[15] it may well be that bixin in prepared foods will be considered an important nutritional factor for human health in the future.

Conclusion

We have presented a procedure for the detection and determination of bixin and norbixin in human plasma. With its use we were able to demonstrate for the first time that bixin is absorbed into the blood stream after ingestion. The results also suggest a conversion of bixin to norbixin and *cis–trans* isomerization during the digestive process and in the bloodstream itself.

References

1 Collins, P., *Food Ingred. Process. Int.*, 1992, February, 23.
2 Carughi, A., and Hooper, F. G., *Am. J. Clin. Nutr.*, 1994, **59**, 896.
3 Khachik, F., Beecher, G. R., Goli, M. B., Lusby, W. R., and Smith, C., *Anal. Chem.*, 1992, **64**, 2111.
4 Kostic, D., White, W. S., and Olson, J. A., *Am. J. Clin. Nutr.*, 1995, **62**, 604.
5 Schüep, W., Hess, D., and Schierle, J., in *Carotenoids, Isolation and Analysis*, ed. Britton, G., Liaaen-Jensen, S., and Pfander, H., Birkhäuser Verlag, Basle, 1995, vol. 1-A, pp. 261–264.
6 Dinesen, N., personal communication.
7 Scotter, M. J., Thorpe, S. A., Reynolds, S. L., Wilson, L. A., and Strutt, P. R., *Food Addit. Contam.*, 1994, **11**, 301.
8 Parker, R. S., paper presented at the 11th International Symposium on Carotenoids, Leiden, 1996.
9 Schipalius, L. E., and Strahan, M., paper presented at the 11th International Symposium on Carotenoids, Leiden, 1996.
10 Bowen, P., paper presented at the Pre-EB Carotenoid Research Interaction Group, Washington, DC, 1996.
11 Emenheiser, C., paper presented at the pre-EB Carotenoid Research Interaction Group, Washington, DC, 1996.
12 DiMascio, P., Davasagayan, T. P. A., Kaiser, S., and Siess, H., *Biochem. Soc. Trans.*, 1990, **18C**, 1054.
13 Canfield, L. M., and Valenzuela, J. G., *Ann. N.Y. Acad. Sci.*, 1993, **691**, 192.
14 Zhang, L. W., Cooney, R. V., and Bertram, J. S., *Carcinogenesis*, 1991, **12**, 2100.
15 Krinsky, N. J., *Pure Appl. Chem.*, 1994, **66**, 1003.

Overoxidized Poly{pyrrole-co-[3-(pyrrol-1-yl)-propanesulfonate]}-coated Platinum Electrodes for Selective Detection of Catecholamine Neurotransmitters

Joseph Wang[*a], **Prasad V. A. Pamidi**[a], **Gemma Cepria**[a], **Sanjay Basak**[b] and **Krishnan Rajeshwar**[b]

[a] *Department of Chemistry and Biochemistry, New Mexico State University, Las Cruces, NM 88003, USA*

[b] *Department of Chemistry, The University of Texas at Arlington, Arlington, TX 76019, USA*

The cation-exchange and anion-exclusion properties of the poly{pyrrole-co-[3-(pyrrol-1-yl)propanesulfonate]}-(PPy-PS) copolymer are exploited for imparting higher selectivity to measurements of primary neurotransmitters in the presence of ascorbic acid. Such incorporation of ionizable sulfonated groups in the pyrrole ring prior to its electropolymerization leads to effective rejection of the anionic ascorbate species and preferential collection of the cationic dopamine and norepinephrine. Overoxidized PPy-PS films thus offer better discrimination against ascorbic acid than Nafion or overoxidized polypyrrole coatings. Experimental variables influencing the permselective behavior of the PPy-PS layer, including the electropolymerization time and solution pH, were explored. The selectivity and sensitivity improvements associated with the increased electrostatic character of overoxidized polypyrrole films hold promise for neurochemical electrochemical studies.

Keywords: Poly{pyrrole-co-[3-(pyrrol-1-yl)-propanesulfonate]}; permselectivity; dopamine; ascorbic acid

Amperometric microelectrodes have been widely used for *in vivo* monitoring of catecholamine neurotransmitters, particularly dopamine and norepinephrine in small animal brains.[1,2] A major problem facing such electrochemical brain studies is the lack of resolving power between the neurotransmitters of interest and other co-existing oxidizable compounds, particularly ascorbic acid. One common route to impart higher selectivity to these microelectrodes is to cover their surface with an appropriate permselective coating. Cation-exchange polymers, such as Nafion[3,4] have been particularly attractive in connection with neurochemical studies of neurotransmitter release. Because of the cation-exchange properties associated with their sulfonated moiety, such surface layers allow facile transport of the cationic neurotransmitters, while excluding the anionic ascorbate interference.

Recent reports have proposed the use of overoxidized polypyrrole (PPy) films for enhancing the selectivity towards catecholamines.[5–7] In particular, Pihel *et al.*[6] have illustrated that overoxidized PPy films are as effective as Nafion in rejecting the interfering ascorbate and Dopac anions, and that this electropolymerization avenue leads to uniform films on electrodes of different shapes (for which Nafion coatings are often non-uniform). The improved selectivity has been attributed to the removal of positive charges on the polymer and the introduction of oxygenated functionalities (such as carbonyl groups).[5,8] Additional improvements in the selectivity have been reported recently for overoxidized polypyrrole films prepared in the presence of bulky anions such as dodecylsulfate.[9,10]

In this paper, we describe the utility of poly{pyrrole-co-[3-(pyrrol-1-yl)propanesulfonate]} (PPy-PS) films for enhancing the selectivity of electrochemical measurements of biogenic amines. This copolymer consists of repeated units of pyrrole and 3-(pyrrol-1-yl)propanesulfonate.[11,12] Similar substitution of the pyrrole ring with an ionizable sulfonated pendant group has been used previously for binding multiply charged complex ions such as $Ru(NH_3)_6^{3+}$.[11] Here we demonstrate the utility of overoxidized PPy-PS copolymers for imparting higher selectivity and sensitivity on measurements of primary neurotransmitters in the presence of ascorbic acid. Such a surface layer possesses improved ascorbate exclusion properties (compared with both overoxidized PPy and Nafion coatings), while trapping cationic catecholamine species. These attractive cation-exchange/anion-rejection properties of the overoxidized PPy-PS film are obtained without the incorporation of large anion dopants.

Experimental

Apparatus

Cyclic voltammetric and amperometric measurements were performed using a Bioanalytical systems (BAS) (W. Lafayette, IN, USA) Model CV-27 voltammetric analyzer in connection with a BAS *X–Y–t* recorder. A platinum disk electrode (1.6 mm diameter, BAS Model MF-2013), modified with the polymer, served as the working electrode. An Ag/AgCl (3 M NaCl) electrode (BAS Model RE-5) was used as the reference electrode and a platinum wire acted as the auxiliary electrode. The three electrodes were connected to the 10 ml electrochemical cell (BAS Model VC-2) through the holes of the Teflon cover. A magnetic stirrer and stirring bar provided the desired convective transport during amperometric measurements.

Reagents

Ascorbic acid, arterenol (norepinephrine) and 5- hydroxytyramine (dopamine) were purchased from Sigma (St. Louis, MO, USA). Pyrrole (98%) from Aldrich (Milwaukee, WI, USA) was distilled prior to use. 3-(Pyrrol-1-yl)propanesulfonate (Py-PS) was synthesized as described.[11,12] Nafion (5% m/m solution in lower aliphatic alcohols) from Aldrich was used for modifying the surface in comparative studies. Sodium hydroxide (VWR Scientific, Media, PA, USA) was used as the electrolyte during the overoxidation step. Potassium chloride (Fisher Scientific, Pittsburgh, PA, USA), along with 0.05 M phosphate buffer (pH 7.4), served as the electrolyte in the electropolymerization, while 0.05 M phosphate buffer (pH 7.4) was used as the supporting electrolyte during the voltammetric and amperometric measurements. Doubly distilled, de-ionized water was used for preparing the various reagents.

Electrode Preparation

Electropolymerization of pyrrole was carried out in 10 ml of 0.05 M phosphate buffer solution (pH 7.4) containing 0.35 M

pyrrole and 10 mM KCl, by cycling the potential twice between −0.20 and +1.12 V at 50 mV s⁻¹. Coating of the PPy-PS film was carried out in a similar fashion using a phosphate buffer solution containing 0.07 M pyrrolesulfonate and 0.28 M pyrrole. Overoxidation of the PPy and PPy-PS electrodes was performed in stirred 0.1 M NaOH solution by holding their potential at +0.6 V for 10 min. Nafion-modified electrodes were prepared by drop casting 20 µl of the 0.5% m/m ionomer solution and allowing to dry in air under ambient conditions.

Procedure

All measurements were carried out at room temperature. Amperometric measurements were carried out after applying the potential to the electrode and allowing the transient signal to reach its steady-state value.

Results and Discussion

The discriminative and detection properties of the overoxidized PPy-PS film were compared with those of the common Nafion and overoxidized polypyrrole coatings. Fig. 1 displays the amperometric response of the (a) Nafion, (b) overoxidized polypyrrole and (c) overoxidized PPy-PS-coated platinum electrodes (at +0.6 V) to (A) dopamine and (B) norepinephrine in the presence of increasing levels of ascorbic acid. While the Nafion and polypyrrole-modified electrodes exhibit a fast response for both neurotransmitters, they also display a small ascorbic acid contribution. This contribution is greatly suppressed at the PPy-PS-coated electrode; this electrode also displays enhanced sensitivity towards the catecholamine analytes (compared with the overoxidized polypyrrole-coated surface). Note also the slower response of the PPy-PS-modified electrode, which is attributed to its ion-exchange equilibration process. Overall, such coupling of effective charge repulsion of

ascorbic acid with the enhanced dopamine or norepinephrine response results in excellent selectivity towards the target neurotransmitter analytes.

Cyclic voltammetry can shed additional insights into the enhanced selectivity of the PPy-PS-coated electrode. Fig. 2 compares cyclic voltammograms obtained over the −0.2 to +0.6 V range for (a) dopamine, (b) norepinephrine, and (c) ascorbic acid at the overoxidized (A) PPy and (B) PPy-PS-modified electrodes. The latter displays an enhanced anodic response for both dopamine and norepinephrine. Note also the higher oxidation potentials and the reduction peaks (in the cathodic scan). Careful examination reveals also a significantly smaller ascorbic acid response.

Experimental variables affecting the discriminative properties of the PPy-PS film were elucidated. As expected for its charge repulsion and uptake properties, the solution pH has a profound effect on the observed selectivity (Fig. 3). The dopamine/ascorbate current ratio (0.1 mM DA/1.0 mM AA), I_{da}/I_{aa}, increases rapidly on raising the pH from 4.0 to 6.0 and then it starts to level off. Around the physiological pH the ratio is 42 (*i.e.*, a selectivity factor $k_{DA/AA}$ of 420 for equal concentrations). This pH profile reflects the fact that while the dopamine response remains nearly the same (approximately 900 nA) on raising the pH from 4.0 to 9.0, the ascorbate signal decays rapidly between pH 4.0 and 6.0, and remains negligible (approximately 20 nA) at higher pH values (not shown). Apparently, charge repulsion plays a more profound role in the observed selectivity–pH relationship than the ion-exchange collection. Using the bare platinum surface, ascorbic acid displays a current of 1.2 µA over the entire pH range, while dopamine yields a signal of around 100 nA. Hence the PPy-PS-modified electrode results in a nine-fold enhancement of the catecholamine response at pH 7.4 and a 600-fold suppression of
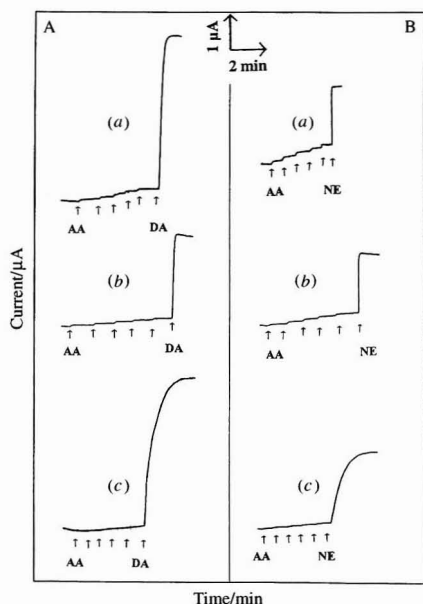
Fig. 1 Current *versus* time recordings for five successive additions of 1 × 10⁻³ M ascorbic acid followed by an addition of (A) 1 × 10⁻⁴ M dopamine or (B) 1 × 10⁻⁴ M norepinephrine. Platinum electrodes coated with (a) Nafion, (b) PPy and (c) PPy-PS. Applied potential, + 0.6V; stirring rate, 600 rpm; electrolyte, 0.05 M phosphate buffer (pH 7.4).
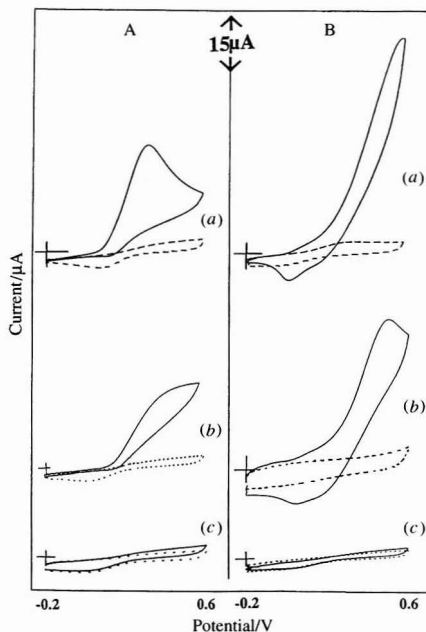
Fig. 2 Cyclic voltammograms for (a) 1 × 10⁻² M dopamine, (b) 1 × 10⁻² M norepinephrine and (c) 1 × 10⁻² M ascorbic acid at (A) polypyrrole- and (B) PPy-PS-coated platinum electrodes. Dotted lines represent the corresponding blank voltammograms. Scan rate, 50 mV s⁻¹; electrolyte, phosphate buffer (pH 7.4).

the ascorbate signal, *i.e.*, increasing the $k_{DA/AA}$ by a factor of 5400.

Fig. 4 displays the effect of the number of voltammetric scans during the film preparation (electropolymerization) on the response of the (A) PPy-PS and (B) PPy-coated electrodes. One (*a*) and ten (*b*) potential cycles in the presence of pyrrolesulfonate had no effect on the effective rejection of ascorbic acid (up to 5 mM). The resulting PPy-PS-modified electrodes also maintains a large dopamine response [(*a*) 3.80 and (*b*) 2.92 µA]. Similar results were observed following five electropolymerization cycles (not shown; dopamine current of 2.85 µA). A different behavior is observed at the polypyrrole-coated electrode (B). One voltammetric scan in the presence of pyrrole results in a large (2.0 µA) dopamine response, and also in small ascorbate contributions. Increasing the number of cycles to five and ten decreases both the ascorbate and dopamine signals. The five-scan preparation still displayed a small ascorbic acid response, along with a dopamine signal of 0.4 µA (not shown). While the ten-scan preparation of the PPy layer offers elimination of the ascorbate contribution, it also results in a substantial diminution of the dopamine response (down to 0.1 µA). Apparently, increasing the thickness of the polypyrrole
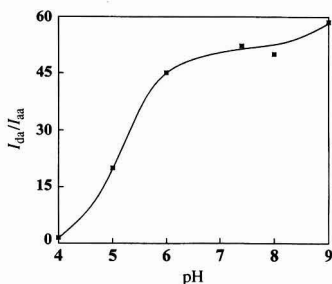
Fig. 3 Effect of pH on the relative amperometric response of 1×10^{-4} M dopamine *versus* 1×10^{-3} M ascorbic acid. Conditions as in Fig. 1(*c*), except that phosphoric acid or potassium hydroxide were used for pH adjustment.
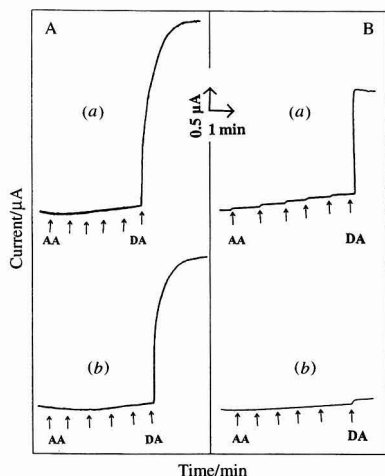
Fig. 4 Current *versus* time recordings for five successive additions of 1×10^{-3} M ascorbic acid followed by an addition of 1×10^{-4} M dopamine. Traces (*a*) and (*b*) are for electrodes prepared with one and ten potential cycles, respectively. Platinum electrode coated with (A) PPy-PS and (B) PPy. All other conditions as in Fig. 1(*c*).

film hinders greatly the transport of both analytes. In contrast, the small changes of the dopamine peak at thicker PPy-PS coatings indicate that this hindrance is balanced by higher cation-exchange capacity. Note also that the electropolymerization time had little effect on the response time of both electrodes.

As expected from their cation-exchange properties, the improved selectivity of PPy-PS-coated electrodes (compared with PPy-modified electrodes) is accompanied by enhanced sensitivity. Fig. 5 displays current–time recordings obtained at the (*a*) PPy-PS and (*b*) PPy-modified electrodes for successive 10 µM additions of (A) dopamine and (B) norepinephrine. While both electrodes respond favorably to these micromolar concentration increments, the PPy-PS film results in about four- and six-fold sensitivity enhancements for dopamine and norepinephrine, respectively. The resulting calibration plots (shown as insets) display some curvature at concentrations higher than 60 and 80 µM for the PPy-PS- and PPy-coated electrodes, respectively. The slopes of the initial linear portions correspond to 11.5 (PPy-PS) and 2.6 nA µM^{-1} (PPy) for dopamine and 9.3 (PPy-PS) and 1.5 nA µA^{-1} (PPy) for norepinephrine.

In conclusion, this study has illustrated that increasing the electrostatic character of overoxidized polypyrrole films, through the incorporation of ionizable sulfonated moieties, provides higher selectivity in measurements of dopamine and norepinephrine in the presence of excess ascorbic acid. The resulting overoxidized PPy-PS layer couples very effective ascorbate exclusion properties with the preferential uptake of cationic neurotransmitters. Realization of these selectivity and sensitivity enhancements for various neurochemical studies
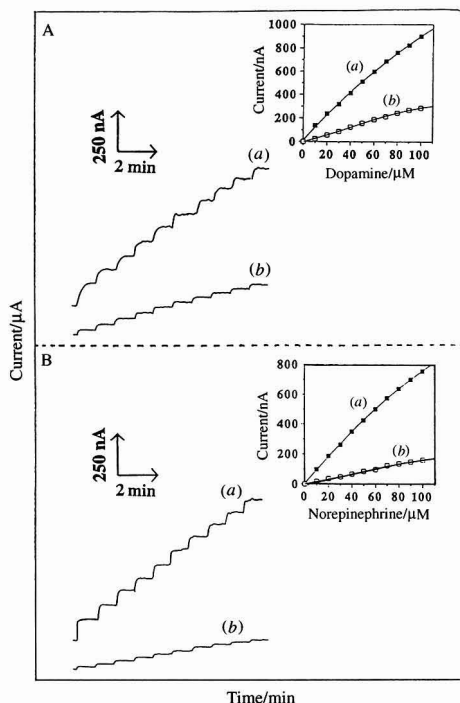
Fig. 5 Amperometric recordings for the successive additions of 1×10^{-5} M (A) dopamine and (B) norepinephrine at (*a*) PPy-PS and (*b*) PPy-coated platinum electrodes. All other conditions as in Fig. 1(*c*). Also shown (as insets) are the corresponding calibration plots.

would require similar modification of miniaturized (carbon-fiber) electrodes and the attainment of faster response times.

References

1 Schenk, J., Miller, E., and Adams, R. N., *J. Chem. Educ.*, 1983, **60**, 311.
2 Stamford, J., and Justice, J., *Anal. Chem.*, 1996, **68**, 359A.
3 Capella, P., Ghasemzadeh, B., Mitchell, K., and Adams, R. N., *Electroanalysis*, 1990, **2**, 175.
4 Kristensen, E., Kuhr, W. G., and Wightman, R. M., *Anal. Chem.*, 1987, **59**, 1752.
5 Witkowski, A., and Brajter-Toth, A., *Anal. Chem.*, 1992, **64**, 635.
6 Pihel, K., Walker, Q., and Wightman, R. M., *Anal. Chem.*, 1996, **68**, 2084.
7 Kang, T., Shen, G., and Yu, R., *Talanta*, 1996, **43**, 2007.
8 Palmisano, F., Malitesa, C., Centonze, D., and Zambonin, P., *Anal. Chem.*, 1995, **67**, 2207.
9 Gao, Z., and Ivaska, A., *Anal. Chim. Acta*, 1993, **284**, 393.
10 Gao, Z., Zi, M., and Chen, B., *Anal. Chim. Acta*, 1994, **286**, 213.
11 Basak, S., Rajeshwar, K., and Kaneko, M., *Anal. Chem.* 1990, **62**, 1407.
12 Basak, S., Bose, C., and Rajeshwar, K., *Anal. Chem.* 1992, **64**, 1813.

Amperometric Determination of Hydrogen Peroxide With a Manganese Dioxide-modified Carbon Paste Electrode Using Flow Injection Analysis

Klemens Schachl[a], Hailemichael Alemu[b], Kurt Kalcher[*a], Jitka Ježkova[c], Ivan Švancara[c] and Karel Vytřas[c]

[a] *Institut für Analytische Chemie, Karl-Franzens Universität Graz, Universitätsplatz 1, A-8010 Graz, Austria*
[b] *Department of Chemistry, Addis Ababa University, P.O. Box 1176, Addis Ababa, Ethiopia*
[c] *Department of Analytical Chemistry, University of Pardubice, nam Cs. legii 565, Cz-53210 Pardubice, Czech Republic*

A carbon paste electrode bulk modified with MnO_2 was investigated as an amperometric detector for hydrogen peroxide in flow injection analysis (FIA). With an operating potential of +0.46 V *versus* Ag/AgCl, H_2O_2 produces catalytic oxidation currents which can be exploited for quantitative determinations. Factors influencing the analytical performance of the electrode, such as paste composition and pH, were studied both for batch voltammetry and for FIA. For the flow system the influence of the injection volume and flow rate were examined. The amperometric signals are linearly proportional to H_2O_2 concentrations in the range 0.5–350 mg l^{-1}, showing a detection limit (three times the signal-to-noise ratio) of 45 µg l^{-1}.

Keywords: Manganese dioxide; hydrogen peroxide; flow injection analysis; amperometry; modified carbon paste electrode

Hydrogen peroxide is a very important intermediate in environmental and biological reactions. It also has wide application in industrial processes as a universal oxidant.[1] The monitoring of hydrogen peroxide with a reliable, rapid and economic method is of great significance for numerous processes. Several analytical techniques have been employed for its determination but most of them suffer from interferences, long analysis time and use of expensive reagents.[2–4] Electroanalytical methods have also been found suitable since they achieve low detection limits and rapid response times.[4,5] They are based on direct reduction or oxidation of hydrogen peroxide, where the electrode reactions are subject to large overvoltages and electrochemical irreproducibility.[6] A number of studies have been carried out to improve the electrochemical response of H_2O_2 by immobilizing substances on the electrode surface that have catalytic (mediating) activity.[7,8] Immobilization of transition metals, their oxides or complexes on the electrode surface is widely applied.[6,9–22]

Determination of H_2O_2 was attempted with different modified electrodes: graphite and carbon electrodes with vacuum-deposited palladium and gold,[9] graphite powder with platinum, palladium and ruthenium complexes,[10] glassy carbon with manganese dioxide,[5] with copper heptacyanonitrosylferrate(II)[11] or with palladium–iridium[12] and graphite coated with montmorillonite which was loaded with a ruthenium–ammonia complex.[13]

The modification of carbon paste electrodes (CPE) with catalytic metals, metal oxide micro-particles or their complexes for the determination of H_2O_2 has received considerable attention.[6,10,14–17] Modifiers used were palladium, platinum black, cobalt(II) phthalocyanine, palladium–gold and cobalt(II)

and cobalt(III) oxides. Prussian Blue was frequently used for modification of CPE, glassy carbon electrodes, noble metal electrodes and metal oxide electrodes.[18–22] Linders *et al.*[23] investigated the oxidation of H_2O_2 using an iron phthalocyanine-modified CPE which could be employed for the quantitative determination of concentrations up to 1.7 mg l^{-1}. Wang *et al.*[24] determined H_2O_2 concentrations up to 340 µg l^{-1} by accumulation at mediatorless peroxidase/carbon paste electrodes. The application of CPE modified with enzymes, tissues and cells as amperometric sensors was reviewed by Gorton.[25]

The aim of this work was to find a simple and cheap procedure for the determination of H_2O_2 at low concentrations based on a manganese dioxide bulk-modified CPE. In alkaline medium manganese dioxide oxidizes H_2O_2 to O_2 whereas it is reduced to oxides containing manganese in lower oxidation states.[26] This reaction was investigated for its applicability to the electroanalytical determination of hydrogen peroxide.

Experimental

Apparatus

Batch experiments

Cyclic voltammetric (CV) measurements were carried out with a PAR 174A polarograph (EG&G Princeton Applied Research, Princeton, NJ, USA), combined with a universal programming unit (PARC 175, EG&G Princeton Applied Research). The cell compartment was a laboratory-constructed electrode assembly of Plexiglas,[27] equipped with a titration vessel of glass (Model 6.1415.220; Metrohm, Herisau, Switzerland). A platinum wire served as the counter electrode and an Ag/AgCl electrode (Model 6.1227.000; Metrohm) equipped with a salt bridge (1 M KCl) with a Vycor frit as reference electrode. A magnetic stirrer and a Teflon-coated stirring bar (approximately 300 rpm) provided the convective transport. Fresh measuring solutions were purged for at least 5 min with argon (99.999%) *via* a Teflon tube. During measurements, argon was passed over the solutions.

Voltammetric curves were registered with an *X–Y* recorder (RE 0089; EG&G Princeton Applied Research). Display graphs were recorded on a personal computer with an appropriate interface for analogue-to-digital conversion.[28]

Flow injection system

The flow injection system consisted of an HPLC pump (Model 510; Waters, Milford, MA, USA), a sample injection valve (U6K; Waters) and a thin-layer electrochemical detector (LC-4C; BAS, West Lafayette, IN, USA) with a flow-through cell (CL-5; BAS). Two carbon paste electrodes (in parallel configuration) acted as working electrodes (total electrode surface

0.14 cm²); the thickness of the layer in the cell was 0.0127 cm. An Ag/AgCl electrode (3 M KCl), (RE-1; BAS) served as the reference electrode. The counter electrode was the back plate of the cell, made of stainless steel. Response curves were registered either with a strip-chart recorder (*X–Y* 7KC 1924-8AD; Pharmacia, Uppsala, Sweden), or the data were transferred to a personal computer *via* an appropriate interface (900 Series interface; Nelson, San Jose, CA, USA) and processed by integration software (PC-Integrator; Nelson).

Reagents and Solutions

Analytical-reagent grade chemicals were used. De-ionized water was distilled twice in a quartz still and then purified with an ion-exchange system (Nanopure; Barnstead, Dubuque, IA, USA). Ammonia–ammonium chloride buffer was prepared by dissolving 5.349 g of ammonium chloride (Merck, Darmstadt, Germany) in 7.5 ml of 25% ammonia (Merck) and diluting to 1000 ml with water. Hydrogen peroxide (30%) (Merck) was standardized by iodimetric titration.[29] An aqueous stock standard solution containing 10 g l^{-1} H_2O_2 was prepared freshly each day. Working standard solutions of lower concentrations were prepared immediately before use. Manganese dioxide and all other compounds used were obtained from Merck.

Working Electrodes

Batch voltammetry and voltammetric procedures

A Teflon rod (11 mm od) with a hole at one end (7 mm diameter, 3 mm deep) for the carbon paste filling served as the electrode body. Electrical contact was made with a platinum wire through the centre of the rod. Unmodified carbon paste was prepared by adding 1.58 g of paraffin oil (Uvasol; Merck) to 5.00 g of spectral carbon powder (RWB; Ringsdorff-Werke, Bad Godesberg, Germany). Modified carbon pastes were prepared by replacing corresponding amounts of the carbon powder (2.5, 5, 10, 15 and 20% m/m) with manganese dioxide and then adding the paraffin oil. The mixtures were homogenized carefully and allowed to rest for at least 24 h. The carbon paste was packed into the hole of the electrode and smoothed with a PTFE spatula. When using the modified paste for voltammetric measurements, the electrode was activated once a day by repeating 10 times the application of a potential of -0.8 V and 0.4 V for 30 s each and scanning to the negative potential.

Cyclic voltammetric measurements were performed from 0.8 to -1.5 V *versus* Ag/AgCl with a scan rate of 20 mV s^{-1} after an equilibration period of 15 s with the initial potential applied.

Flow injection analysis

The modified carbon paste was filled into the electrode body of the thin-layer cell. It was activated in the same way as with batch measurements. The operating potential was 0.46 V *versus* Ag/AgCl. The flow rate was set to 0.9 ml min^{-1}; the usual injection volume was 50 μl. The carrier solution was deaerated with helium (>99.999%), (Messer Griesheim, Gumpoldskirchen, Austria) for 20 min before use in order to prevent the formation of gas bubbles in the flow system.

Analysis of Samples

A medical solution containing hydrogen peroxide (Bio-Garten; Köttmannsdorf, Austria) and a blonding booster (Spray Blond; Chattem, Basingstoke, UK) were bought in a shop and stored in a refrigerator. The samples were diluted 1 : 1000 and 1 : 2500 (v/v), respectively, with water immediately before analysis. Quantitative determinations were made with flow injection

analysis by injecting the sample solutions directly and after spiking with 20, 40 and 60 mg l^{-1} H_2O_2 as internal standards (10 injections of 50 μl).

Results and Discussion

Voltammetric Behavior of H_2O_2 at MnO_2-modified Carbon Paste Electrodes

Fig. 1 illustrates the cyclic voltammograms of hydrogen peroxide at a plain and an MnO_2-modified CPE.

At the unmodified electrode, reduction of H_2O_2 appears at negative potentials overlapped by the reduction of oxygen-containing groups of the carbon particles at -1.2 V and of electrolyte components at even more negative potentials (Fig. 1, curve b).[30] No oxidation can be observed within the applied potential range.

A CPE modified with MnO_2 shows in the absence of hydrogen peroxide, a broad reduction wave from around -0.2 to -0.8 V (curve c). The current response decreases with increasing number of cycles. It can be assigned to an overall reduction of MnO_2 to oxides with manganese in lower oxidation states.[31] Above -0.2 V oxidation occurs, where $Mn^{II,III}$ is re-transformed into MnO_2. During cycling there is obviously a thin film of MnO_2 produced from the bulk modifier.

In the presence of H_2O_2, the cyclic voltammogram displays a distinct reduction at -1.0 V (curve d). This is again assignable to the reduction of Mn^{IV} and/or H_2O_2, maybe in concordance with the reduction of C–O-groups of the carbon paste.[32,33] The much lower currents as compared with an unmodified carbon paste electrode indicate that H_2O_2 decomposes catalytically at the surface. Above -0.3 V oxidation occurs with a more distinct signal at 0.4–0.5 V. Thus, the oxidation of manganese oxides to MnO_2 is significantly increased in the presence of H_2O_2. The characteristic shape of the cyclic voltammogram in this potential region indicates catalytic (mediating) activity of the modifier towards the analyte.

The MnO_2-modified CPE can be used directly without activation for monitoring H_2O_2. Practical investigations showed that the reproducibility of the current response is better after alternating application of positive and negative potentials (+0.4,
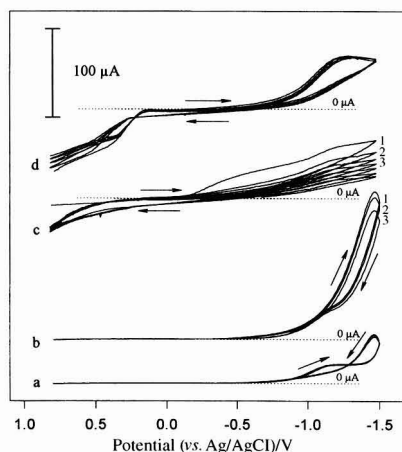
Fig. 1 Cyclic voltammograms of hydrogen peroxide at an unmodified (a, b) and an MnO_2-modified CPE (c, d). Equilibration time, 30 s; initial potential, 0.8 V; final potential, -1.5 V *versus* Ag/AgCl; scan rate, 20 mV s^{-1}; supporting electrolyte, NH_3–NH_4Cl buffer (0.2 M); H_2O_2 concentration, 0 (a, c) and 50 mg l^{-1} (b, d).

−0.8 V). This conditioning procedure forms MnO_2 films at the electrode surface which can react more intimately with the analyte than the modifier in the electrode bulk.

All measurements were carried out in ammonia–ammonium chloride buffer at pH 9.5. The concentration of MnO_2 in the carbon paste has a significant influence on the voltammetric signal. The maximum current increase in CV was obtained when the MnO_2 concentration was 3.8–5.7% (mass ratio of MnO_2 in the paste). Higher concentrations of MnO_2 decreased the current significantly, the reason for which is unclear. Presumably more MnO_2 at the electrode surface reduces the amount of conductive areas (carbon particles) so that the chemical decomposition of H_2O_2 in the presence of MnO_2 becomes more probable and thus reduces the extent of the electrochemical reaction. Hence an electrode modified with 3.8% MnO_2 was employed throughout this work.

Flow Injection Analysis

For flow injection analysis, the modified electrode was used as an amperometric detector in a thin-layer cell using the supporting electrolyte as a carrier. A sample amperogram is shown in Fig. 2.

The MnO_2-modified CPE responds rapidly to dynamic changes in the H_2O_2 concentration. In the absence of the modifier in the paste, no response was observed on injecting the analyte, whereas MnO_2 produces sharp peaks with excellent reproducibility. Evaluation of the responses is best done from their heights.

The dependence of the signal on the applied working potential is shown in Fig. 3. A maximum current could be observed with a potential of around 0.46 V. At lower values the current decreases significantly; the reason for which is that the electrochemical oxidation is less efficient, allowing the chemical decomposition of H_2O_2 to become dominant.

The injection volume also influences the amperometric signal. The current increases with increasing volume up to 150 µl and then levels off. The best reproducibility was obtained with 50 µl of injected sample.

A significant dependence of the amperometric response on the flow rate could be observed under the injection conditions as well as in the steady state (Fig. 4).

Under steady-state conditions when H_2O_2 is present permanently in the carrier, the response increases sharply with slow flow rates, and only gradually with faster flow rates. For Faradaic processes one would expect a dependence of the current on the cube root of the flow rate in a thin-layer cell.[34] However, a plot of the current *versus* the cube root of the flow rate does not give a linear relationship, implying that apart from the electrochemical reaction, also a chemical reaction could be involved. Obviously, there is more intense contact of H_2O_2 with the modifier (reduced state) at higher flow rates (thinner diffusion layer) which facilitates chemical re-oxidation to MnO_2. Under injection conditions the peak height increases almost linearly and sharply up to 0.9 ml min^{-1}, whereas it decreases at higher flow rates. The decrease is significant and suggests that apart from increased dispersion of H_2O_2 in the carrier, a chemical reaction is involved which precedes the electrochemical reaction and which is kinetically slow.
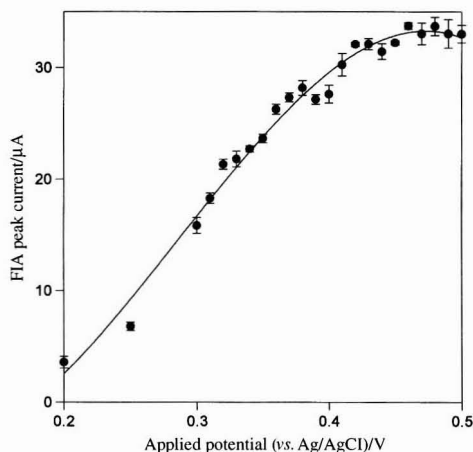
Fig. 3 Dependence of the current response in FIA on the applied working potential. Flow rate, 0.9 ml min^{-1}; carrier, NH_3–NH_4Cl buffer (0.2 M); injections of 50 µl H_2O_2 (20 mg l^{-1}).

Fig. 2 FIA responses of H_2O_2. Operating potential, 0.46 V; carrier, NH_3–NH_4Cl buffer (0.2 M), flow rate, 0.9 ml min^{-1}; H_2O_2 concentration, (a) 20, (b) 40 and (c) 60 mg l^{-1}; injection volume, (1) 25, (2) 50 and (3) 100 µl.
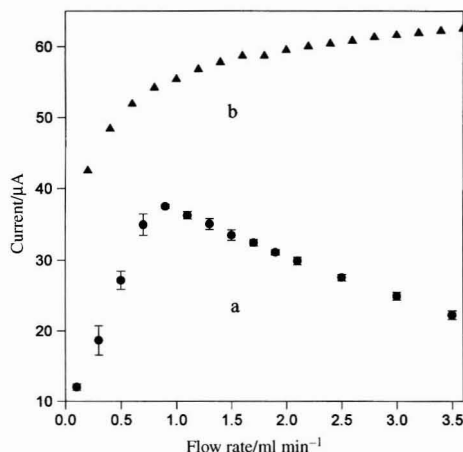
Fig. 4 Flow rate dependence of the peak height in FIA and of the amperometric signal under steady-state conditions. Operating potential, 0.46 V *versus* Ag/AgCl. a, Carrier, NH_3–NH_4Cl buffer (0.2 M); injections of 50 µl H_2O_2 (20 mg l^{-1}); b, carrier, NH_3–NH_4Cl buffer (0.2 M) containing H_2O_2 (20 mg l^{-1}).

Linear Range, Detection Limit and Reproducibility

The relationship between the amperometric peak current and the concentration of H_2O_2 was investigated for the range 0.5–1000 mg l^{-1}. A linear relationship exists up to 350 mg l^{-1} and the linear regression y (μA) = 0.975 × (mg l^{-1} H_2O_2) + 0.2 shows a correlation coefficient of 0.999. With higher concentrations a deviation occurs, probably owing to an unfavourably high ratio of H_2O_2 to MnO_2. It may be also concluded that in the presence of large amounts of hydrogen peroxide chemical oxidation of the reduced modifier becomes increasingly dominant. The detection limit (three times the signal-to-noise ratio) was determined to be 0.045 mg l^{-1} H_2O_2 for an injection volume of 50 μl. For a concentration of 0.5 mg l^{-1} (ten injections of 50 μl of H_2O_2 solution) the RSD was determined as 1.6%.

Interferences

Several cations and anions were investigated for their interference with the amperometric determination of H_2O_2 (Table 1).

Sodium and potassium did not show any effect in a 50-fold mass excess with respect to H_2O_2. Cadmium interferes slightly, probably owing to reduction of the effective electrode surface by adsorption of the hydroxide. This effect is even more pronounced for copper and higher concentrations of iron and lead. In the latter case formation of the dioxide, which behaves electrochemically different, can be assumed.

Anions such as nitrate, sulfate, chlorate, perchlorate, peroxodisulfate and phosphate do not or only slightly interfere in a 50-fold mass excess. Tartrate, borate, hypochlorite and vanadate diminish the signal of hydrogen peroxide if they are present in the same concentration as H_2O_2 or in five-fold excess. Probably H_2O_2 in the sample solution is consumed by the interferents due to a chemical redox process. On the other hand, perborate at higher concentrations increases the current response because it is hydrolysed, yielding hydrogen peroxide.

Ascorbic acid consumes hydrogen peroxide by formation of dehydroascorbic acid, with a decrease in the amperometric signal until all H_2O_2 is reduced. With increasing concentration of ascorbic acid again an increase in the response can be observed owing to reduction of MnO_2.

A slight influence of the amperometric signal (increase and decrease) can be observed with concentrations of paracetamol up to 20 ppm. High concentrations lead to an enormous increase in the amperometric signal, which is caused by chemical oxidation of paracetamol by MnO_2.

Uric acid slightly decreases the amperometric signal.

Sample Analysis

Commercially available products containing H_2O_2, such as a hair blonding booster (Spray Blond) and a mouth wash (Bio-Garten medical H_2O_2 solution) were analysed using the FIA system. The results obtained by the amperometric method were 6.23 ± 0.11 and 2.73 ± 0.02%, respectively (three determinations employing the standard additions method). These corresponded excellently with values from the reference method (iodimetric titration), which gave 6.21 ± 0.06 and 2.80 ± 0.01%.[29]

Conclusion

The method presented here is a simple and fast procedure for the determination of H_2O_2 based on flow injection analysis. Its low detection limit and its applicability in neutral and slightly alkaline media suggest that the MnO_2 bulk-modified carbon paste can probably act as a useful electrode material for the development of biosensors. In this respect, the CPE bulk modified with MnO_2 supersedes a film-modified glassy carbon electrode, which shows a better detection limit of 4 μg l^{-1}, but is operated in strongly alkaline solutions.[5]

Compared with a platinum electrode, the optimum operating potential of the modified CPE is only slightly decreased.[35] However, the ease of modifying and handling the latter makes the MnO_2 modified electrode superior to Pt. Additionally, interferents which give a response at platinum electrodes at potentials comparable to that of H_2O_2 show an overpotential at CPEs and, therefore, interfere less severely.

Table 1 Relative changes in the current response of H_2O_2 in FIA in the presence of interferents. Flow rate, 1.2 ml min^{-1}; operating potential, 0.46 V *versus* Ag/AgCl; carrier, NH_3–NH_4Cl buffer (0.2 M); injection of 50 μl of an aqueous solution of H_2O_2 (20 mg l^{-1}) containing the interferent

Interferent	Changes in current (%)					
	1 mg l^{-1}	2 mg l^{-1}	5 mg l^{-1}	20 mg l^{-1}	100 mg l^{-1}	1000 mg l^{-1}
Na^+	0	0	0	0	0	0
K^+	0	0	0	0	0	0
Cd^{2+}	−8	−8	−11	−11	−22	−34
Cu^{2+}	−29	−36	−56	−70	−78	−100
Fe^{3+}	−3	−3	−8	−37	−80	−100
Pb^{2+}	0	−2	−5	−12	−100	
NO_3^-	0	0	0	0	0	0
SO_4^{2-}	0	0	0	0	0	0
ClO_3^-	0	0	0	0	0	0
ClO_4^-	0	0	0	0	0	0
$S_2O_8^{2-}$	0	0	0	0	0	0
PO_4^{3-}	0	0	0	0	0	−9
Tartrate	0	0	0	−4	−100	
BO_3^{3-}	0	0	−5	−100		
ClO^-	−23	−31	−45	−100		
VO_3^-	−9	−10	−26	−90	−100	
BO_3^-	0	0	0	0	+25	+194
Ascorbic acid	−14	−91	−89	−84	−57	+256
Paracetamol	−21	+9	−19	−9	+40	+351
Uric acid	−21	−23	−23	−19	−12	

References

1 Meiattini F., in *Methods of Enzymatic Analysis*, ed. Bergmeyer, H. U., VCH, Weinheim, 3rd edn., 1985, vol. 7, pp. 566–571.
2 Vogel, A. I., *Textbook of Quantitative Inorganic Analysis*, Longman, New York, 4th edn., 1981, p. 381.
3 Matsubura, C., Kawamoto, N., and Takamura, K., *Analyst*, 1992, **117**, 1781.
4 Oungpipat, W., Alexander, P., and Southwell-Kelly, P., *Anal. Chim. Acta*, 1995, **309**, 35.
5 Taha, Z., and Wang, J., *Electroanalysis*, 1991, **3**, 215.
6 Cai, X., Kalcher, K., Kölbl, G., Neuhold, C., Diewald, W., and Ogorevc, B., *Electroanalysis*, 1995, **7**, 340.
7 Kalcher, K., *Electroanalysis*, 1990, **2**, 419.
8 Kalcher, K., Kauffmann, J. M., Wang, J., Svancara, I., Vytras, K., Neuhold, C., and Yang, Z., *Electroanalysis*, 1995, **7**, 5.
9 Gorton, L., and Svensson, T., *J. Mol. Catal.*, 1986, **38**, 49.
10 Wang, J., Naser, N., Angnes, L., Wu, H., and Chen, L., *Anal. Chem.*, 1992, **64**, 1285.
11 Gao, Z., Ivaska, A., Li, P., Lui, K., and Yang, J., *Anal. Chim. Acta*, 1992, **259**, 211.
12 Cox, J. A., and Jaworski, R. K., *Anal. Chem.*, 1989, **61**, 2176.
13 Oyama, N., and Anson, F. C., *J. Electroanal. Chem.*, 1986, **199**, 467.
14 Rice, M. E., Galus, Z., and Adams, R. M., *J. Electroanal. Chem.*, 1983, **143**, 89.
15 Mizutani, F., Yabuki, S., and Katsura, T., *Denki Kagaku*, 1992, **60**, 1141.
16 Gorton, L., and Jönsson, G., *J. Mol. Catal.*, 1986, **38**, 157.
17 Mannino, S., Cosino, M. S., and Ratti, S., *Electroanalysis*, 1993, **5**, 145.
18 Itaya, K., Shoji, N., and Uchida, I., *J. Am. Chem. Soc.*, 1984, **106**, 3423.
19 Boyer, A., Kalcher, K., and Pietsch, R., *Electroanalysis*, 1990, **2**, 155.
20 Karyakin, A. A., Gitelmacher, O. V., and Karyakina, E. E., *Anal. Chem.*, 1995, **67**, 2419.
21 Chi, Q., and Dong, S., *Anal. Chim. Acta*, 1995, **310**, 429.
22 Karyakin, A. A., Karyakina, E. E., and Gorton, L., *Talanta*, 1996, **43**, 1597.
23 Linders, C. R., Vincke, B. J., and Patriarche, G. J., *Anal. Lett.*, 1986, **19**, 1831.
24 Wang, J., Ciszewski, A., and Naser, N., *Electroanalysis*, 1992, **4**, 777.
25 Gorton, L., *Electroanalysis*, 1995, **7**, 23.
26 *Gmelin Handbuch der Anorganischen Chemie*, Verlag Chemie, Weinheim, 8th edn., 1966, System Nummer 3 (O), Lieferung 7, pp. 2357–2359.
27 Kalcher, K., *Fresenius' Z. Anal. Chem.*, 1986, **323**, 238.
28 Kalcher, K., and Jorde, C., *Comput. Chem.*, 1986, **10**, 201.
29 Poetke, W., *Praktikum der Massanalyse*, Harri Deutsch, Thun, 3rd edn., 1987, pp. 178–179.
30 Stadlober, M., Kalcher, K., Raber, G., and Neuhold, C., *Talanta*, 1996, **43**, 1915.
31 Farsang, G., and Tomcsanyi, L., *Acta Chim. Acad. Sci. Hung.*, 1967, **52**, 123.
32 Engstrom, R. C., and Strasser, V. A., *Anal. Chem.*, 1984, **56**, 136.
33 Engstrom, R. C., *Anal. Chem.*, 1982, **54**, 2310.
34 Wang, J., *Analytical Electrochemistry*, VCH, New York, 1st edn., 1994, p. 61.
35 Tay, B.-T., Ang, K.-P., and Gunasingham, H., *Analyst*, 1988, **113**, 617.

Adsorptive Stripping Voltammetry of Bleomycin

Xuecai Tan, Jingbo Hu and Qilong Li*

Department Of Chemistry, Beijing Normal University, Beijing 100875, China

In 0.05 M H_2SO_4 solution, two reductive peaks, P_1 and P_2, of bleomycin were obtained. The peak potentials E_{P_1} and E_{P_2} were -0.83 and -1.09 V (*versus* Ag/AgCl), respectively. The sensitivity of P_2 was much higher than that of P_1. The peak current of P_2 was proportional to the concentration of bleomycin over the range 1.0×10^{-9}–1.0×10^{-7} M with a detection limit of 5.0×10^{-10} M using adsorptive voltammetry at an accumulation time of 120 s ($E_i = -0.80$ V). The behaviour of the reduction wave was studied and applied to the determination of bleomycin in mouse serum. The reduction process of P_1 was irreversible with adsorptive characteristics and the adsorption behaviour obeyed the Frumkin adsorptive isotherm. The adsorptive coefficient β was 8.9×10^5, the interaction factor α was 0.94 and the Gibbs energy of adsorption $\Delta G°$ was -33.93 kJ mol^{-1}. P_2 was an irreversible adsorption peak with catalytic hydrogen properties.

Keywords: Adsorptive stripping voltammetry; bleomycin; irreversible wave

Bleomycin (BLM) is a member of a family of structurally similar glycopeptide antibiotics recognized as antitumour drugs used in the treatment of Hodgkin's lymphoma and carcinomas of the testis, head, skin and neck. Its structure is shown in Fig. 1. The determination of BLM by gas chromatography and high-performance liquid chromatography has been reported.[1-3] However, the voltammetric behaviour of BLM and its determination have not been investigated so far. In this work, the voltammetric behaviour of BLM was studied and a method for the determination of trace amounts of BLM was developed. In 0.05 M H_2SO_4, two reductive peaks, P_1 and P_2, of BLM were obtained. The peak potentials E_{P_1} and E_{P_2} were -0.83 and -1.09 V (*versus* Ag/AgCl), respectively. The sensitivity of P_2 was much higher than that of P_1. A linear relationship held between the peak current of P_2 and the concentration of BLM in the concentration range 1.0×10^{-7}–1.0×10^{-9} M with good

precision and accuracy. After concentration for 120 s, the detection limit was 5.0×10^{-10} M. The method was applied to samples of mouse serum and satisfactory results were obtained. The electrode reaction mechanism is discussed.

Experimental

Apparatus

A Model 370 Electrochemistry System (EG&G Princeton Applied Research, Princeton, NJ, USA) was used for linear sweep and cyclic voltammetry, with a three-electrode system consisting of a hanging mercury drop electrode (HMDE) as the working electrode, an Ag/AgCl (saturated KCl) reference electrode and a platinum counter-electrode. The electrolytic cell was a 10 ml beaker. All experiments were performed at room temperature and dissolved oxygen was removed by passing pure nitrogen through the solutions.

Reagents

BLM was obtained from the Institute of Materia Medica, Chinese Academy of Medical Science (Beijing, China), with a purity of 98%. A 2.7×10^{-4} M stock standard solution of BLM was prepared by dissolving 10.2 mg in a small volume of triply distilled water and diluting to 25.0 ml; it was stored in the dark. The supporting electrolyte was 0.5 M H_2SO_4. All chemicals were of analytical-reagent grade. Triply distilled water was used throughout.

Procedure

A 10 ml volume of 0.05 M H_2SO_4 containing a specific amount of sample solution was added to the cell and purged with purified nitrogen for 4 min to remove oxygen. The pre-concentration potential (-0.80 V) was applied to a new mercury drop for 120 s. The voltamperogram was recorded by using a linear sweep scan. The scan was terminated at -1.15 V.

Results and Discussion

In 0.05 M H_2SO_4, two reductive waves, P_1 and P_2, of BLM were obtained by dc polarography. The wave of P_2 was a sharp peak and its height was much higher than that of P_1 (see Fig. 2).

Adsorptive Properties

Repetitive cyclic voltamperograms

Fig. 3 shows repetitive cyclic voltamperograms for 1.0×10^{-6} M BLM, recorded after preconcentration at -0.60 V for 30 s. Two cathodic peaks, P_1 and P_2, are observed in the first scan (curve a) at -0.83 and -1.09 V. The peak current of P_2 was much higher than that of P_1. Subsequent scans (curves band c) exhibited a substantial decrease in the peak to a stable value, showing that BLM has adsorptive characteristics at the mercury electrode.
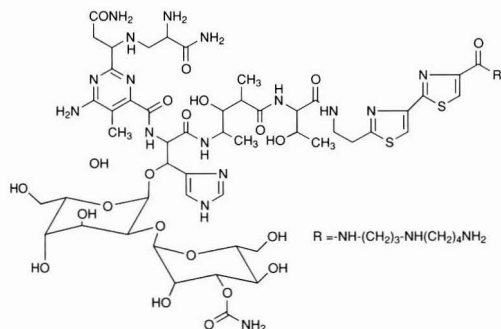
Fig. 1 Structure of BLM.

Effect of accumulation time

Fig. 4 shows plots of the cathodic peak currents (i_{pc}) of P_1 and P_2 in linear sweep voltammetry *versus* accumulation time (t) for different concentrations of BLM. At first, i_{pc_1} increased linearly with t, indicating that before adsorptive equilibrium is reached, the longer the accumulation time, the more BLM was adsorbed and the larger was the peak current. However, after a specific
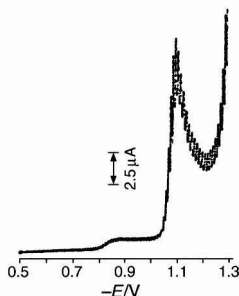
Fig. 2   Dc polarogram of BLM. Conditions: 0.05 M H_2SO_4, 6.5×10^{-5} M BLM, $V = 20$ mVs^{-1}, $t = 0.5$ s.
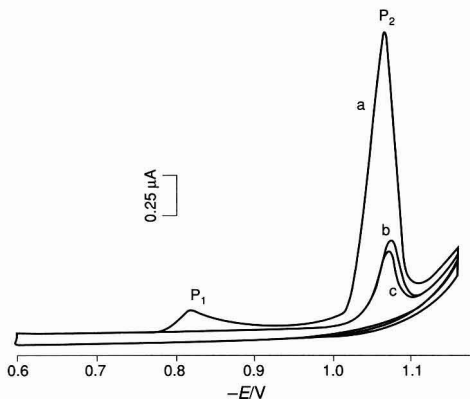
Fig. 3   Repetitive cyclic voltamperograms. Conditions: 0.05 M H_2SO_4, 1.0×10^{-6} M BLM, $V = 100$ mV s^{-1}, $t_{acc} = 30$ s.
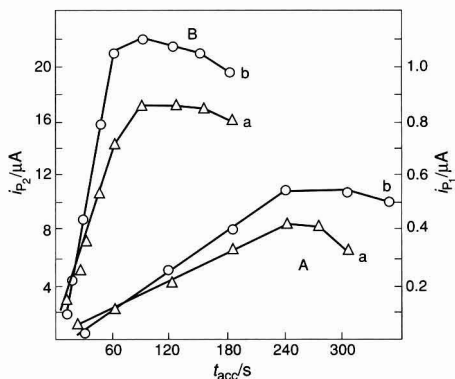
Fig. 4   Effect of accumulation time. A, P_1; B, P_2. BLM concentration: a, 1.0×10^{-7}; b, 5.0×10^{-7} M. Other conditions as in Fig. 2.

period of accumulation time, the peak current tended to level off, illustrating that adsorptive equilibrium of BLM on the mercury electrode surface was achieved.

Effect of scan rate

Fig. 5 shows the effect of scan rate on the peak current. The peak currents i_{pc_1} and i_{pc_2} increased with increasing scan rate. The experiments indicate further that when $t_{acc} = 0$ s, i_{pc_1} and i_{pc_2} show a linear relationship with $v^{1/2}$, illustrating that the reduction of BLM is diffusion controlled. When $t_{acc} = 60$ s, the i_{pc_1}–v and i_{pc_2}–v curves became a straight line, suggesting that the electrode process was adsorption-controlled.[4]

Measurement of amount of BLM adsorbed

After peak P_1 in the linear sweep voltammogram, the current decreased to the background level and the area under the peak was determined and the quantity of charge (Q) transferred by reduction was calculated. The amount of BLM adsorbed per unit area (Γ) was then obtained from $\Gamma = Q/nFA$, where A is the electrode area. A plot of $nF\Gamma$ as a function of BLM concentration (c_{BLM}) is shown in Fig. 6. A linear relationship between $\ln[c_{BLM}(1 - \theta)/\theta]$ *versus* θ was found, where $\theta = \Gamma/\Gamma_{max}$ and Γ_{max} is the maximum surface coverage, showing that BLM adsorption satisfies the Frumkin isotherm $\beta c_{BLM} = \theta \exp[\alpha\theta/(1 - \theta)]$ with adsorption coefficient $\beta = 8.9 \times 10^5$ l mol^{-1} and the interaction factor $\alpha = 0.94$.[5] The Gibbs energy of adsorption $\Delta G^0 = -33.93$ kJ mol^{-1}, indicating that the
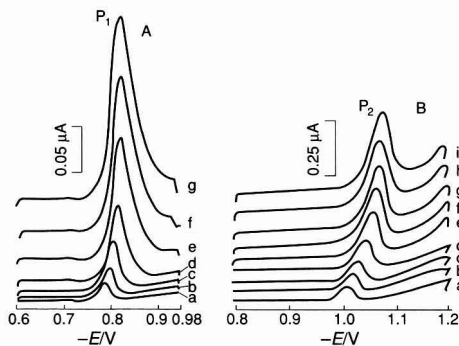
Fig. 5   Effect of scan rate (0.05 M H_2SO_4). A, P_1. Conditions: 2.0×10^{-6} M BLM, $t_{acc} = 60$ s, scan rate = a, 5; b, 10; c, 20; d, 50; e, 100; f, 150; and g, 200 mV s^{-1}. B, P_2. Conditions: 5.0×10^{-7} M BLM, $t_{acc} = 10$ s, scan rate = a, 5; b, 10; c, 20; d, 50; e, 100; f, 150; g, 200; h, 250; and i, 300 mV s^{-1}.
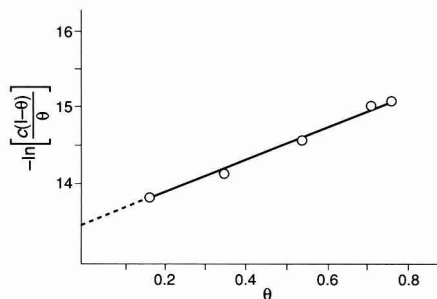
Fig. 6   Plot of $\ln[c_{BLM}(1 - \theta)/\theta]$ *versus* θ. Conditions: 0.05 M H_2SO_4, $t_{acc} = 30$ s, $v = 100$ mVs^{-1}.

reaction species has a stronger adsorption. The value of α depends primarily on the structure of the adsorbed particles and may also be a function of potential. The value of α is positive, indicating that the interactions between the adsorbed species on the electrode surface are attractive.

As mentioned above, BLM has adsorption characteristics, which can be used in an effective preconcentration step before the voltammetric measurement, hence a highly sensitive adsorptive stripping voltammetry of the drug can be obtained. Because the sensitivity of P_2 was much higher than that of P_1, peak P_2 was used in the determination of BLM.

Reversibility

In Fig. 3, it can be seen that no peaks are observed on the anodic branch of P_1 and P_2, indicating that the reduction of BLM at the Hg electrode is irreversible.

Hydrogen bubbles occur near the electrode when electrolysis is performed at the peak potential of P_2. The peak current of P_2 increased with increasing Britton–Robinson buffer capacity at the same pH value (4.35). These experiments indicated that P_2 showed catalytic hydrogen properties.

Measurement of the number of electrons transferred[6,7]

The number of electrons was determined by constant potential coulometry with a large area of the mercury cathode. Three portions of 0.05 M H_2SO_4 and concentrations of 7.7×10^{-5}, 6.5×10^{-5} and 8.5×10^{-5} M BLM were electrolysed at -0.85 V (*versus* SCE) for P_1, with consumption of 0.62, 0.52 and 0.73 C, respectively. The values of n, the number of electrons transferred, thus obtained were 1.9, 1.8 and 2.0, respectively, hence $n = 2$. For P_2, the electrolysis experiment was performed at -1.09 V after P_1 was completely electrolysed. A large current was still found after electrolysis for 200 min and indicated that the number of electrons was not determined because P_2 showed the properties of catalytic hydrogen.

Determination of α n and α

According to the Laviron equation[8] for the irreversible reduction wave:

$$W_{1/2} = 2.44RT/(\alpha nF) = 62.5/(\alpha n)\ (25\ °C)$$

where $W_{1/2}$ is the half-width of the peak. αn can be calculated to be 1.39 for P_1 when the scan rate $v = 100$ mV s^{-1}. P_1 of BLM undergoes a two-electron reduction, *i.e.*, $n = 2$, hence $\alpha = 0.69$.

In summary, in 0.05 M H_2SO_4, two reduction peaks of BLM, P_1 and P_2, were obtained. P_1 was an irreversible adsorption peak with a two-electron reduction process. P_2 was an irreversible adsorption peak with catalytical hydrogen properties.

Measurement by adsorptive stripping voltammetry

Selection of experimental conditions

In order to choose the optimum experimental conditions for the determination of BLM by adsorptive stripping voltammetry, a series of experiments were carried out. Various supporting electrolytes, such as H_2SO_4, HCl, NaOH, KCl, NH_3–NH_4Cl and HOAc–NaOAc buffer solutions were tested. H_2SO_4 was found to be the best because of the fairly well defined voltamperogram and reasonably high sensitivity. The effect of supporting electrolyte concentration on i_{pc_2} was examined. The results showed that i_{pc_2} increased with increasing H_2SO_4 concentration, and between 0.01 and 0.10M, i_{pc_2} remained almost constant at a high level, so 0.05 M H_2SO_4 was chosen for subsequent experiments. The effect of the preconcentration potential was also studied. i_{pc_2} increased with increasing preconcentration

Table 1 Analytical results for BLM in mouse serum

Sample No.	Found/µg ml^{-1}	Mean/µg ml^{-1}	RSD (%)
1	59.8		
	62.2		
	57.4	60.2	3.5
	61.2		
2	64.5		
	62.3		
	65.8	64.3	2.3
	64.6		
3	64.5		
	63.7		
	62.7	63.5	1.2
	63.2		

potential in the negative direction, then reached a constant value. A potential of -0.80 V was chosen as the optimum preconcentration potential. The stability of the system was fairly good.

Calibration graph and detection limit

Under the optimized conditions of 0.05 M H_2SO_4, a preconcentration potential of -0.80 V and a scan rate of 100 mV s^{-1}, the peak current of BLM was found to be proportional to its concentration over the range 1.0×10^{-9}–1.0×10^7 M when $t_{acc} = 120$ s.

According to IUPAC, the detection limit $DL = 3s/k$, where s is the standard deviation of replicate determination values under the same conditions as for the sample analysis in the absence of the analyte; k is the sensitivity, namely the slope of the calibration graph. Now, $n = 10$, $\bar{x} = 1.25 \times 10^{-2}$ µA, $s = 2.2 \times 10^{-4}$ µA, $k = 0.031 \times 10^8$ µA mol^{-1} l^{-1}, hence $DL = 3s/k = 3 \times 2.2 \times 10^{-4}/(0.031 \times 10^8) = 5.03 \times 10^{-10} \approx 5 \times 10^{-10}$ mol l^{-1}.

Analysis of Samples

Measurement of BLM in mouse serum was performed by adsorptive stripping voltammetry. The mouse serum was provided by the Biological Department in this university, which is engaged in studies of the action mechanism for anticancer drugs. BLM was administered to mice and the serum was analysed for BLM. No sample preparation was used other than dilution with the supporting electrolyte. The determination was accomplished by the standard additions method and the results of a few analyses are given in Table1. The relative standard deviation was about 1.2–3.5%. In addition, some recovery experiments were carried out and the recovery was 93.0–101.2%. The results confirm the usefulness of the proposed method for the determination of BLM.

References

1 Shiu, G. K., and Geehl, T. J., *J. Chromatogr.*, 1980, **181**, 127.
2 Aszalos, A., Gawfor, J., and Vollmer, P., *J. Pharm. Sci.*, 1981, **70**, 878.
3 Chang, T., Lee, T. M., and Borders, B., *J. Antibiot.*, 1984, **79**, 1098.

4 Li, Q. L., and Chen, S. A., *Anal. Chim. Acta*, 1993, **282**, 145.
5 Moncelli, M. R., Nucci, L., Mariani, P., and Guidelli, R., *J. Electroanal. Chem.*, 1985, **183**, 285.
6 Li, Q. L., *Huaxue Tongbao*, 1994, **10**, 13.
7 Li, Q. L., and Ji, G., *Talanta*, 1990, **37**, 937.
8 Laviron, E., *J. Electroanal.Chem.*, 1974, **52**, 355.

Trace Determination of Strong Acids in Nitro Plasticizers

Sylvain Désilets* and Sylvie Villeneuve

Defence Research Establishment Valcartier, 2459 Pie-XI Blvd. North, Val-Bélair, Québec, Canada G3J 1X5

A titration method was applied to the trace determination of strong acids in a variety of nitro plasticizers. The analyses were performed in acetonitrile using an automatic titrator and a calomel combined glass electrode for non-aqueous solutions. A dilute solution of sodium hydroxide (5.00×10^{-4} M) in methanol was used as the titrant. The sensitivity and precision of the method were greatly increased by the addition of a known volume of dilute nitric acid to the solvent in which the titrations were performed. Very low acid content values were detected in the plasticizers with the experimental conditions used. The detection limit was found to be 0.001 mg g^{-1} of NaOH in the sample (0.000 025 m equiv. g^{-1}) and the measured acid content values were reproducible.

Keywords: *Trace analysis; acids; nitric acid; plasticizers; non-aqueous solutions; titration*

The strong acid content in nitro plasticizers may play an important role in determining the condition of this class of components. Indeed, trace acidity can influence the processing and long-term stability of the various formulations made with these plasticizers. Since all the plasticizers involved in this study contained nitro (–NO$_2$), nitrate esters (–O–NO$_2$) or nitramine (–N–NO$_2$) functions, they may undergo some chemical decompositions which lead to the production of nitrogen dioxide (NO$_2$) over time, as is especially well documented in the case of the nitrate esters.[1]

The newly formed radical species of nitrogen dioxide readily react with the nearby molecules of RCH$_2$ONO$_2$. As a result, gaseous products, such as NO, N$_2$O, N$_2$O$_4$, N$_2$, CO$_2$, CO and H$_2$O, are formed.[2] Subsequent reaction of nitrogen oxide and nitrogen dioxide with trace amounts of water or moisture contribute to the presence of nitric acid[2,3] in the medium. Also, some residual nitric acid may be left from the processes used in the synthesis of the plasticizers. Consequently, the acidity detected in these compounds is mainly attributed to trace amounts of strong acids such as nitric acid.

Trace determination of nitric acid has already been carried out for low concentrations in polar snow[4] and for moderate concentrations in non-aqueous solution,[5–7] in aqueous solution,[8–10] in freshwater,[11] in various complex aqueous mixtures[12–14] and in atmospheric aerosol.[15,16] In our case, these procedures were found to be inappropriate for the trace determination of acids in an organic environment such as that of nitro plasticizers. In fact, the activity of the diluted acid species measured by the electrode is weaker in an organic medium than in an aqueous solution. Therefore, this phenomenon may strongly decrease the sensitivity of the analytical method. In spite of this factor, the present study shows how the acid content of nitro plasticizers may nevertheless be determined at a very low level in an organic medium.

Experimental

Nitro Plasticizers

The trace level of strong acid was determined for the following eight nitro plasticizers: (1) bis(2,2-dinitropropyl) acetal/formal [BDNPA/F, a 1 + 1 mixture by mass of bis(2,2-dinitropropyl)acetal (BDNPA) and bis(2,2-dinitropropyl) formal (BDNPF)], (2) butane-1,2,4-triol trinitrate (BTTN), (3) trimethylolethane trinitrate (TMETN), (4) triethylene glycol dinitrate (TEGDN), (5) diethylene glycol dinitrate (DEGDN), (6) butyl-2-nitratoethylnitramine (BuNENA), (7) ethyl-2-nitratoethylnitramine (EtNENA) and (8) methyl/ethyl-2-nitratoethylnitramine [Me/EtNENA, a 58 + 42 mixture by mass of methyl-2-nitratoethylnitramine (MeNENA) and ethyl-2-nitratoethylnitramine (EtNENA)]. Their structural formulae are shown in Fig. 1. For some of these plasticizers, the acid content was determined for more than one lot. The manufacturers of the plasticizers and their lot numbers are given in Table 1.
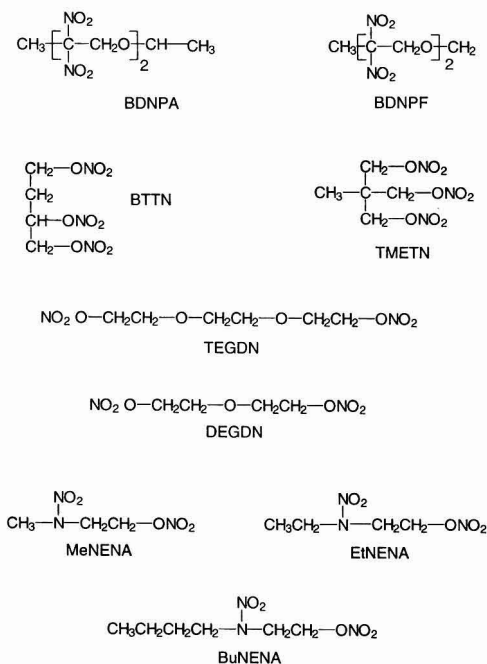
Fig. 1 Structural formulae of the nitro plasticizers analysed.

Reagents Used for Titrations

The titrations in an organic medium involved the use of various chemicals. Acetonitrile from Caledon Laboratories (Georgetown, ON, Canada) was used as the solvent. Concentrated nitric acid (15 M) from J. T. Baker (Phillipsburg, NJ, USA) was used to prepare a dilute 1.50×10^{-2} M solution in acetonitrile that was subsequently added in very small volumes to the pure acetonitrile solvent. The titrant consisted of a 5.00×10^{-4} M solution that was prepared with sodium hydroxide (J. T. Baker) in anhydrous analytical-reagent grade methanol (Caledon Laboratories) (water content <0.03%). This dilute titrant had to be stored in an airtight container in order to keep its concentration from changing over time. Potassium hydrogenphthalate (KHP, $M_r = 204$) from Fisher Scientific (Pittsburgh, PA, USA) was used to calibrate the titrant.

Automatic Titrator

The titrations were performed using a Mettler (Highstown, NJ, USA) DL21 automatic titrator with a Mettler DG 113-SC calomel combined glass electrode with movable sleeve designed for titrations in non-aqueous solutions. The reference electrolyte contained in the electrode consisted of a saturated AgCl solution of 1 M LiCl in ethanol. As a pre-operational treatment, the glass membrane was activated by placing the electrode in de-ionized water for 1 d. The electrode was stored in the 1 M LiCl solution. The maximum volume of the Mettler DV905 interchangeable burette was 10 ml.

Titration Parameters

Various parameters were configured on the automatic titrator to allow the titrations to be performed under specific conditions. The standard titration mode and with the 'steepest jump' titration method were chosen. The increment in the steep region of the titration curve was reduced to 0.01 ml. A stirring time of 60 s was chosen to allow homogenization and dissolution of the sample before measurement of the initial potential and before the start of the titration. The chosen units were mol l^{-1} for the calibration of the titrant and mg g^{-1} for the determination of strong acids in the nitro plasticizers. Before starting a series of titrations, the electrode was pre-soaked in acetonitrile solvent for the purpose of improving performance which is critical for trace determinations. Between titrations, the electrode was cleaned by stirring it for 60 s first in acetone and then in acetonitrile.

Table 1 Acid content of nitro plasticizers as determined by the titration method

Plasticizer	Manufacturer*	Lot number	Acid content/ mg g^{-1}
BDNPA/F	Aerojet	2Q-118-007	0.009
TEGDN	Trojan	EJ-02E	0.018
TEGDN	Trojan	JD-04E	0.004
TEGDN	ICI	XDP-664-001	0.027
TMETN	Trojan	EE-31M	0.002
TMETN	Trojan	ID-07M	0.005
TMETN	ICI	A-624-001/4472	0.006
BTTN	Trojan	GC-07B	0.047
BTTN	Trojan	JE-10B	0.018
BTTN	ICI	D-623-003	0.009
DEGDN	Trojan	EI-10D	0.018
BuNENA	ICI	RXL-647	0.106
EtNENA	ICI	RXL-663	0.063
Me/EtNENA	ICI	RXL-692	0.045

* Aerojet, (Sacramento, CA, USA); Trojan, (Spanish Fork, UT, USA); ICI, (Tamaqua, PA, USA).

Results and Discussion

Standardization of the Titrant

The mother solution used to prepare the actual titrant was obtained by dissolving 1.00 g of NaOH in 1 l of anhydrous methanol. It was readily calibrated by titration with KHP. This procedure involved drying 0.02 g of KHP in an oven overnight, dissolving it in 60 ml of distilled water and titrating it with the 2.50×10^{-2} M NaOH mother solution. The mother solution was then diluted by a factor of 50 in order to obtain a 5.00×10^{-4} M NaOH solution to be used as the actual titrant. A dilution factor of 50 might lead one to think that the accuracy could be affected by introducing additional CO_2 or water possibly present in methanol. However, by using the anhydrous or a low water content grade of methanol (water content <0.03%), the concentration of carbonic acid present in methanol would be expected to be low. It is also assumed that a solvent of such quality has been treated with appropriate purification procedures.[5] In any case, the direct standardization of the diluted titrant (5.00×10^{-4} M) would clearly eliminate the possible error from the dilution factor of 50. However, this would need a very small amount of KHP, probably added from a diluted standard solution, which may lead to a 'steepest jump' smoothed and/or to the absence of an end-point from the weak stimulation of the electrode by the diluted KHP.

A determination was also performed with an added volume of a calibrated diluted HNO_3 solution subsequently titrated with the 5.00×10^{-4} M NaOH solution. The similarity between the expected value and the result obtained demonstrated that the titrant had not been significantly changed by factors other than the dilution factor of 50. Actually, changes in the molarity originating from the presence of carbonic acid in the methanol were not detected and were thus deduced to be lower than the precision of the titration method.

Blank Determination

The need to use a blank arose from unsuccessful attempts at performing direct titrations on the plasticizer samples. As an example, the direct titration of 2.0 g of BDNPA/F in 60 ml of acetonitrile with the 5.00×10^{-4} M NaOH solution is presented in Fig. 2. The curve does not show any well defined equivalence point. Many trials were performed with dilute NaOH solutions of various concentrations from 2.50×10^{-2} to 5.00×10^{-4} M, but no significant changes were observed.

From these results, it was deduced that the titration medium needed the addition of some nitric acid to stimulate the electrode and to act as a blank for the subsequent trace determinations of strong acids. The addition of a compound such as a tetraalkylammonium salt in the titration medium[5] could also have been a valuable alternative with the advantage of introducing no additional HNO_3 in the titrated plasticizers. However, considering the fact that the plasticizers already contained HNO_3 and
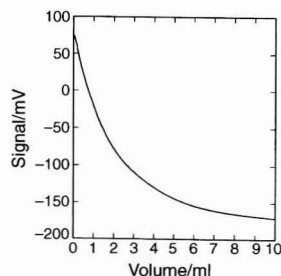
Fig. 2　Direct titration curve for BDNPA/F. Titrant: 5.00×10^{-4} M NaOH solution in methanol.

that no decomposition or formation of more acid in all the nitro plasticizers over a period of many months had been observed (by subsequent titrations), it was determined that HNO_3 was the best compound to be used in order to stimulate the electrode. The approach of adding a tetraalkylammonium salt should be considered in the case of nitro plasticizers showing a degradation in additional HNO_3.

It was decided to determine the lowest nitric acid volume that would give a successful titration in acetonitrile by showing a well defined curve. Many unsuccessful attempts were made with HNO_3 and NaOH solutions of various concentrations. As shown in Fig. 3, typical titration curves for blank determination were finally obtained with added volumes of 45, 22 and 11 µl of 1.50×10^{-2} M HNO_3 using the 5.00×10^{-4} M NaOH solution as the titrant. The 22 and 45 µl curves show a well defined equivalent point identified by dotted lines whereas the 11 µl curve can be considered as the limiting volume since it has no significant equivalent point. In the 22 and 45 µl titration curves, the positive jump of the potential observed at the beginning of the titration (from 0 to 0.5 ml) is caused by the drastic polarity change of the acetonitrile solution induced by the first drops of methanol that were added from the titrant. In fact, in one experiment, 1.0 ml of pure methanol added before the titration completely eliminated this positive jump in the curve and could possibly be used to increase the precision in other experiments. However, since this additional procedure did not significantly change the shape of the curve in the 'steepest jump' region specifically, it did not actually improve the determination of the end-point and was thus not incorporated in the analytical method.

Since the 22 µl volume gave a well defined curve with an equivalent point, it was chosen as the volume to be added to the acetonitrile solvent in order to perform the blank and acid content determinations.

Determination of Strong Acid Concentrations

The titrations for the determination of the strong acid content in nitro plasticizers were performed in 60 ml of acetonitrile to which 22 µl of 1.50×10^{-2} M HNO_3 was added to stimulate the electrode. Between 1.5 and 2.0 g of a given nitro plasticizer was used. However, about 0.2 g of material was used with the NENAs because the acid content of these plasticizers was higher.

The addition of HNO_3 significantly improved the sensitivity and precision of the titration method, as may be observed in Fig. 4, where titration curves for various nitro plasticizers are depicted. For all these curves, the equivalence points are sharp and well defined. It is also noticeable in all cases that the end-points do not appear at 0 mV, but rather at a positive potential value. The curves show that the strong acid determination, even at the trace level, can readily be achieved.
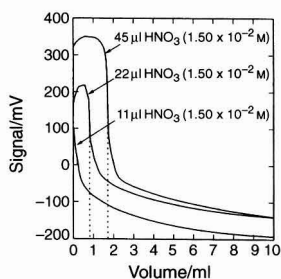
Table 1 shows the acid content values in mg g^{-1} of NaOH in the sample for each of the nitro plasticizers as determined by the titration method. The following equation was used by the titrator to calculate the acid content:

$$\text{acid content (mg g}^{-1}\text{NaOH)} = (V_S - V_B) C_T \frac{M_{rT}}{M_S} \qquad (1)$$

where V_S = volume of the NaOH titrant (ml) used to titrate the plasticizer sample to which 22 µl of 1.5×10^{-2} M HNO_3 were added, V_B = volume of the NaOH titrant (ml) used to titrate the 22 µl of the blank 1.5×10^{-2} M HNO_3 solution, C_T = concentration of the NaOH titrant (mol l^{-1}), M_{rT} = relative molecular mass of NaOH titrant (40.0 g mol^{-1}) and M_S = mass of the plasticizer sample (g).

Each value for the 14 plasticizers in Table 1 corresponds to an average of between three and nine measurements. The RSDs calculated from these results varied between 6 and 20%. Many lots were analysed twice or three times at intervals varying between 2 and 6 months. For these lots, the acid content measured from month to month was found to be constant within an identical lot. It is interesting to note that for various lots of the same material, the difference between acid content values could be considerable (e.g., 0.004 mg g^{-1} for TEGDN JD-04E and 0.027 mg g^{-1} for TEGDN XDP-664-001). Also, the NENAs showed the highest acid content values, ranging between 0.045 and 0.106 mg g^{-1}.

Once again considering the problem of the dilution of the titrant and its absorption of CO_2, all the analyses of the same plasticizers performed with the same dilute 5×10^{-4} M NaOH solution over a period of a few months showed reproducible results for the acid content, suggesting a negligible effect of additional atmospheric water and/or CO_2 absorbed by an older NaOH titrant. With the analytical procedure used in this paper and from many hundreds of titration experiments with either the same NaOH solution (5×10^{-4} M) or with a new freshly prepared solution, no significant changes of the titrant concentration with time or from the dilution factor of 50 were ever observed, probably because of the low water content or possibly because of the low solubility of CO_2 in methanol.

As for the accuracy of the determination, Grunwald[17] observed that the titration activity coefficients of ionic species may deviate greatly from unity in organic media of low and intermediate dielectric constants. The short-range ion-pair formation (from a low dielectric solvation shell) responsible for this deviation of the ion activities may also affect the position and the accuracy of the inflection point in potentiometric titrations.[17] Consequently, in our case, the accuracy of the acid content determination had to be demonstrated by using additional calibrated volumes (similar to the amount of acid contained in the plasticizer) of the dilute nitric acid solution which were added to the BDNPA/F plasticizer sample. The additional nitric acid was therefore measured with an accuracy

Fig. 3 Blank determinations in acetonitrile for which the added volume of the 1.50×10^{-2} M HNO_3 solution in acetonitrile was varied. Titrant: 5.00×10^{-4} M NaOH solution in methanol.
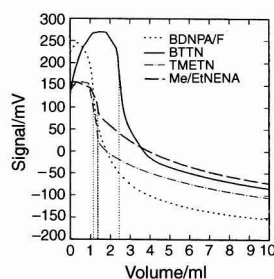
Fig. 4 Titration curves for various plasticizers with 22 µl 1.50×10^{-2} M HNO_3 solution in acetonitrile added to the solvent. Titrant: 5.00×10^{-4} M NaOH solution in methanol.

of better than 10% for BDNPA/F, which suggests an acceptable accuracy of the titration method made on the nitro plasticizers.

The limit of detection of the titration method was evaluated from the TMETN plasticizer results which had the lowest acid content. In fact, the acid concentration of TMETN evaluated at 0.002 mg g^{-1} NaOH was almost undetectable from the titration curve. The limit of detection was deduced to be 0.001 mg g^{-1} NaOH (0.000025 mequiv. g^{-1}) from a titration experiment performed with a TMETN sample of half its usual size. From our experience, the limiting factors of detection at a lower concentration are the solubility of the plasticizer in acetonitrile and the high viscosity of the solutions.

Conclusions

A titration method for the trace determination of strong acids in nitro plasticizers was successfully applied with an automatic titrator and a calomel combined glass electrode designed for titrations in non-aqueous solutions. The acidity in the compounds studied was mainly attributed to trace amounts of nitric acid.

The direct titration of nitro plasticizer samples was found to be inappropriate for the trace determination of strong acids. The organic medium in which the titrations were performed needed the addition of a known volume of a dilute solution of HNO$_3$ which would act both as an electrode activator and a blank. The addition of HNO$_3$ significantly increased the sensitivity and precision of the titration method.

Reproducible acid content values were obtained from month to month for the titration of nitro plasticizers. The method was sensitive enough to detect very low acid contents (0.001 mg g^{-1} NaOH in the sample).

References

1 Hiskey, M. A., Brower, K. R., and Oxley, J. C., *J. Phys. Chem*, 1991, **95**, 3955.
2 Druet, L. M., and Asselin, M., *J. Energ. Mater.*, 1988, **6**, 27.
3 *The Merck Index—An Encyclopedia of Chemicals, Drugs and Biologicals*, Merck, Rahway, NJ, USA, 10th edn., 1983, p. 947.
4 Legrand, M. R., Aristarain, A. J., and Delmas, R. J., *Anal. Chem.*, 1982, **54**, 1336.
5 Kucharsky. J., and Safarik, L., *Titrations in Non-aqueous Solvents*, Elsevier, Amsterdam, 1965.
6 Saigal, B., Joshi, G. K., and Khatri, H. K., *Asian J. Chem.*, 1993, **5**, 366.
7 Denisova, N. I., and Golubeva, A. A., *J. Anal. Chem. USSR*, 1972, **27**, 1221.
8 Molt, K., and Cho, Y. J., *J. Mol. Struct.*, 1995, **349**, 345.
9 Meites, L., Faneli, N., and Papoff, P., *Anal. Chim. Acta*, 1987, **192**, 33.
10 Wu, Y. C., Feng, D., and Koch, W. F., *J. Solution Chem.*, 1989, **18**, 641.
11 Rogeberg, E. J., and Kallqvist, T., *Vatten*, 1988, **44**, 89.
12 Lindroos, K., *Analyst*, 1987, **112**, 71.
13 Nakashima, T., and Lieser, K. H., *Radiochim. Acta*, 1986, **39**, 149.
14 Shutov, G. M., Berg, V. K., Chirkova, R. G., and Orlova, E. Y., *J. Anal. Chem. USSR*, 1972, **27**, 807.
15 Tanner, R. L., *Adv. Chem. Ser.*, 1993, **232**, 229.
16 Koutrakis, P., Wolfson, J. M., and Spengler, J. D., *Atmos. Environ.*, 1988, **22**, 157.
17 Grunwald, E., *Anal. Chem.*, 1954, **26**, 1696.

AUTHOR INDEX

Where on the paper an asterisk appears against the name of one or more authors, it indicates the author(s) to whom correspondence should be addressed.

Book Reviews

Flow Injection Analysis of Pharmaceuticals Automation in the Laboratory
Edited by J. Martinez Calatayud. Pp. vii + 394. Taylor & Francis. 1996. Price £75.00. ISBN 0-7484-0445-7.

Flow injection analysis (FIA) is now well accepted as a sample handling technique in the laboratory. Since it was introduced about 20 years ago there has been a rapid growth in research output relating to FIA including a vast number of methods for every conceivable analyte. In this book the author gives an overview of flow injection analysis as applied to the analysis of pharmaceuticals and related products. It is split into five parts; part one is an introduction to automation in the laboratory, part two is a general overview of flow injection analysis and parts three to five are devoted to FIA applications to pharmaceuticals classified by the method of detection, *i.e.*, UV/VIS absorption, fluorescence, chemiluminescence, biochemical, *etc.*

> ## This is a good comprehensive text on the theory and practice of FIA.

This is a good comprehensive text on the theory and practice of FIA, the general overview is very full and while all of the applications are pharmaceutical, each separate section has a general introduction before describing specific applications. The only criticism is the lack of a chapter on the control of FIA systems by computers. While a few FIA systems are commercially available, most workers configure their own systems and such a chapter would have been very useful. There is a good index, diagrams are clear and the cited references are as up to date as can be expected for a book (1995).

Overall I can thoroughly recommend this book, not only to pharmaceutical chemists but to any analytical scientist with an interest in flow injection.

S. W. Lewis
6/90127A   *Deakin University*
Australia

Strategies in Size Exclusion Chromatography
Edited by Martin Potschka and Paul L. Dubin. *ACS Symposium Series 635.* Pp. xiii + 415. American Chemical Society. 1996. Price $109.95. ISBN 0-8412-3414-0.

Size exclusion chromatography (SEC) is still expanding; while it enjoys the status of a mature technique with increasing numbers of applications in polymer and biological chemistry, there is also active development of the understanding of the fundamentals. The American Chemical Society (ACS) continues to reflect progress in SEC through the publication of symposium proceedings, and this volume is the latest in a distinguished series. It is developed from a symposium held at the 209th ACS National Meeting in 1995 in Anaheim, California, and contains 21 chapters by a total of 51 authors, the majority from Europe and USA.

> ## Progress is being made with the long-term problem of defining molecular 'size' in the context of SEC.

There are four main themes which mirror major current research areas in SEC: detector technologies; column based

analysis; synthesis and characterization of stationary phase packings; and applications to new polymer systems. Progress in detection is represented by two chapters, one on the determination of the molecular weights of copolymers by SEC with light scattering detection, and one on coupled multi-angle light scattering and viscometric detection. Eight chapters then take up column based analysis, with discussions of the modelling of SEC to the fore. Here it is gratifying to learn that progress is being made with the long-term problem of defining molecular 'size' in the context of SEC. A unified thermodynamic model for polymer separations by SEC, hydrodynamic chromatography and gel electrophoresis will be of special interest to separation scientists from other disciplines. New stationary phases are discussed in two further chapters, which are introduced by a review chapter. There is appropriate emphasis here on media for aqueous SEC. Applications are a strong feature, and eight final chapters describe the use of SEC in topics as diverse as studies of 'critical chromatography', micelle formation, poly(styrenesulfonates), glucans and other polysaccharides, and polyvinyl alcohol. There is a comprehensive index.

The level of the discussion in virtually all of the chapters makes this very much a book for the SEC expert. The more general analyst wishing to learn of current progress in this important branch of chromatography will, however, also find material of interest.

Keith D. Bartle
6/901231   *University of Leeds*

Instrumental Element and Multi-element Analysis of Plant Samples. Methods and Applications
By Bernd Markert. Translated by Brooks Haderlie. Pp. xvi + 296. Wiley. 1996. Price £65.00. ISBN 0-471-95865-4.

This is a comprehensive text that covers all the aspects of the relevant information of the occurrence and significance of chemical elements in plants, and all aspects of the analytical procedure from sampling, through sample processing to the analytical instrument. A lot of information is covered in relatively few (296) pages and hence some areas are limited, *e.g.*, a description of different instrumental measuring methods.

The book is conveniently divided into three parts: 'Occurrence and Significance of Chemical Elements in Plants'; 'Use of Plants in Bioindication'; and 'Instrumental Analysis of Plant Samples'. The former part consists of four chapters; a brief review of some of the previous studies dealing with the broad field of elemental occurrence in the biosphere.

In the second part there is one chapter which treats the use of plants as bioindicators, with emphasis on the peculiarities of the elemental status of mosses.

In Chapter 6, the individual analytical steps and their effect on the accuracy and precision of the analytical results are described in some details (49 pages). Thereafter, this chapter covers a range of applications of the instrumental measuring methods for the analysis of environmental samples. The emphasis here is on the comparison of the capabilities of direct methods [*e.g.*, neutron activation analysis (NAA), and X-ray fluorescence analysis (XRFA)] and composite methods (*e.g.*, atomic emission spectrometry with inductively coupled plasma (ICP-AES), mass spectrometry with inductively coupled plasma (ICP-MS), and atomic absorption spectrometry (AAS).

However, there is one substantial omission. As would be apparent from the title, simultaneous electrothermal atomic absorption spectrometry is not described in this book. However, this is not an important objection, because most of the up to date books that cover analytical instrumentation treat all the previous techniques in depth.

Overall, the book gives an excellent overview of the elemental composition of plants, describing the influence of their surroundings on element uptake by different plant species, and of some multi-element techniques.

The data provided in the six appendices are very useful, such as: essentiality, occurrence, toxicity, and uptake form of naturally occurring elements in the environment (Appendix 1); estimated annual production of individual elements for the year 2000 (appendix 2); correlation matrix for 45 different elements from 13 plant species (Appendix 3); analytical flow chart for the instrumental multi-element analysis of environmental samples (Appendix 4); the quality control of related, original analytical data by comparison of analytical results using the different instrumental techniques for different plant materials are included for particular elements (Appendix 5); and the spectrum of concentration and methods for the instrumental multi-element analysis of environmental samples (Appendix 6).

Overall, the book gives an excellent overview of the elemental composition of plants, describing the influence of their surroundings on element uptake by different plant species, and of some multi-element techniques. The authors have done a splendid job of making the subject 'accessible' for undergraduate and postgraduate students in environmental and analytical chemistry. Also, this book will be a useful source of material for those workers involved in environmental analysis.

J. L. Burguera
7/90037F   *Los Andes University*
Venezuela

Conference Diary

1997

Pollutec 97 Industrie

September 30-October 3

Paris, France

For further details contact: Michele Jackson or Gerard Witty, Promosalons UK Ltd. Telephone: +44 (0)171 221 3660; Fax: +44 (0)171 792 3525

4th International Symposium on Environmental Geochemistry

October 5-10

Vail, CO, USA

For further details contact: R. C. Severson, U.S. Geological Survey, Federal Center, Box 25046, MS 973, Denver, CO 80225, USA. Telephone: +1 303 236 5514; Fax: +1 303 236 3200; E-mail: iseg@helios.cr.usgs.gov

Metals in Environmental Health and Disease - Chemical Analysis and Biological Monitoring of Metal Exposures

October 6-8

Washington, DC, USA

For further details contact: Course Coordinator: Ruth Murphy, Department of Education Services, Armed Forces Institute of Pathology, Washington, DC 20306-6000, USA. Telephone: (202) 782 5021; Fax: (202) 782 7164; Internet: came@email.afip.osd.mil; Web Site: http://www.afip.mil

Solvent Selection for Pesticide Residue Analysis - Extraction, Partitioning from Agricultural Environmental Samples: Plants, Soil, Water

October 6-9

Angers, France

For further details contact: Congres Scientifiques Services (C2S), Solvent Selection, Chantal Iannarelli, 2 rue de Villarmains, 92210 Saint Cloud, France. Telephone (33) 01 47 71 90 04; Fax: (33) 01 47 71 90 05; E-mail: c2s@club-internet.fr

1st Euroconference on Environmental Analytical Chemistry

October 11-17

Neusiedl, Austria

For further details contact: Dr Erwin Rosenberg, Institute of Analytical Chemistry, TU Wien, Getreidemarkt 9, A-1060 Wien, Austria. Fax: +43 1 5867813; E-mail: erosen@fbch.tuwien.ac.at; WWW-page: http://www.iac.tuwien.ac.at/~euconeac/welcome.html

BCEIA '97, The 7th International Beijing Conference and Exhibition on Instrumental Analysis

October 14-18

Shanghai, China

For further details contact: BCEIA '97 General Service Office, Room 585, Chinese Academy of Sciences Building, San Li He, Xi Jiao, PO Box 2143, Beijing 100045, China. Telephone: +86 10 8511133 Ext. 1585, +86 10 8511814; Fax: +86 10 8511814; E-mail: bceia@aphy01.iphy.ac.cn

Chiral Europe '97

October 16-17

London, UK

For further details contact: Spring Innovations Ltd., 185A Moss Lane, Bramhall, Stockport, Cheshire, UK SK7 1BA. Telephone: +44 (0)161 440 0082; Fax: +44 (0)161 440 9127; E-mail: spring.innovations@dial.pipex.com; http://www.spring-innovations.co.uk/

35th International Exhibition of Chemistry, Analysis, Research, Test Equipment and Biotechnology

October 21-24

Milan, Italy

For further details contact: General Secretariat, 20149 Milano, Italy - Via Domenichino, 11 (C.P. 15117 - 20150 Milano, Italy). Telephone: +39 2 4815541; Fax: +39 2 4980330; E-mail: assoexpo@assoexpo.com; http://www.assoexpo.com

15th MOSAN (Congress-Exhibition of Health Equipment, Products, Services, Technologies and Events)

October 21-24

Milan, Italy

For further details contact: General Secretariat, 20149 Milano, Italy - Via Domenichino, 11 (C.P. 15117 - 20150 Milano, Italy). Telephone: +39 2 4815541; Fax: +39 2 4980330; E-mail: assoexpo@assoexpo.com; http//www.assoexpo.com

24th Annual Meeting of the Federation of Analytical Chemistry and Spectroscopy Societies

October 26-30

Providence, RI, USA

For further details contact: Jo Ann Brown, Federation of Analytical Chemistry and Spectroscopy Societies, 210B Broadway Street, Frederick, MD 21701, USA. Telephone: +1 301 694 8122; Fax: +1 301 694 6890; E-mail: jbrownsas@aol.com

8th Symposium on Handling of Environmental and Biological Samples in Chromatography. 26th Scientific Meeting of the Group of Chromatography and Related Techniques of the Spanish Royal Society of Chemistry

October 26-29

Almeria, Spain

For further details contact: M. Frei-Häusler, IAEAC Secretariat, Postfach 46, CH-4123 Allschwil 2, Switzerland. Fax: +41 61 482 08 05

ISPPP '97: 17th International Symposium on the Separation of Proteins, Peptides and Polynucleotides

October 26-29

Washington, DC, USA

For further details contact: Janet Cunningham, Barr Enterprises, P.O. Box 279, Walkerville, MD 21793, USA. Telephone: +1 301 898 3772; Fax: +1 301 898 5596; E-mail: Janetbarr@aol.com

Fourth PharmAnalysis Europe Conference and Table-Top Exhibition

October 27-28

London, UK

For further details contact: Advanstar Communications, Conference Division, Advanstar House, Park West, Sealand Road, Chester CH1 4RN, UK. Telephone: +44 (0)1244 378 888; Fax: +44 (0)1244 370 011

1997 Eastern Analytical Symposium

Somerset, NJ, USA

November 16-21

For further details contact: EAS, P.O. Box 633, Montchanin, DE 19710-0633, USA. Telephone: (302) 738-6218; Fax: (302) 738-5275; E-mail easinfo@aol.com; Internet: http://www.eas.org/index.htmlanlcd

NanoTech '97

Montreux, Switzerland

November 17-21

For further details contact: Dave Morehouse, Conference Coordinator, Scitec, Conference Coordination Office, Av. de Provence 20, CH-1000 Lausanne 20, Switzerland. Telephone: +41 21 626 46 30/626 23 53; Fax: +41 21 624 15 49; E-mail: symposia@worldcom.ch; http://www.sitec-robotics.com

Inchem Tokyo '97 - The 21st International Trade Fair for Chemical and Process Engineering

Tokyo, Japan

November 18-21

For further details contact: The Secretariat of Inchem Tokyo, Convention Division, c/o Japan Management Association, 3-1-22 Shiba-koen, Minato-ku, Tokyo 105, Japan. Telephone: +81 3 3434 1391; Fax: +81 3 3434 8076; http://www.jma. or.jp/CONVENTION/INCHEM97/inframe.htm

The 2nd Mediterranean Basin Conference on Analytical Chemistry

November 23-28

Rabat, Morocco

For further details contact: Professor Abderrahmane Laachach, Laboratoire de Chimie Analytique, Ecole Nationale de l'Industrie Minerale, Av. Hadj Ahmed Cherkaoui, B.P. 753 Agdal Rabat, Morroco. Telephone: +212 (7) 77 13 60 and 77 16 67; Fax: +212 (7) 77 45 37 and 77 10 55

Symposium on Radionuclide Containment in Radioactive Waste Disposal

December 10

Loughborough, UK

For further details contact: Dr. P. Warwick. Telephone: 01509 222585; E-mail P.Warwick@lboro.ac.uk or from Dr S. J. King. Telephone: 01509 222545; E-mail: S.J.King@lboro.ac.uk. Department of Chemistry, Loughborough University, Loughborough, Leics., UK LE11 3TU

3rd BMSS LC/MS Symposium

December 17-18

Cambridge, UK

For further details contact: Dr J. Oxford, BMSS, P.O. Box 38, Royston, Herts, SG8 5BX, UK

1998

2nd Symposium on the Analysis of Well Characterized Biotechnology Pharmaceuticals

January 5-7

San Francisco, CA, USA

For further details contact: Joan Saluzzi, Rhema Association Management, P.O. Box 411106, San Francisco, CA 94141-1106, USA. Telephone: 415-487-9876; Fax: 415-487-9875; E-mail: society@hooked.net; Website: http://www.hpl.hp.com/casss/wcbp

1998 Winter Conference on Plasma Spectrochemistry

January 5-10

Scottsdale, AZ, USA

For further details contact: Ramon Barnes, Department of Chemistry, Lederle GRC Towers, University of Massachusetts, Box 34510, Amherst, MA 01003-4510. Telephone:+1 413 545 2294; Fax: +1 413 545 3757; E-mail: winterconf@chem.umass.edu

HPCE '98 - Eleventh International Symposium on High Performance Capillary Electrophoresis and Related Microscale Techniques

January 31-February 5

Orlando, Florida, USA

For further details contact: Shirley Schlessinger, Symposium Manager, 400 East Randolph Street, Suite 1015, Chicago, IL, USA. http://www.hpl.hp.com/casss/hpce98

International Conference on Arsenic Pollution of Ground Water in Bangladesh: Cause, Effect and Remedy

February 9-11

Dhaka, Bangladesh

For further details contact: In Bangladesh: Professor Quazi Quamruzzaman, Chairman, Dhaka Community Hospital Trust, 1089 Malibagh Choudhurypara, Dhaka 1219, Bangladesh. Telephone: 88-02-834887/88-02-416583; E-mail: dch@bangla.net. In India: Dr Dipankar Chakraborti, Director, School of Environmental Studies, Jadavpur University, Calcutta-700032, India. Telephone: 00-91-33-473-5233; Fax: direct 00-91-33-473-4266; E-mail: dcsoesju@giascl 01.vsnl.net.in

Fifth International Symposium on Hyphenated Techniques in Chromatography and Hyphenated Chromatographic Analyzers

February 11-13

Bruges, Belgium

For further details contact: Ordibo bvba, Lucas Henninckstraat 18, B-2610 Wilrijk Antwerp, Belgium. Telephone: +32 3 561 2831 or +32 3 217 2905; Fax: +32 3 827 8439; E-mail: smitsr@innet.be

28th Annual International Symposium on Environmental Analytical Chemistry

March 1-5

Geneva, Switzerland

For further details contact: Mrs M. Frei-Haeusler, IAEAC Secretariat, P. O. Box 46, CH-4123 Allschwil 2, Switzerland. Fax: +41 61 482 0805; E-mail: iaeacmfrei@access.ch

PITTCON '98

March 1-6

New Orleans, LA, USA

For further details contact: The Pittsburgh Conference, 300 Penn Center Blvd., Suite 332, Pittsburgh, PA 15235-5503, USA. Tel: +1 412 825 3220; Fax: +1 412 825 3224; E-mail: expo@pittcon.org

28th Annual International Symposium on Environmental Analytical Chemistry

March 2-5

Geneva, Switzerland

For further details contact: Mrs M. Frei-Hausler, IAEAC Secretariat, Postfach 46, CH-4123 Allschwil 2, Switzerland. Telephone: +41 61 481 2789; Fax: +41 61 482 0805

InCom '98, International Symposium on Instrumentalized Analytical Chemistry and Computer Technology

March 23-27

Dusseldorf, Germany

For further details contact: Werner Gunther, InCom Bureau, Postfach 30 10 45, 40410 Dusseldorf, Germany. Tel: +49 211 45 08 54; Fax: +49 211 45 42 442; E-mail: incom@mail.graffix.de; http://www.incom-symposium.de

7th Latin American Congress on Chromatography and Related Techniques

March 25-27

Aquas de Sao Pedro, Brazil

For further details contact: Prof. Dr. Fernando Lancas, University of Sao Paulo, Institute of Chemsitry at Sao Carlos, 13560-970 Sao Carlos (SP), Brazil. E-mail: colacro7@iqsc.sc.usp.br; Telephone: +55 (16) 274 9178; Fax: +55 (16) 274 9179; http://www.iqsc.sc.usp.br/dqfm/croma/colacro7.htm

Europt(r)ode IV

March 29-April 1

Muenster, Germany

For further details contact: Europt(r)ode IV Conference Office, Ines Pleggenkuhle, ICB - Institut fur Chemo- und Biosensorik, Mendelstr. 7, D-48149 Muenster, Germany. Telephone: +49 251 980 2800; Fax: +49 251 980 2802; E-mail: cammann@uni-muenster.de; http://www.uni-muenster.de/ChemoBioSensorik/Welcome-e

4th International Symposium on Hygiene and Health Management in the Working Environment

April 27-29

Ostend, Belgium

For further details contact: Technologisch Instituut vzw, Desguinlei 214, B-2018 Antwerpen, Belgium. Telephone: +32 3 216 09 96; Fax: +32 3 216 06 89; E-mail: hygiene@ti.kviv.be

IV International Symposium Chemistry Forum '98. Microsymposium on Miniaturized Analytical Devices

April 27-29

Warsaw, Poland

For further details contact Dr. Wojciech Wroblewski, Faculty of Chemistry, Warsaw University of Technology, ul. Noakowskiego 3, 00-664 Warsaw, Poland. Telephone: 48 22 6605427; Fax: 48 22 6607408; E-mail: forum@ch.pw.edu.pl; URL http://www.ch.pw.edu.pl/forum/index.html

The First International Conference on Trace Element Speciation in Biomedical, Nutritional and Environmental Sciences

May 4-7

Neuherbert/Munchen, Germany

For further details contact: First Speciation Conference, c/o Ulla Schrodel, GSF - Forschungszentrum, Congress Service, Postfach 1129, D-85758 Oberschleissheim, Germany. Telephone: +89 3187 3030 (2669); Fax: +89 3187 3362

HPLC '98—22nd International Symposium on High Performance Liquid Phase Separations & Related Techniques

St. Louis, MO, USA

May 3-8

For further details contact: Janet Cunningham, Barr Enterprises, P.O. Box 279, Walkersville, MD 21793, USA. Telephone: (301) 8983772; Fax: (301) 898 5596; E-mail: Janetbarr@aol.com

5th International Symposium on Metal Ions in Biology and Medicine

May 8-10

Neuherberg/Munich, Germany

For further details contact: Mrs Ulla Schroedel, GSF-Forschungszentrum-Congress Service, Ingolstaedter Landstrasse 1, (Neuherberg), D-85764 Oberschleissheim, Germany. Telephone: +49 (089) 3187 3030 or 2669; Fax: +49 (089) 3187 3362; E-mail: schroedel@gsf.de

SCANNING 98

May 9-12

Baltimore, Maryland, USA

For further details contact: Mary K. Sullivan, SCANNING 98, P.O. Box 832, Mahwah, NJ 07430, USA. Telephone: (201) 818-1010; Fax: (201) 818-0086; E-mail: fams@holonet.net; Internet: www.scanning-fams.org

The Scientific Instrument Association Conference 1998

May 11-14

London, UK

For further details contact: David Lofty/Rosemary Gregory, SIA '98 Conference Office. Telephone: +44 (0)1280 822873

7th European Conference on Electroanalysis

May 24-28

Coimbra, Portugal

For further details contact: Prof. C. Brett, Departmento de Quimica, Universidade de Coimbre, P-3049 Coimbra, Portugal. Telephone/Fax: +351-39-35295

20th International Symposium on Capillary Chromatography

Riva del Garda, Italy

May 25-29

For further details contact: Prof. Dr. P. Sandra, I.O.P.M.S., Kennedypark 20, B-8500 Kortijk, Belgium. Telephone: (32) 56-204960; Fax: (32) 56-204859; E-mail: ric.sandra@ven.be

VIIIth International Symposium on Luminescence Spectrometry in Biomedical and Environmental Analysis-Detection Techniques and Applications in Chromatography and Capillary Electrophoresis

May 26-29

Las Palmas de G.C., Spain

For further details contact: Dr Jose Juan Santana Rodriguez, Department of Chemistry, Faculty of Marine Sciences, University of Las Palmas de G.C., 35017 Las Palmas de G.C., Spain. Telephone: +34 28 452915; Fax: +34 28 452922; E-mail: josejuan.santana@quimica.ulpgc.es

Symposium on High Performance Liquid Phase Micro Separations

May 31-June 3

Lund, Sweden

For further details contact: Marit Johansson, The Swedish Academy of Pharmaceutical Sciences, Box 1136, 111 82 Stockholm, Sweden. Telephone: +46 8 723 50 00; Fax: +46 8 20 55 11; E-mail: marit.johansson@swepharm.se; http://www.swepharm.se/English/

Third International Symposium on Hormone and Veterinary Drug Residue Analysis

June 2-5

Bruges, Belgium

For further details contact: Prof. C. Van Petegheim, Symposium Chairman, Faculty of Pharmaceutical Sciences, University of Ghent, Harelbekestraat 72, B-9000 Ghent, Belgium. Telephone: +32 (0) 9264 81 34; Fax: +32 (0) 9264 81 99; E-mail: carlos.vanpeteghem@rug.ac.be; Website: http://allserv.rug.ac.be/~cvpetegh

5th World Congress on Biosensors

June 3-5

Berlin, Germany

For further details contact: Phillipa Orme, Biosensors 98, The Boulevard, Langford Lane, Kidlington, Oxford, UK, OX5 1GB. Telephone: +44 (0)1865 843691; Fax: +44 (0)1865 843958; E-mail: p.orme@elsevier.co.uk

AIRS III, 3rd International Symposium on Advanced Infrared and Raman Spectroscopy

July 5-9

Vienna, Austria

For further details contact: Dr Bernhard Lendl, Institute for Analytical Chemistry, Vienna University of Technology, Getreidemarkt 9/151, A-1060 Vienna, Austria. Telephone: +43 1 588 01 4848/4837; Fax: +43 1 586 78 13; E-mail: blendl@fbch.tuwien.ac.at; http://.iac.tuwien.ac.at/~airsiii

Ninth Biennial National Atomic Spectroscopy Symposium

July 8-10

Bath, UK

For further details contact: BNASS Secretariat, c/o Professor S J Hill, Department of Environmental Sciences. University of Plymouth, Drake Circus, Plymouth PL4 8AA, UK. Telephone: +44 (0)1752 233 000; Fax: +44 (0)752 233 035; E-mail: sjhill@plym.ac.uk

Geocongress '98

July 8-10

Pretoria, South Africa

For further details contact: Congress Secretary, Telephone: +27 12 8411167; Fax: +27 12 8411221; E-mail: eaucamp@geoscience.org.za; Internet address: geoscience.org.za/geocongress

SFC/SFE '98 - 8th International Symposium and Exhibit on Supercritical Fluid Chromatography and Extraction

July 12-16

St. Louis, MO, USA

For further details contact: Janet Cunningham, Barr Enterprises, P.O. Box 279, Walkersville, MD 21793, USA. Telephone: (301) 898 3772; Fax: (301) 898 5596; E-mail: Janetbarr@aol.com

Euroanalysis 10

September 6-12

Basel, Switzerland

For further details contact: The Congress Secretariat, Convention Center Basel, PO Box, CH-4021 Basel, Switzerland. Telephone: +41 61 686 2828; Fax: +41 61 686 2185; E-mail: congress@messebasel.ch

The 135th British Pharmaceutical Conference

September 8-11

Eastbourne, UK

For further details contact: BPC Secretariat Royal Pharmaceutical Society of Great Britain, 1 Lambeth High Street, London UK SE1 7JN. Telephone: +44(0) 171 820 3241; Fax: +44(0) 171 735 7629

22nd International Symposium on Chromatography ISC '98

September 13-18

Rome, Italy

For further details contact: F. Dondi, Department of Chemistry, Universita di Ferrara, Via L. Borsari, 46, I-44100 Ferrara, Italy. Telephone: +39 (532) 291154; Fax: +39 (532) 240707; E-mail: mo5@dns.unife.it; Internet: http://www.unife.it/isc22

112th AOAC International Annual Meeting and Exposition

September 13-17

Montreal, Ontario, Canada

For further details contact: Carolyn Dell, Meetings and Education Department, AOAC International, 481 North Frederick Ave., Suite 500, Gaithersburg, MD 20877, USA. Telephone: +1 301 924 7077; E-mail: cdell@aoac.org

SPICA 98 - International Symposium on Preparative and Industrial Chromatography and Allied Techniques

September 23-25

Strasbourg, France

For further details contact: Secretariat SPICA 98, Mlle Francoise Brionne, E.N.S.I.C., 1 rue Grandville, BP 451, F-54001 Nancy Cedex, France. Telephone: 33-(0) 383 17 50 03; Fax: 33-(0) 383 35 08 11; E-mail: brionne@ensic.u-nancy fr

XIVth Conference on Analytical Chemistry

September 24-26

Piatra Neamt, Romania

For further details contact: Dr G. L. Radu, Romanian Society of Analytical Chemistry, 13 Bvd, Republicii, 70346 Bucharest III, Romania. Telephone and Fax: +40 1 410 2279

6th Symposium on Kinetics in Analytical Chemistry (KAC 98)

September

Chaldiki, Greece

For further details contact: Prof. M. Karayannis, University of Ioannina, Ioannina, Greece. Telephone: +30 0651 98406; Fax: +30 0651 98407; E-mail: mkaragia@cc.uoi.gr

μ-TAS '98 - Micro-Total Analysis Systems

October 12-16

Alberta, Canada

For further details contact: Professor D. Jed Harrison, Chair, μ-TAS '98, Department of Chemistry, University of Alberta, Canada, T6G 2G2. Telephone: 1-403-492-2790; Fax: 1-403-492-8231; E-mail: MicroTAS@chem.ualberta.ca

1999

HPCE '99, Twelfth International Symposium on High Performance Capillary Electrophoresis & Related Microscale Techniques
January 23-28

Palm Springs, CA, USA

For further details contact: Joan Saluzzi, HPCE'99 Symposium Manager, c/o Rhema Association Management, PO Box 411106, San Franciso, CA 94141-1106, USA. Telephone: +1 415 487 9876; Fax: +1 415 487 9875; E-mail: society@hooked.net

23rd International Symposium on High Performance Liquid Phase Separations and Related Techniques HPLC '99

May 30-June 4

Granada, Spain

For further details contact: HPLC '99 Secretariat, Ana Costeja, Palacio de Congresos, Department de Convencions, Av. Reina Ma Cristina, s/n. 08004 Barcelona, Spain. Telephone: +34 3 233 23 77; Fax: +34 3 426 28 45; E-mail: hplc99@website.es; http://www.website.es/hplc99

SAC 99

Dublin, UK

July 25-30

For further details contact: Conference Officer (Anaytical Division), The Royal Society of Chemistry, Burlington House, Piccadilly, London, UK W1V 0BN. Telephone: +44 (0)171 437 8656; Fax: +44 (0)171 734 1227

Twenty Second International Symposium on Capillary Chromatography

November 8-12

Gifu, Japan

For further details contact: Kiyokatsu Jinno, School of Materials Science, Toyohashi University of Technology, Toyohashi 441-8122, Japan. Voicemail: 81-532-44-6805; Fax: 81-532-48-5833; E-mail: jinno@chrom.tutms.tut.ac.jp

Courses

1997

Hands-on LC-MS Training Course

September 1-5

Zeist, Netherlands

For further details contact: Rob J Vreeken, Course Organizer. Telephone: +31 30 6944276; Fax: +31 30 6956742; E-mail: vreeken@voeding.tno.nl

Field GC/MS - Hands-on-Training Clinic

September 9-11

Bel Air, MD, USA

For further details contact: Lori Sather, University of Utah, MARC 214 EMRL, Bldg 61, Salt Lake City, UT 84112, USA. Telephone: (801) 581-8431; Fax: (801) 581-4526; E-mail: sather@mail.marc.utah.edu

Workshop in Liquid Scintillation Counting

September 15-19

Loughborough, Leics, UK

For further details contact: Dr P. Warwick. Telephone: +44 (0)1509 222585 or Mrs C. Bartrop, Department of Chemistry, Loughborough University, Loughborough, Leics, LE11 3TU, UK. Telephone: +44 (0)1509 222545

HPLC Troubleshooting Course

September 16-17

Prestbury, Cheshire, UK

For further details contact: HPLC, Wellington House, Waterloo Street West, Macclesfield, Cheshire, SK11 6PJ, UK. Telephone: +44 (0)1625 613848; Fax: +44 (0)1625 616916; E-mail: hplc@silk.u-net.com

NMR Spectroscopy

September 17-19

Heslington, York, UK

For further details contact: Dr Terry Threlfall, Department of Chemistry, University of York, Heslington, York, YO1 5DD, UK. Telephone: +44 (0)1904 432576/434079; Fax: +44 (0)1904 432516; E-mail: js20@york.ac.uk

Hands-on LC-MS Training Course

September 22-26

Zeist, Netherlands

For further details contact: Rob J Vreeken, Course Organizer. Telephone: +31 30 6944276; Fax: +31 30 6956742; E-mail: vreeken@voeding.tno.nl

EURACHEM Uncertainty Workshop

September 29-30

Berlin, Germany

For further details contact: Dr Werner Hasselbarth, Federal Institute for Materials Research and Testing, D-12200 Berlin, Germany. Telephone: +49 30 6392 5861; Fax: +49 30 6392 5972

Interpretation of Infrared Spectra

September 30-October 2

Heslington, York, UK

For further details contact: Dr Terry Threlfall, Department of Chemistry, University of York, Heslington, York YO1 5DD, UK. Telephone: +44 (0)1904 432576/434079; Fax: +44 (0)1904 432516; E-mail: js20@york.ac.uk

Quality Assurance for the Analytical Laboratory

October 13-16

Amsterdam, The Netherlands

For further details contact: The Center for Professional Advancement, Oudezijds Voorburgwal 316A, 1012 GM Amsterdam, The Netherlands. Telephone: +31 20 638 28 06; Fax: +31 20 620 21 36

Hands-on LC-MS Training Course

October 13-17

Zeist, Netherlands

For further details contact: Rob J Vreeken, Course Organizer. Telephone: +31 30 6944276; Fax: +31 30 6956742; E-mail: vreeken@voeding.tno.nl

HPLC Beginners Course

October 28-30

Prestbury, Cheshire, UK

For further details contact: HPLC, Wellington House, Waterloo Street West, Macclesfield, Cheshire, SK11 6PJ, UK. Telephone: +44 (0)1625 613848; Fax: +44 (0)1625 616916; E-mail: hplc@silk.u-net.com

CE Small Molecule Analysis

October 29-30

London, UK

For further details contact: Margaret Kermode, Conference Registrar, Advanstar Communications, Advanstar House Park West, Sealand Road, Chester CH1 4RN, UK. Telephone: +44 (0)1244 378 888; Fax: +44 (0)1244 370 011

Entries in the above listing are included at the discretion of the Editor and are free of charge. If you wish to publicize a forthcoming meeting please send full details to: *The Analyst* Editorial Office, Thomas Graham House, Science Park, Milton Road, Cambridge, UK CB4 4WF. Tel: +44 (0)1223 420066. Fax: +44 (0)1223 420247. E-mail:Analyst@RSC.ORG

Future Issues Will Include

IUPAC Announcement

The Quantity 'pH'

The growing awareness amongst analytical chemists of the need for expressing the traceability and uncertainty of results has brought new pressure to reconsider difficulties in determination of the quantity 'pH'. The IUPAC Commission on Electroanalytical Chemistry, V.5, feels responsible for the proper understanding and use of the pH concept[1] throughout the chemistry-based industrial and academic communities. It is proposing new work towards preparation of a unified pH scale, as well as continuing its work on applications.[2-7] The adoption of a scientifically sounder assumption for activity coefficients in mixed electrolytes, *e.g.*, the Pitzer treatment,[8] to replace the Bates-Guggenheim Convention, will lead to the best possible definition of pH, the closest to the 'true', unattainable, pa_H value. By this means, known standard buffers, with or without background electrolyte, can be assigned calculated pH values on the unified pH scale.

Before the unified pH scale is formulated, an extensive further program of experimental work on pH standard buffers is required. It is the intention to enlist the co-operation of some dozen suitably equipped laboratories world-wide to make extensive new emf measurements of Harned cells with buffer substance components over a wide temperature range to derive the necessary information.

A concurrently formed working party will reconsider the current IUPAC (1985) Recommendations.[1] It will provide a forum for discussions among pH experts, metrologists and those in the new research programs, on the validity of newer scientific assumptions for activity coefficients in mixed electrolytes. Among tasks foreseen are

1. Creating a database of the most reliable aqueous emf measurements.

2. Re-analysing these data by multilinear regression and examining extrathermodynamic conventions.

3. Re-examining the realisation of the pH scale by multi-standards, either point-to-point or regression, or by a single standard.

4. Assessing the differences in practical pH measurements of these alternatives on traceability and uncertainty.

A number of laboratories have already offered support. Requests for further details, offers of help, and comments on this proposal and on the existing IUPAC Recommendations for the research collaboration should be sent to: Prof. Arthur K. Covington, Department of Chemistry, University of Newcastle upon Tyne, NE1 7RU, UK. Fax: +44 191 222 6929; E-mail: a.k.covington@newcastle.ac.uk.

Recommendations for the IUPAC Working Party should be sent to Prof. Sandra Rondinini, Department of Chemical Physics and Electrochemistry, University of Milan, 19 Via Golgi, Milan, Italy 20133. Fax +39 (2) 26603 217; E-mail: vertova@icil64.cilea.it.

References

1 Covington, A. K., Bates, R. G., and Durst, A. A., *Pure Appl. Chem.*, 1985, **57**, 531.
2 Mussini, T., Covington, A. K., Longhi, P., and Rondinini, S., *Pure Appl. Chem.*, 1985, **57**, 865.
3 Covington, A. K., Whalley, P. D., and Davison, W., *Pure Appl. Chem.*, 1985, **57**, 877.
4 Covington, A. K., *Pure Appl. Chem.*, 1985, **57**, 887.
5 Rondinini, S., Mussini, P. R., and Mussini, T. *Pure Appl. Chem.*, 1987, **59**, 1549.
6 Covington, A. K., and Whitfield, M., *Pure Appl. Chem.*, 1988, **60**, 865.
7 Durst, R. A., Davison, W., and Koch, W. F., *Pure Appl. Chem.*, 1994, **66**, 649.
8 Covington, A. K., and Ferra, M. I. A., *J. Solution Chem.*, 1994, **23**, 1.

Technical Abbreviations and Acronyms

The presence of an abbreviation or acronym in this list should NOT be read as a recommendation for its use. However, those defined here need not be defined in the text of your manuscript. Abbreviations also cover the plural form.

AAS	atomic absorption spectrometry	mp	melting point
ac	alternating current	MRL	maximum residue limit
A/D	analogue-to-digital	mRNA	messenger ribonucleic acid
ADC	analogue-to-digital converter	MS	mass spectrometry
ANOVA	analysis of variance	NIR	near-infrared
AOAC	Association of Official Analytical Chemists	NMR	nuclear magnetic resonance
ASTM	American Society for Testing and Materials	NIST	National Institute of Standards and Technology
bp	boiling point	od	outer diameter
BSA	bovine serum albumin	OES	optical emission spectrometry
BSI	British Standards Institution	PBS	phosphate buffered saline
CEN	European Committee for Standardization	PCB	polychlorinated biphenyl
		PAH	polycyclic aromatic hydrocarbon
cpm	counts per minute	PGE	platinum group element
CMOS	complementary metal oxide silicon	PIXE	particle/proton-induced X-ray emission
c.m.c.	critical micellization concentration	ppt	parts per trillion (10^{12}; pg g^{-1})
CRM	certified reference material	ppb	parts per billion (10^9; ng g^{-1})
CVAAS	cold vapour atomic absorption spectrometry	ppm	parts per million (10^6; µg g^{-1})
		PTFE	poly(tetrafluoroethylene)
CW	continuous wave	PVC	poly(vinyl chloride)
CZE	capillary zone electrophoresis	PDVB	poly(divinyl benzene)
dc	direct current	QC	quality control
dpm	disintegrations per minute	QA	quality assurance
DRIFT	diffuse reflectance infrared Fourier transform spectroscopy	REE	rare earth element
		rf	radiofrequency
DELFIA	dissociation enhanced lanthanide fluorescence immunoassay	RIMS	resonance ionization mass spectrometry
DNA	deoxyribonucleic acid	rms	root mean square
EDTA	ethylenediaminetetraacetic acid	rpm	revolutions per minute
ELISA	enzyme linked immunosorbent assay	RNA	ribonucleic acid
emf	electromotive force	RSD	relative standard deviation
ETAAS	electrothermal atomic absorption spectrometry	SCE	saturated calomel (reference) electrode
		SE	standard error
EXAFS	extended X-ray absorption fine structure spectroscopy	SEM	scanning/surface (reflection) electron microscopy
EPA	Environmental Protection Agency	SIMS	secondary-ion mass spectrometry
FAAS	flame atomic absorption spectrometry	SIMCA	soft independent modelling of class analogy
FAB	fast atom bombardment		
FAO-WHO	Food and Agriculture Organization, World Health Organization	S/N	signal-to-noise ratio
		SRM	Standard Reference Material
FIR	far-infrared	STM	scanning tunnelling (electron) microscopy
FT	Fourier transform		
FPLC	fast protein liquid chromatography	STP	standard temperature and pressure
FPD	flame photometric detector	TIMS	thermal ionization mass spectrometry
GC	gas chromatography	TLC	thin-layer chromatography
GLC	gas-liquid chromatography	TOF	time-of-flight
HGAAS	hydride generation atomic absorption spectroscopy	TGA	thermogravimetric analysis
		TMS	trimethylsilane
HPLC	high-performance liquid chromatography	TRIS	2-amino-2-(hydroxymethyl)-propane-1,3-diol (reagent)
ICP	inductively coupled plasma	UV	ultraviolet
id	internal diameter	UV/VIS	ultraviolet–visible
INAA	instrumental neutron activation analysis	VDU	visual display unit
		XRD	X-ray diffraction
IR	infrared	XRF	X-ray fluorescence
ISFET	ion-selective effect transistor	YAG	yttrium aluminium garnet
iv	intravenous		
im	intramuscular	***Commonly Used Symbols***	
IGFET	insulated gate field effect transistor	M	molecular mass
ISE	ion-selective electrode	M_r	relative molecular mass
LC	liquid chromatography	r	correlation coefficient
LED	light emitting diode	s	standard deviation of sample
LOD	limit of detection	σ	population standard deviation
LOQ	limit of quantification	u	atomic mass

We have been working hard, and now there is only one thing that may be missing from the 1997 EAS.

Technical Papers

EAS Short Courses

EAS Exhibitor Workshops

Scientific Exposition

Employment Bureau

TUTORIALS

Lunch-time Colloquia

you !
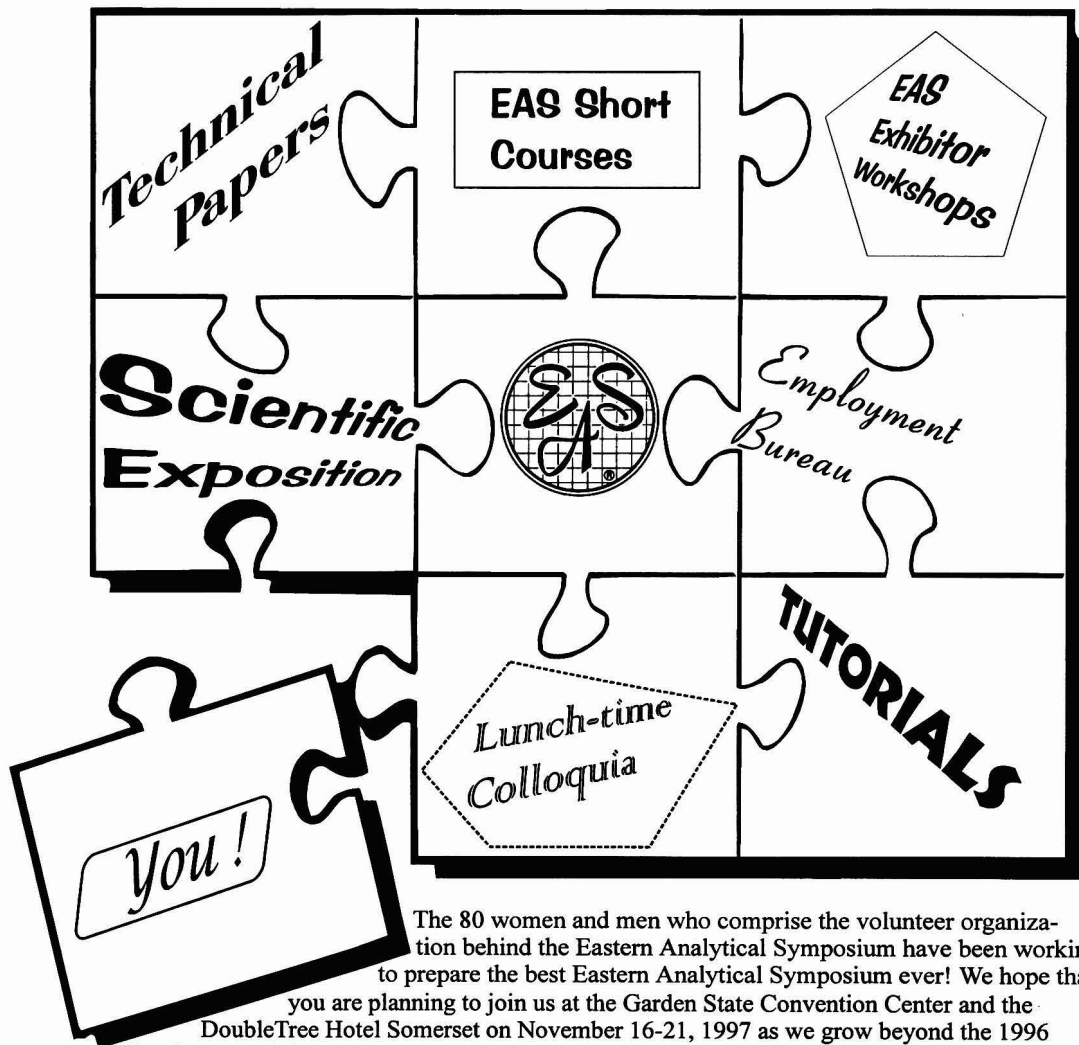
The 80 women and men who comprise the volunteer organization behind the Eastern Analytical Symposium have been working to prepare the best Eastern Analytical Symposium ever! We hope that you are planning to join us at the Garden State Convention Center and the DoubleTree Hotel Somerset on November 16-21, 1997 as we grow beyond the 1996 tally of 318 Exhibit booths, 5115 conferees, and 640 technical papers. The August issue of *The EAS Retort* newsletter is ready now, and the Preliminary Program will be mailed in September. You will find 80 Technical Sessions, 27 EAS Short Courses, 21 EAS Exhibitor Workshops, Housing information, a Registration form, a listing of Exhibitors, and more. Not yet on our mailing list? Don't worry, be happy! More information is available! Simply contact: The EAS HOTLINE at 1-302-738-6218, the EAS FAXLINE at 1-302-738-5275, access the EAS HOMEPAGE at http://www.eas.org/, or send e-mail to EASINFO@AOL.COM.

EAS '97: Continuous Improvement Through Change!

Cover picture: Analysis of additives in polymers. Photograph kindly supplied by H. Vandenburg, School of Chemistry, University of Leeds, Leeds, UK LS2 9JT (see p. 101R).

The Analyst

The analytical journal of The Royal Society of Chemistry

CONTENTS